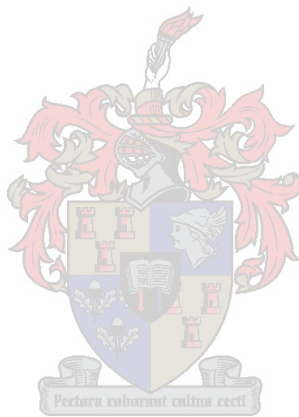


SEDIMENT TRANSPORT REGIME
in the area of the
EAST LONDON HARBOUR ENTRANCE

by

Andre K Theron

**Thesis presented in partial fulfilment of the requirements for the degree of
Master of Engineering (Civil) at the University of Stellenbosch**



Study Leader
Mr DE Bosman

December 2004

Declaration:

I, the undersigned, hereby declare that the work contained in this thesis is my own original work and that I have not previously in its entirety or in part submitted it at any university for a degree.

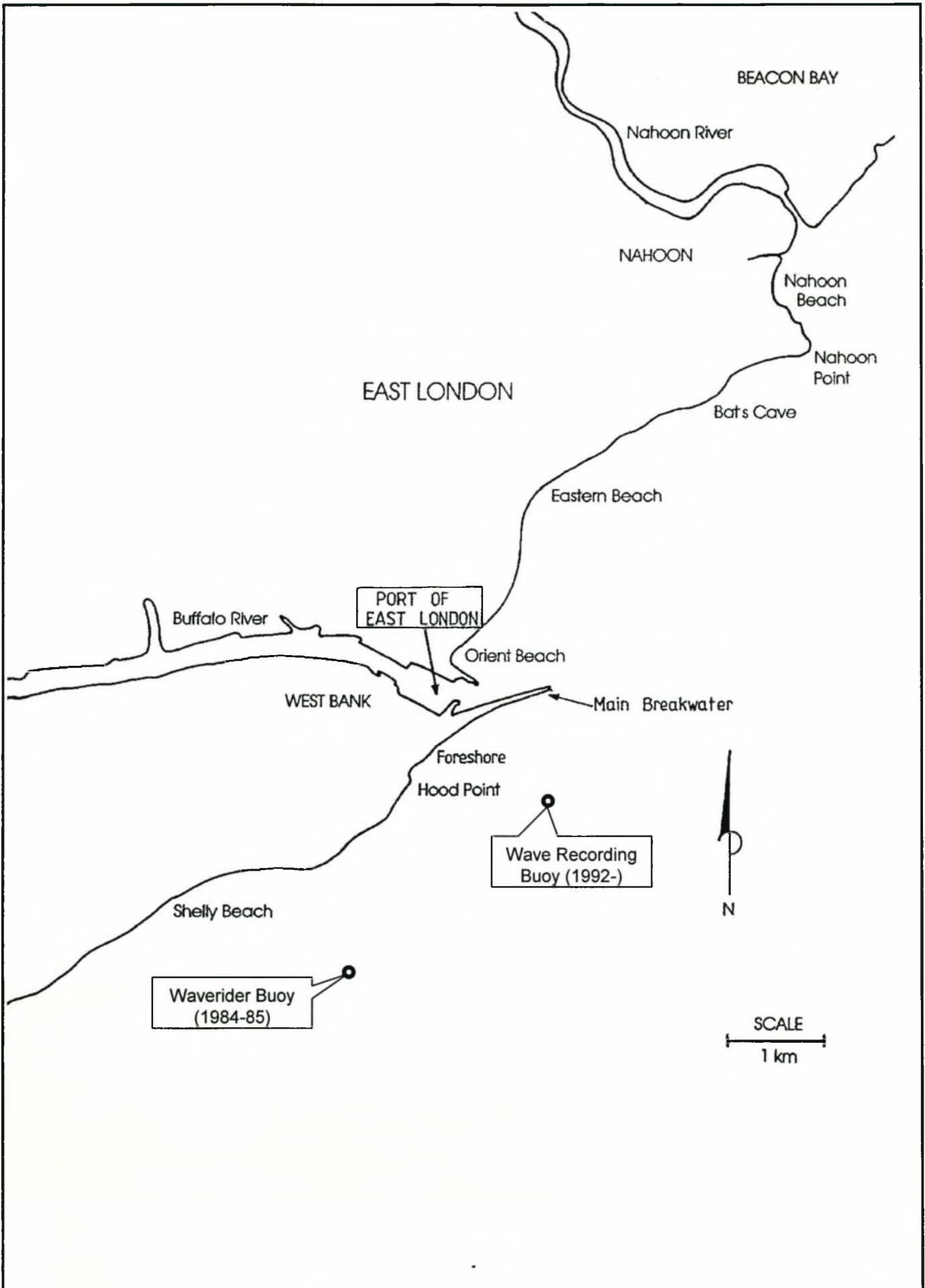
Signature:

Date: 14 October 2004



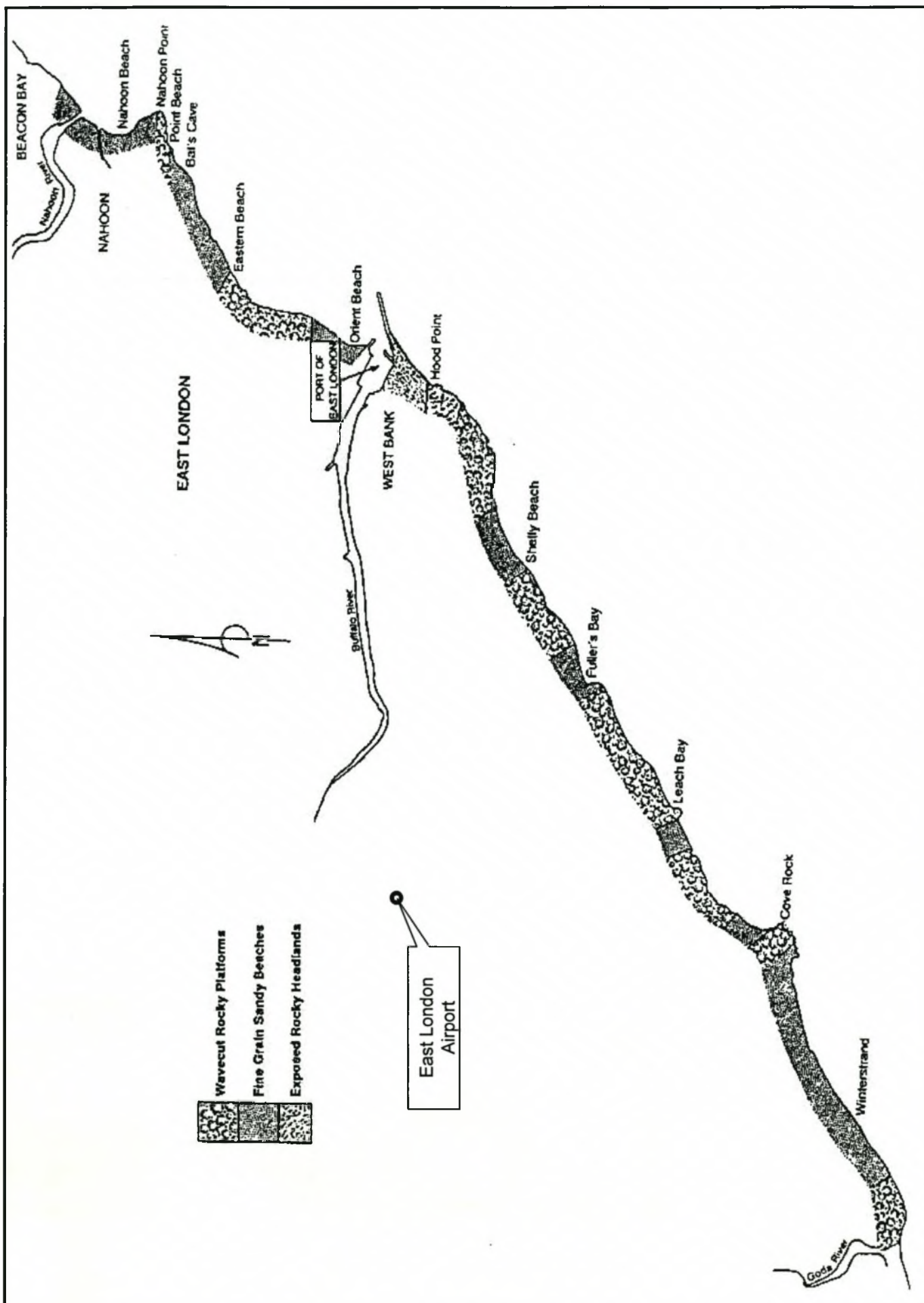
EAST LONDON HARBOUR ON THE BUFFALO RIVER

FIGURE 1.1



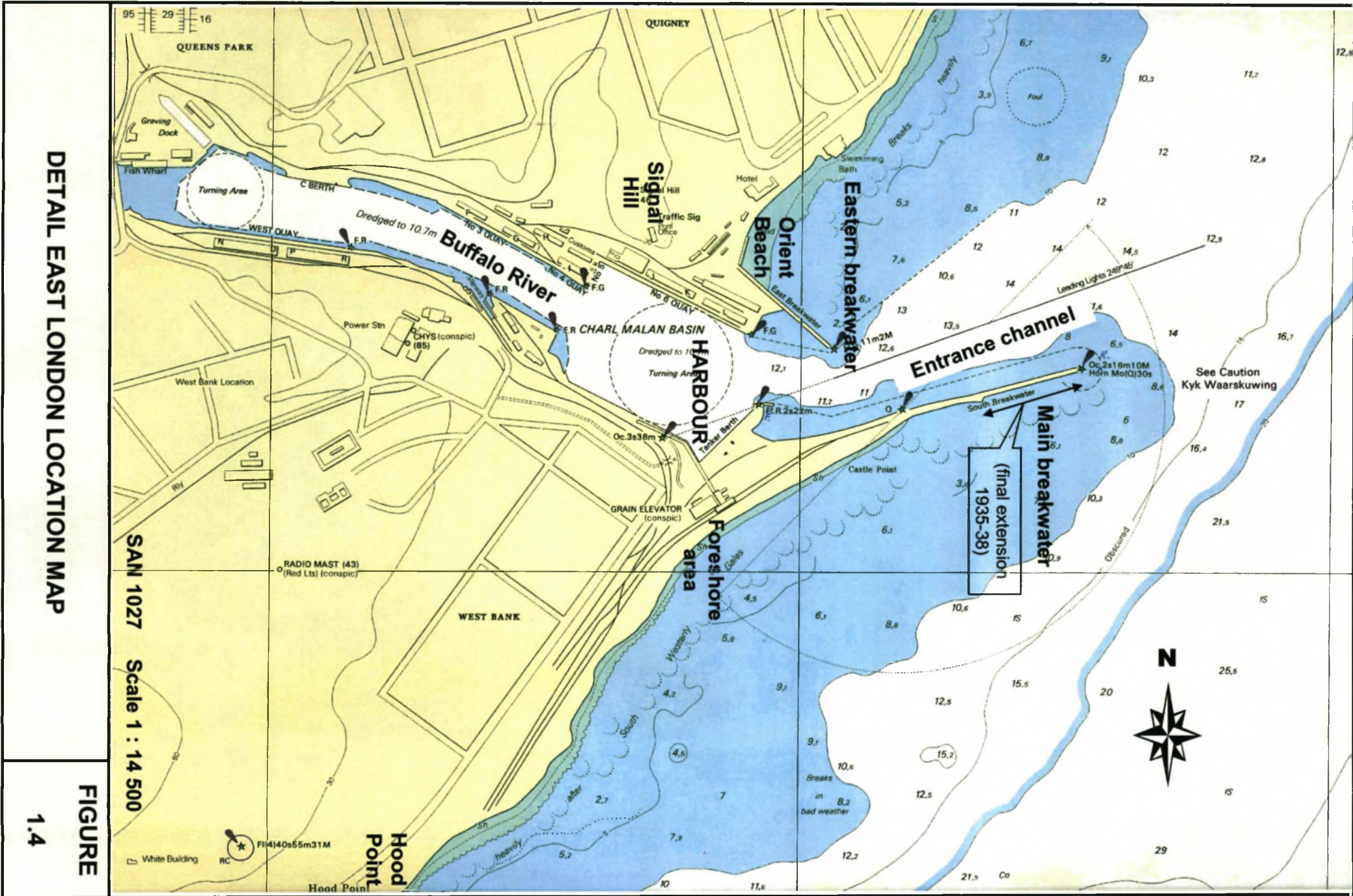
EAST LONDON LOCATION MAP (GENERAL)

**FIGURE
1.2**



EAST LONDON LOCATION MAP SHOWING SHORELINE CHARACTERISTICS (Adapted from Marker, 1988)

FIGURE 1.3

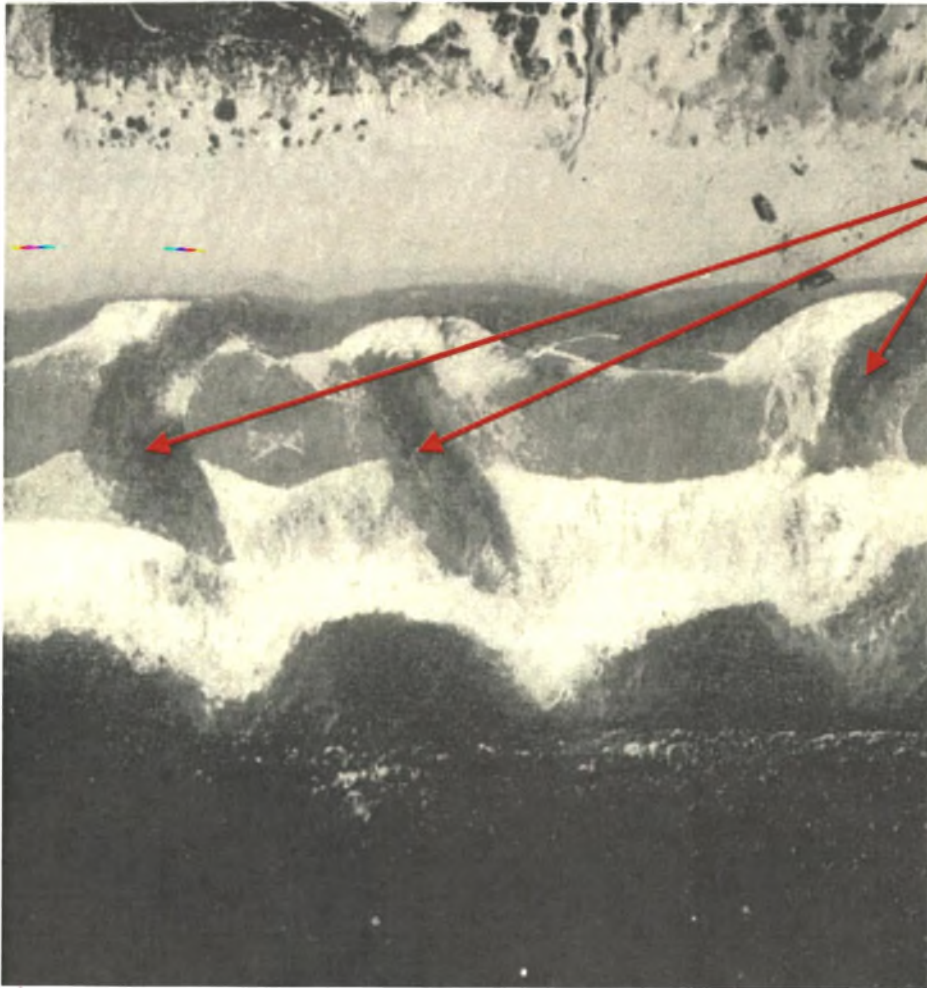


DETAIL EAST LONDON LOCATION MAP

SAN 1027 Scale 1 : 14 500

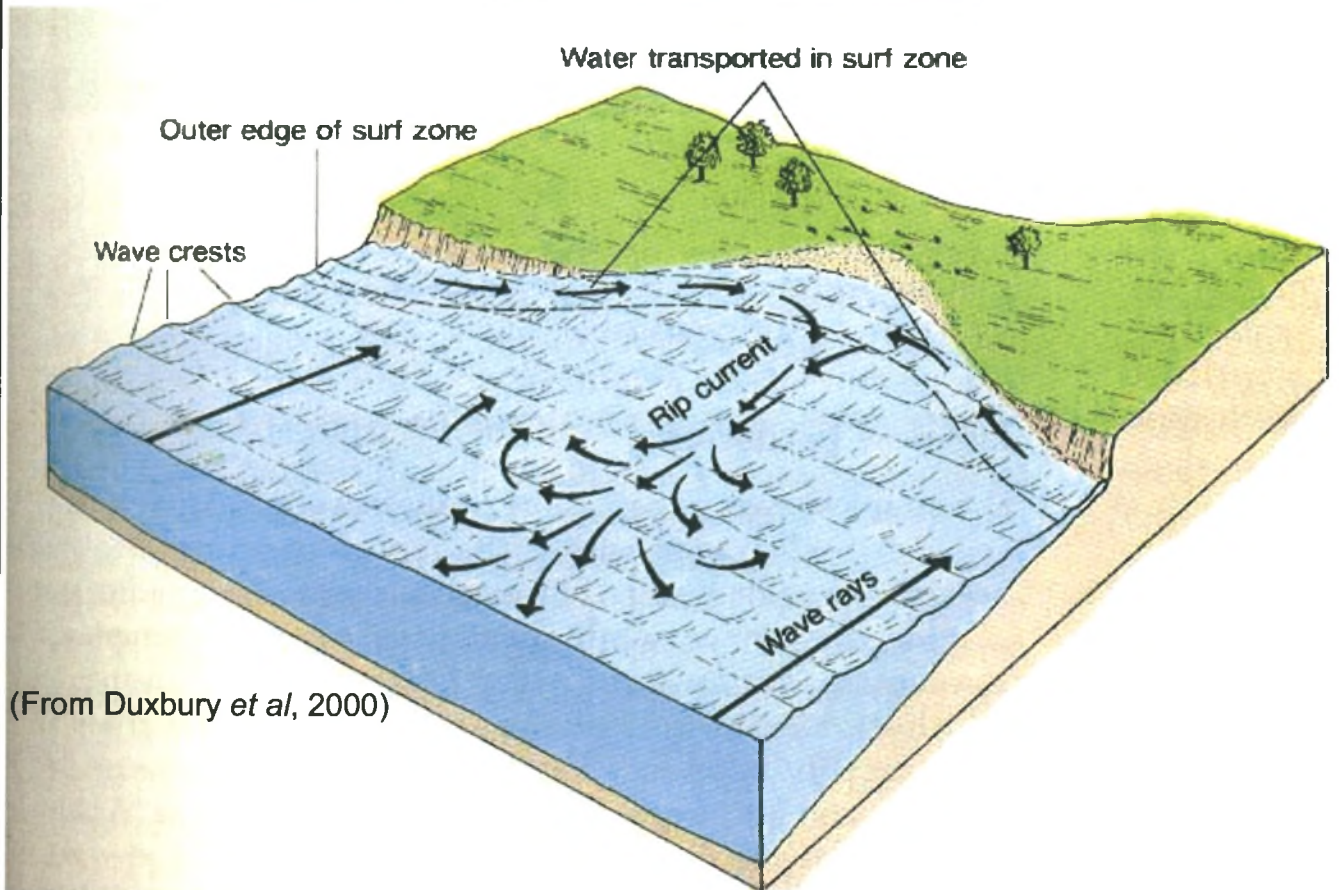
FIGURE

1.4



Rip
Currents

(From <http://duedall.fit.edu/>
Ocean 1010, Coasts and Beaches.URL)



TWO FORMS OF RIP CURRENTS

FIGURE

2.1



**SOME SURF ZONE CONDITIONS BETWEEN
HOOD POINT AND THE MAIN BREAKWATER AREA**

**FIGURE
3.1**



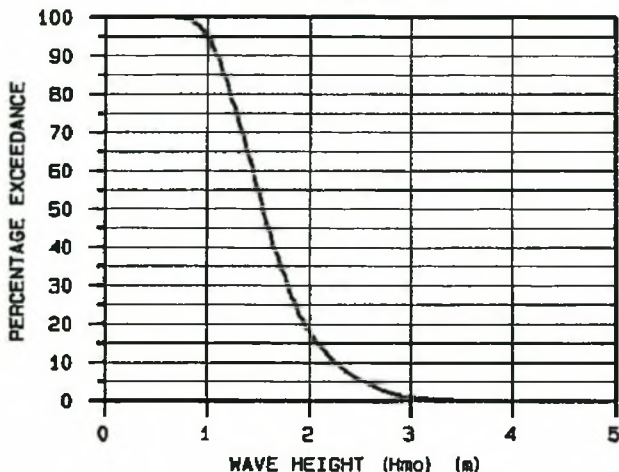
ORIENT BEACH AREA

FIGURE

3.2

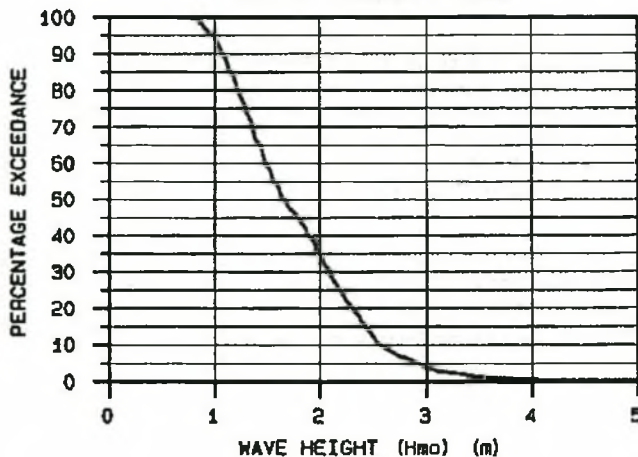
SUMMER

No. of Records = 2608



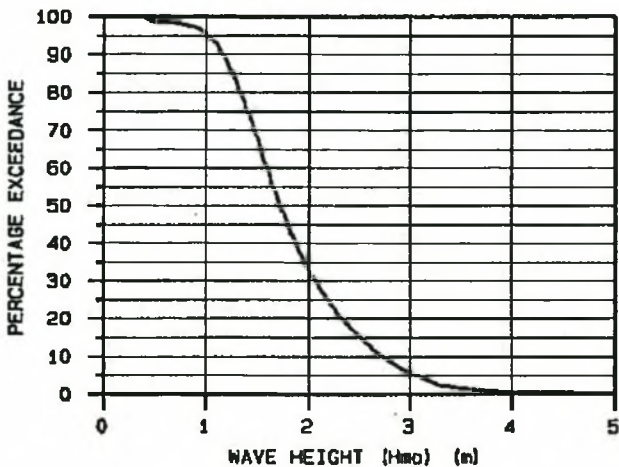
AUTUMN

No. of Records = 1256



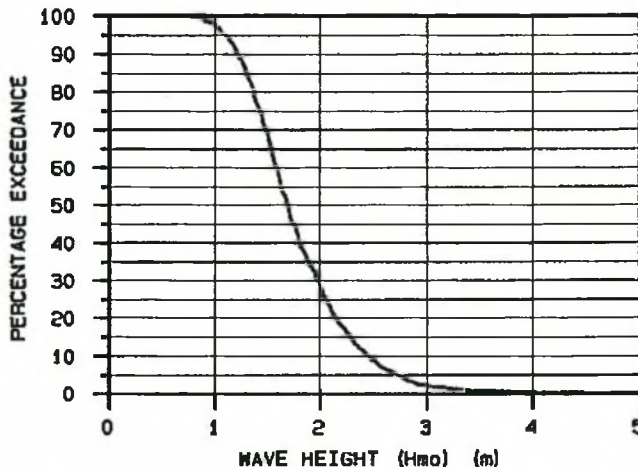
WINTER

No. of Records = 2114



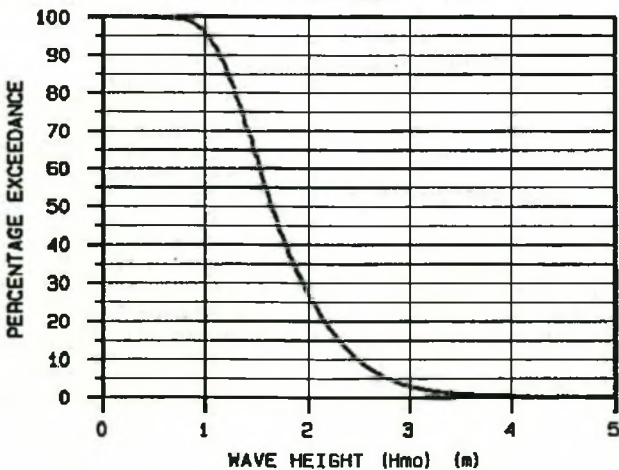
SPRING

No. of Records = 2384



ALL DATA

No. of Records = 8890



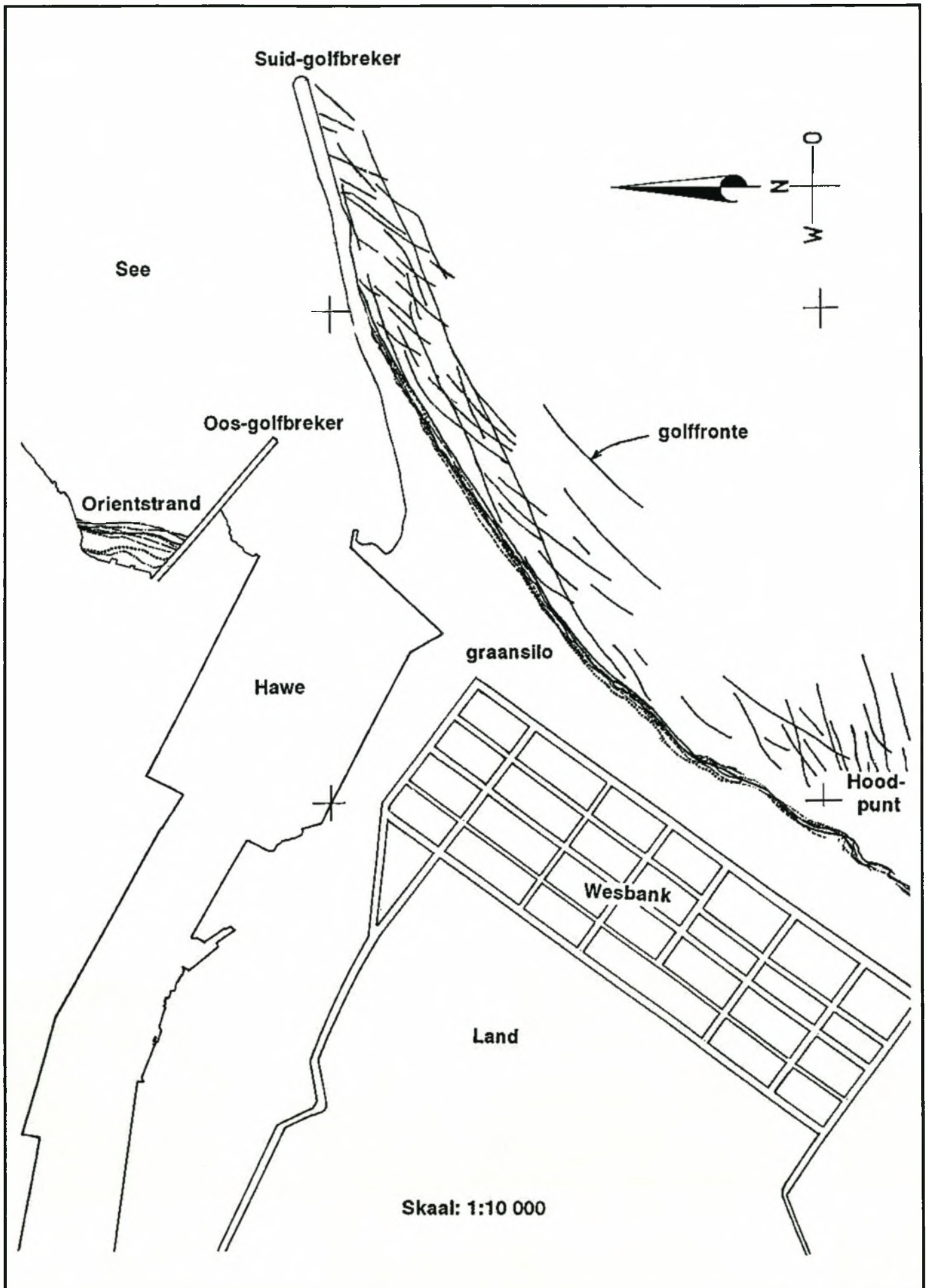
1992/04/22 to 1996/02/28

	WAVE HEIGHT (Hmo) EXCEEDED				
	1%	5%	10%	25%	50%
SUMMER :	3.01	2.55	2.26	1.87	1.55
AUTUMN :	3.69	2.94	2.57	2.19	1.66
WINTER :	3.78	3.09	2.73	2.19	1.73
SPRING :	3.41	2.73	2.44	2.05	1.71
ALL DATA:	3.44	2.78	2.48	2.05	1.64

EAST LONDON WAVE HEIGHT EXCEEDANCE CURVES

FIGURE

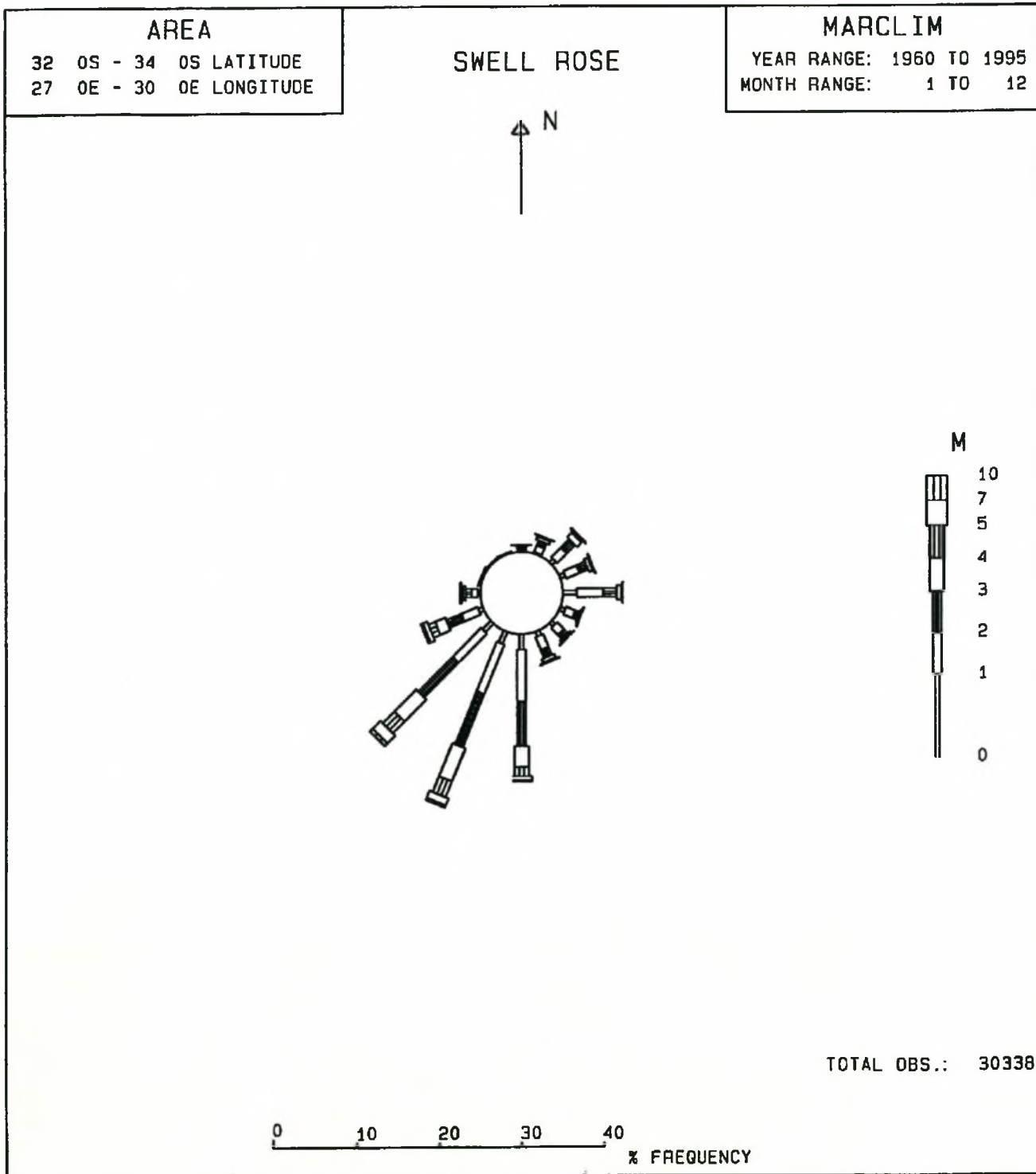
3.3



WAVE CRESTS FROM AERIAL PHOTOGRAPHS

FIGURE

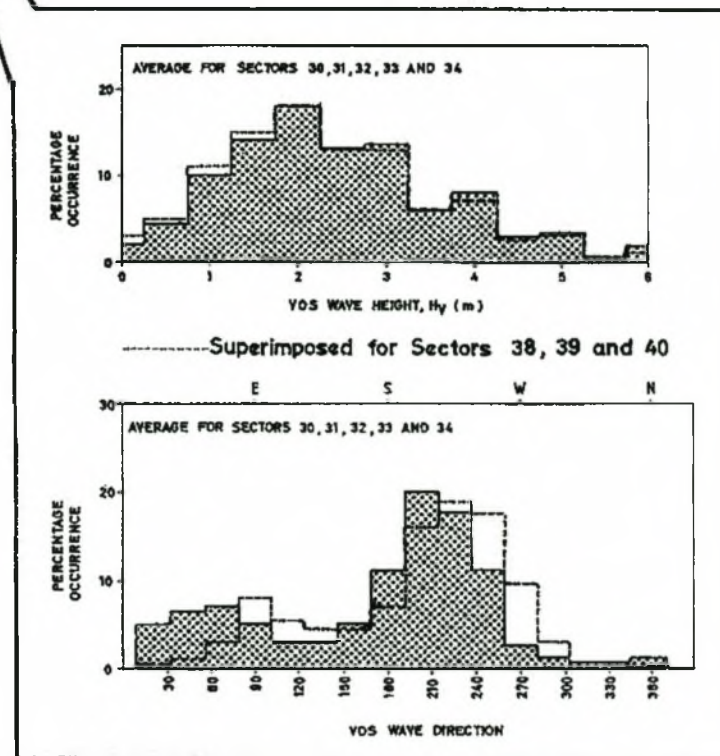
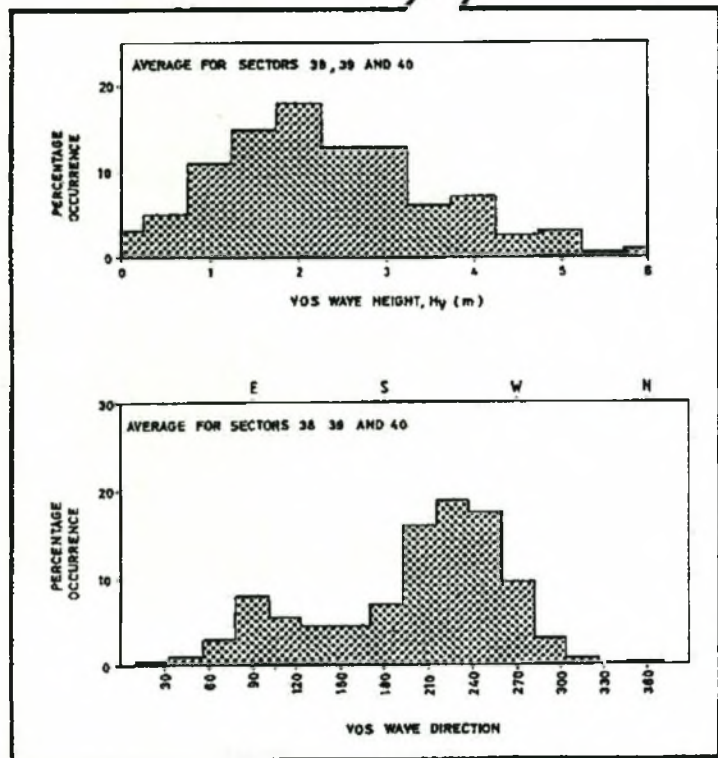
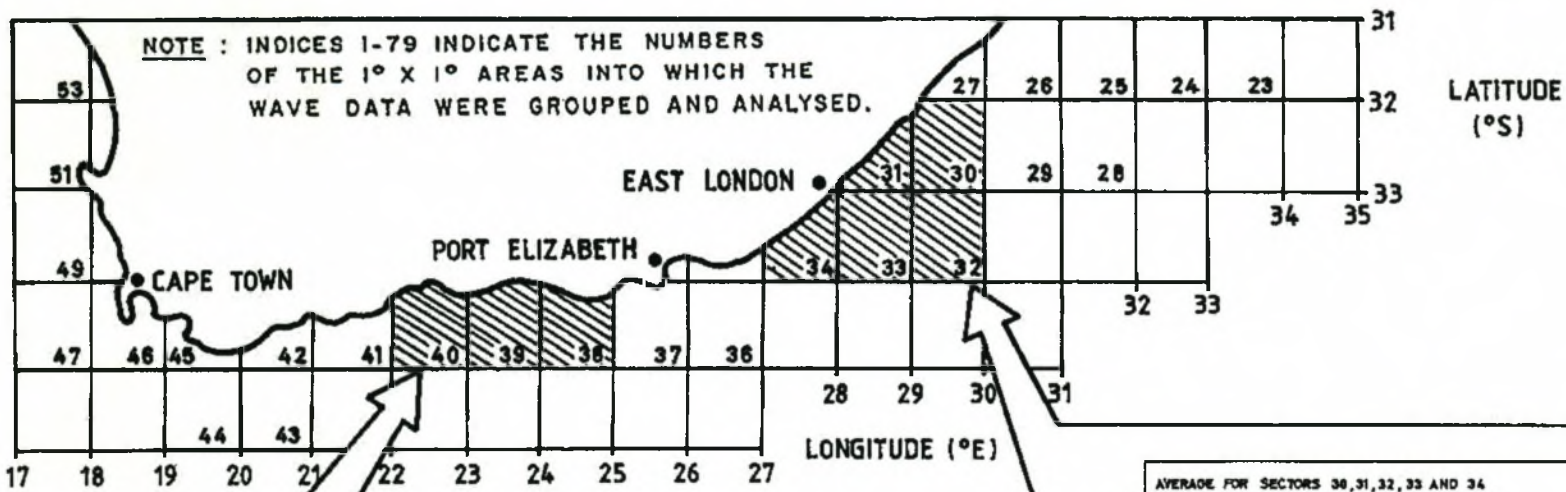
3.4



EAST LONDON VOS SWELL ROSE

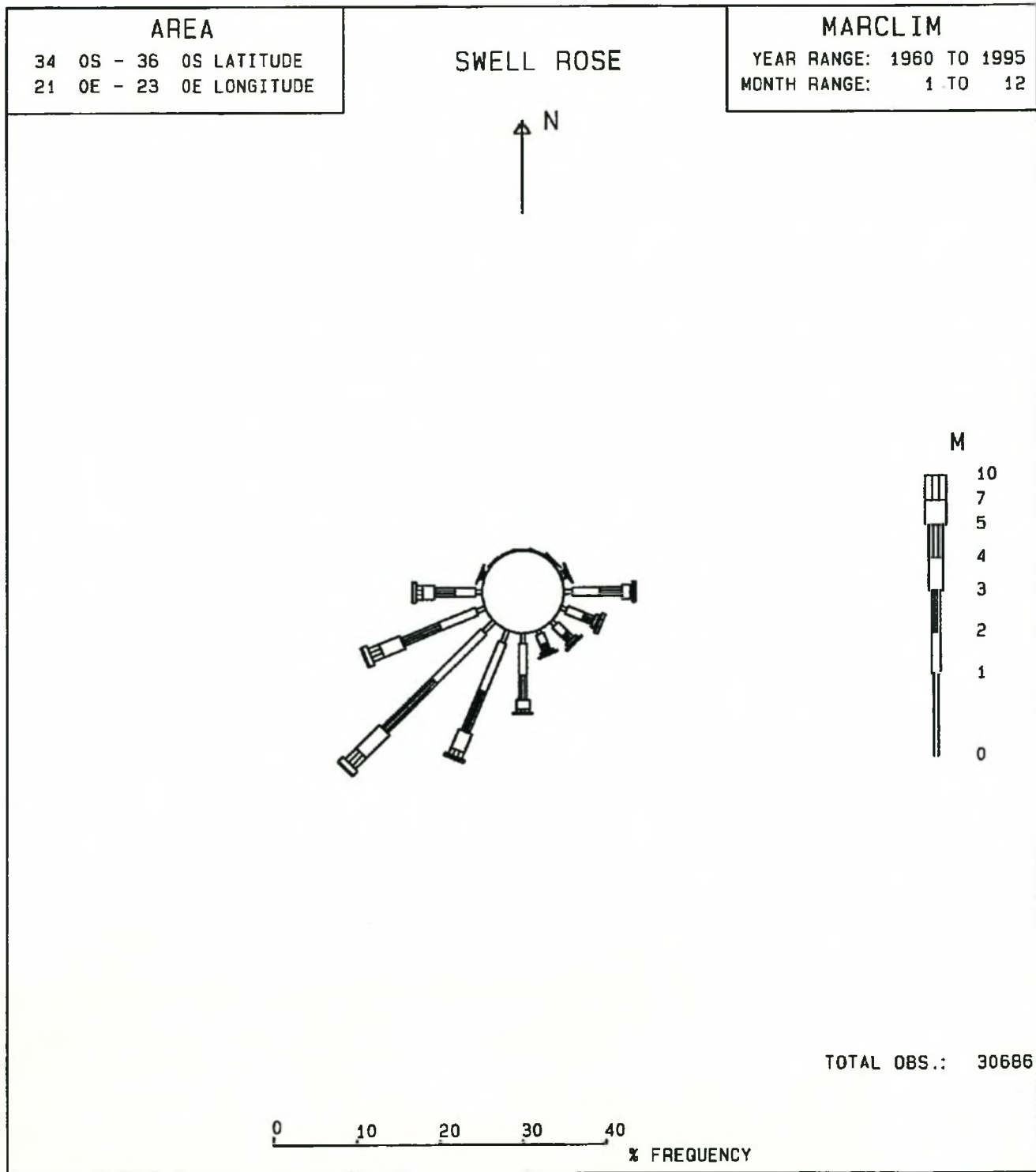
**FIGURE
3.5**

COMPARISON OF VOS WAVE HEIGHTS AND DIRECTIONS



VOS WAVE DATA

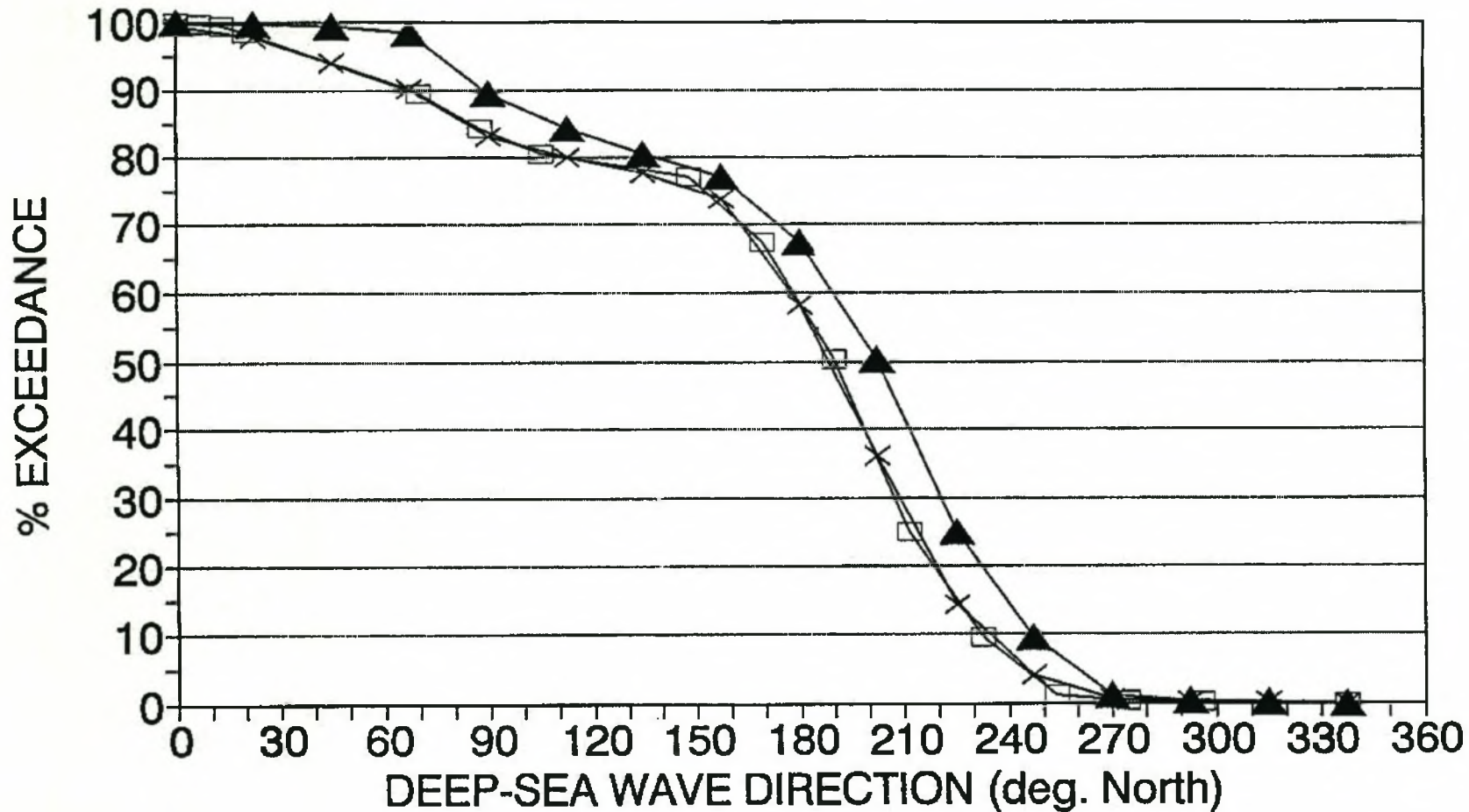
FIGURE 3.6



MOSSEL BAY VOS SWELL ROSE

**FIGURE
3.7**

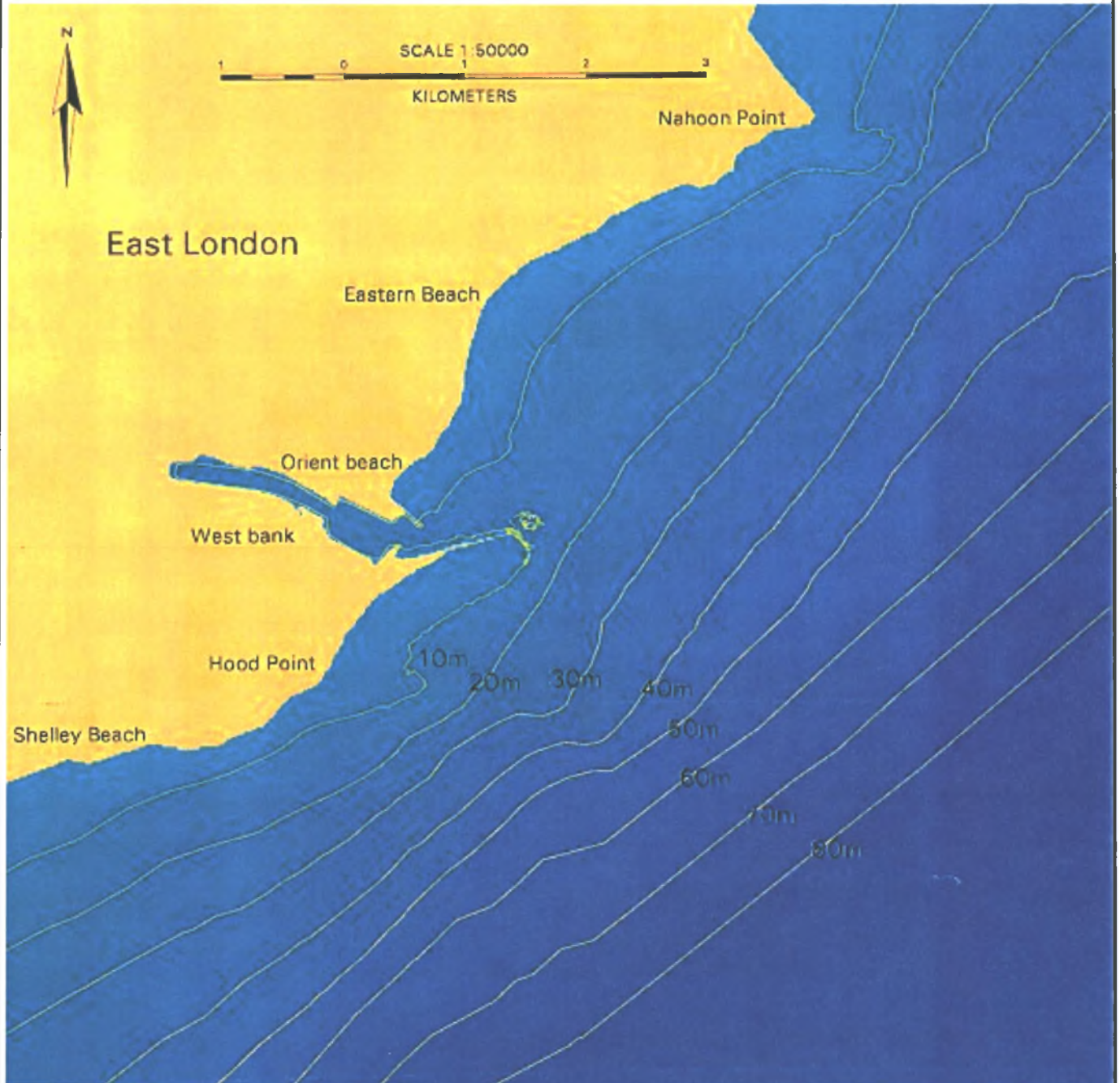
COMPARISON: MOSSEL BAY/ EAST LONDON VOS WAVE DIRECTION EXCEEDANCE CURVE



WAVE DIRECTION EXCEEDANCE CURVES COMPARISON AND ADAPTED MOSSEL BAY CURVE

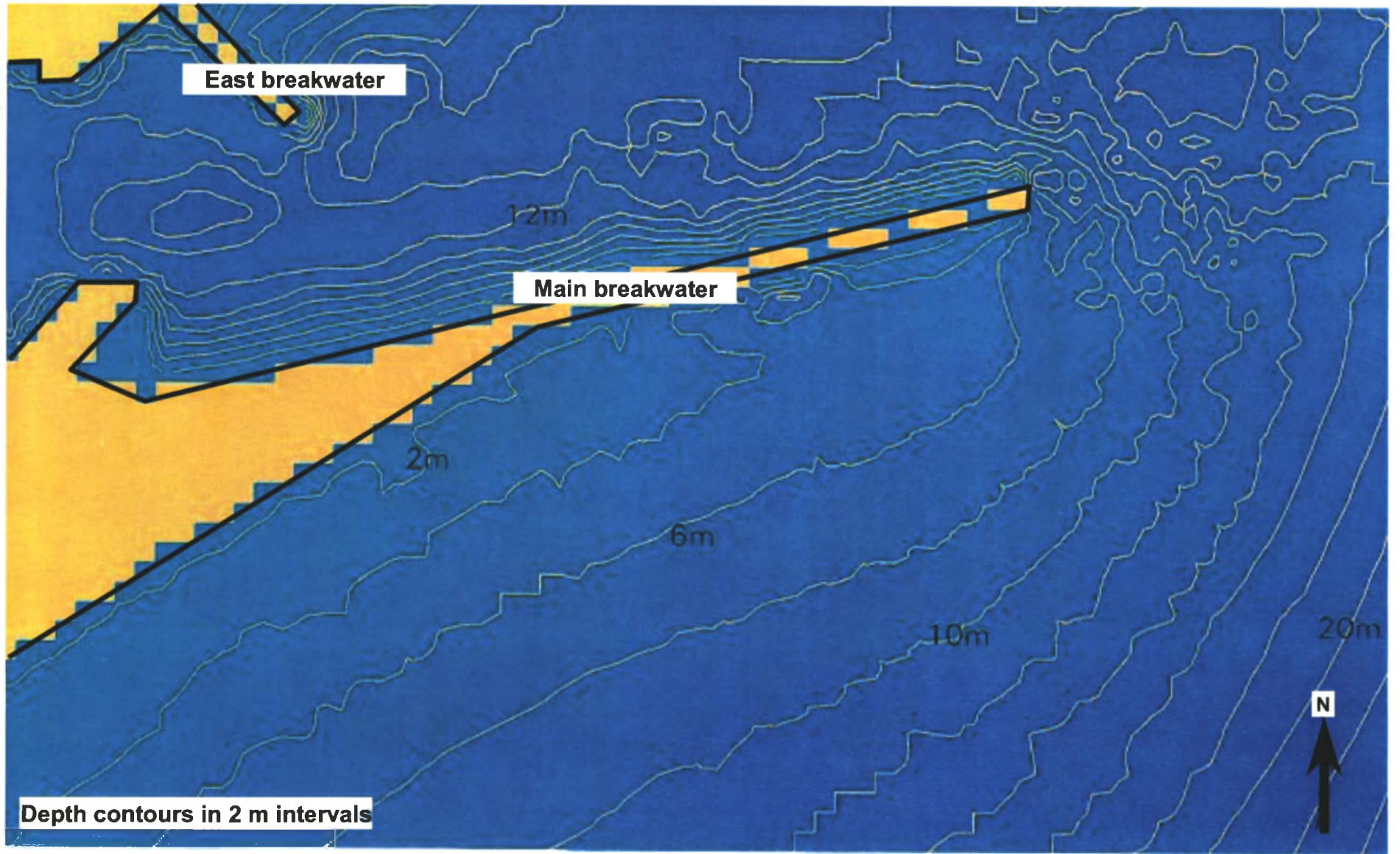
FIGURE 3.8

—x— East London —▲— Mossel Bay —□— MB shifted



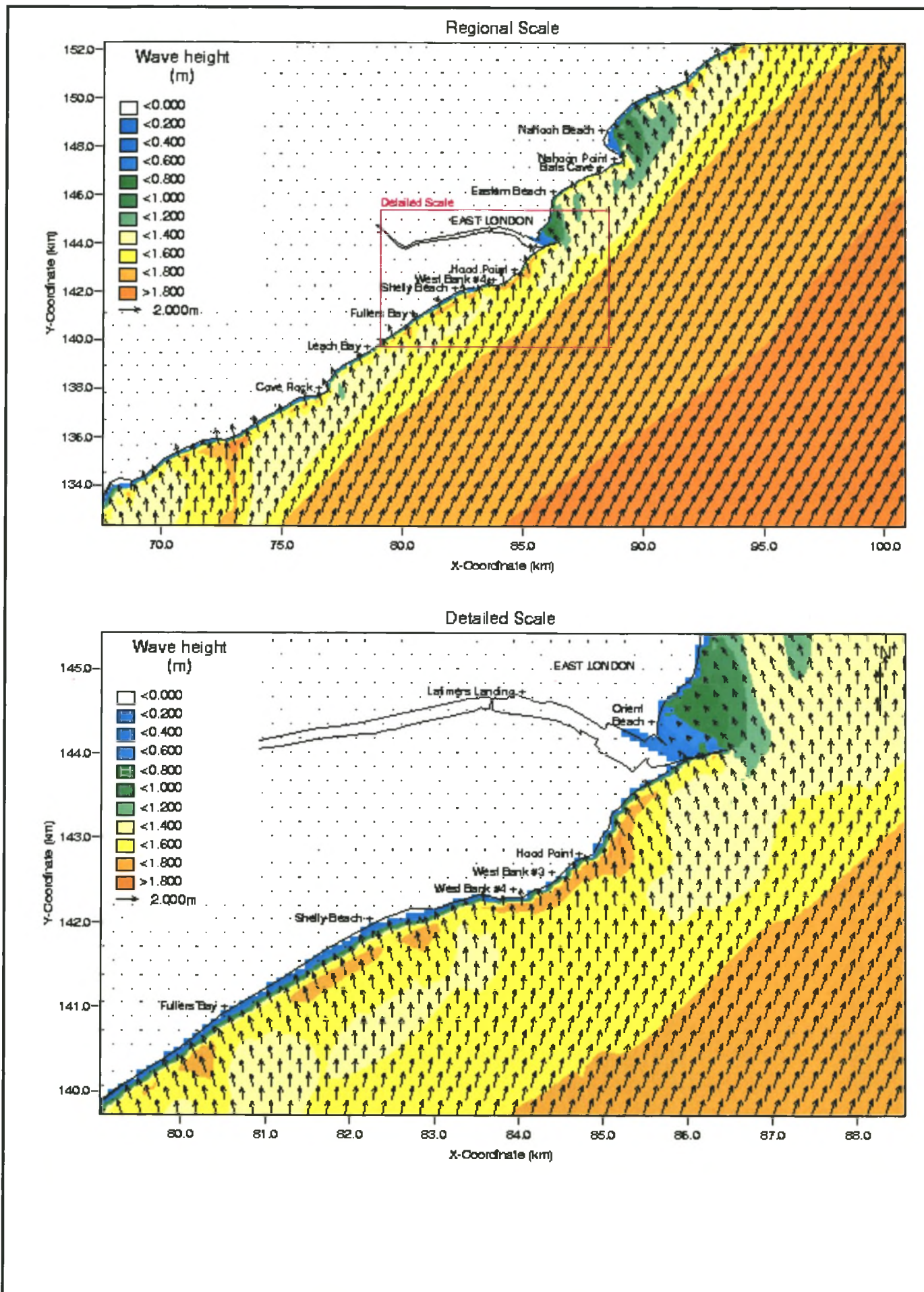
EAST LONDON MODEL BATHYMETRY: SHELLEY BEACH TO NAHOON POINT

**FIGURE
3.9**



EAST LONDON MODEL BATHYMETRY: AREA AROUND THE
MAIN BREAKWATER

FIGURE
3.10

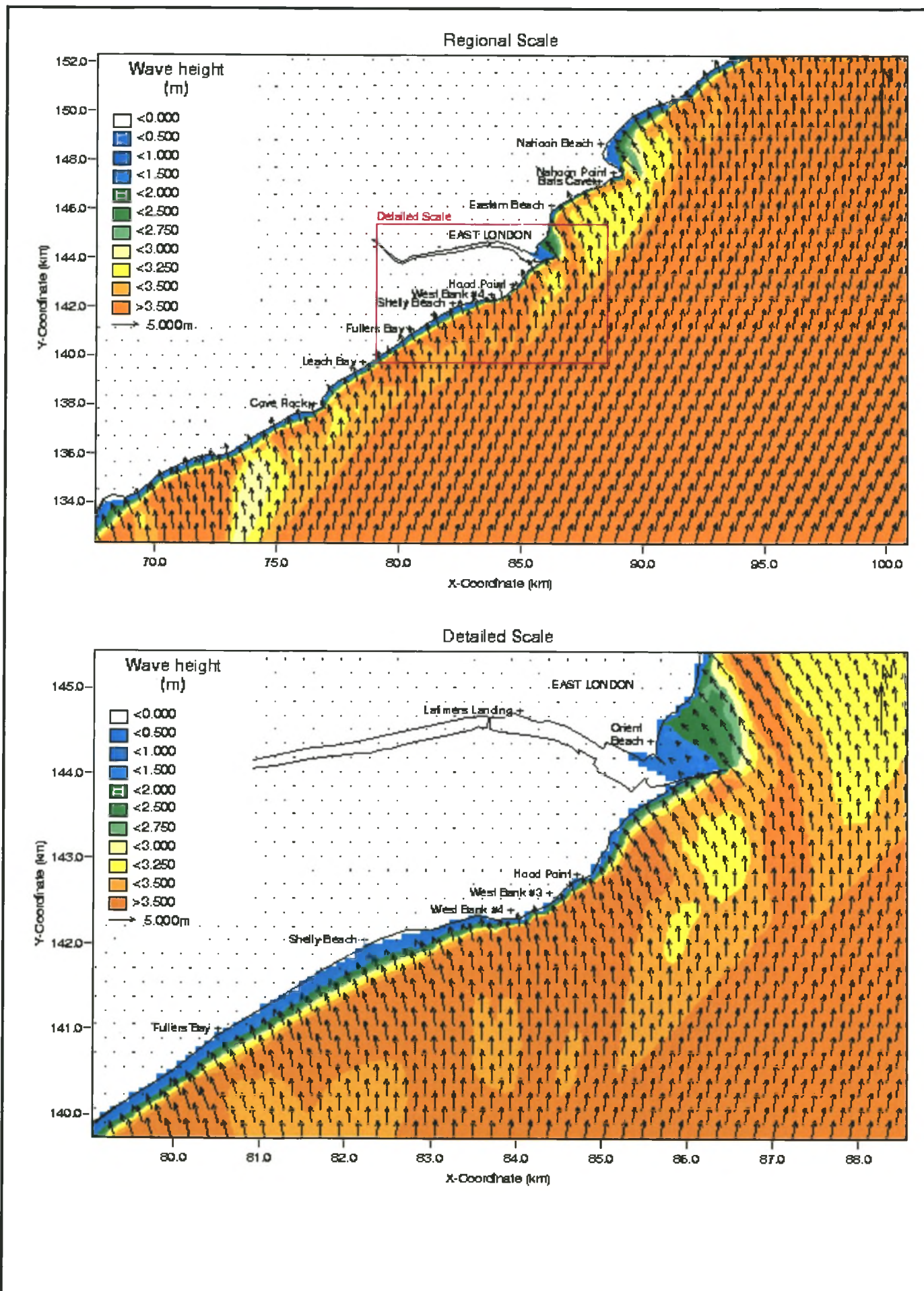


Wave refraction modelling: average condition

(Hmo = 1,9 m; Tp = 12s; Direction = 214 deg. (SW))

FIGURE

3.11



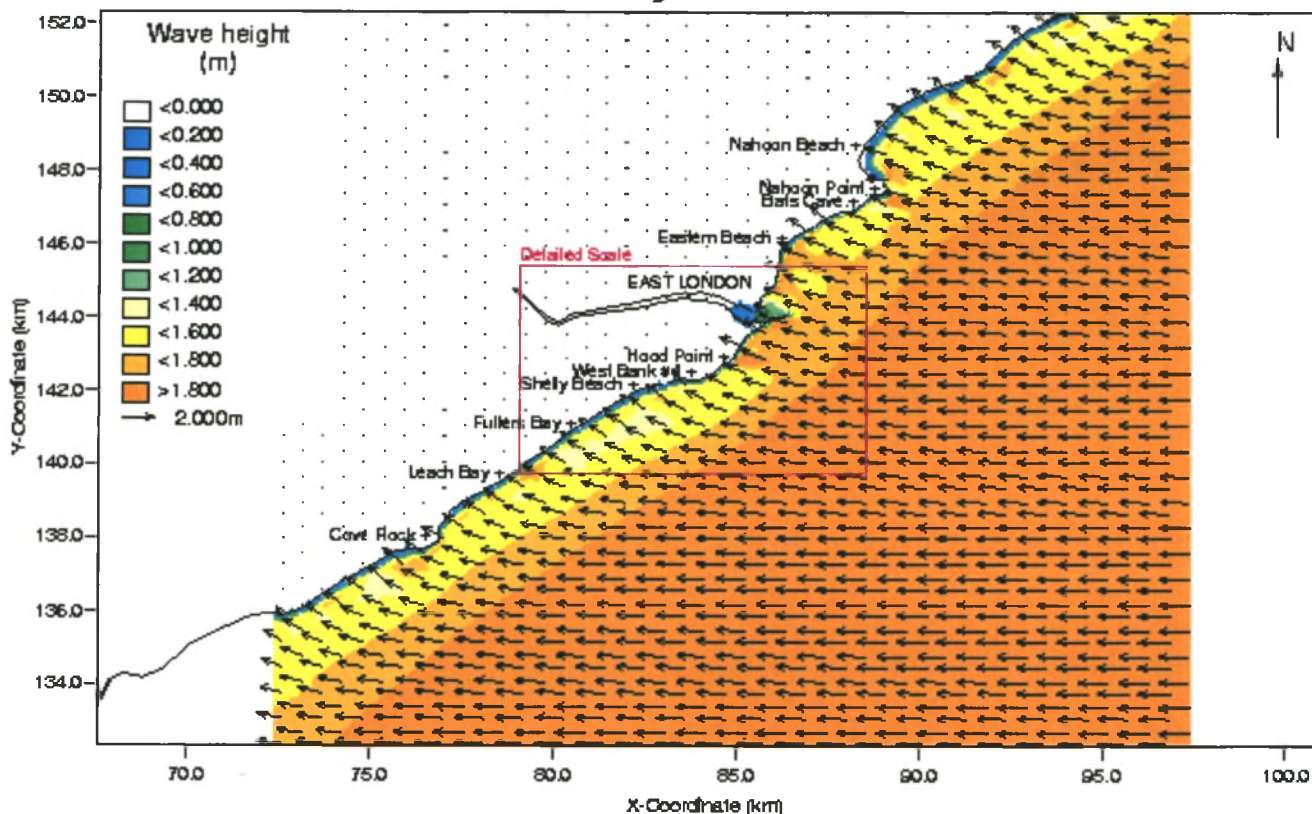
Wave refraction modelling: typical offshore storm condition

($H_{mo} = 4$ m; $T_p = 15$ s; Direction = 214 deg. (SW))

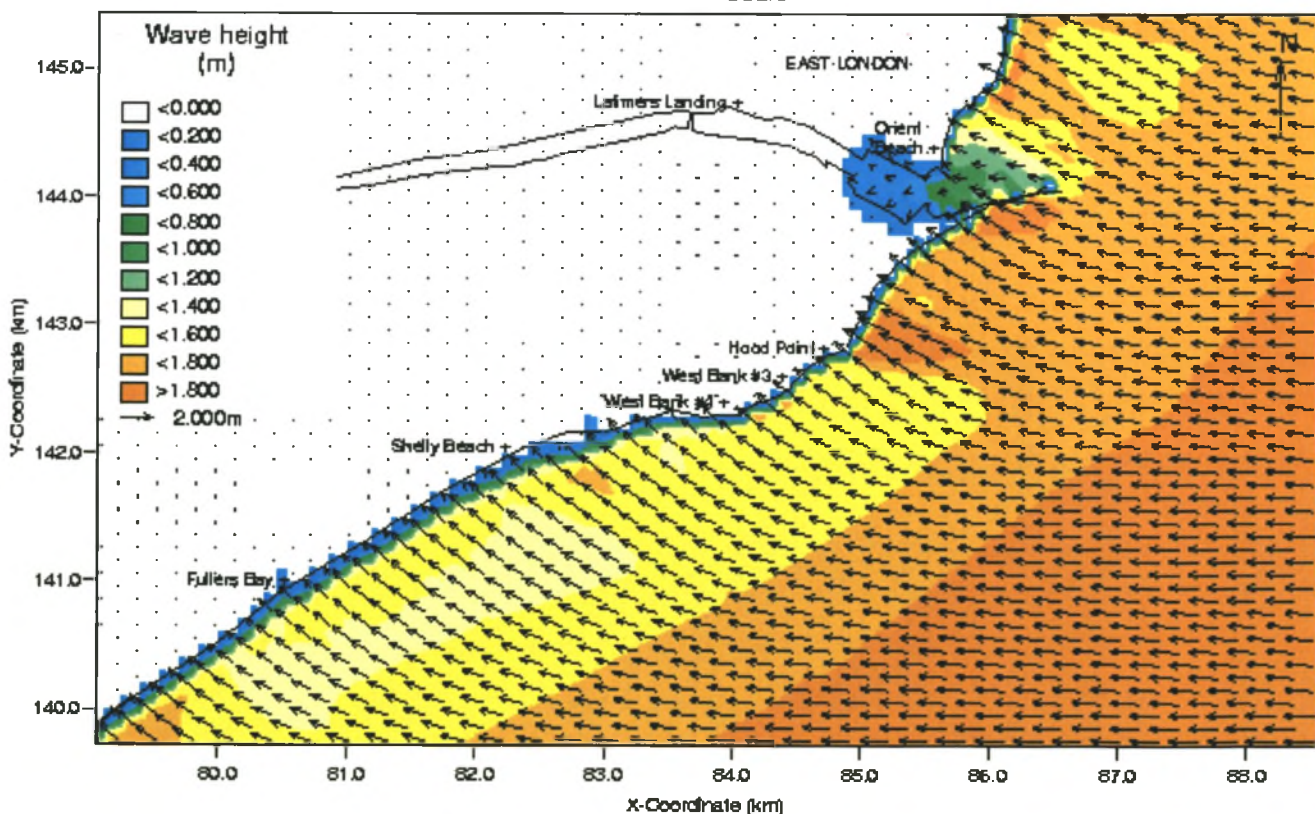
FIGURE

3.12

Regional Scale



Detailed Scale

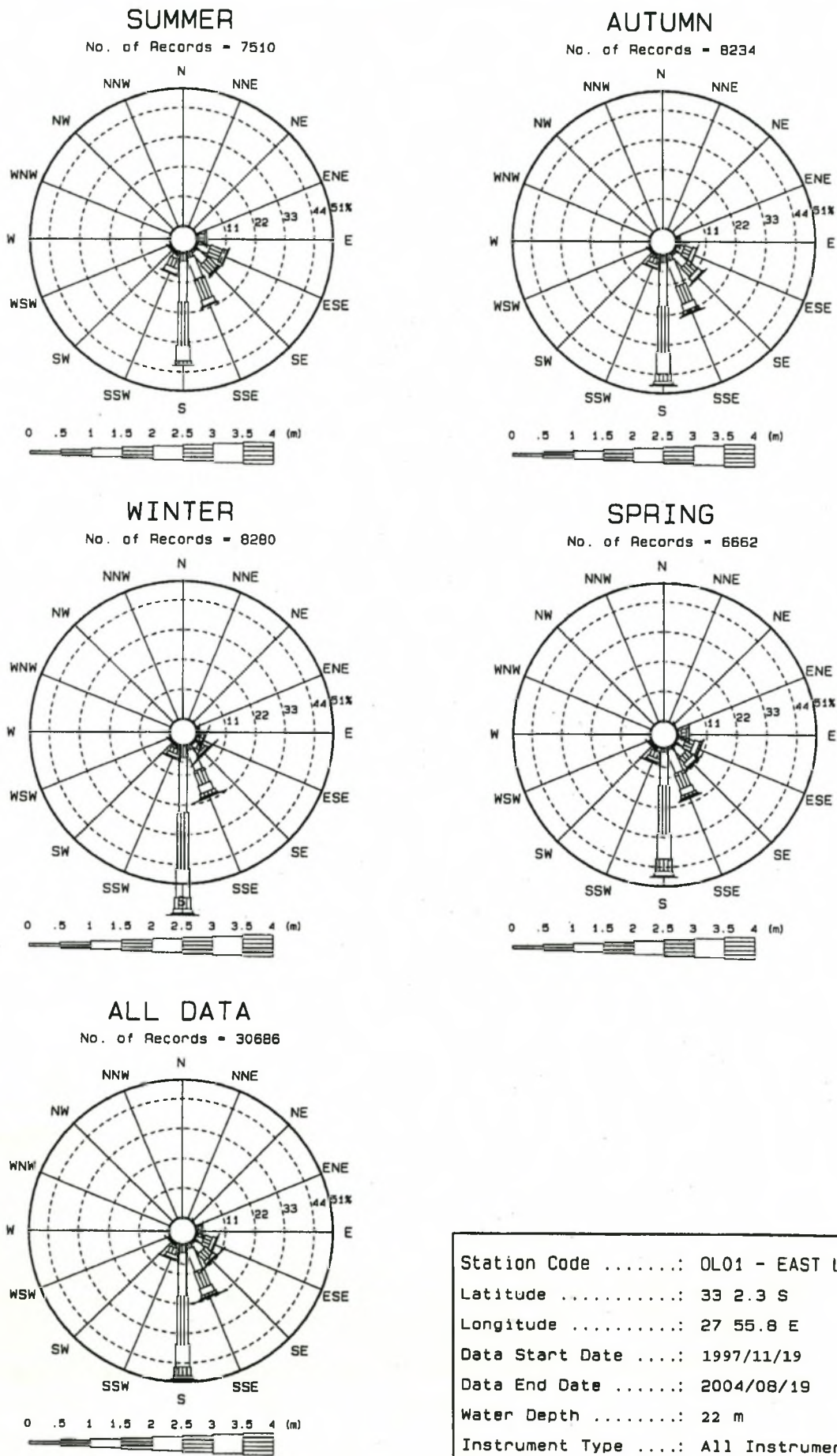


Wave refraction modelling: typical easterly wind wave condition

($H_{mo} = 1,7$ m; $T_p = 10$ s; Direction = 88 deg. (E))

FIGURE

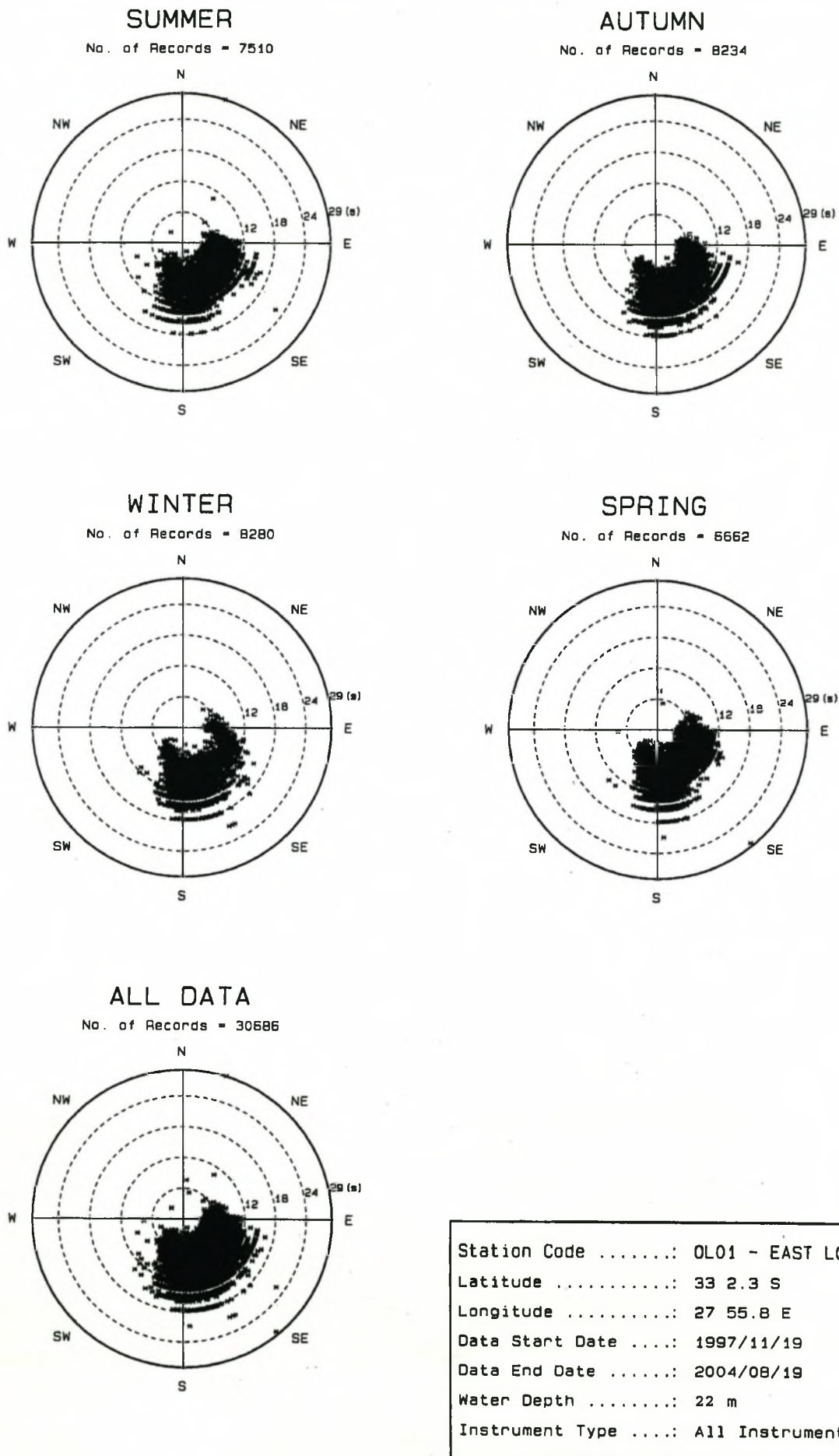
3.13



Station Code: OL01 - EAST LONDON
 Latitude: 33 2.3 S
 Longitude: 27 55.8 E
 Data Start Date: 1997/11/19
 Data End Date: 2004/08/19
 Water Depth: 22 m
 Instrument Type: All Instruments

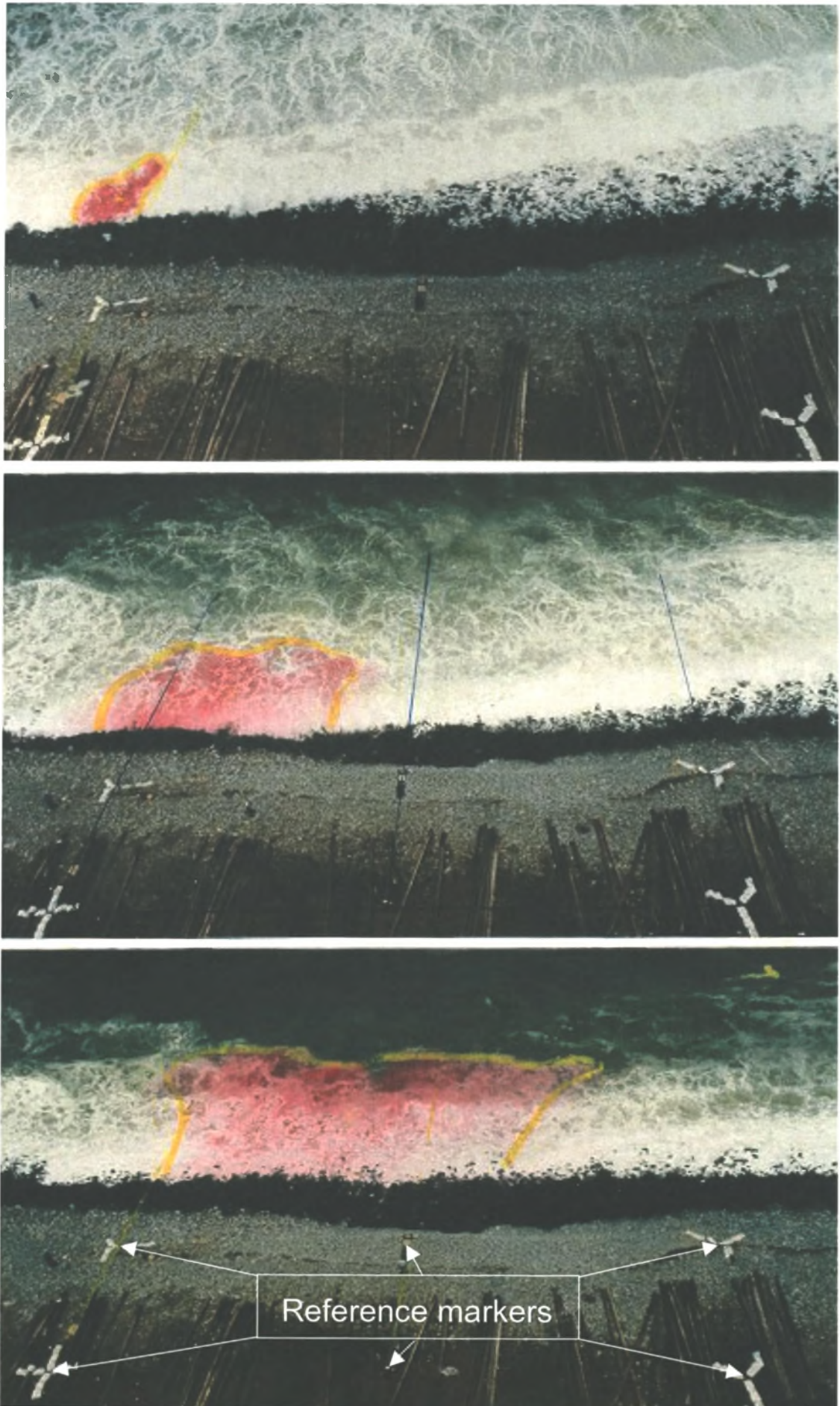
EAST LONDON
WAVE HEIGHT OCCURRENCE PER DIRECTION

FIGURE
3.14



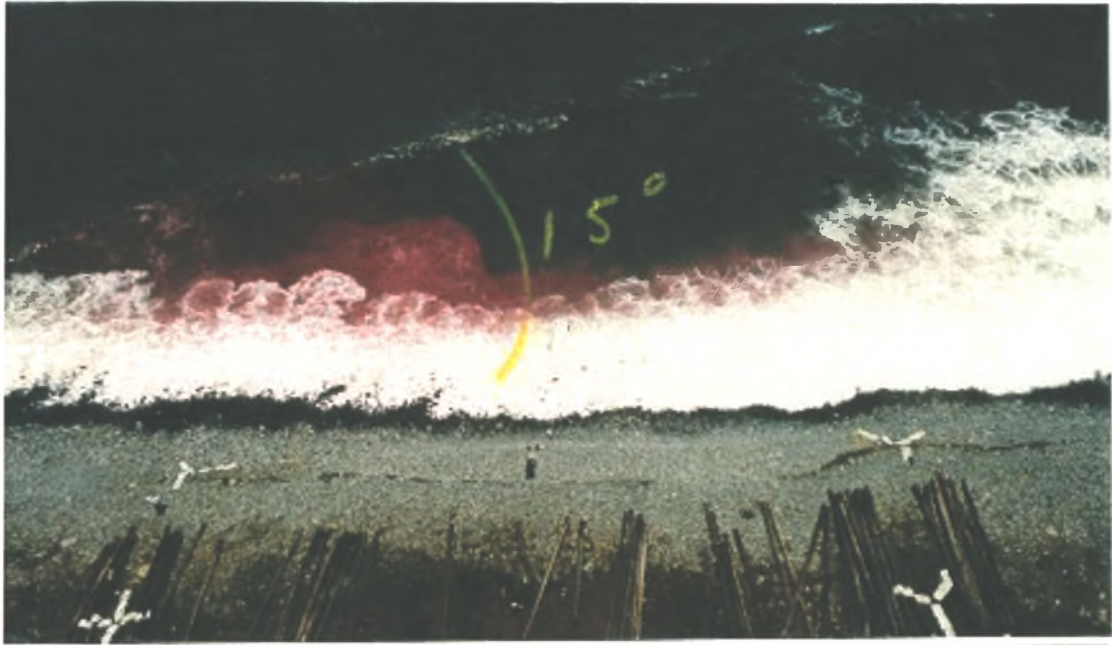
EAST LONDON
WAVE PERIOD (T_p) VERSUS DIRECTION

FIGURE
3.15



**EXAMPLE OF SURF ZONE DYE TRACKING MEASUREMENTS
ALONG THE FORESHORE AREA (1996-11-08)**

**FIGURE
3.16**



a:



b:

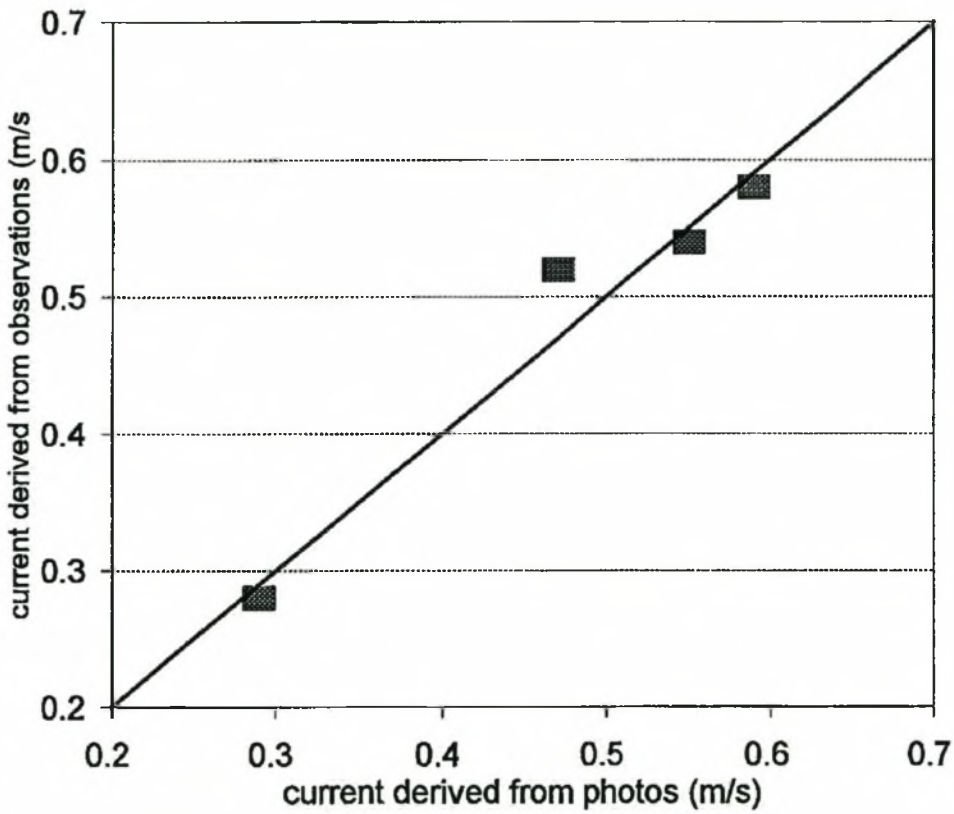


c:

a: WAVE ANGLE AT 13H00 1996-11-08
b: BOAT TRACKING DROGUES 1996-11-08
c: "CALM" CONDITIONS ON 1996-11-06

FIGURE

3.17



—
1:1 correspondence

**COMPARISON OF CURRENT VELOCITIES: OBSERVATIONS
VERSUS PHOTOGRAPH METHOD**

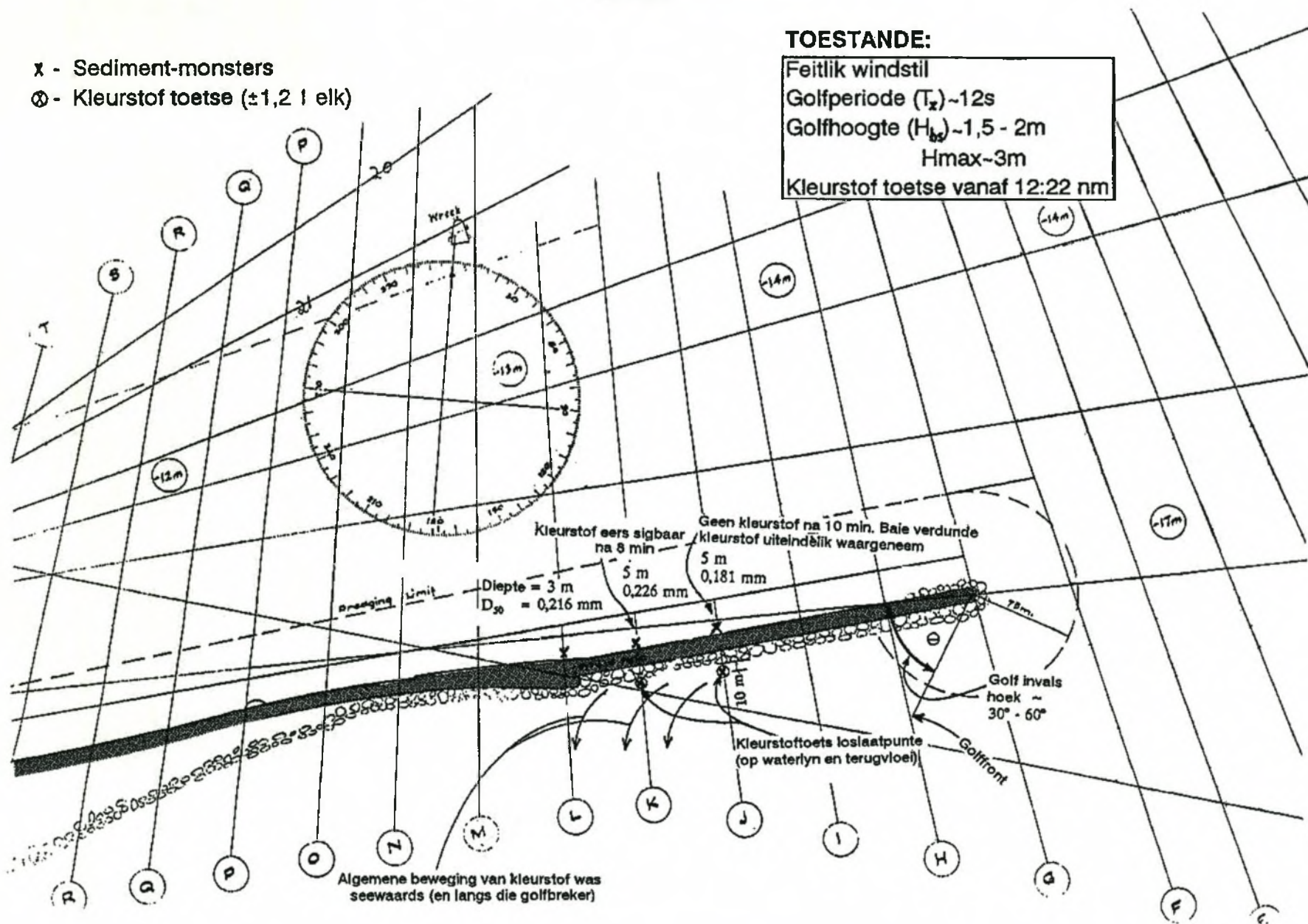
**FIGURE
3.18**

OOS-LONDEN TERREINBESOEK
15/6/93

- x - Sediment-monsters
- ⊗ - Kleurstof toetse (±1,2 l elk)

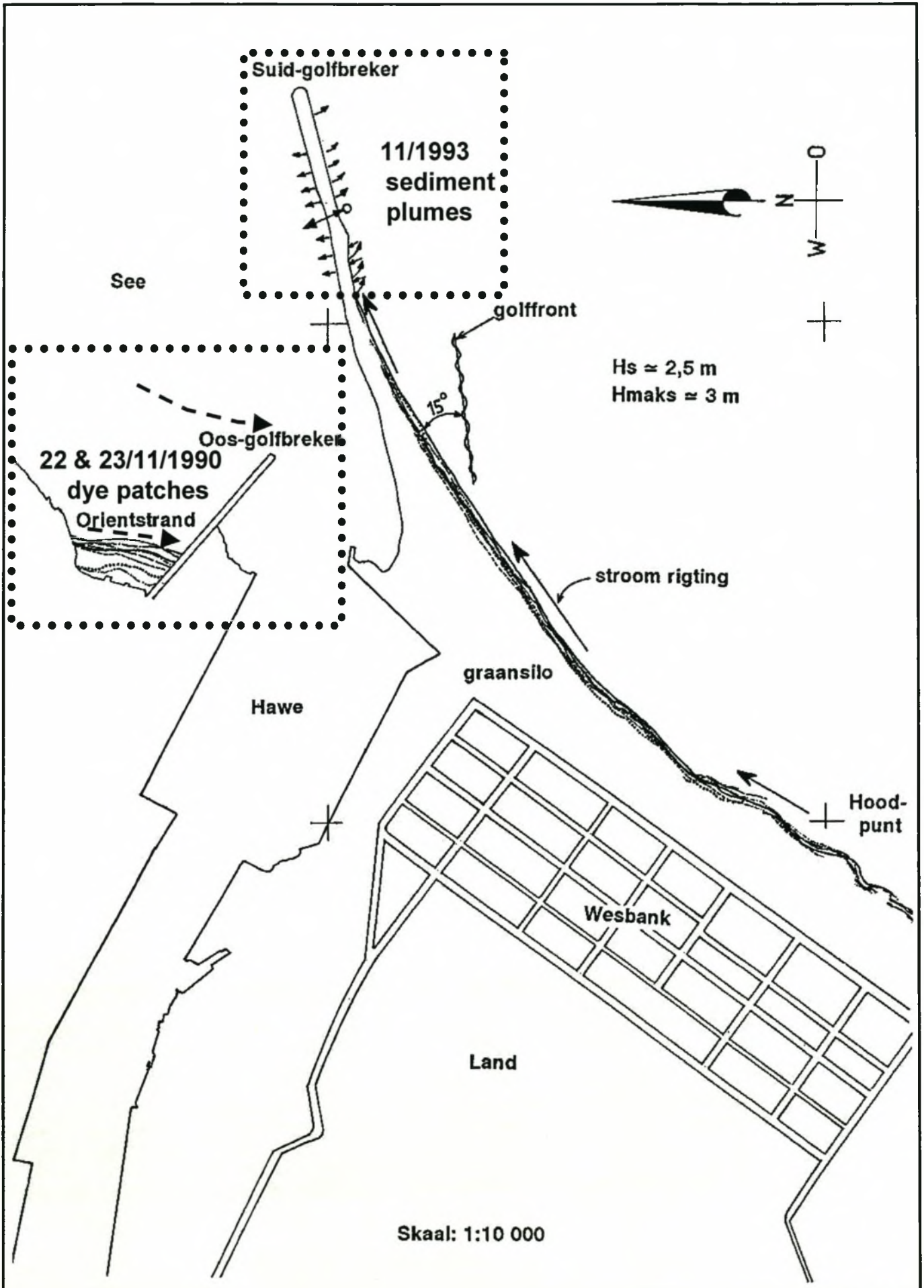
TOESTANDE:

Feitlik windstil
 Golfperiode (T_x) ~12s
 Golfhoogte (H_{bx}) ~1,5 - 2m
 Hmax ~3m
 Kleurstof toetse vanaf 12:22 nm



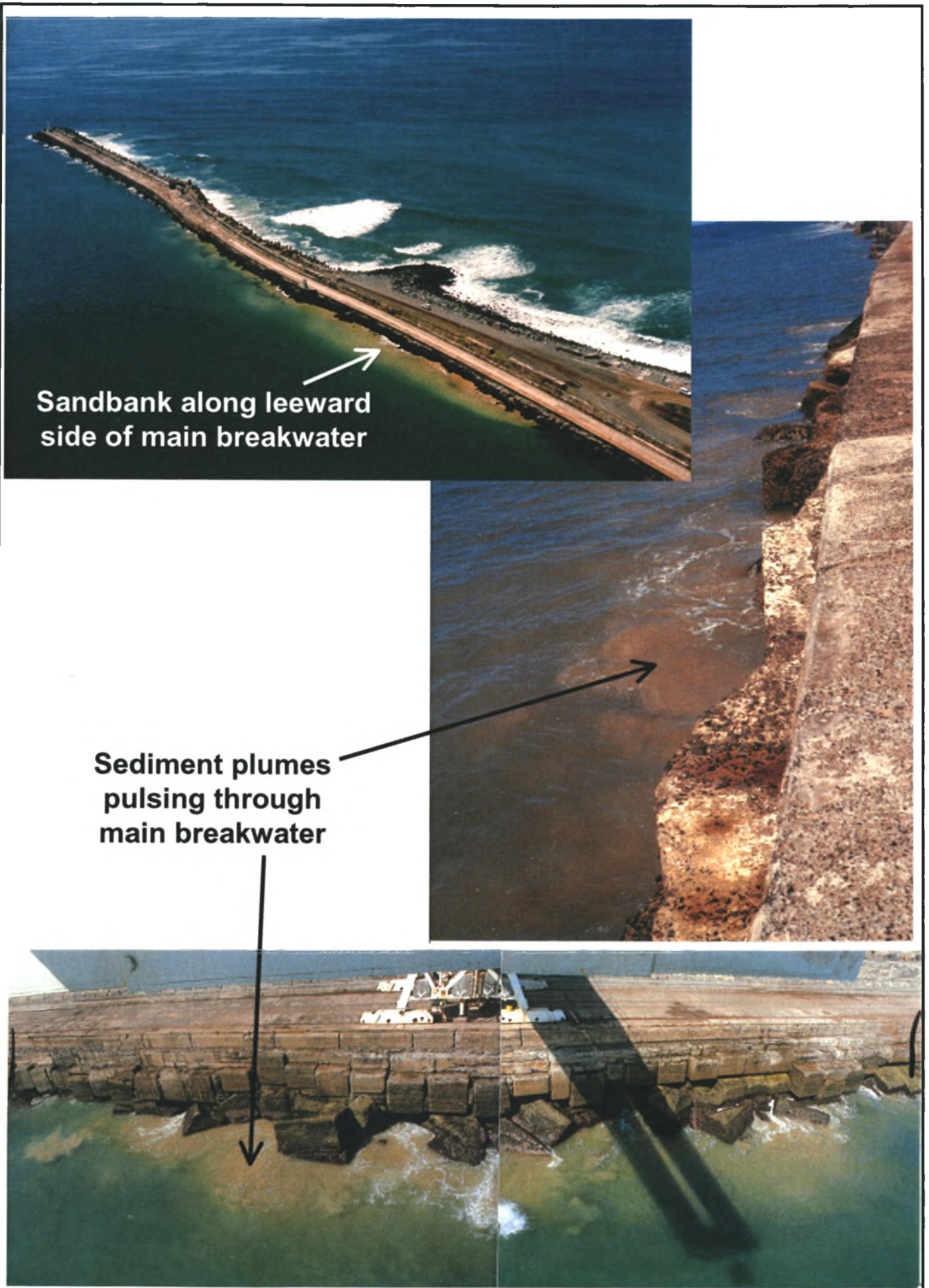
CURRENT OBSERVATIONS: JUNE 1993
(dye patch observations)

FIGURE
3.19



**SURF ZONE SEDIMENT PLUME (1993)
AND DYE (1990) CURRENT PATTERNS**

**FIGURE
3.20**



FIGURE

3.21



SATELLITE IMAGE OF AGULHAS CURRENT

(Image Dr M L Grundlingh)

FIGURE

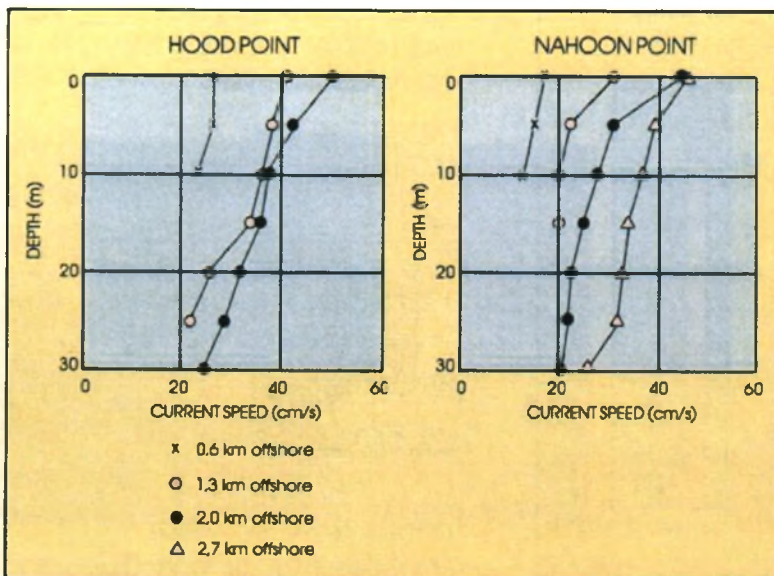
3.22



Measuring Stations

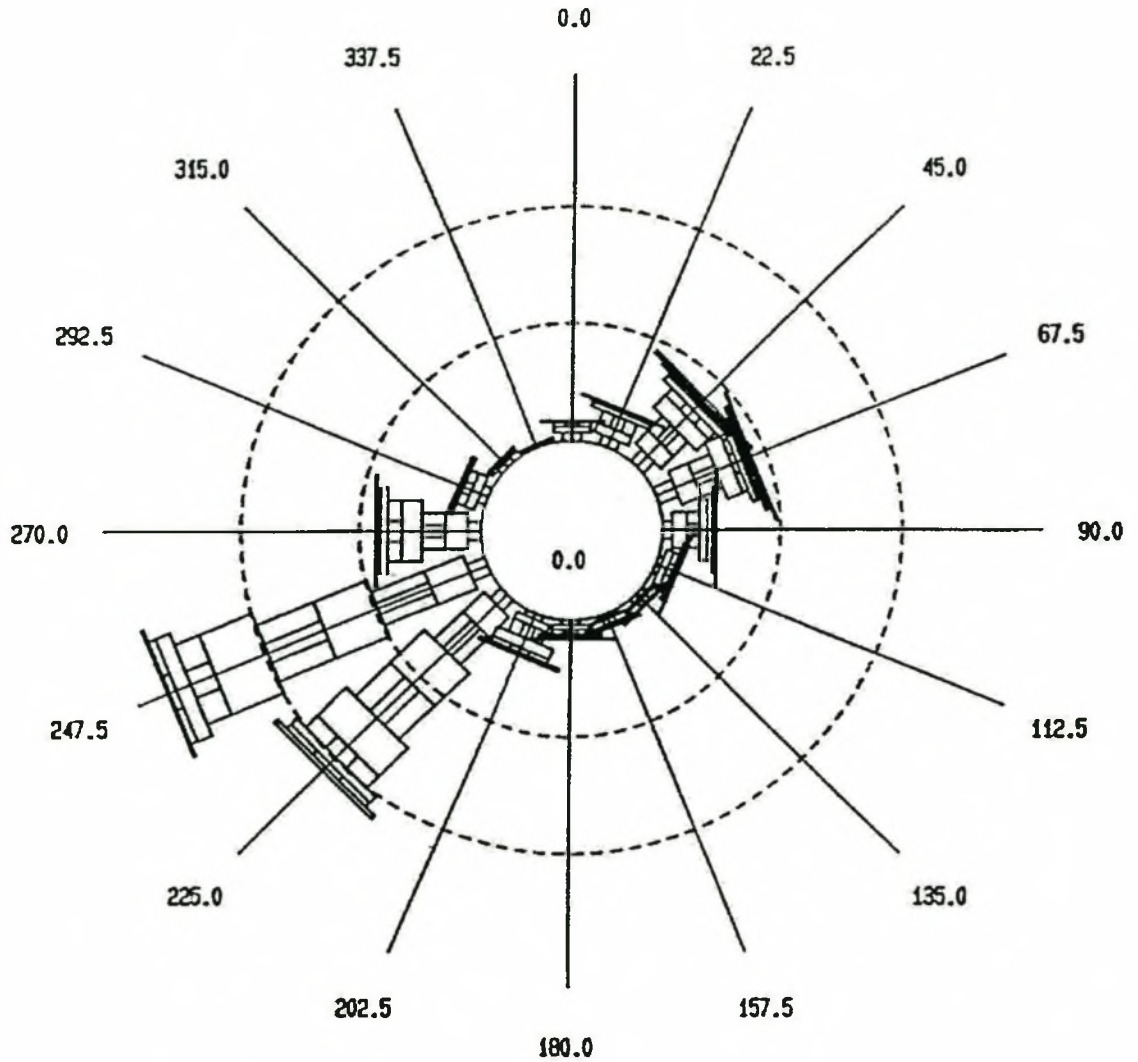
CURRENT PATTERN	Average Velocity cm/sec.	Percentage Occurrence
	46	64
	31	24
	12	8
	11	4

Current Patterns

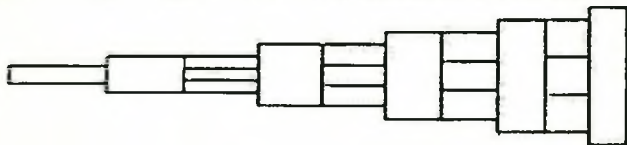


Current Profiles

Annual current rose



cm/s 0.0 5.0 10.0 15.0 20.0 25.0 30.0 35.0 40.0 45.0 50.0



0 10 20 30 40

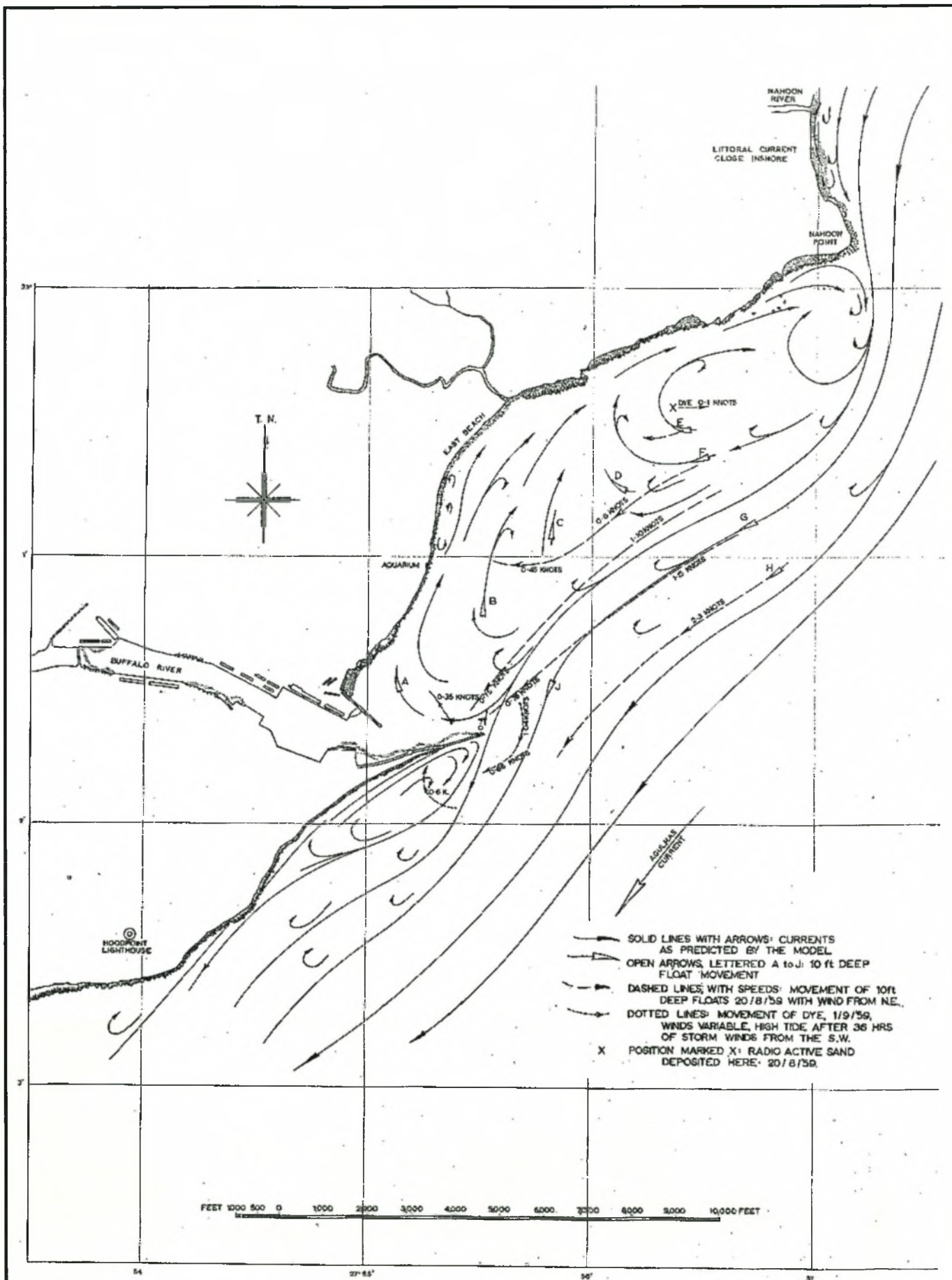
% Occurrence

Notes:

- 1 The rose indicates the direction towards which the current is flowing.
- 2 Based on all current data from Aanderaa ELM1 (location - Figure 3.23, at 30 m water depth, from February 1994 to June 1995).
- 3 These are all nearshore currents seaward of the surf zone.

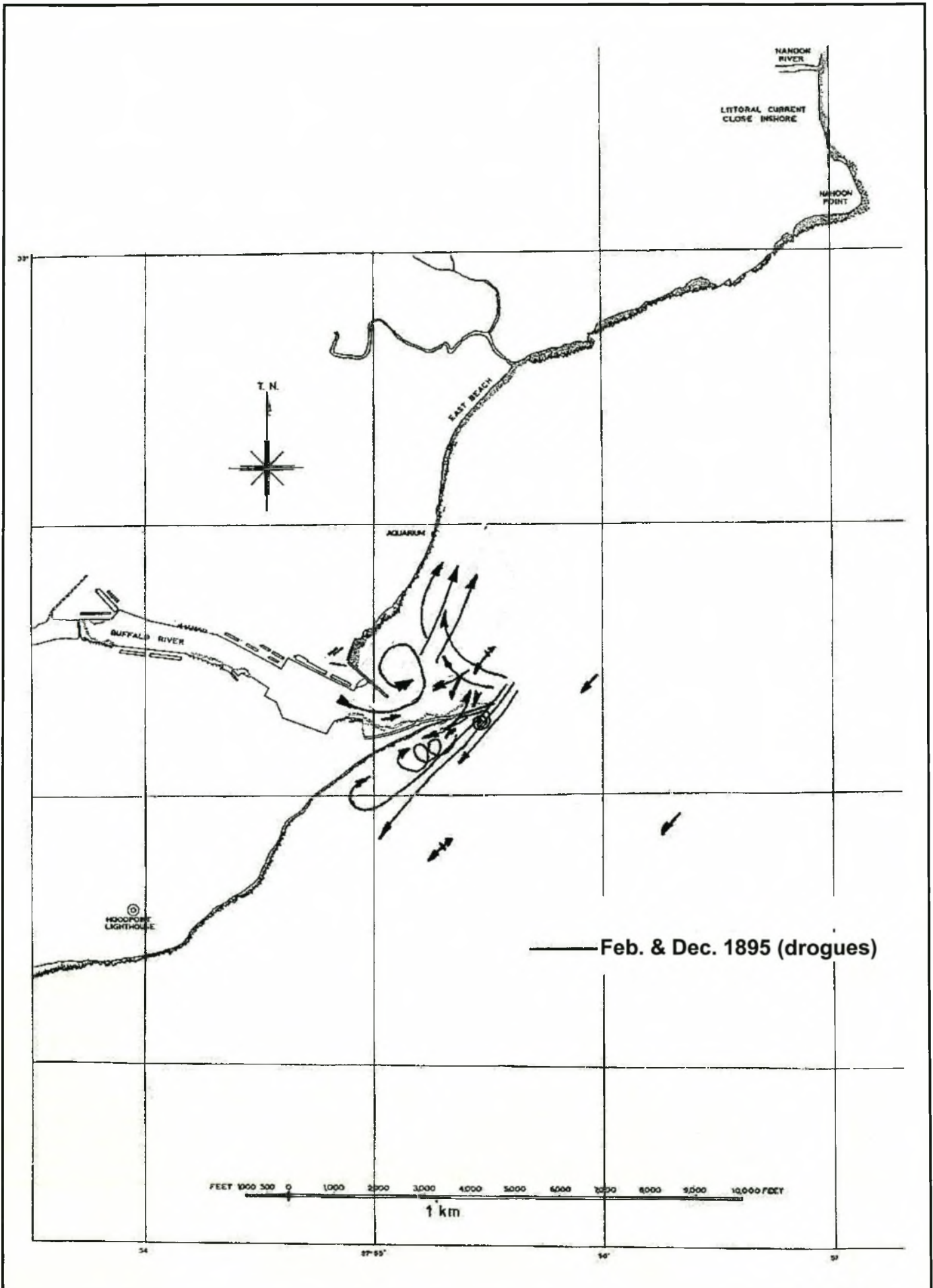
ANNUAL CURRENT ROSE: HOOD POINT TO NAHOON POINT
(CSIR, 1988)

FIGURE
3.24



CURRENT MEASUREMENTS AND PHYSICAL MODEL SIMULATIONS (Whillier, 1962)

FIGURE 3.25

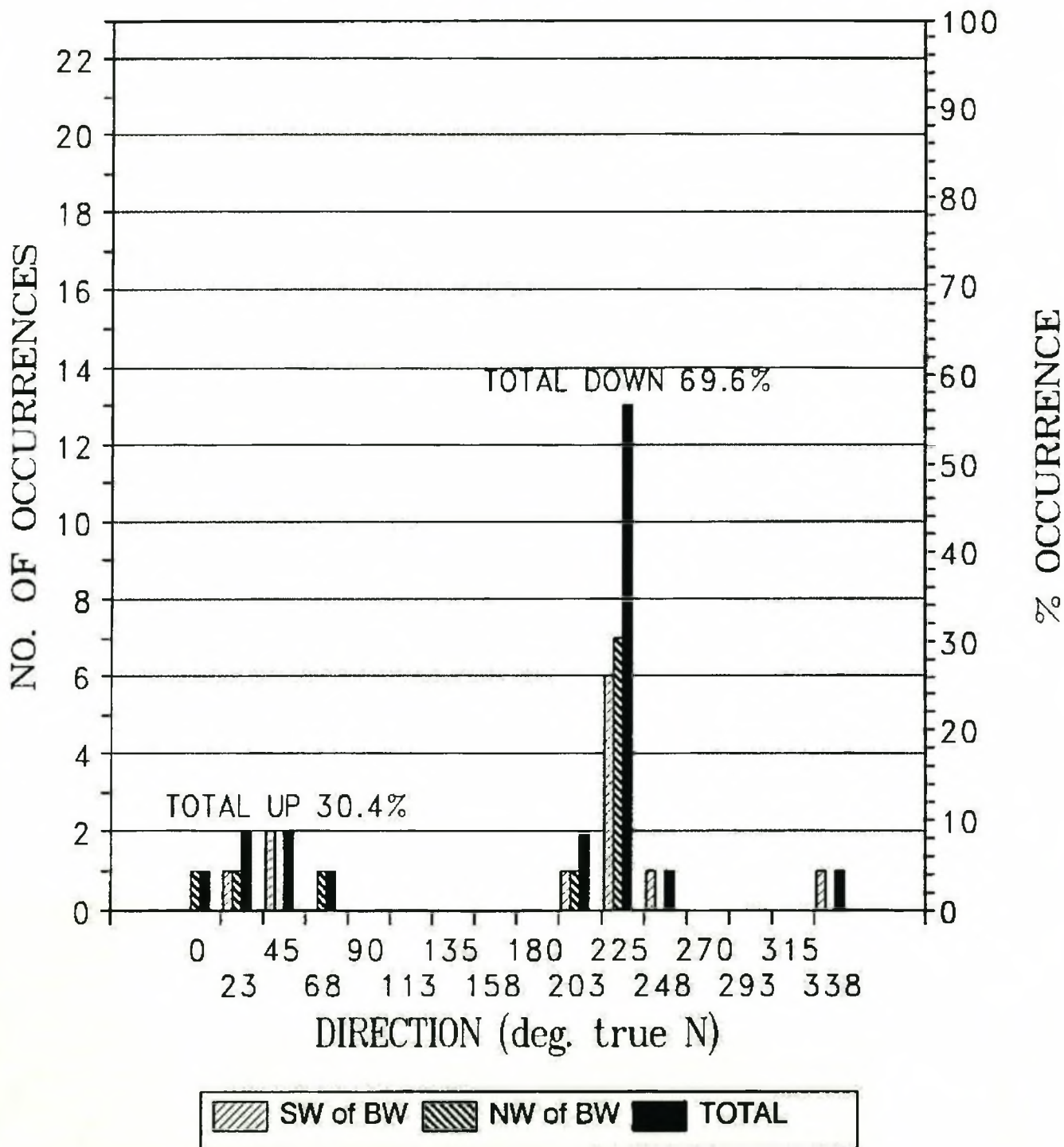


EAST LONDON CURRENT PATTERNS: 1895

FIGURE

3.26

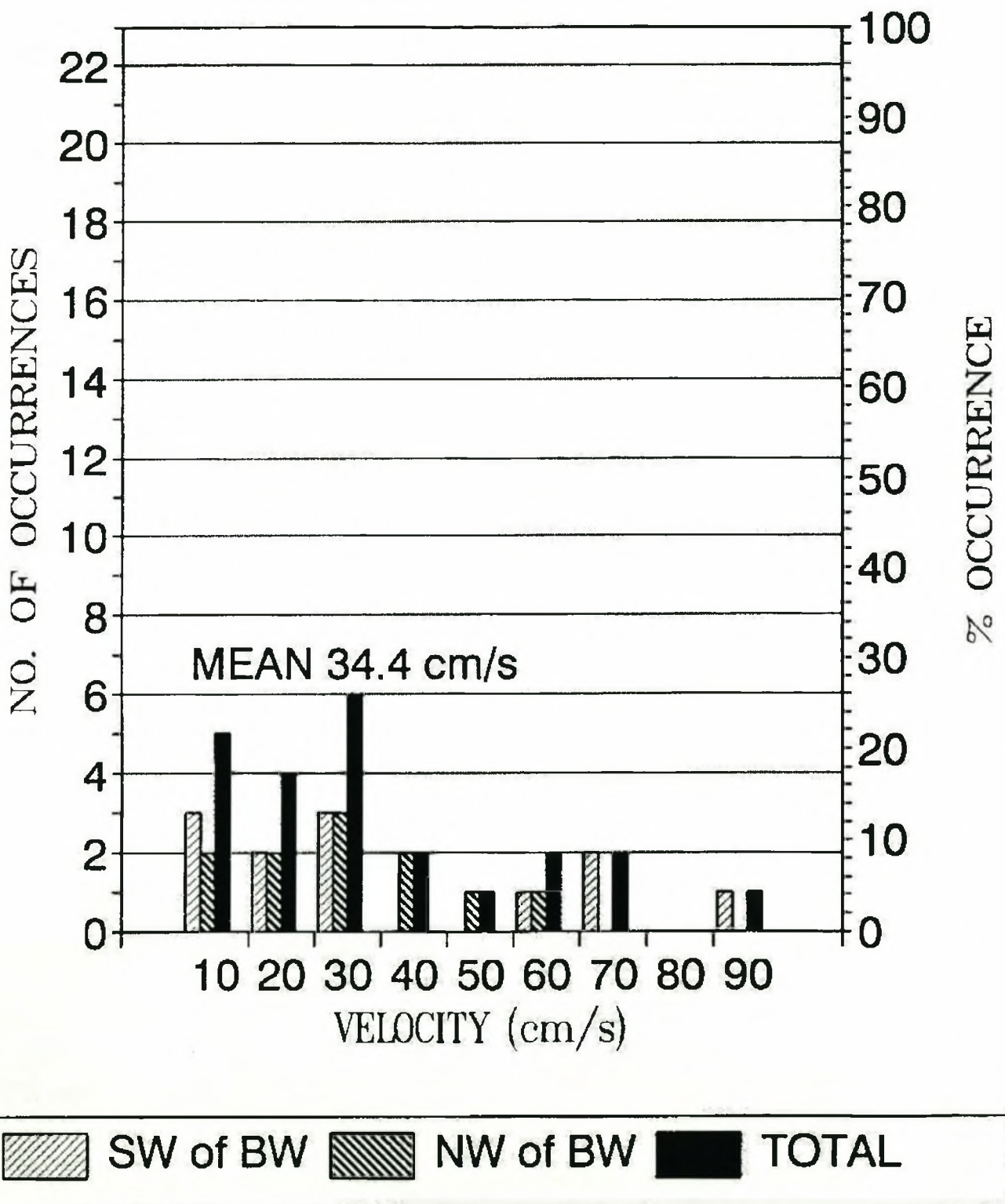
SUB-SURFACE DROGUE MEASUREMENTS DIRECTION OCCURRENCE HISTOGRAM



SUB-SURFACE DROGUE MEASUREMENTS: DIRECTION OCCURRENCE HISTOGRAM

FIGURE 3.27

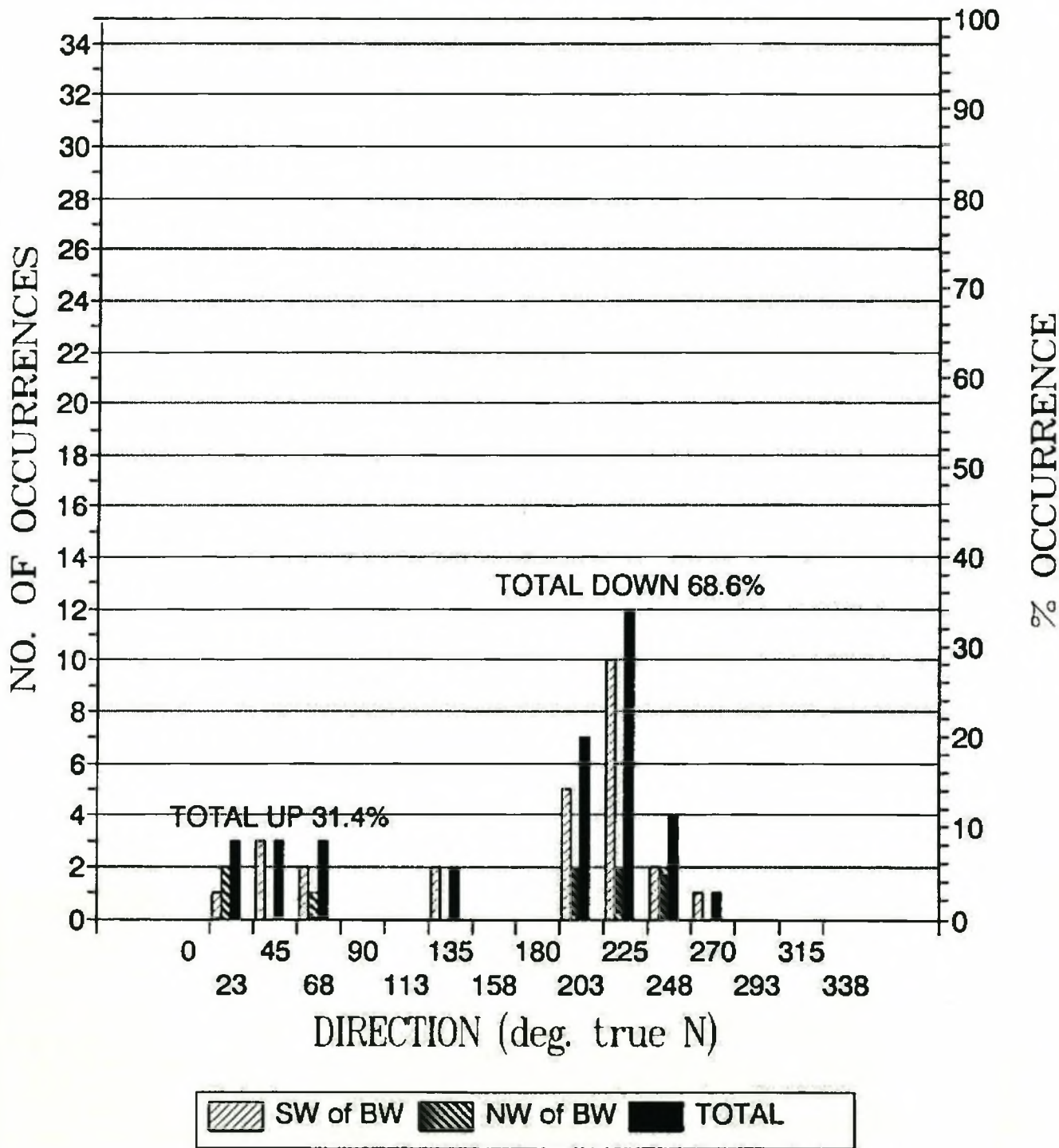
SUB-SURFACE DROGUE MEASUREMENTS VELOCITY OCCURRENCE HISTOGRAM



**SUB-SURFACE DROGUE MEASUREMENTS: VELOCITY
OCCURRENCE HISTOGRAM**

**FIGURE
3.28**

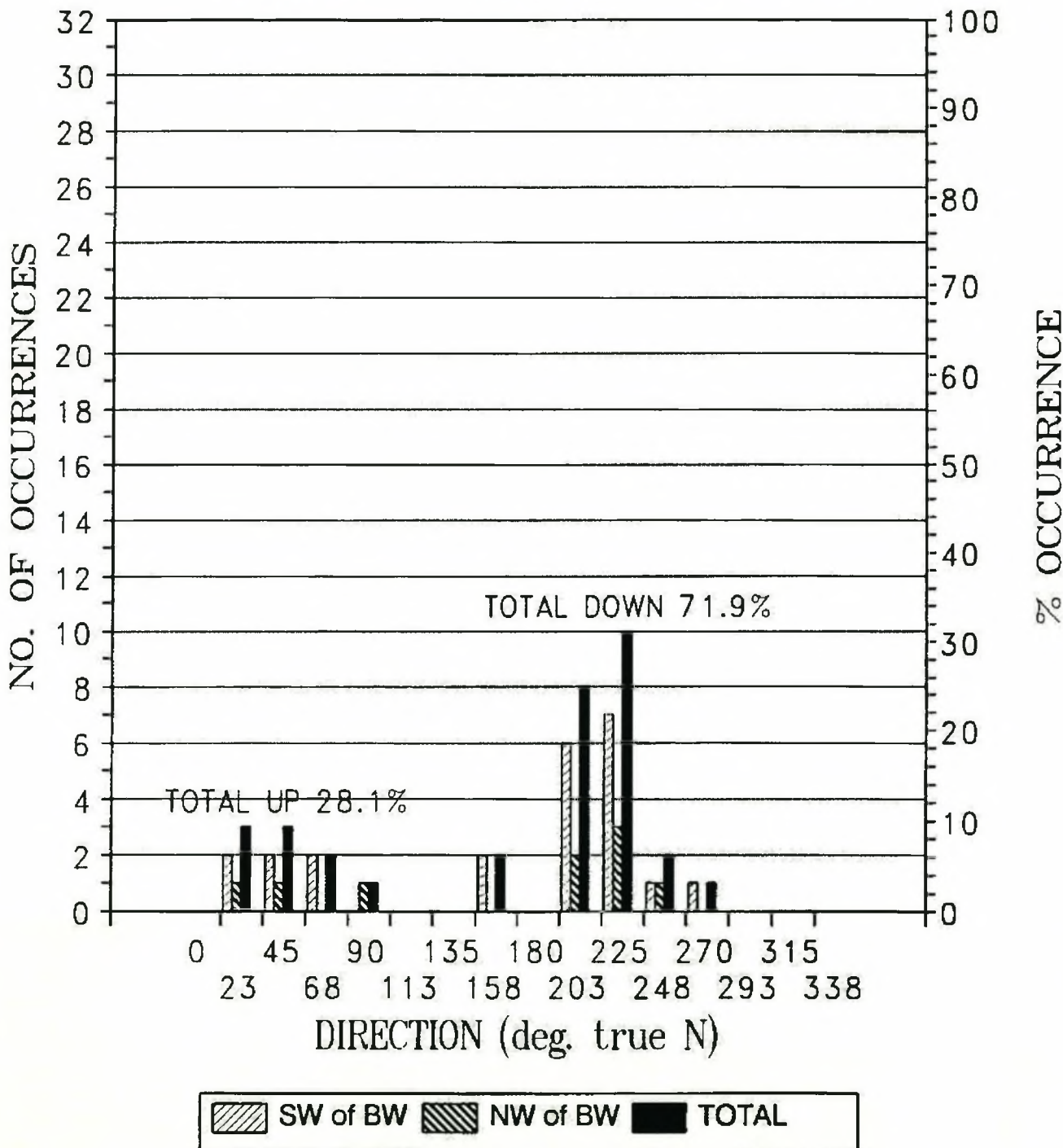
CURRENT VECTOR MEASUREMENTS: 5 m depth DIRECTION OCCURRENCE HISTOGRAM



ENDECO CURRENT VECTOR MEASUREMENTS: DIRECTION OCCURRENCE HISTOGRAM 5 m DEPTH

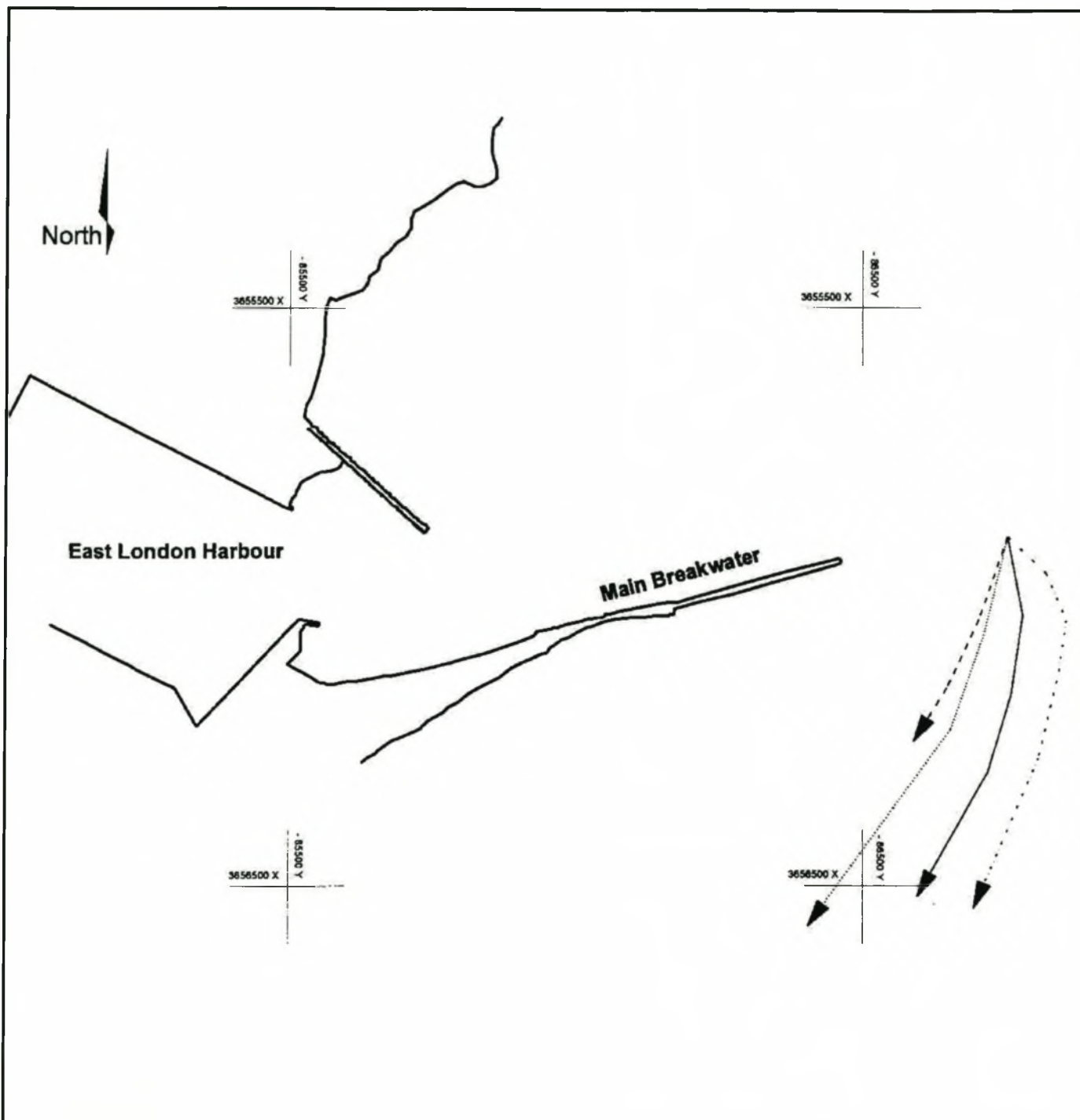
FIGURE 3.29

CURRENT VECTOR MEASUREMENTS: 20m depth DIRECTION OCCURRENCE HISTOGRAM



ENDECO CURRENT VECTOR MEASUREMENTS: DIRECTION OCCURRENCE HISTOGRAM 20 m DEPTH

FIGURE 3.30

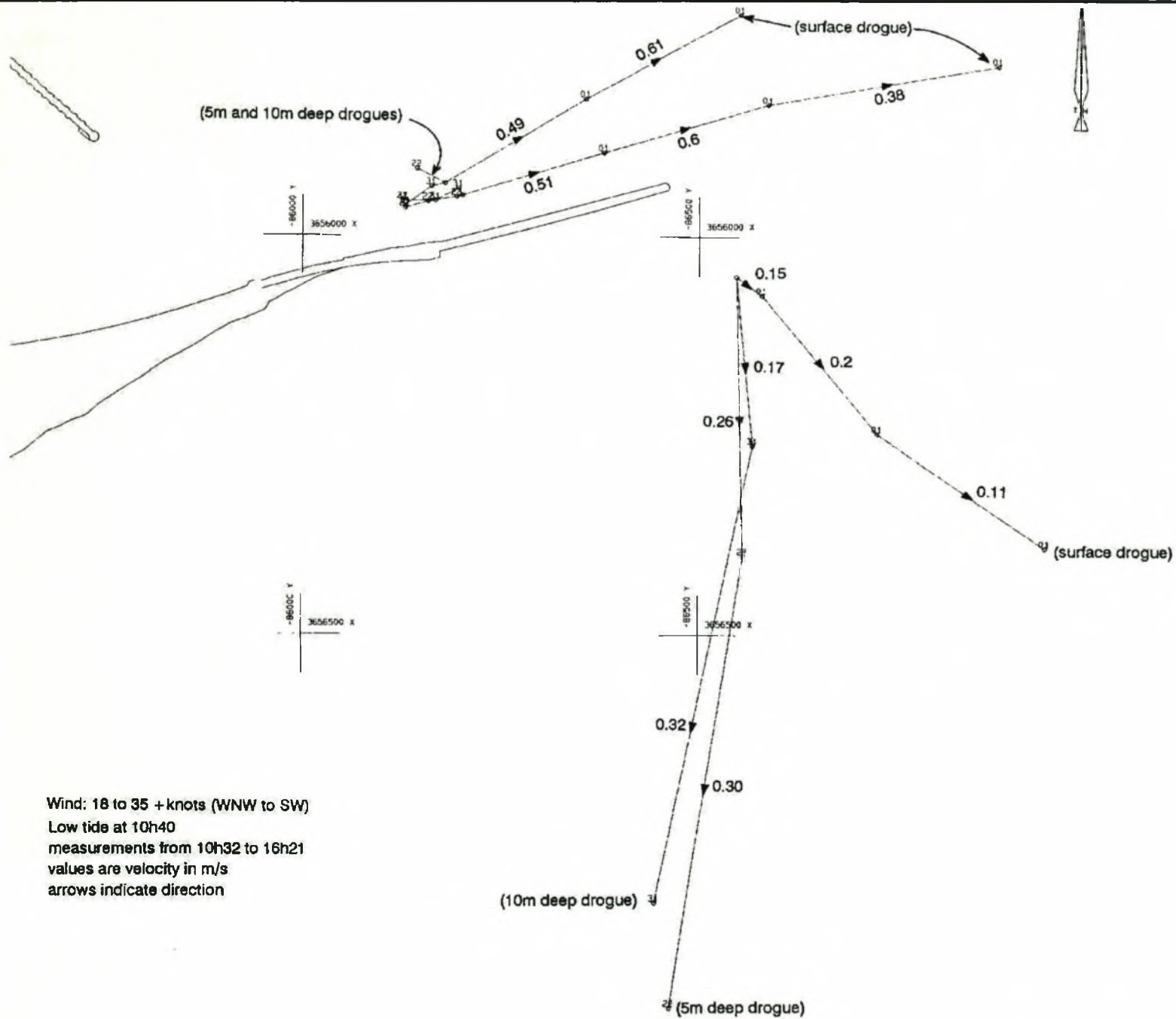


Drogue	Depth	In	Out	Average speed (m/s)	Wind	Swell
.....	surface	16:08	16:40	0,41	18-20 knots SW	2 m
————	-5 m	16:08	16:36	0,41		
.....	-10 m	16:08	16:38	0,44		
-----	-15 m	16:08	16:40			

**DROQUE TRACKING ON 19 MARCH 1996 FROM
16:08 TO 16:40**

**FIGURE
3.31**

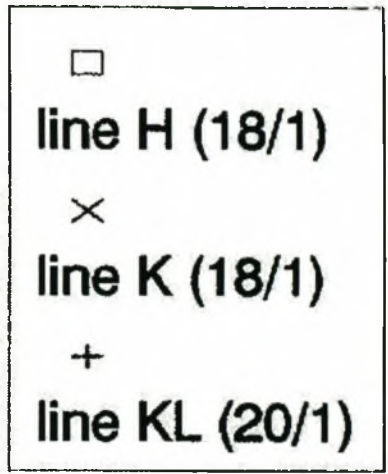
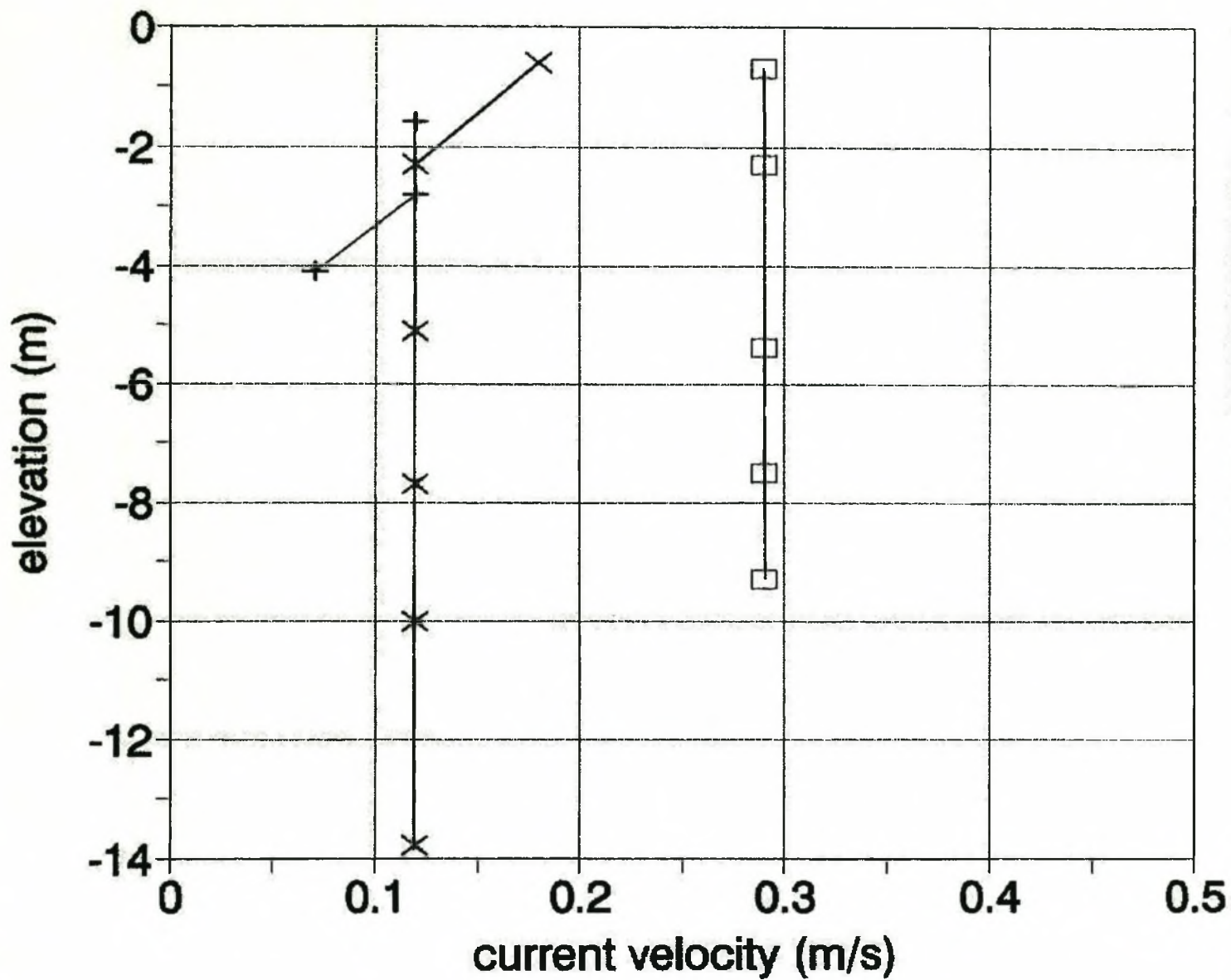
DROUKE TRACKING ON 18 JANUARY 1995



FIGURE

3.32

MEASURED CURRENT PROFILES: 18 & 20/01/1995;
 ENDECO CURRENT METER



Note:
 Locations of lines are indicated on Figure 3.19.

FIGURE
 3.33

CURRENT MEASUREMENTS ON 19 & 20/01/1995: DRIFTER
BOYS AND DYE TRACKING

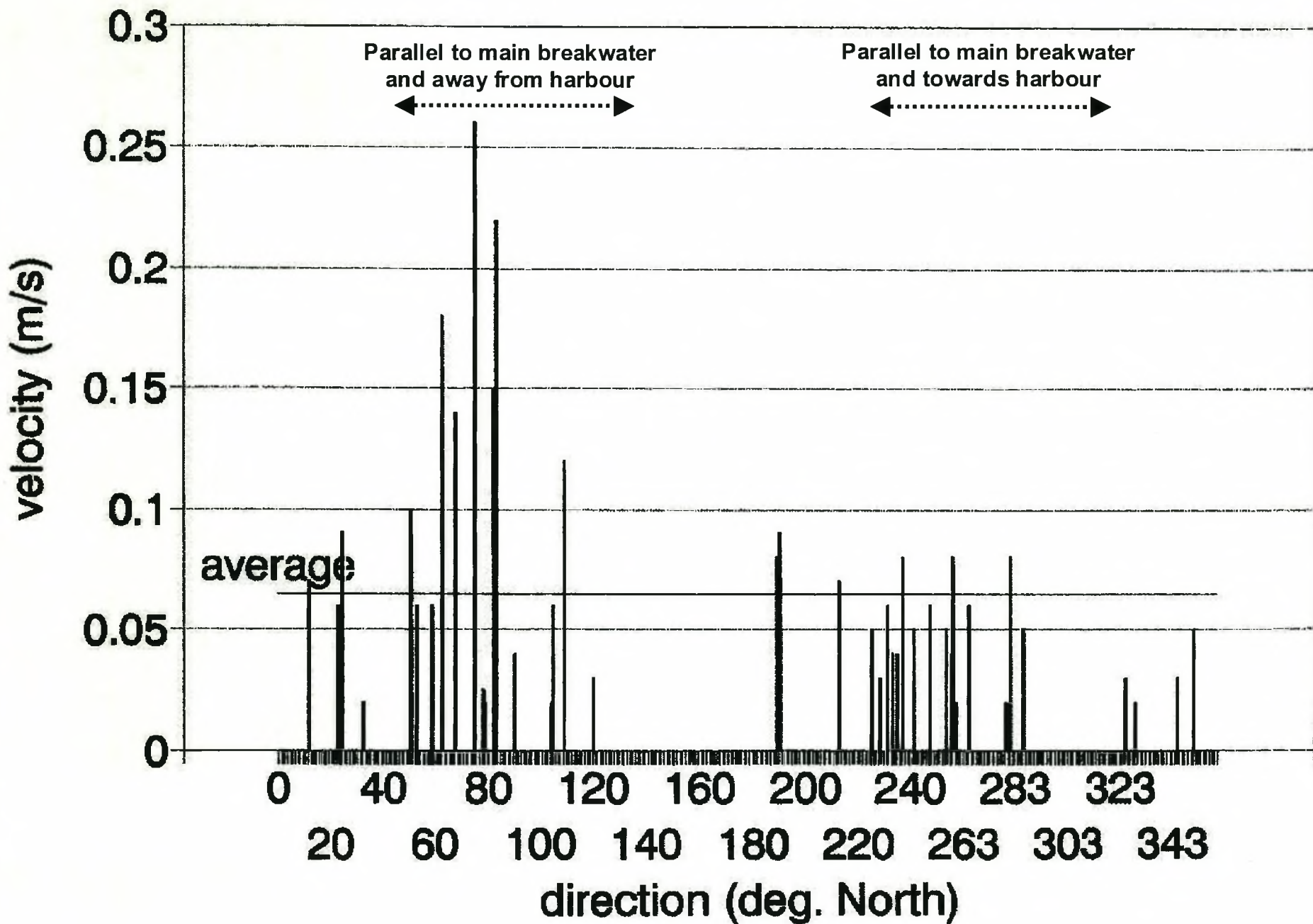
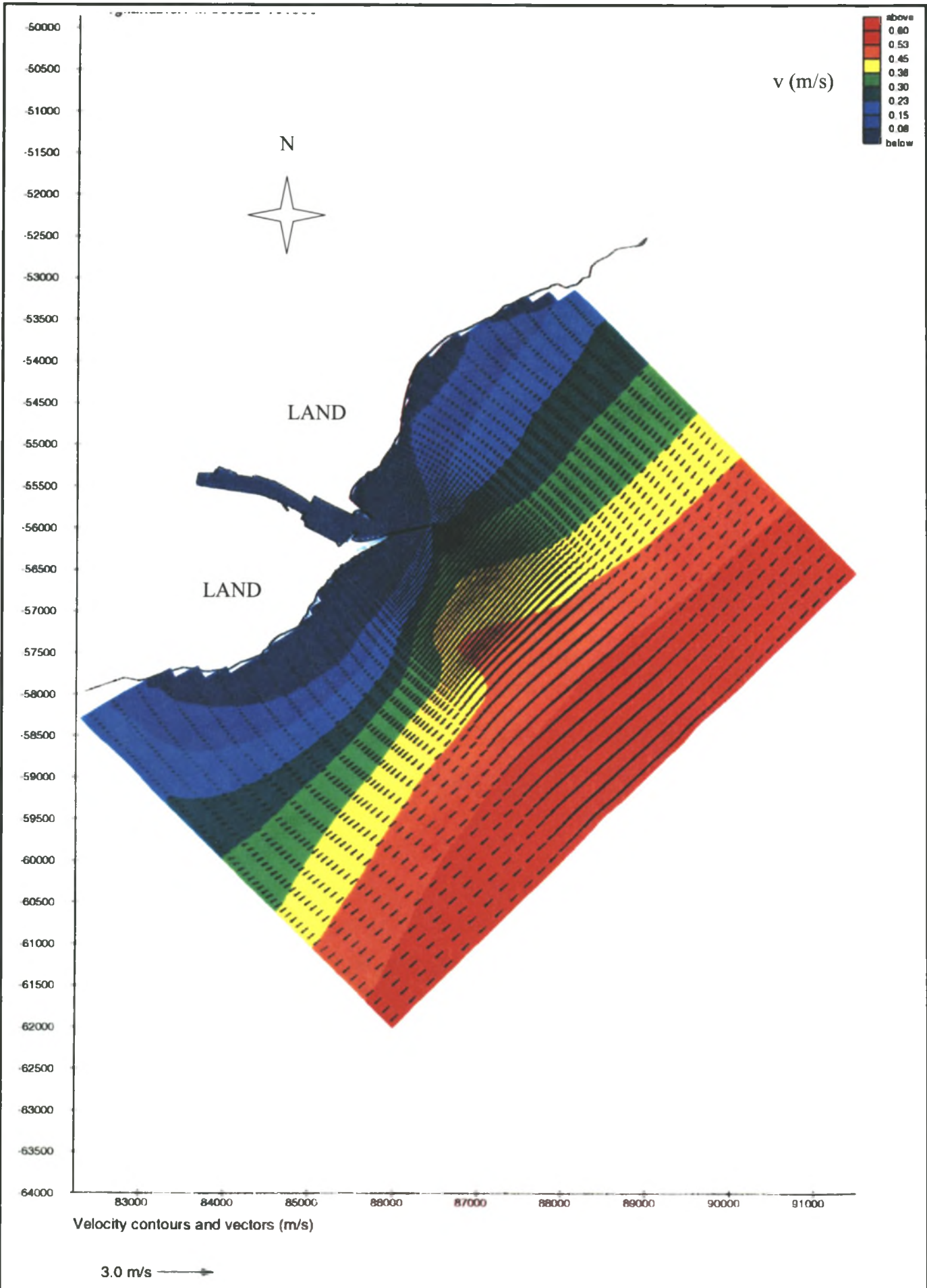
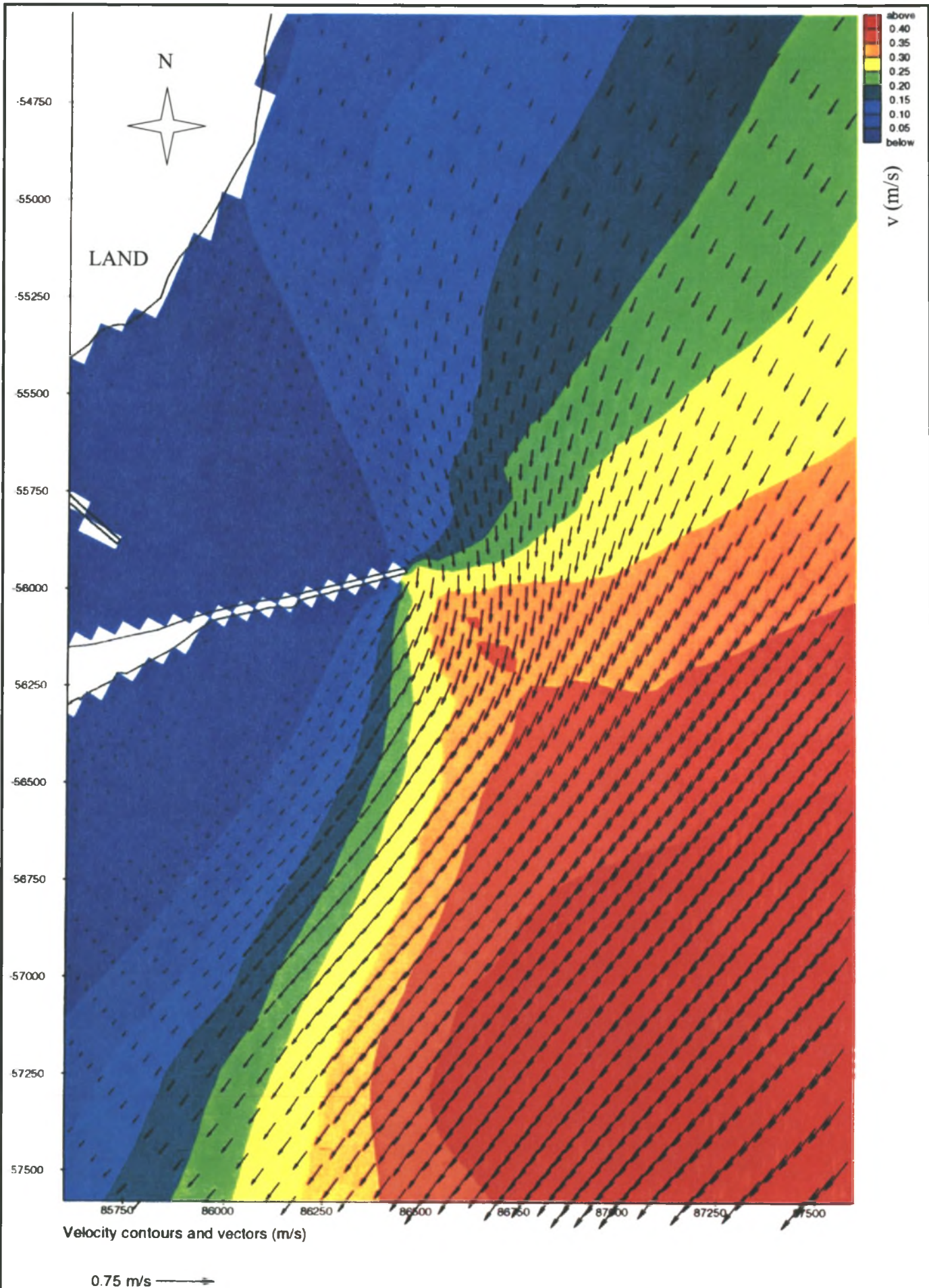


FIGURE
3.34



**NUMERICAL MODELLING OF CURRENTS:
0,3 m/s SW CURRENT – TOTAL GRID AREA**

**FIGURE
3.35**

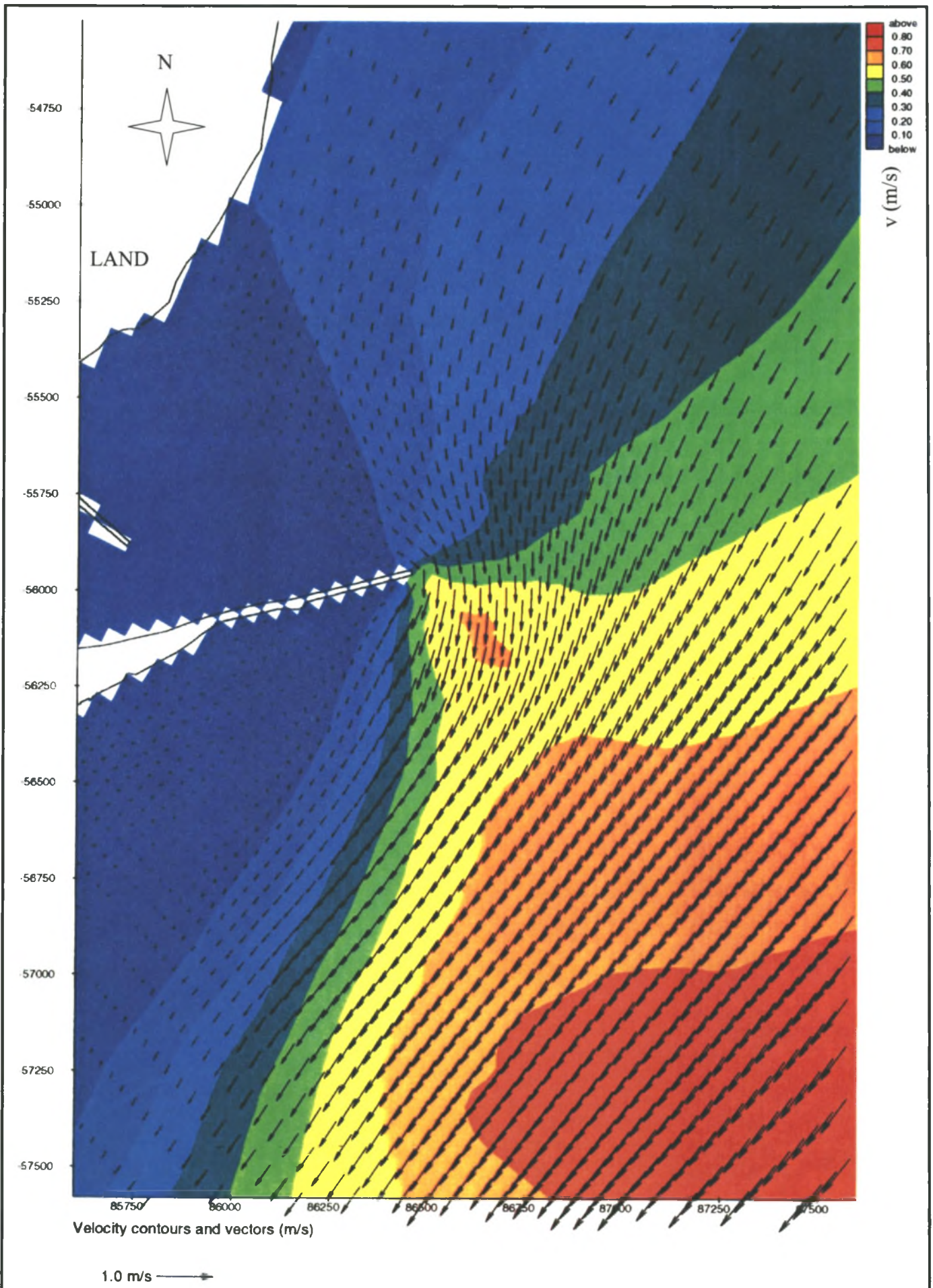


Velocity contours and vectors (m/s)

0.75 m/s →

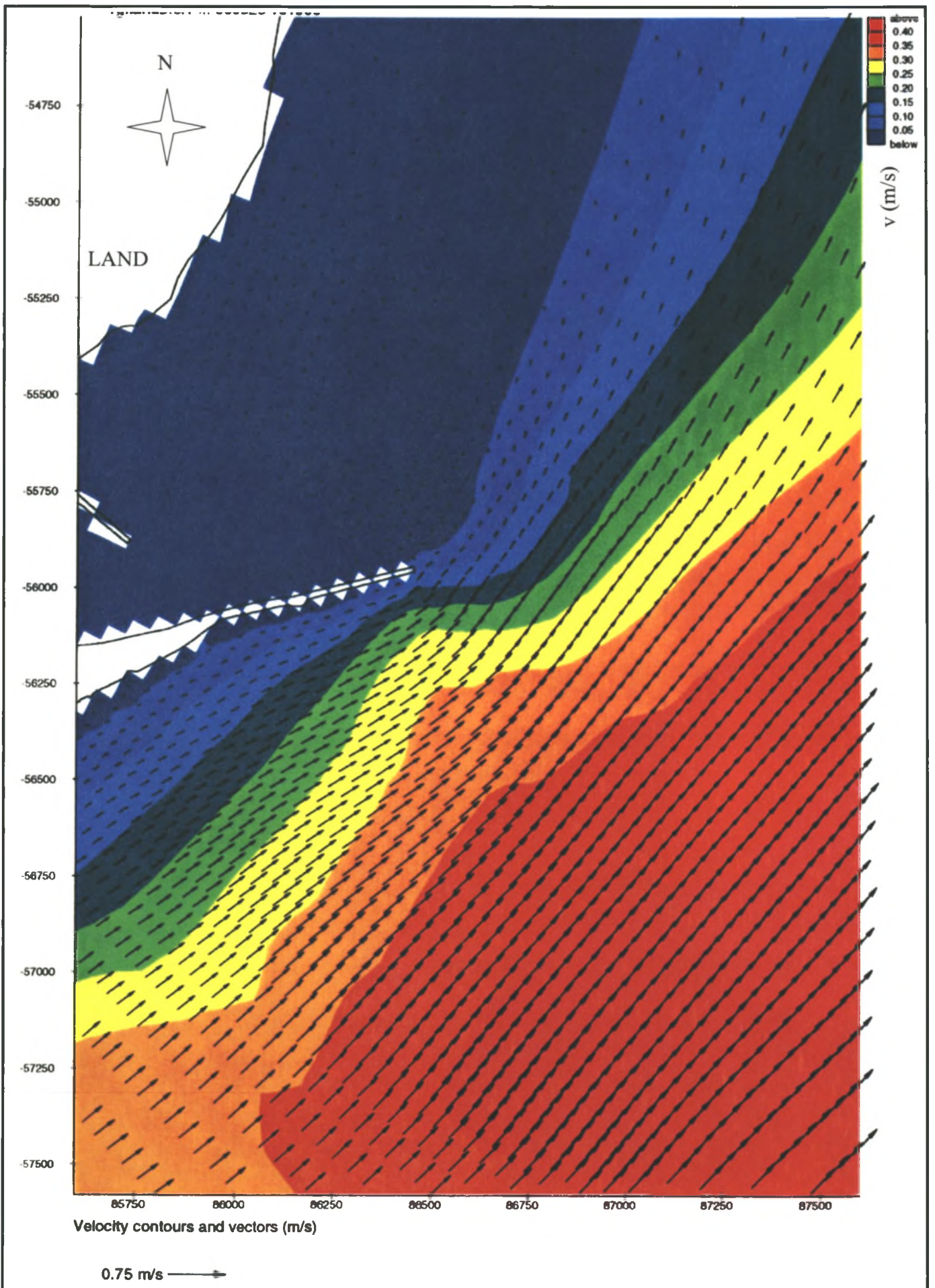
**NUMERICAL MODELLING OF CURRENTS: 0,3 m/s SW
CURRENT – VICINITY OF MAIN BREAKWATER**

**FIGURE
3.36**



**NUMERICAL MODELLING OF CURRENTS:
0,5 m/s SW CURRENT (VICINITY OF MAIN BREAKWATER)**

**FIGURE
3.37**



Velocity contours and vectors (m/s)

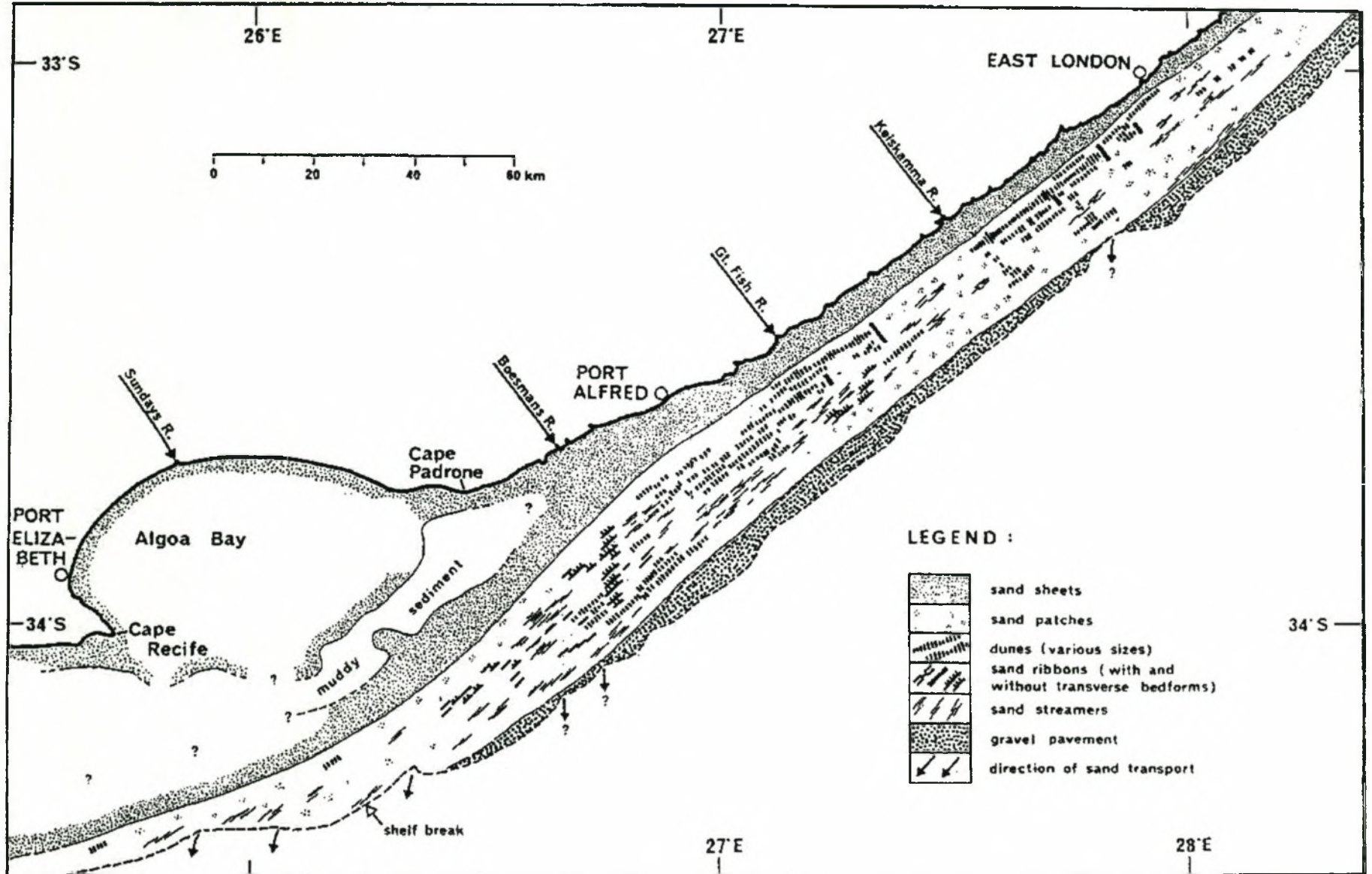
0.75 m/s →

NUMERICAL MODELLING OF CURRENTS:
0,23 m/s NE CURRENT (VICINITY OF MAIN BREAKWATER)

FIGURE

3.38

PHYSIOGRAPHIC FEATURES OF THE CONTINENTAL SHELF
OFF EAST LONDON

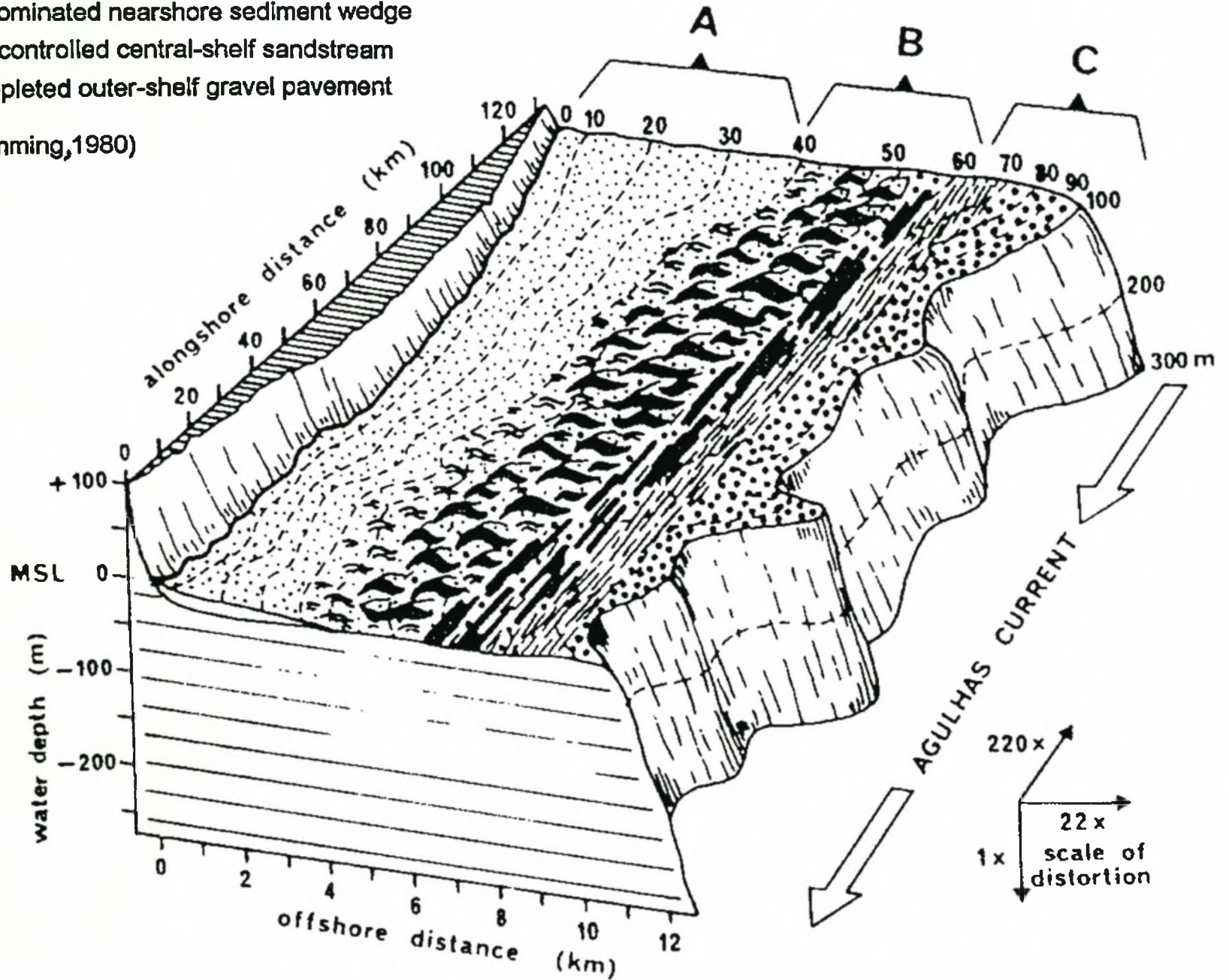


(From Flemming, 1980)

FIGURE
3.39

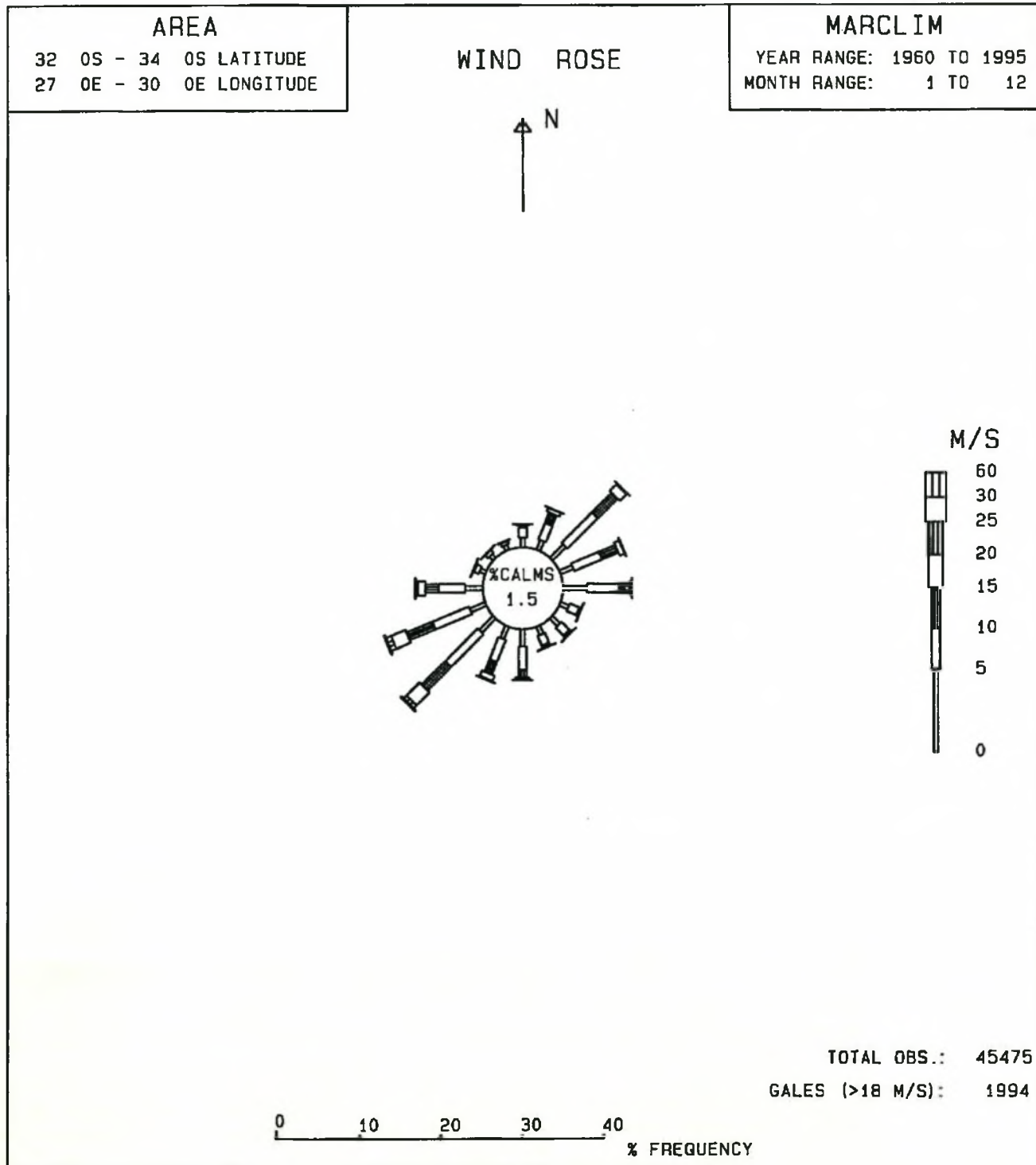
- A: wave-dominated nearshore sediment wedge
- B: current-controlled central-shelf sandstream
- C: sand-depleted outer-shelf gravel pavement

(From Flemming, 1980)



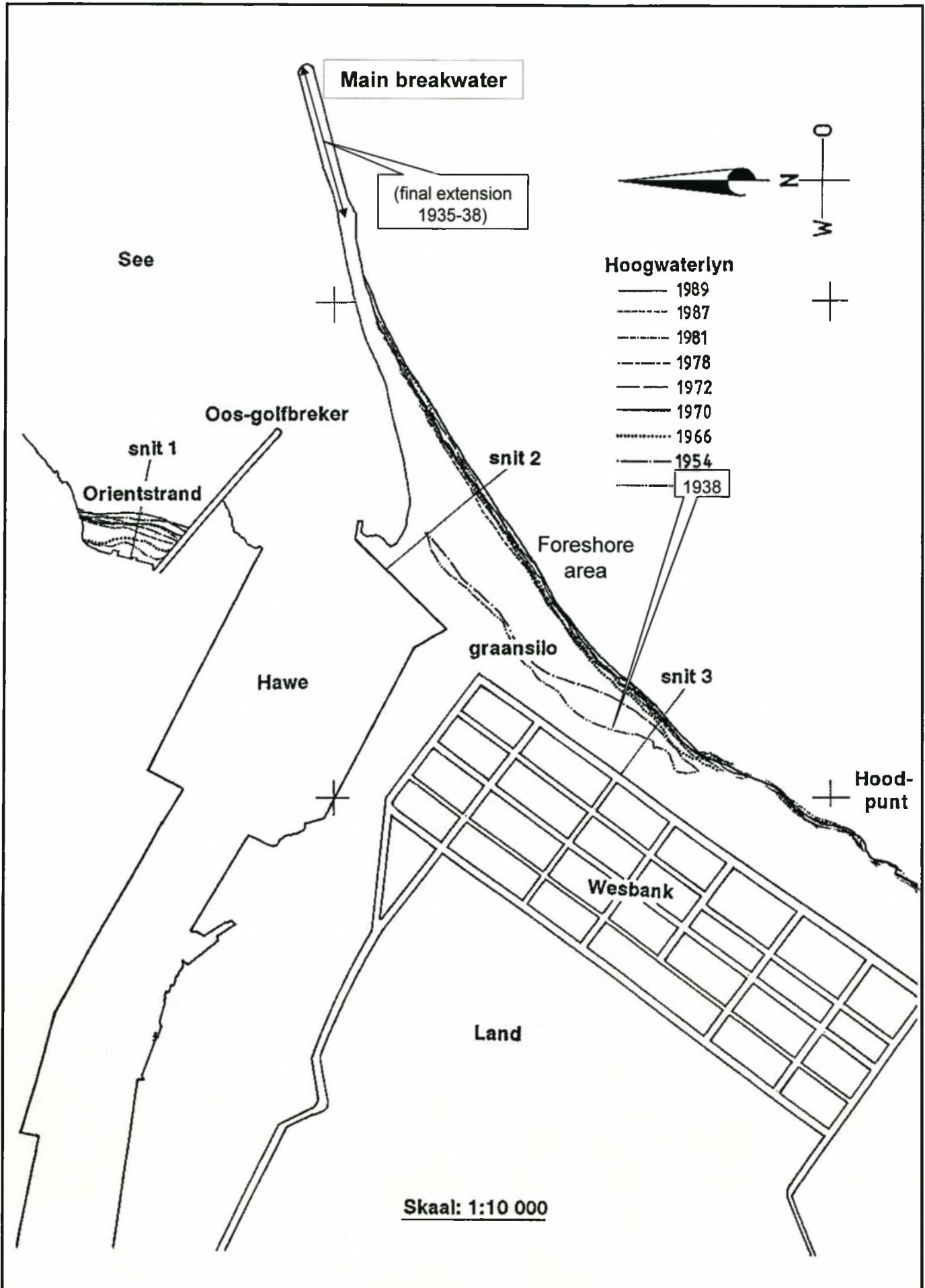
SCHEMATIC BLOCK DIAGRAM OF CONTINENTAL SHELF SECTION: PHYSIOGRAPHIC FEATURES

FIGURE 3.40



EAST LONDON VOS WIND ROSE

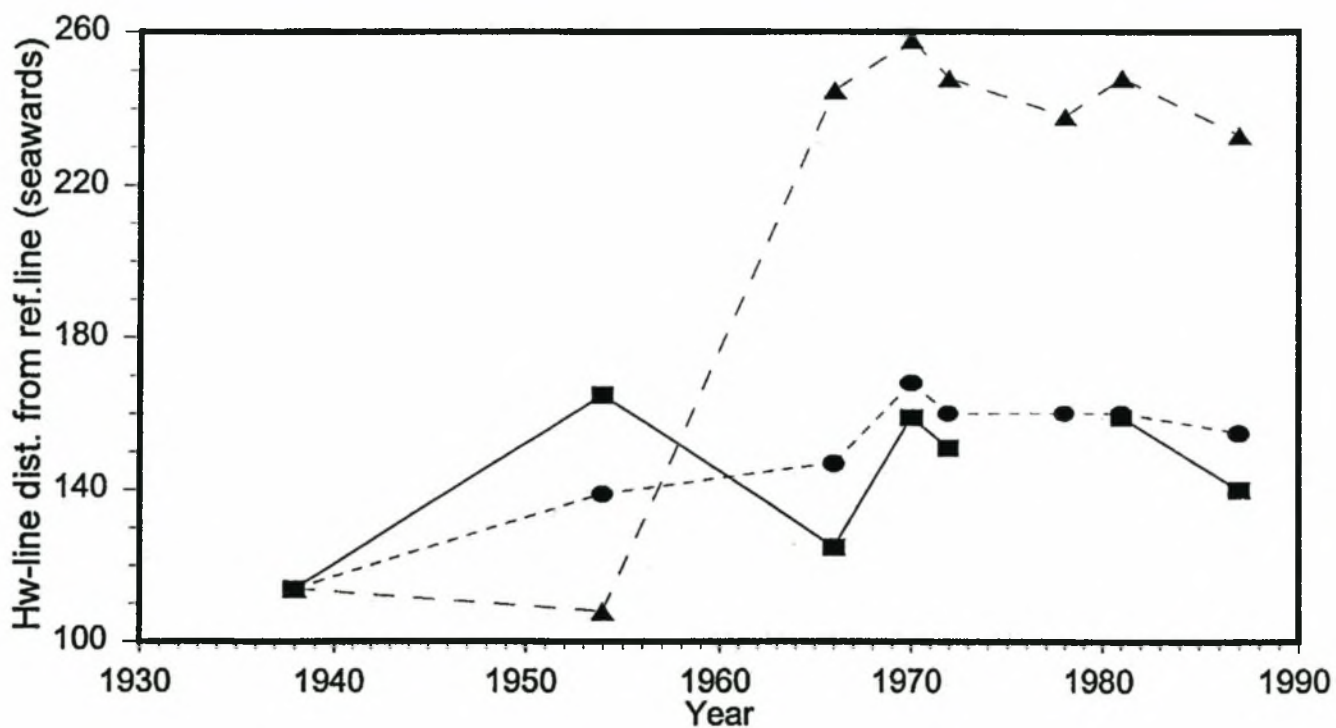
FIGURE
3.41



LOCATION OF HIGH-WATER LINE
FROM AERIAL PHOTOGRAPHS

FIGURE
3.42

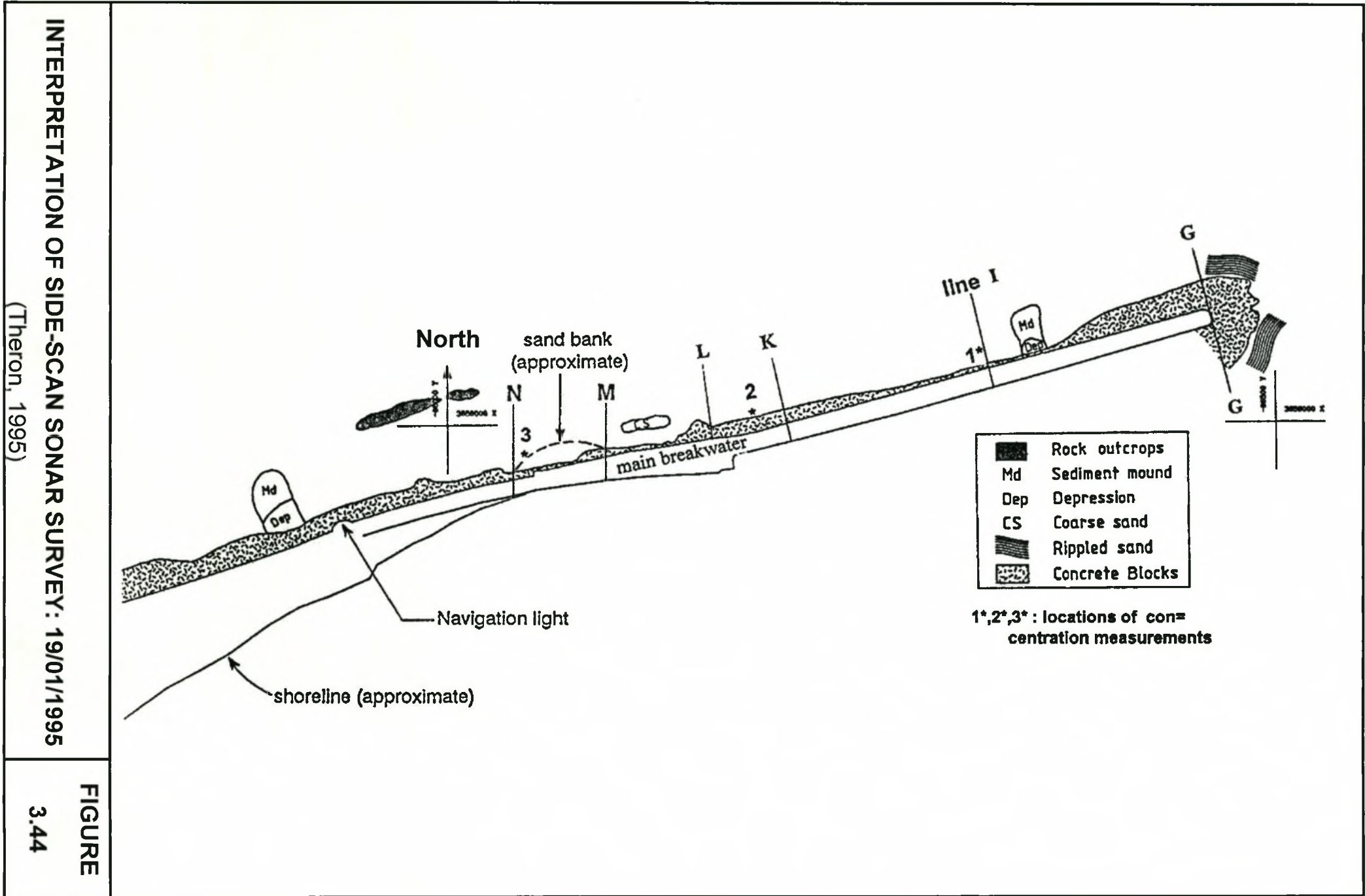
Highwater line variation from photos



Section 1 (Orient)
 Section 2 (main b.w.)
 Section 3 (W. Bank)

VARIATION OF HIGH-WATER LINE FROM AERIAL PHOTOGRAPHS

FIGURE
3.43



FIGURE

3.44

CROSS SECTIONAL PROFILES PERPENDICULAR TO THE MAIN BREAKWATER (SEAWARDS) (Theron, 1995)

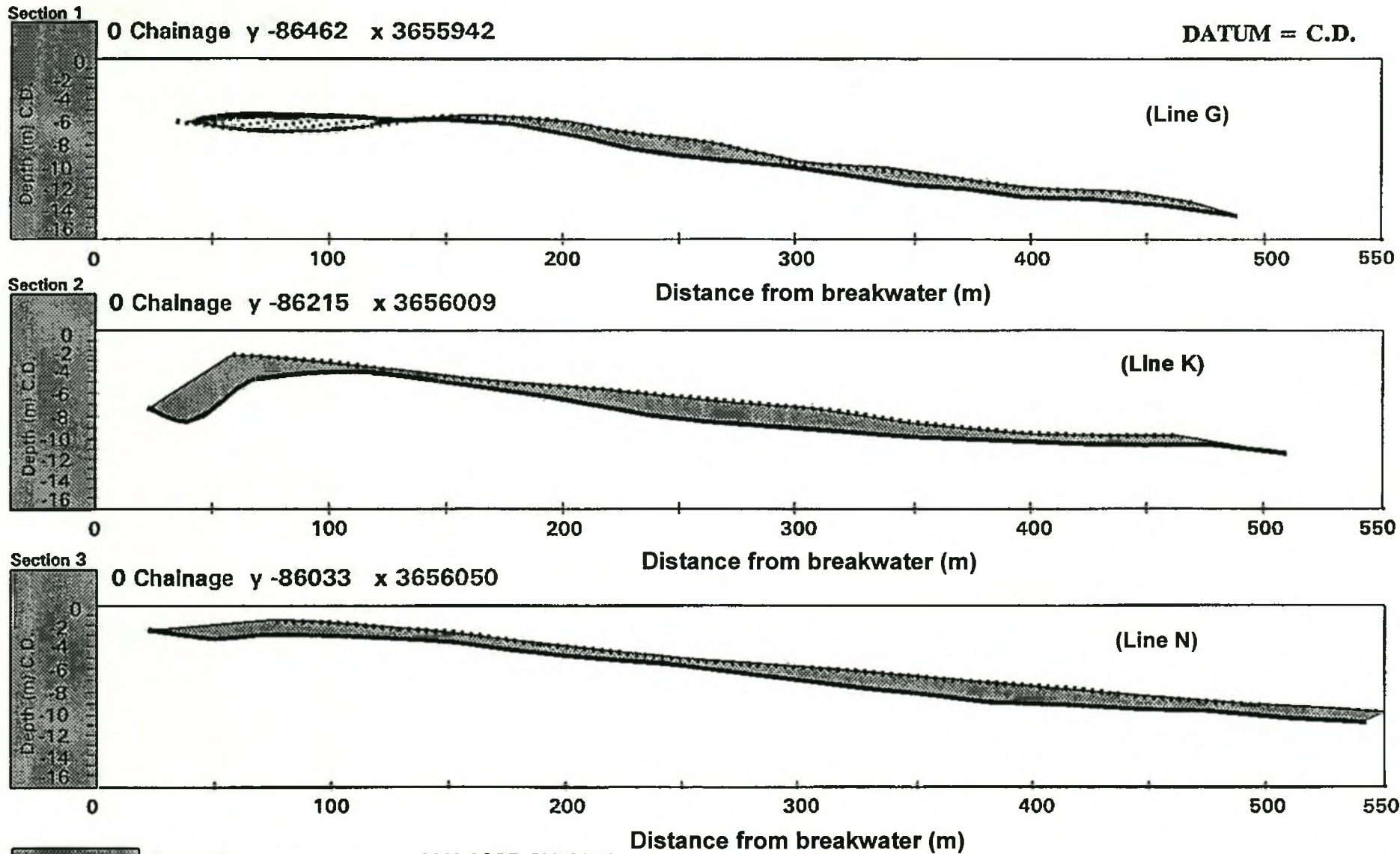
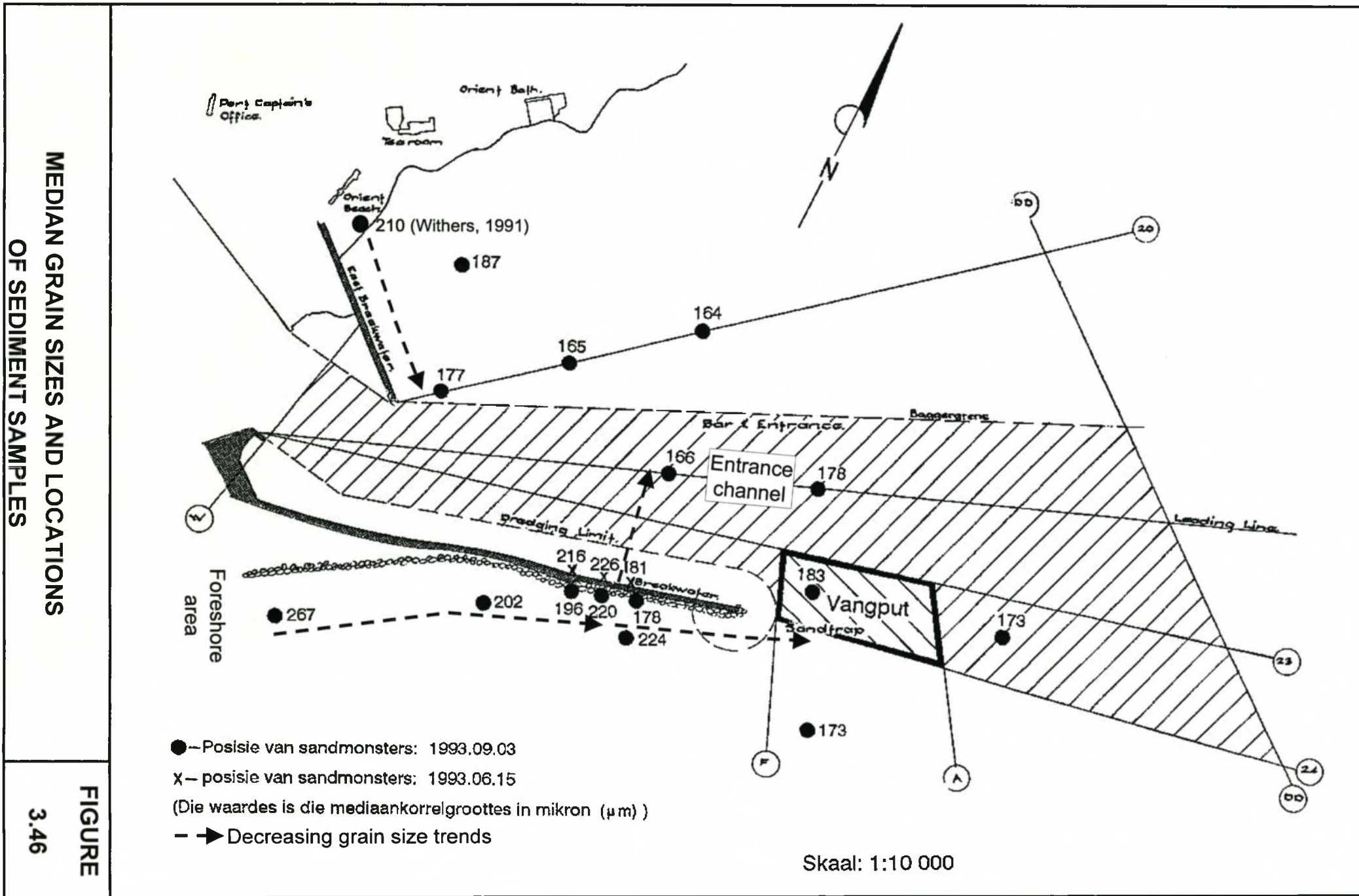
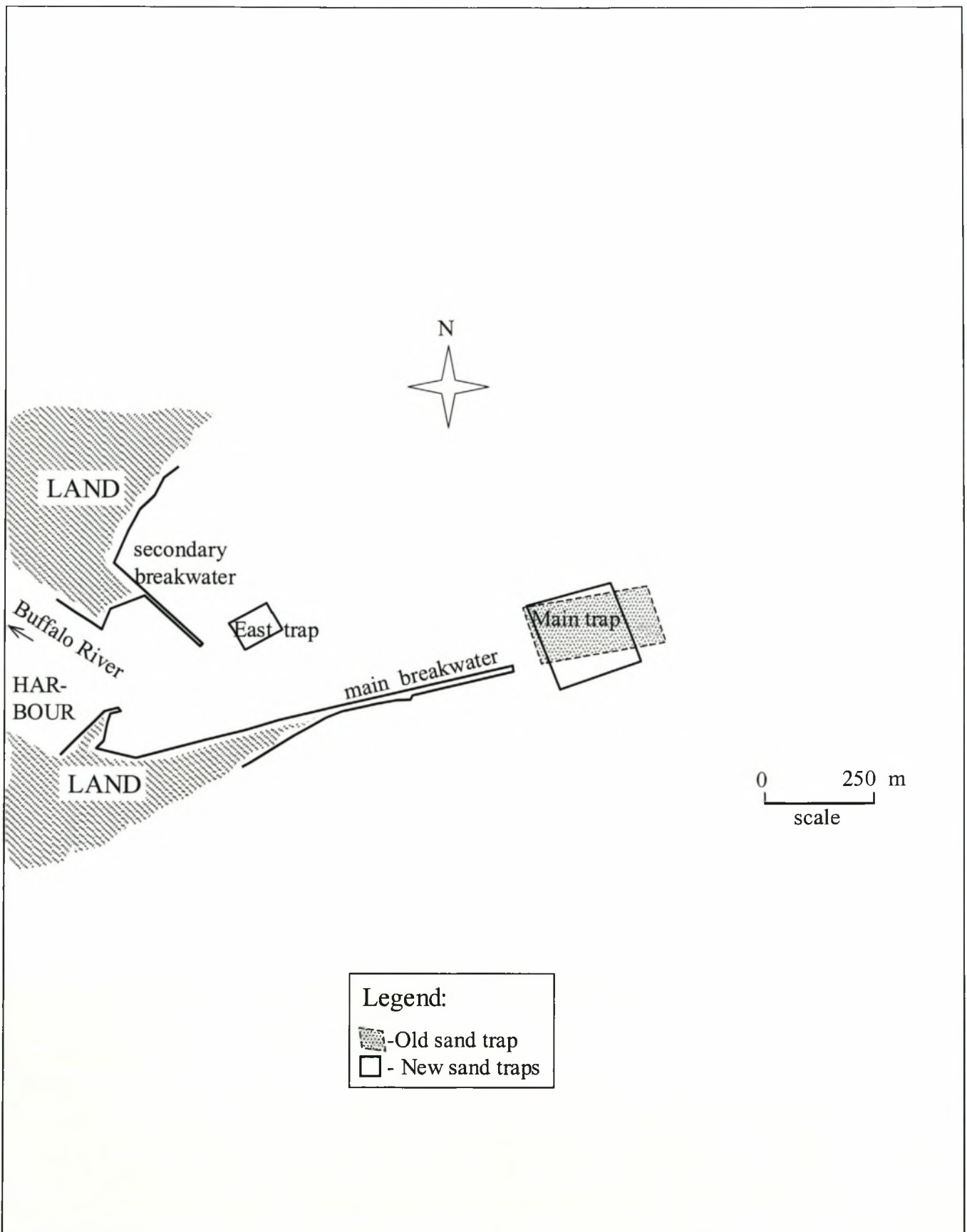


FIGURE 3.45



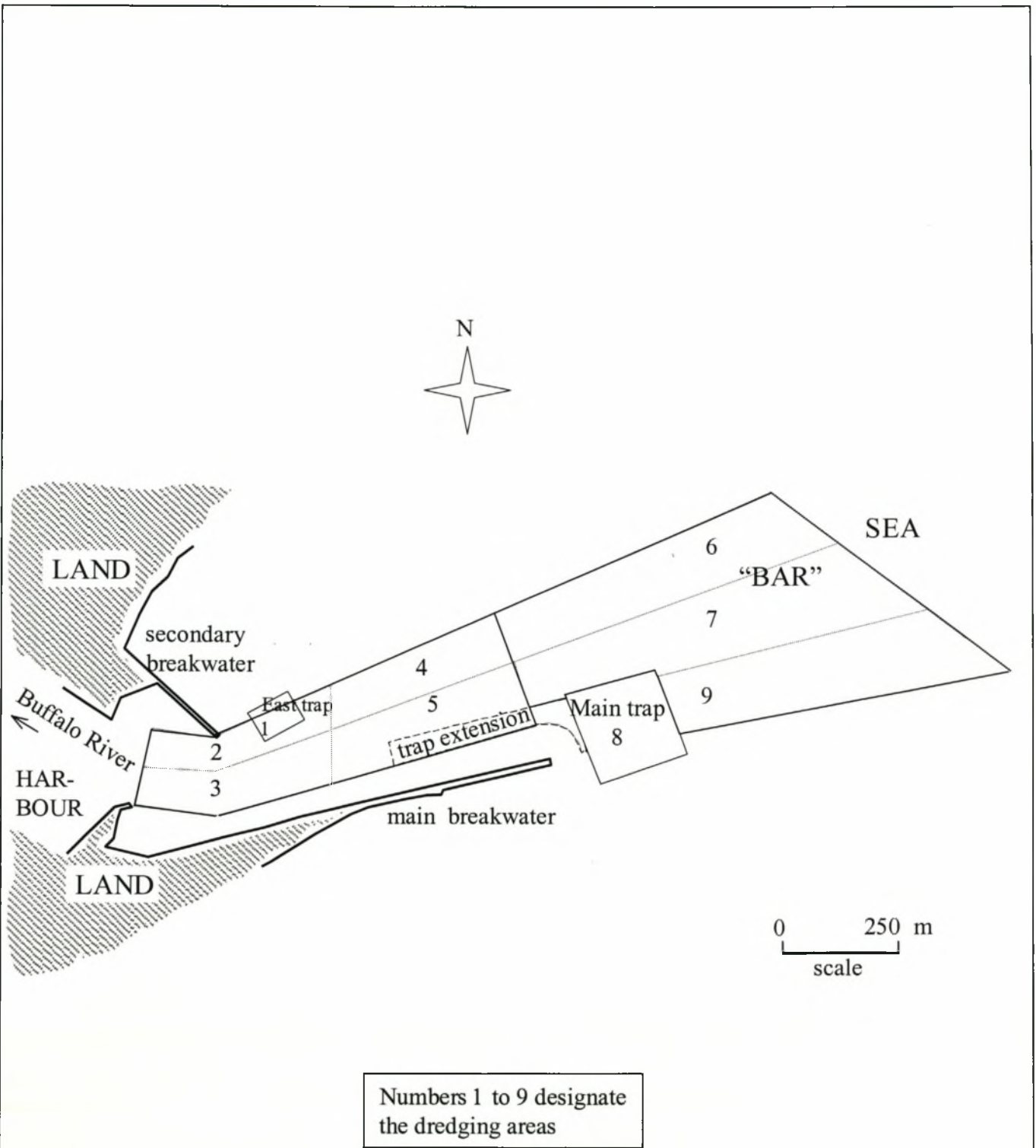
FIGURE

3.46



OLD AND NEW (1994) SAND TRAPS
(Theron and Schoonees, 1998)

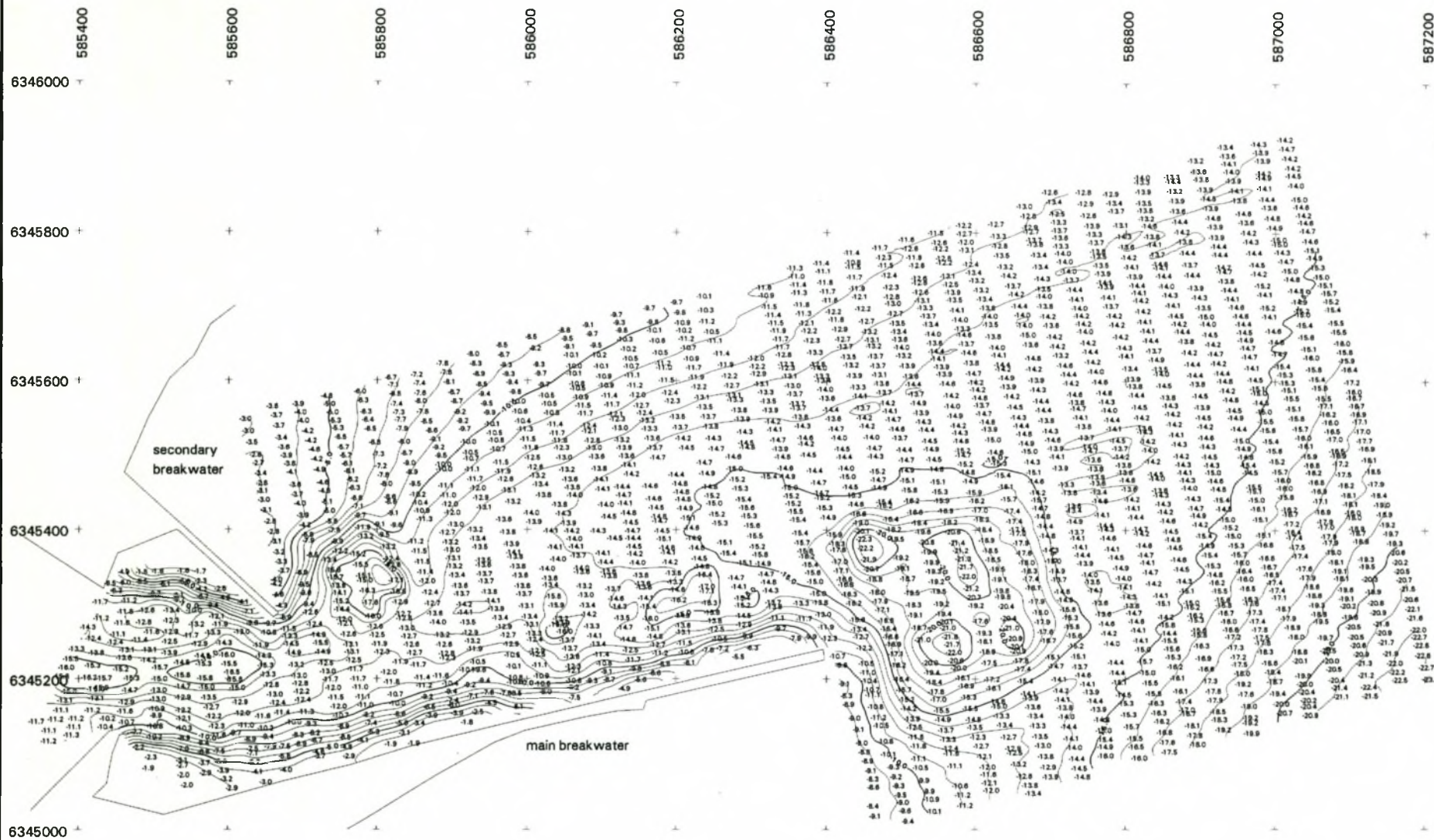
FIGURE
4.1



**EAST LONDON SAND TRAPS, BREAKWATERS
AND DREDGING AREAS**

**FIGURE
4.2**

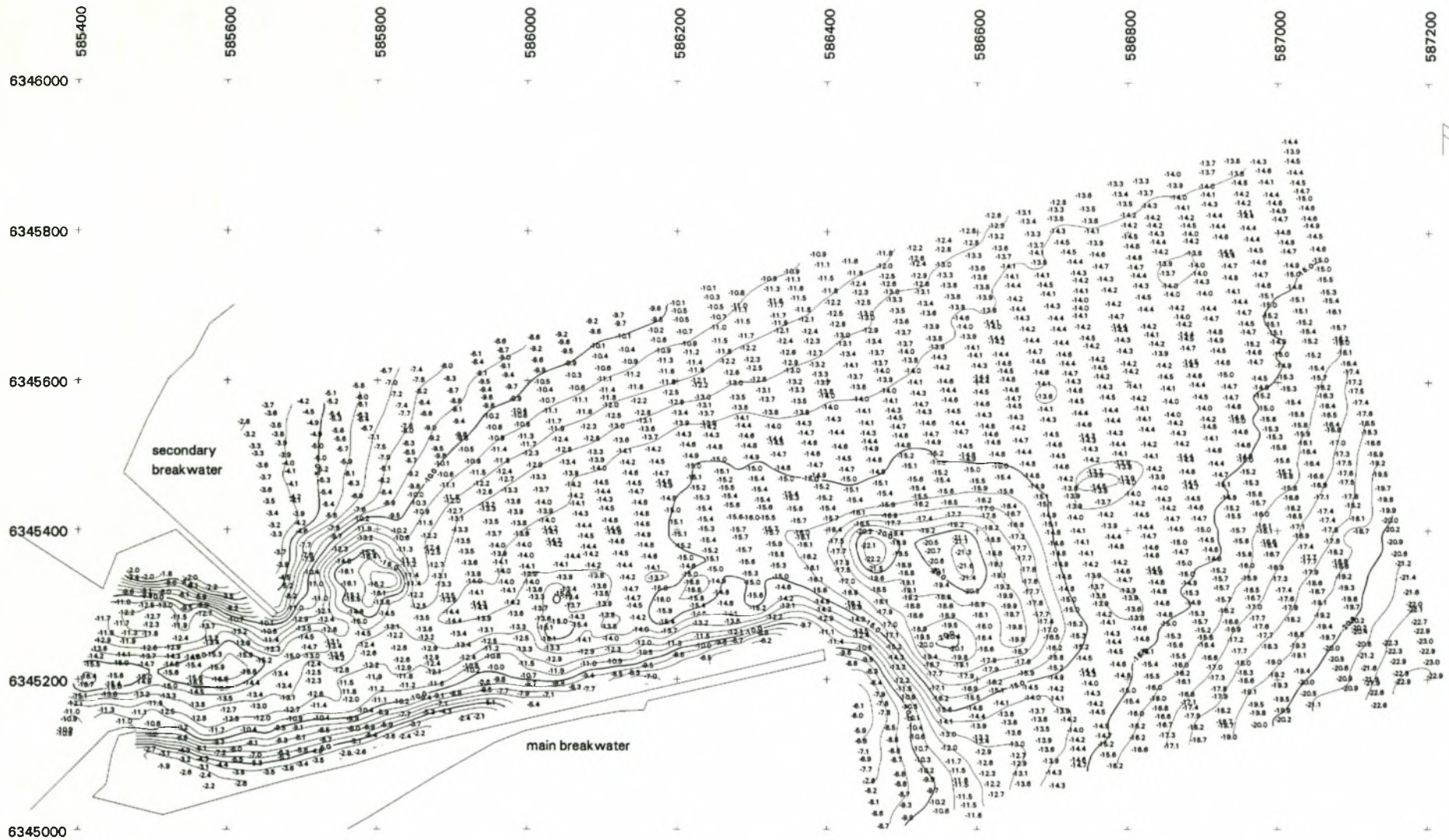
SPOT HEIGHT AND CONTOUR MAP – 25 MAY 1998



Contour Interval : 1 m (to Chart Datum (Port))
Projection : WGS 84 UTM, Lo 27

FIGURE
4.3

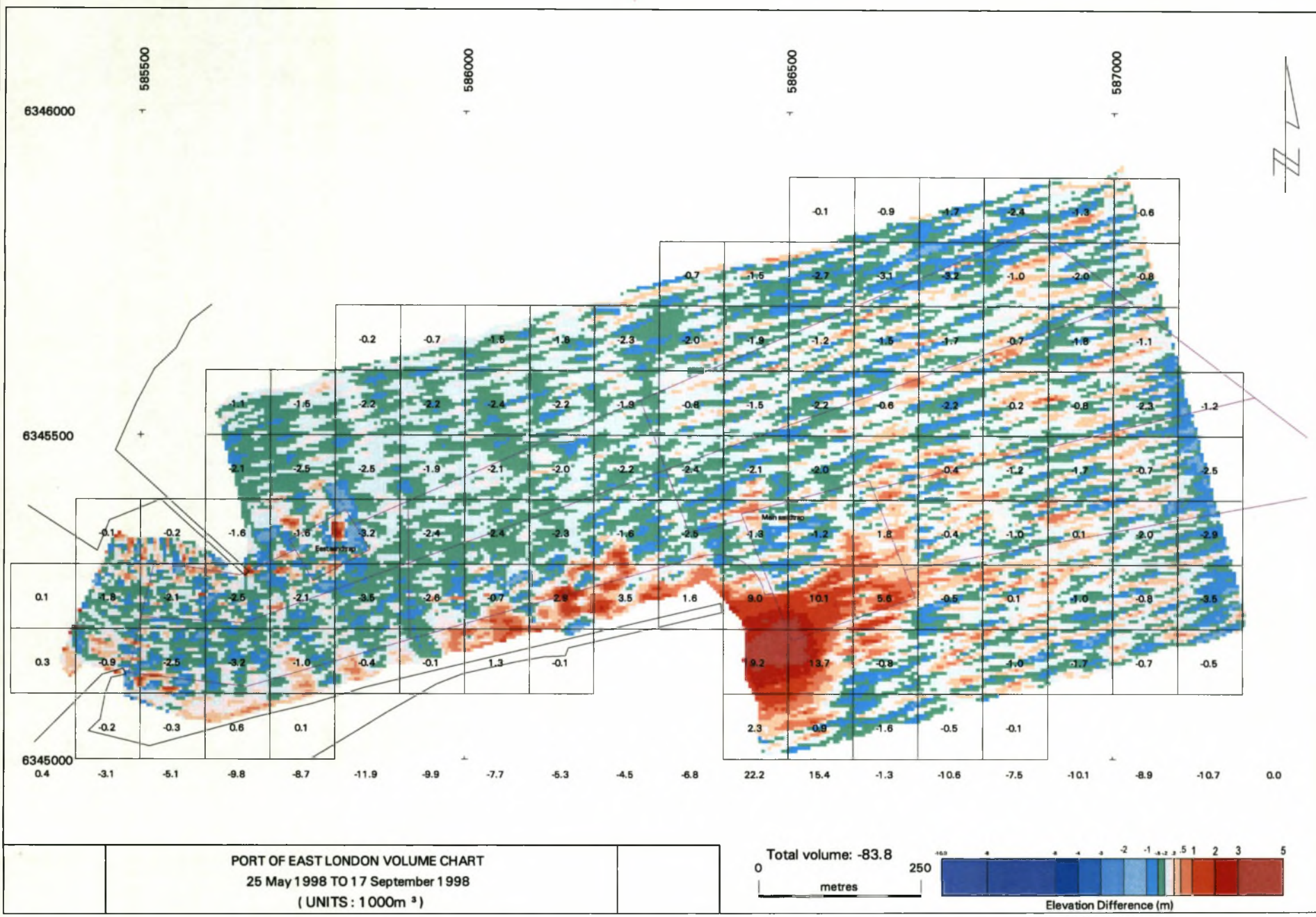
SPOT HEIGHT AND CONTOUR MAP – 17 SEPTEMBER 1998



Contour Interval : 1 m (to Chart Datum (Port))
Projection : WGS 84 UTM, Lo 27

FIGURE 4.4

DIFFERENCE MAP FOR MAY TO SEPTEMBER 1998

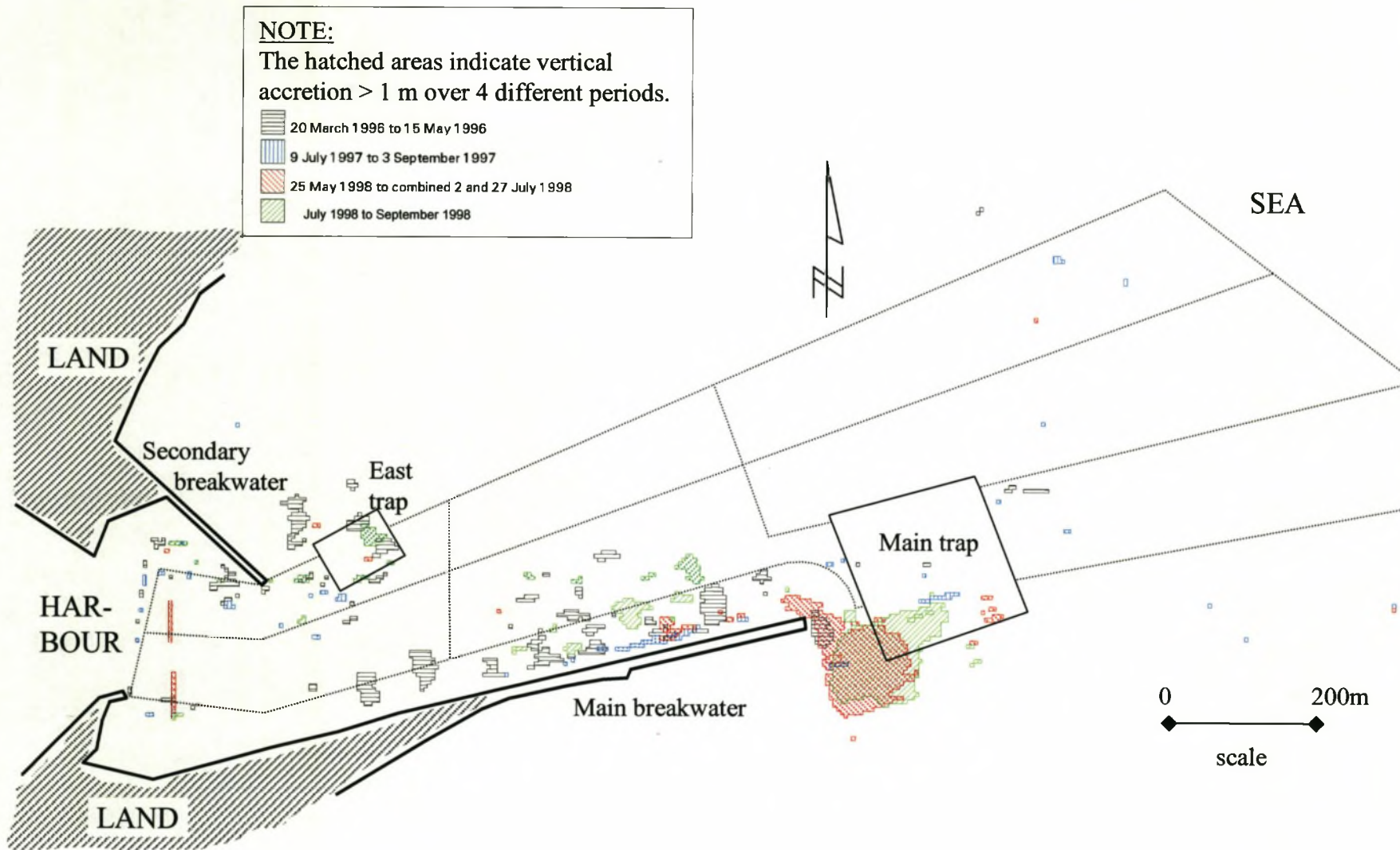


4.5

FIGURE

EAST LONDON - SYNOPSIS OF ACCRETED AREAS (>1 m)

FIGURE 4.6



EAST LONDON - SYNOPSIS OF ACCRETTED AREAS (>0.7 m)

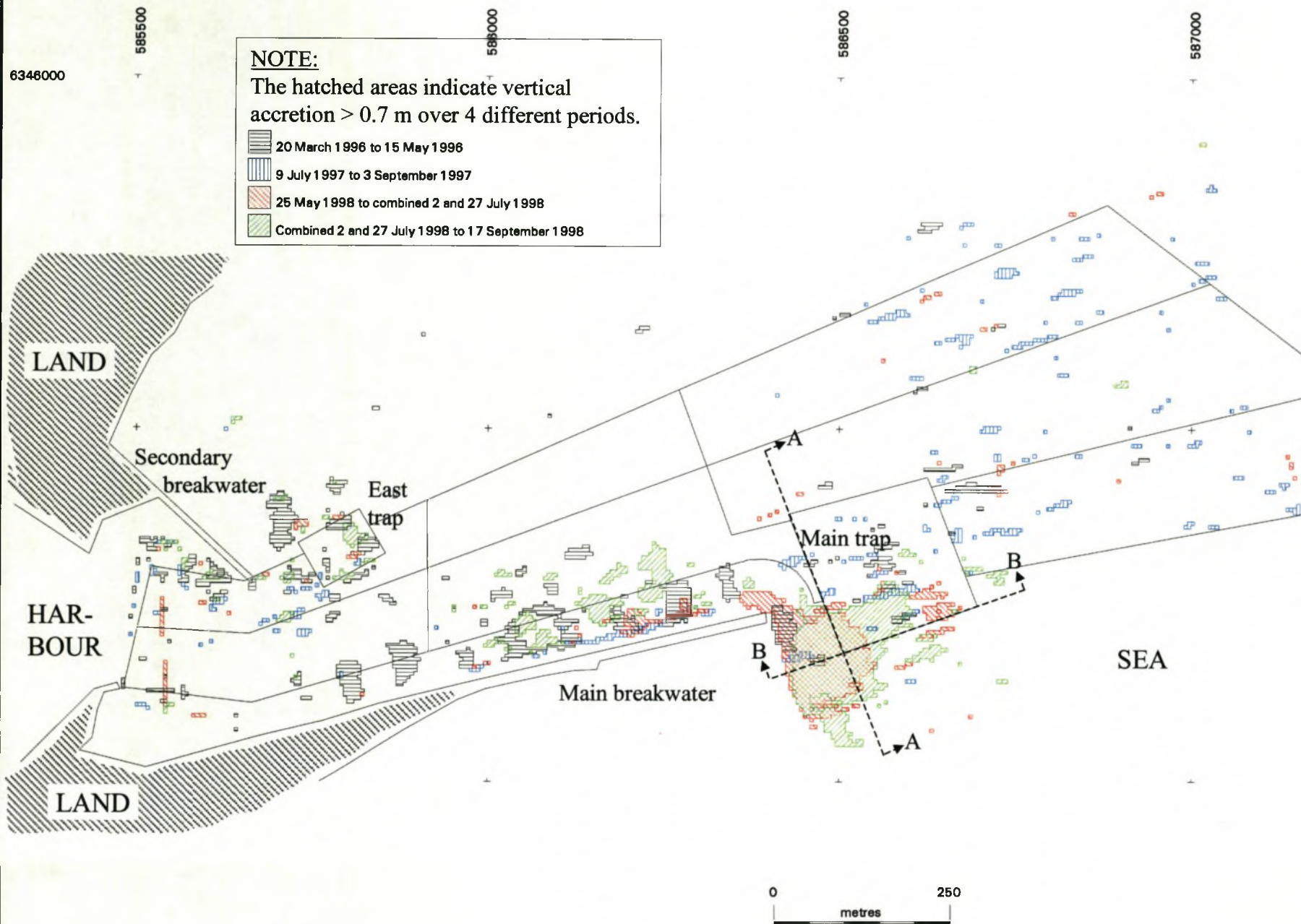
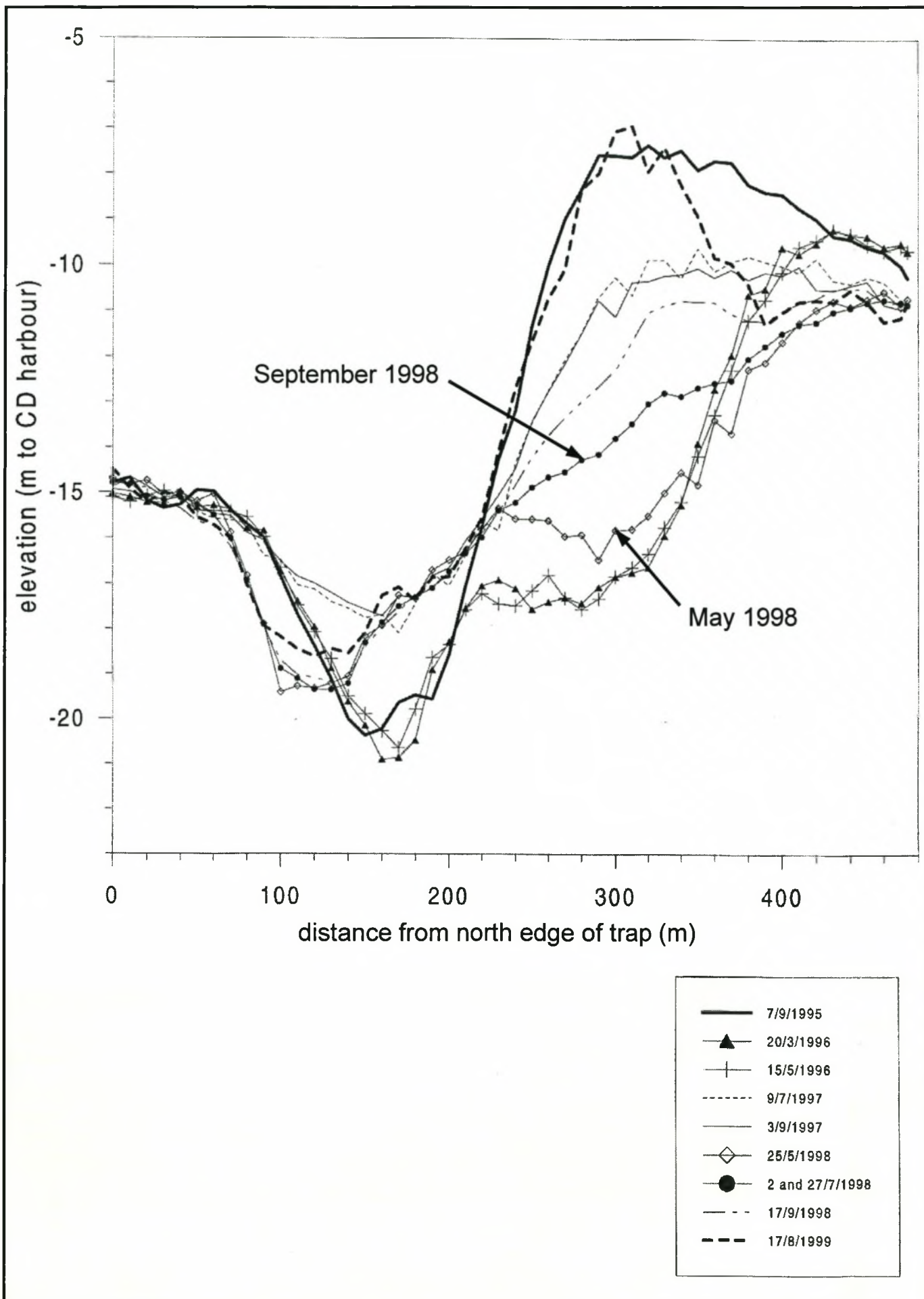
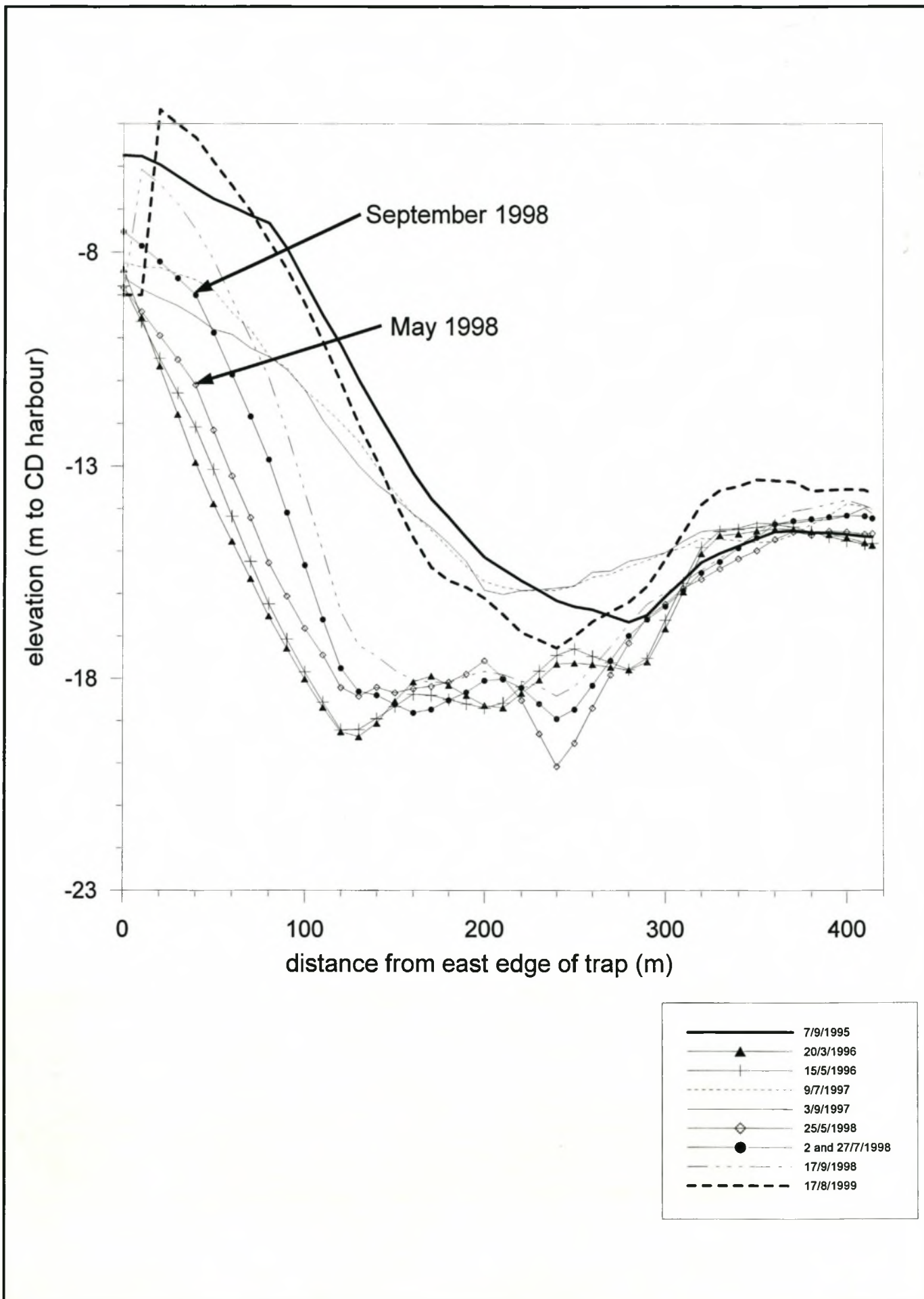


FIGURE
4.7



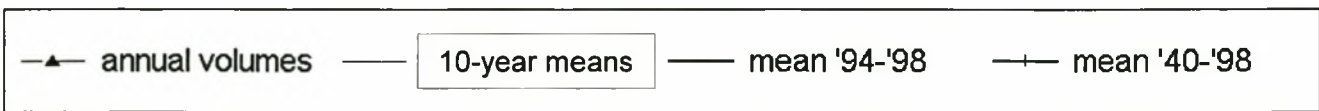
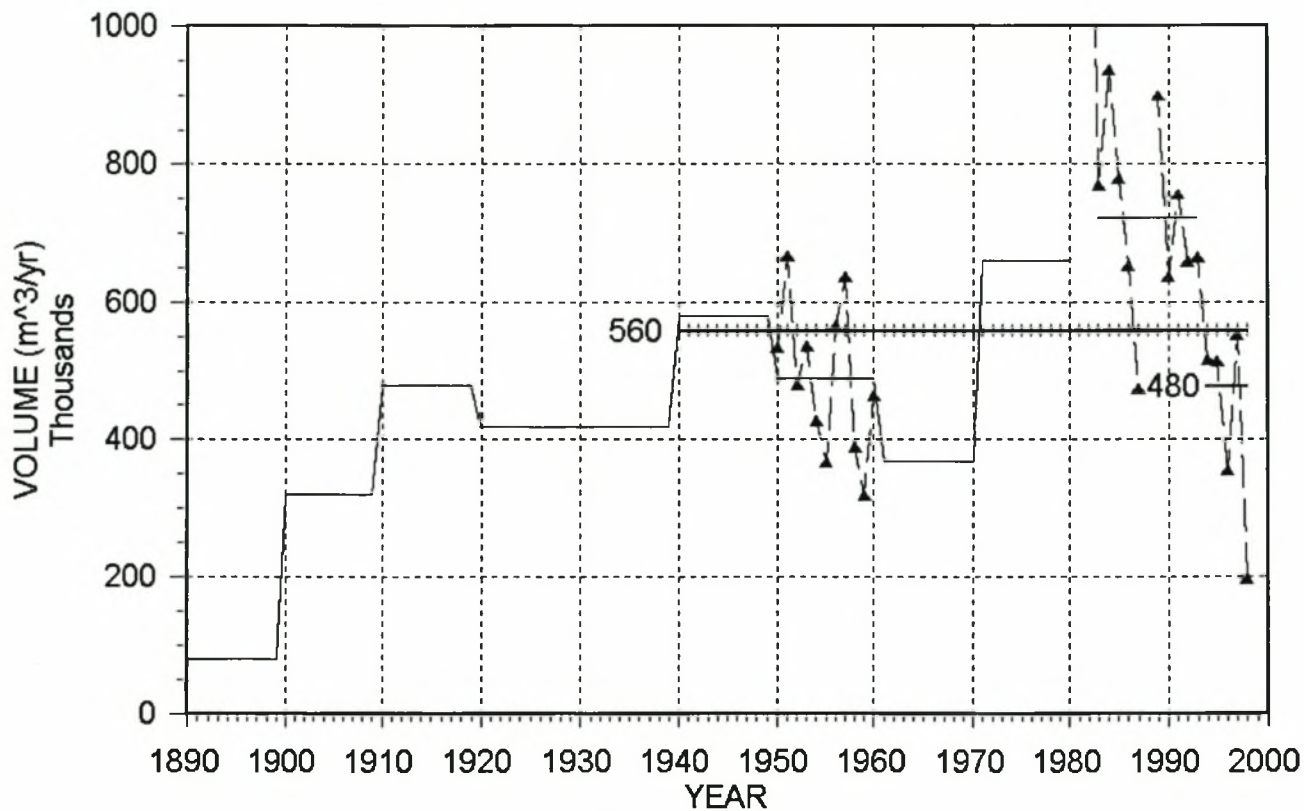
**PROFILES ALONG WESTERN EDGE OF MAIN TRAP
LOOKING EAST (Profile A, Figure 4.7)**

**FIGURE
4.8**



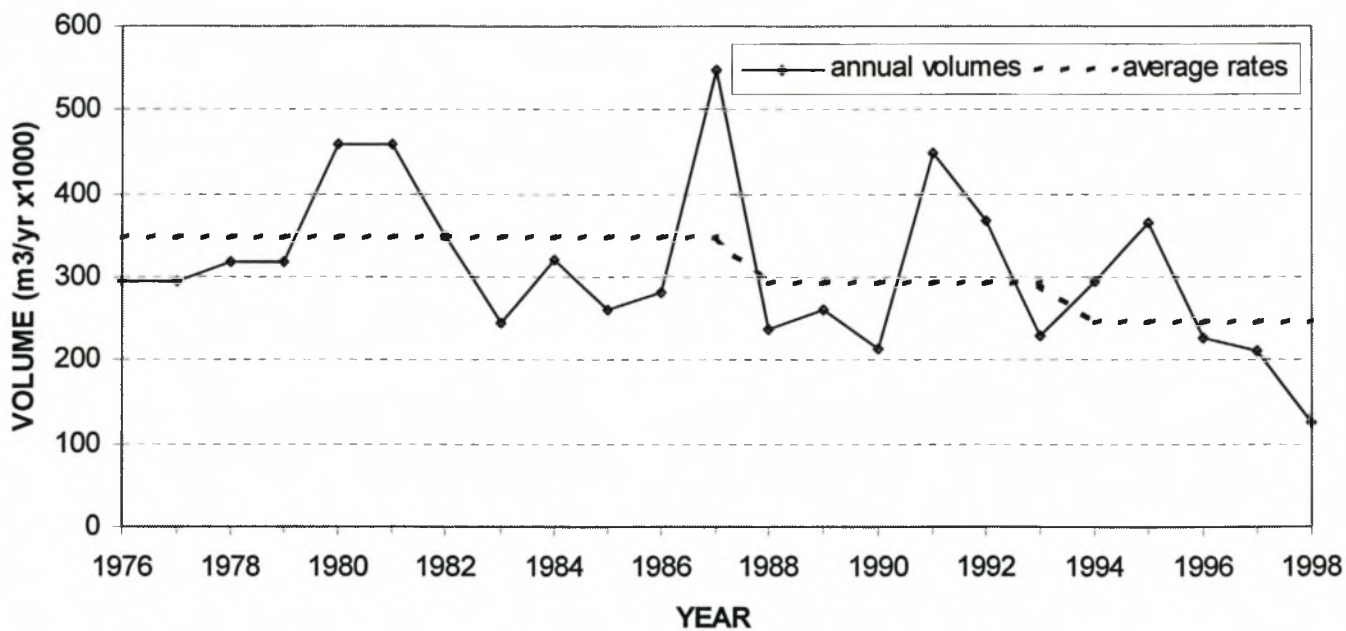
**PROFILES ALONG SOUTHERN EDGE OF MAIN TRAP
LOOKING NORTH (Profile B, Figure 4.7)**

**FIGURE
4.9**



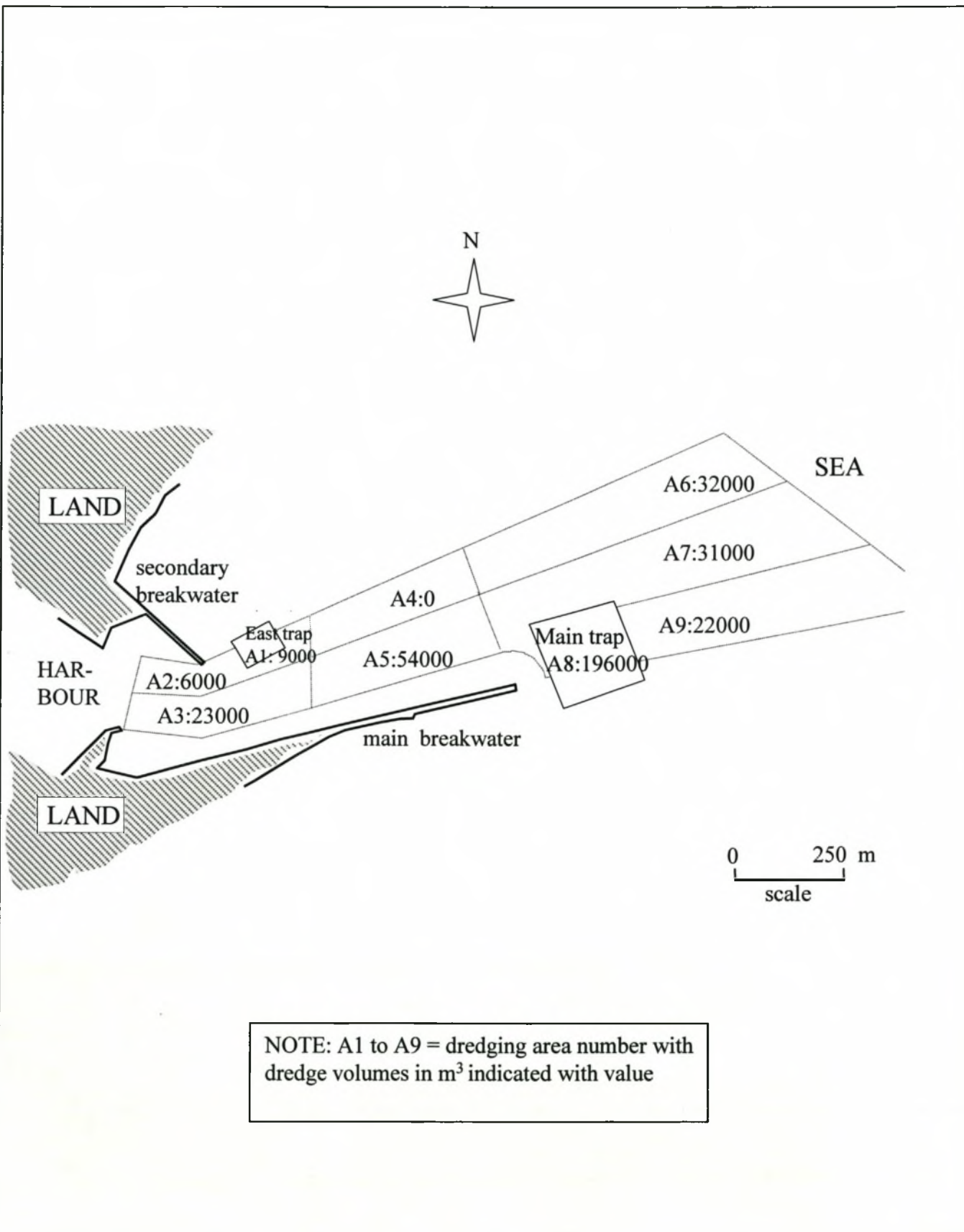
**ANNUAL VOLUMES OF SEDIMENT DREDGED
AT EAST LONDON SINCE 1890 (Theron and Schoonees, 1998)**

**FIGURE
4.10**



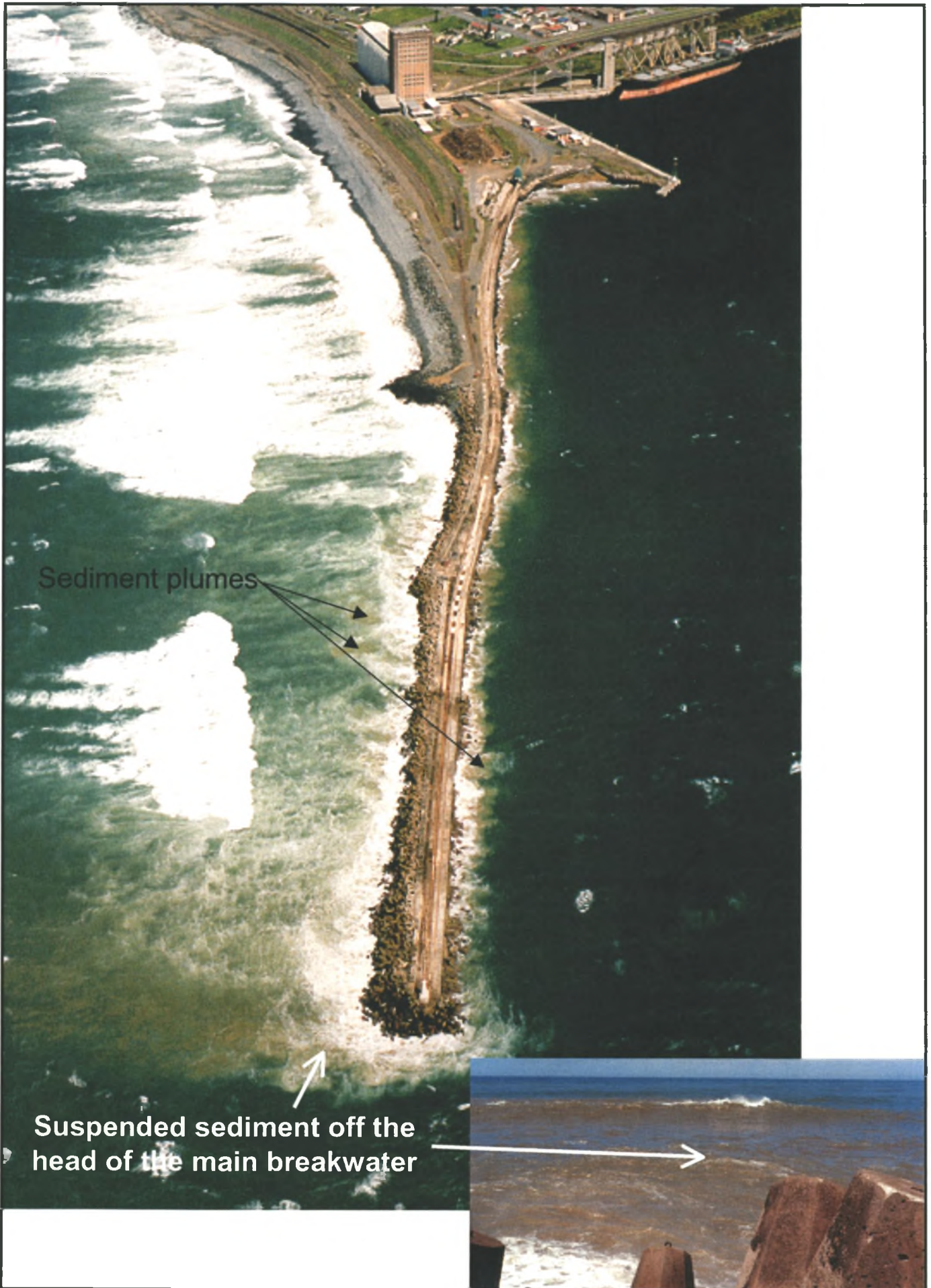
ANNUAL VOLUMES DREDGED FROM MAIN SAND TRAP
(Theron and Schoonees, 1998)

FIGURE
4.11



**MEAN ANNUAL SEDIMENTATION
IN DIFFERENT DREDGING AREAS (1995-1999)**

**FIGURE
4.12**



Sediment plumes

Suspended sediment off the head of the main breakwater

SEDIMENT TRANSPORT ALONG THE SEAWARD SIDE AND AROUND THE HEAD OF THE MAIN BREAKWATER

FIGURE

4.13

**VERTICAL ACCRETION AND MEAN ANNUAL SEDIMENTATION
IN DIFFERENT DREDGING AREAS**

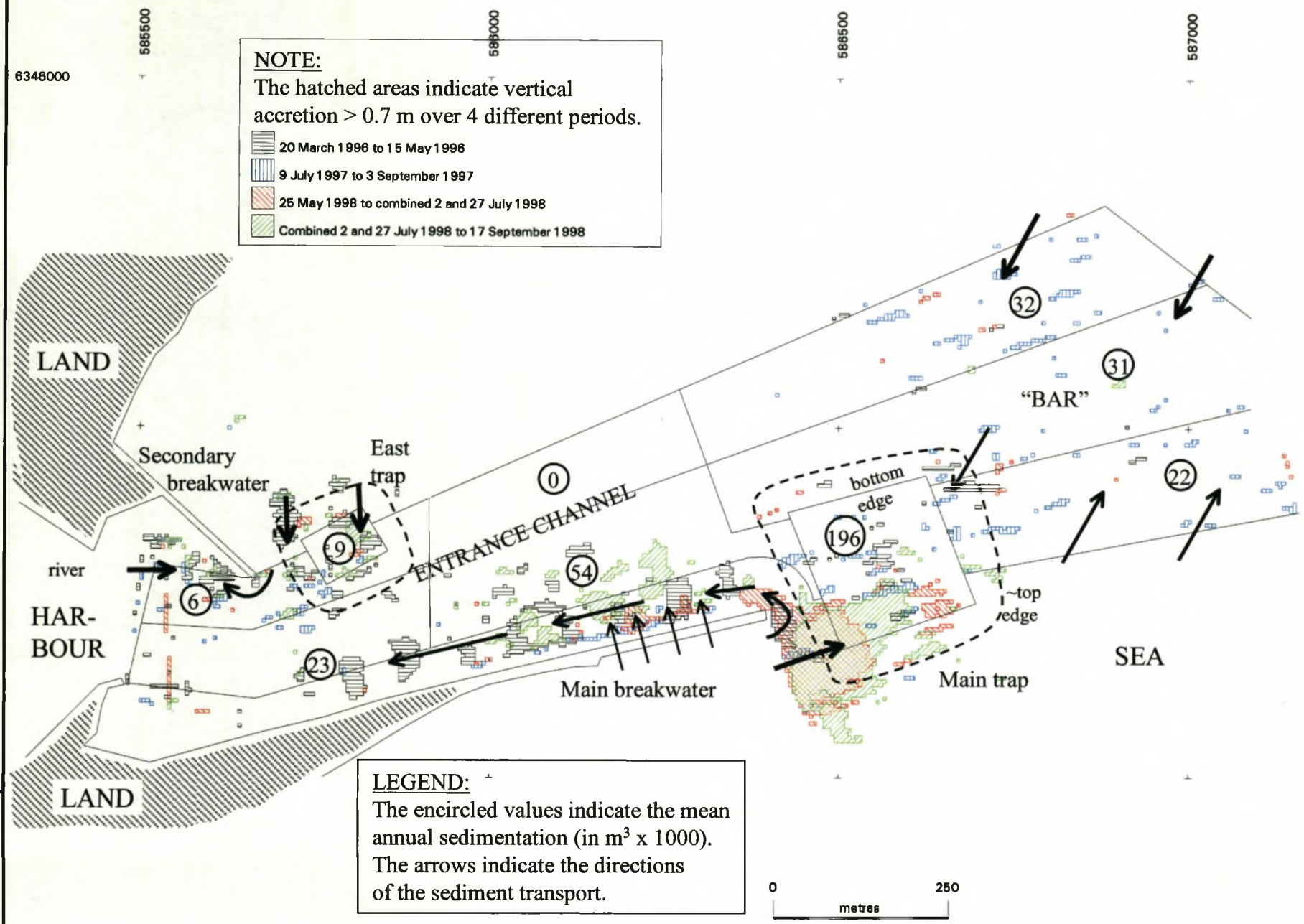
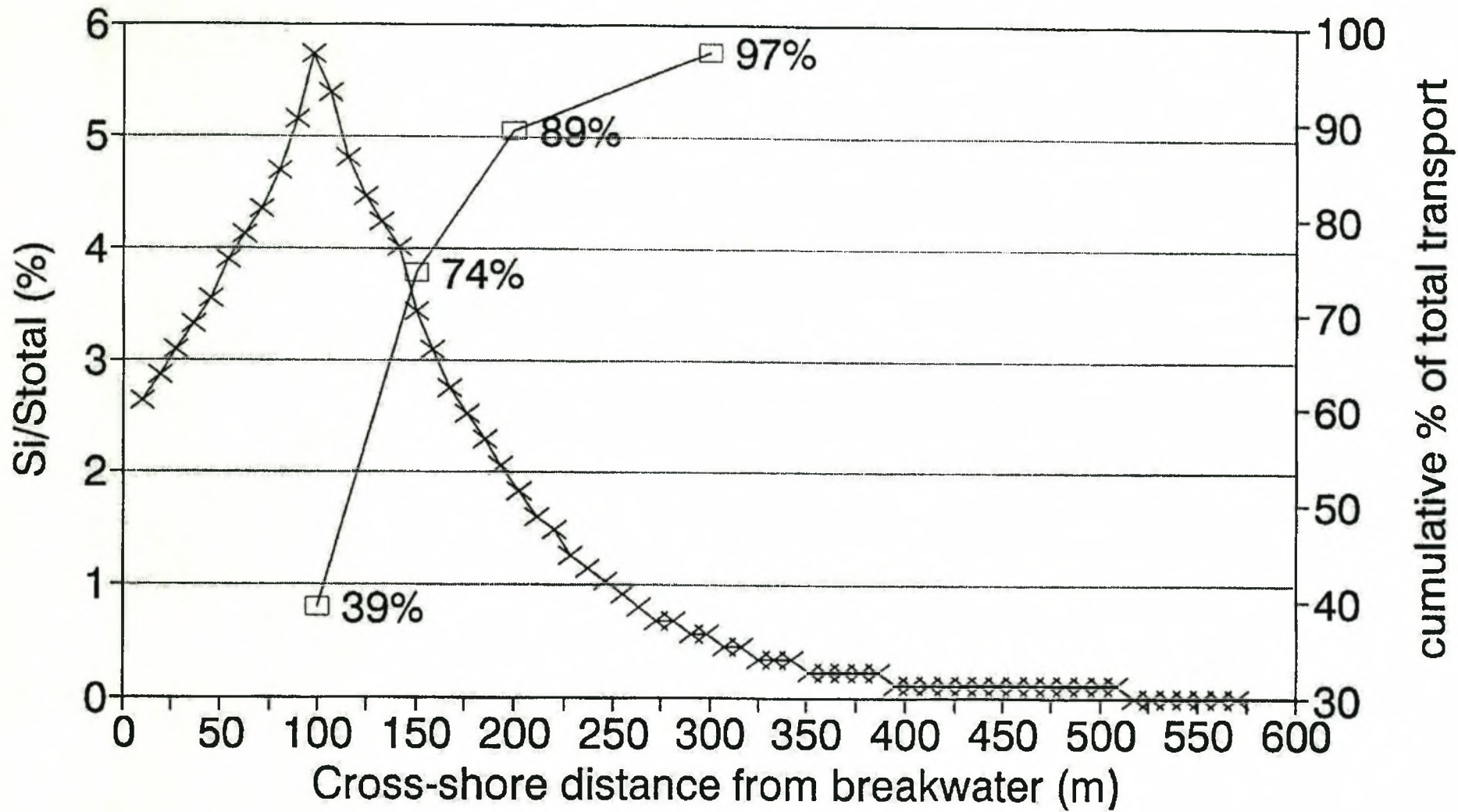


**FIGURE
4.14**

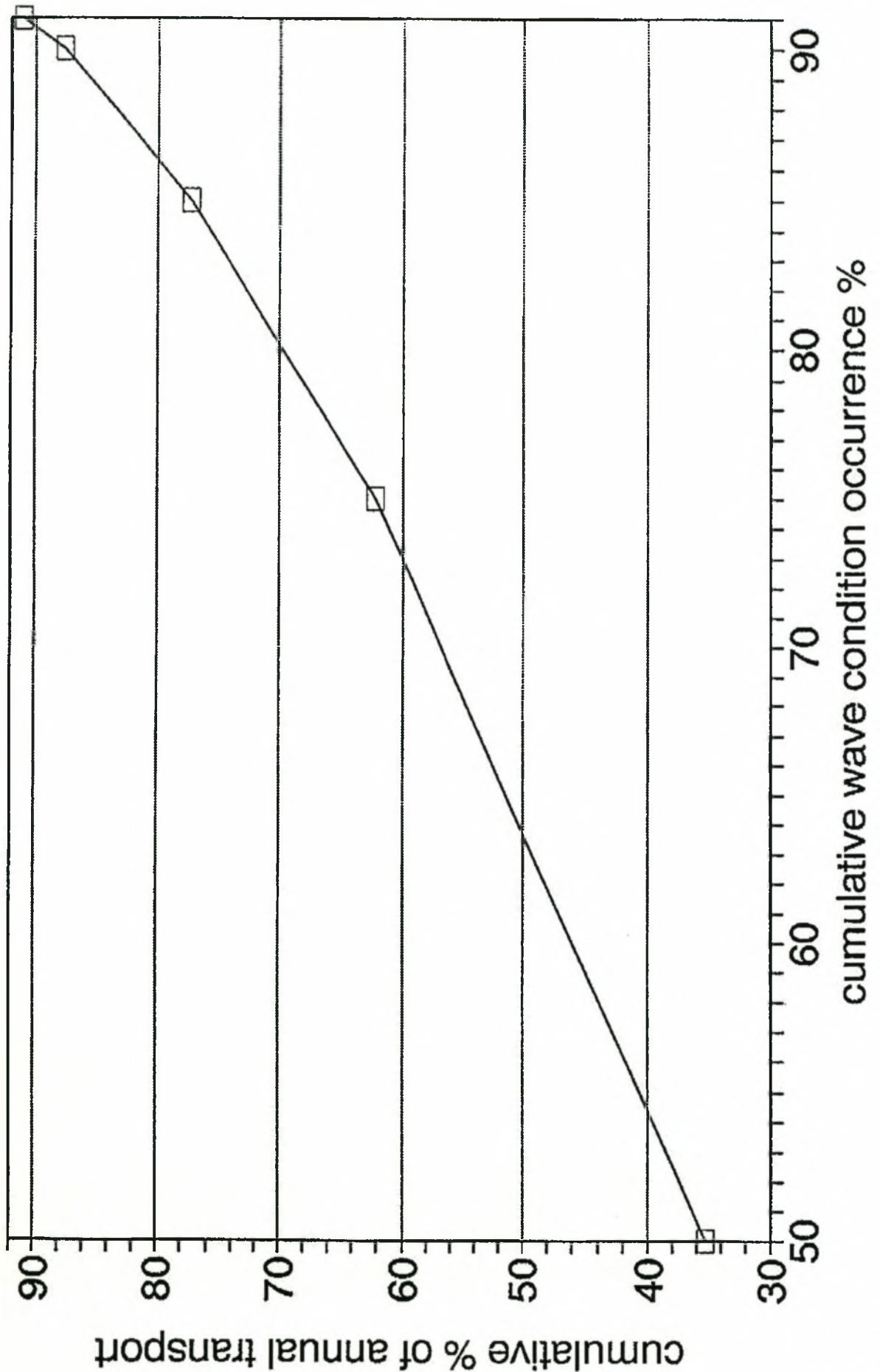
CROSS-SHORE DISTRIBUTION OF LONGSHORE TRANSPORT



NOTE: S_i =local (point) transport rate
 S_t = total across shore transport rate

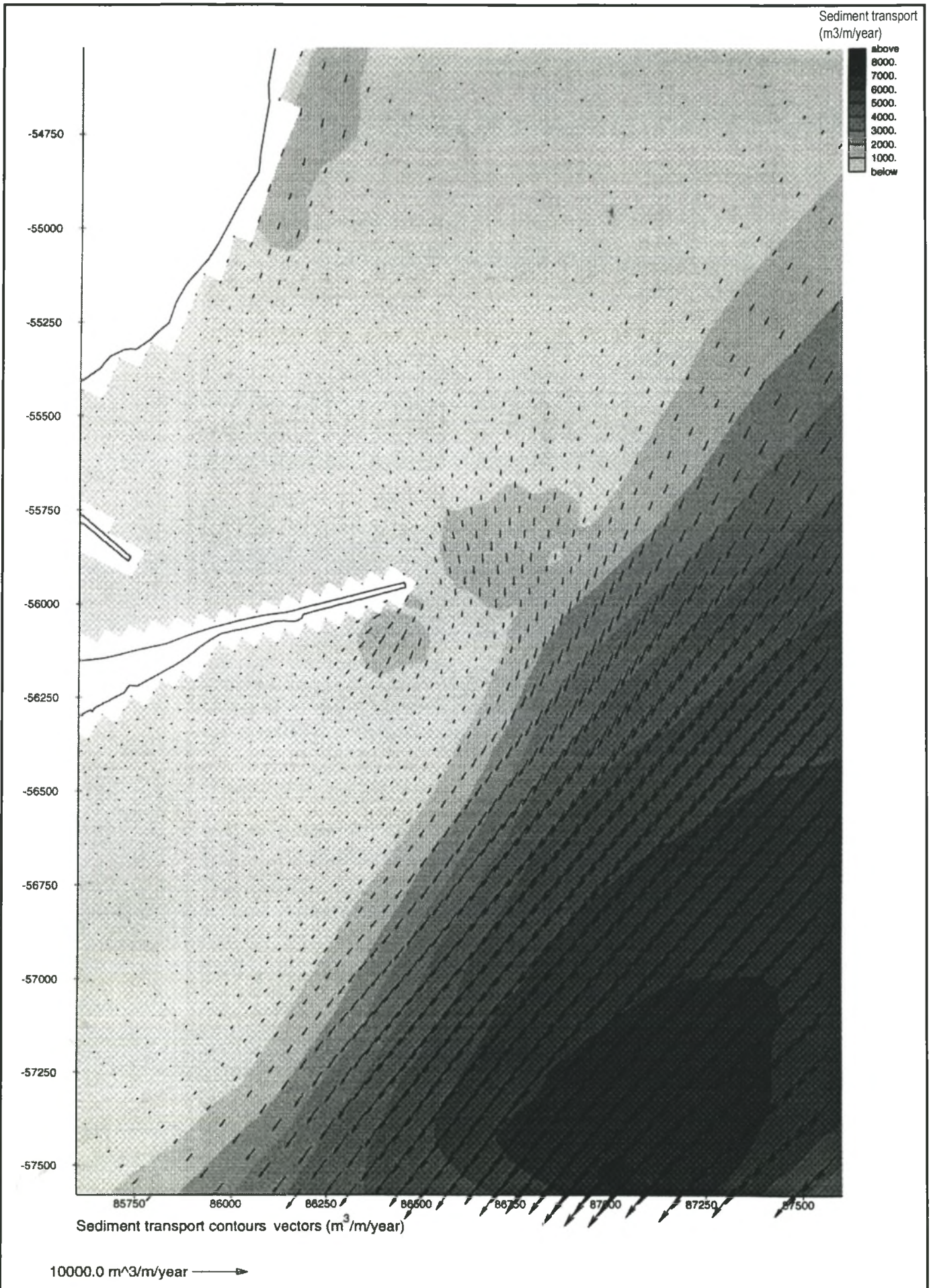
—x— S_i/S_t —□— cum

FIGURE 4.15



DISTRIBUTION OF TOTAL ANNUAL LONGSHORE TRANSPORT OVER WAVE CONDITION OCCURRENCE

FIGURE 4.16

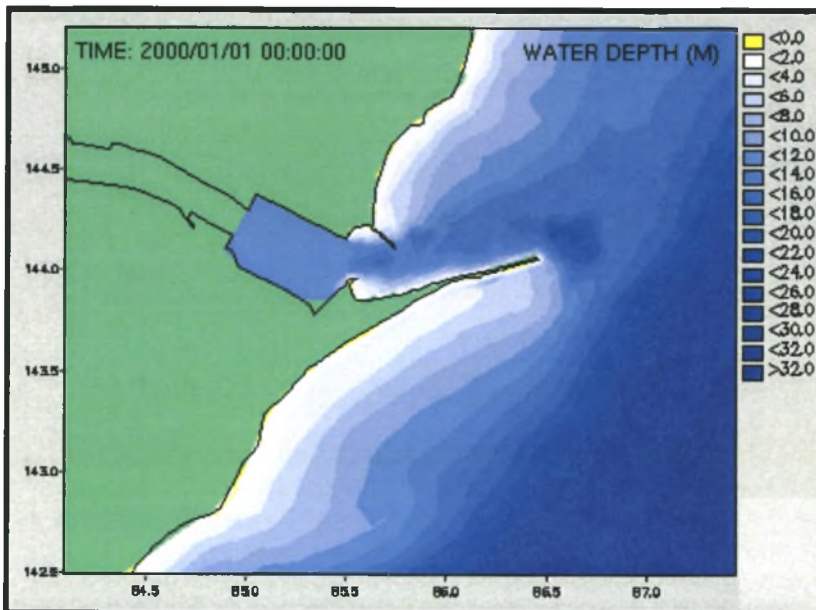


NUMERICAL MODELLING OF SEDIMENT TRANSPORT:

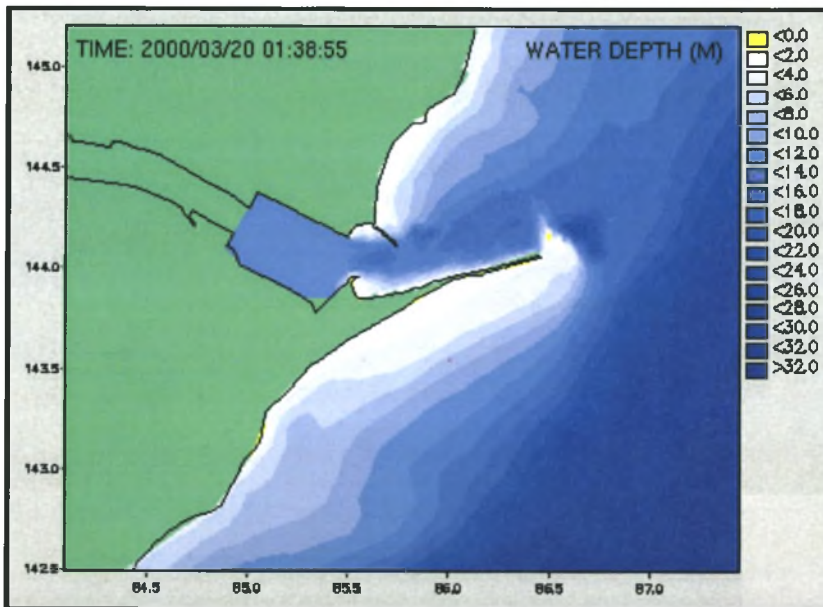
0.3 m/s SW NEARSHORE CURRENT (Hmo =2 m; Tp =12s; Direction =214deg)

FIGURE

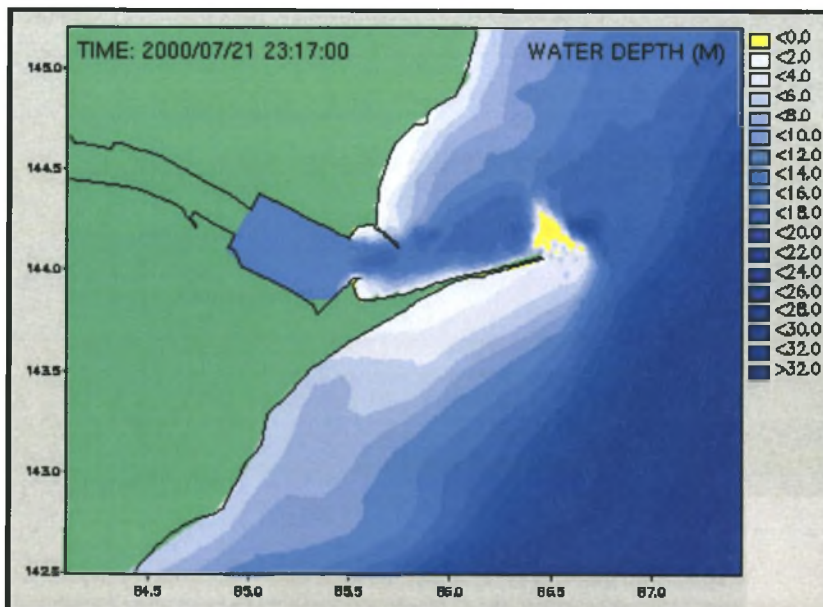
4.17



START



AFTER
78 DAYS

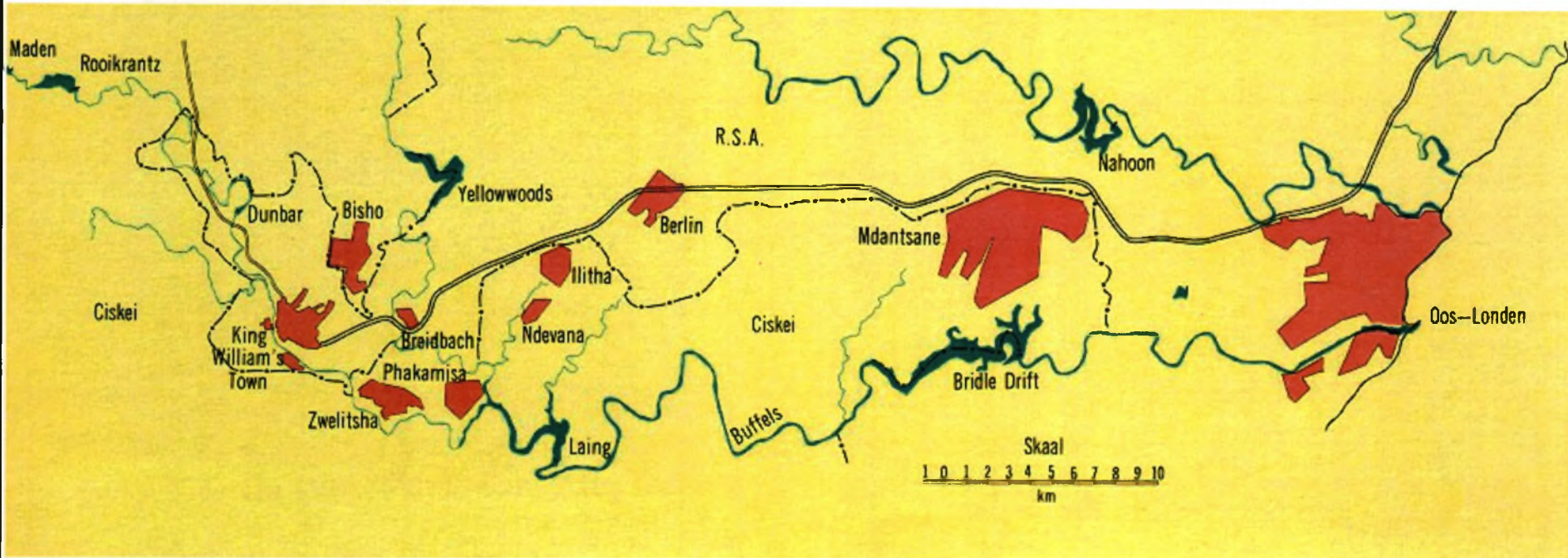


AFTER
171 DAYS

NUMERICAL MODELLING OF BOTTOM CHANGES DUE TO A CONSTANT WAVE CONDITION ($H_{mo} = 2$ m; $T_p = 11.9$ s; Direction = 214deg)

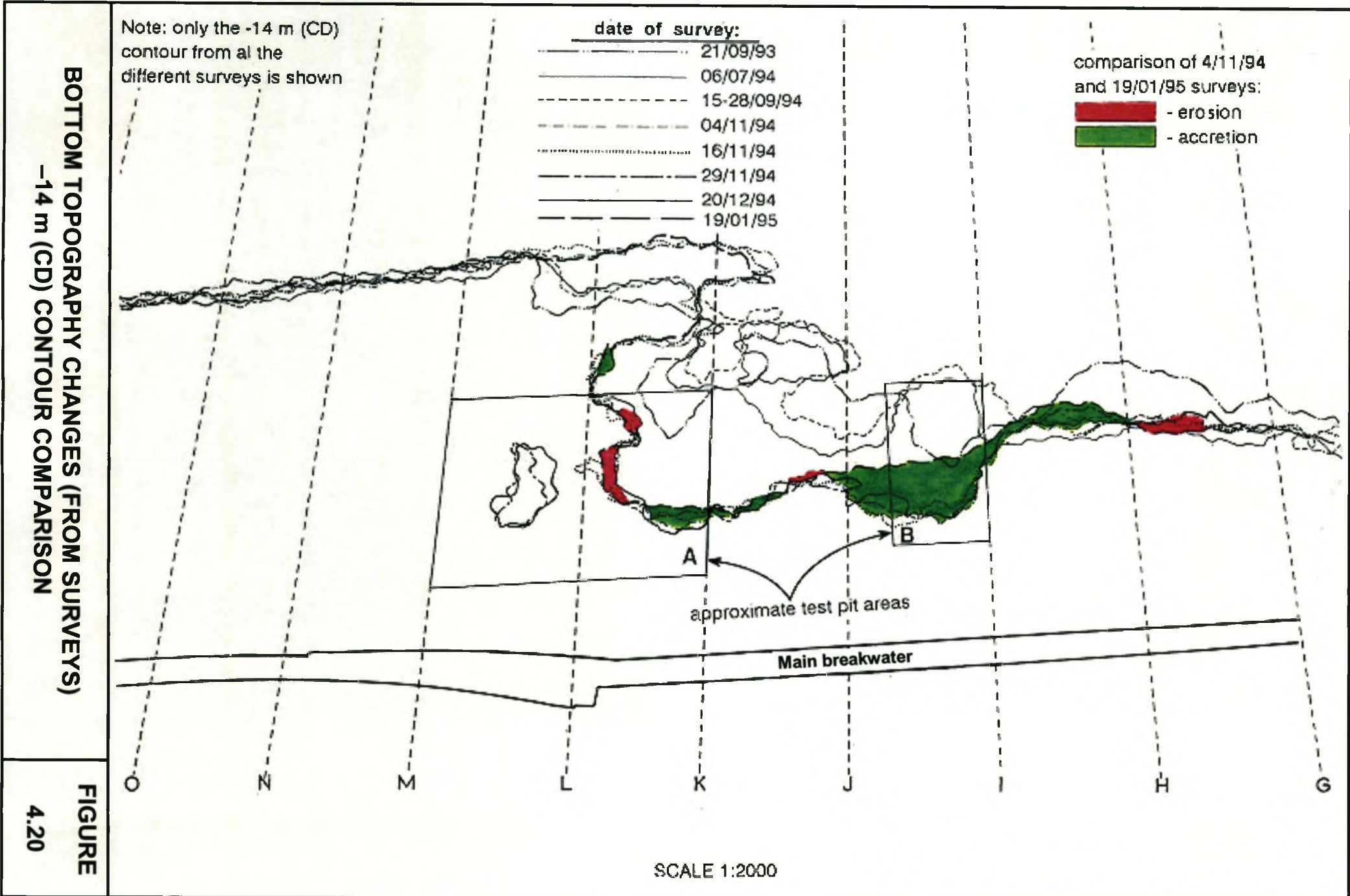
FIGURE

4.18

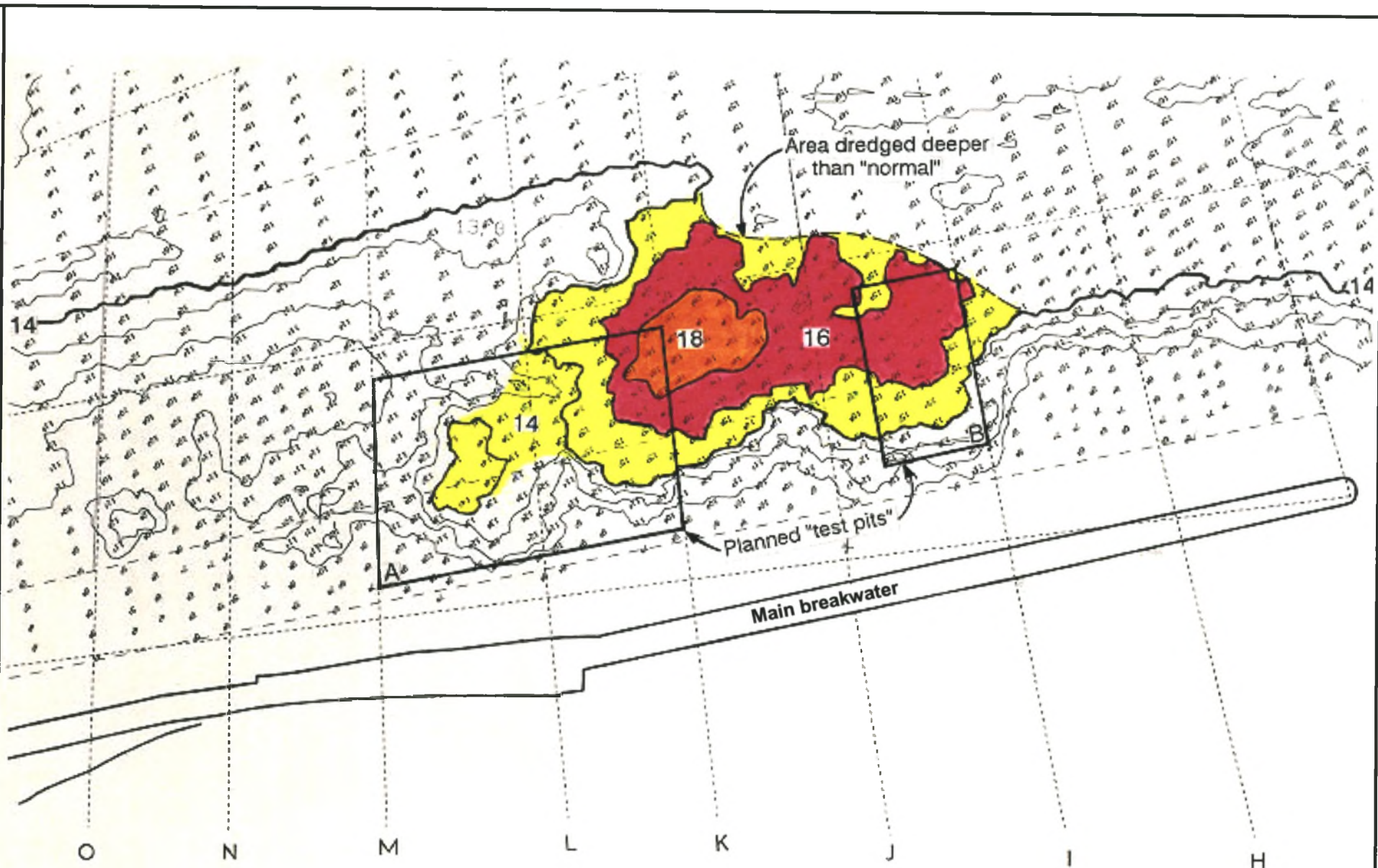


DAMS ON THE BUFFALO RIVER
(from DWA, 1986)

FIGURE
4.19

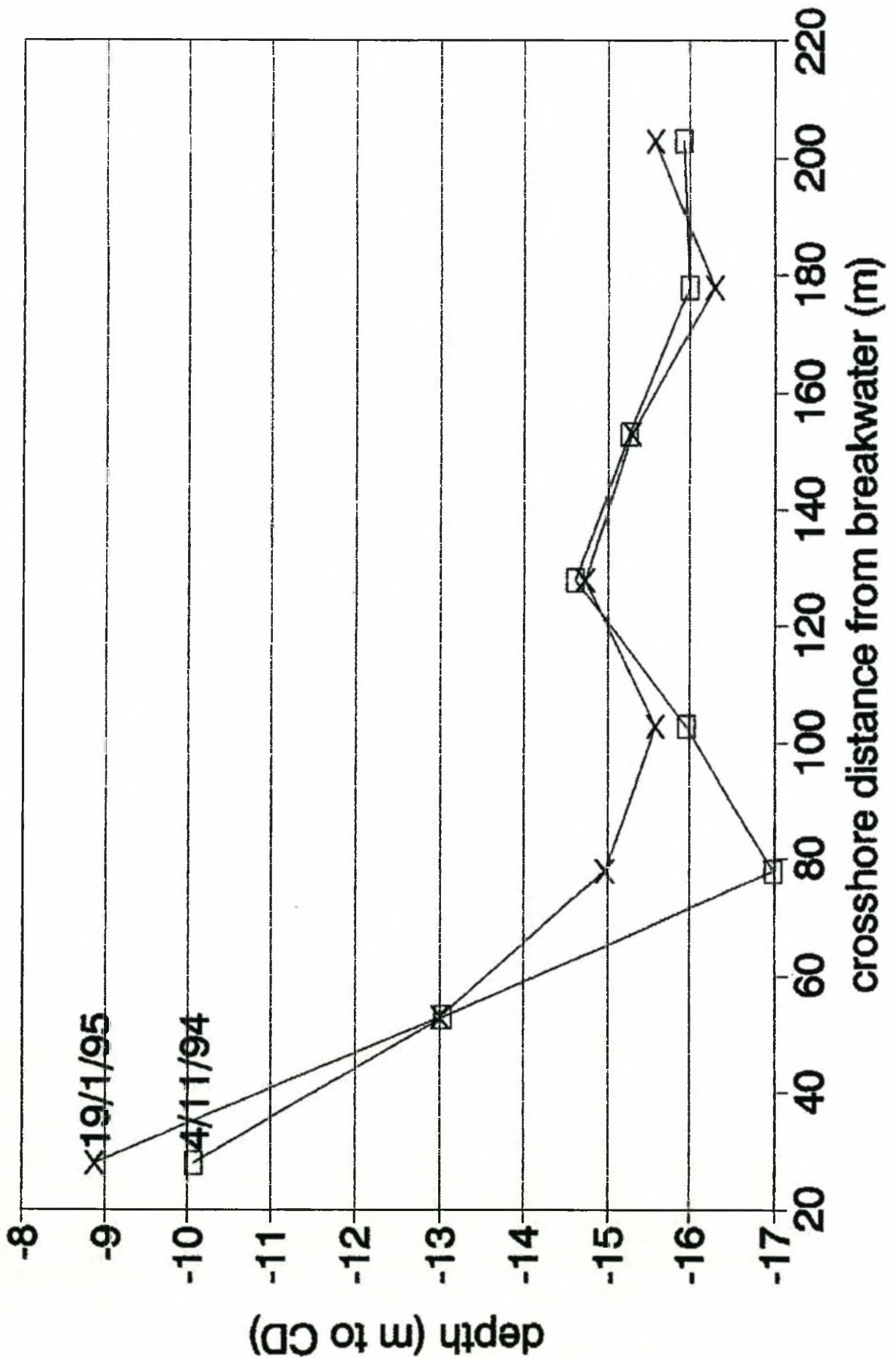


BATHYMETRIC SURVEY OF 04/11/1994



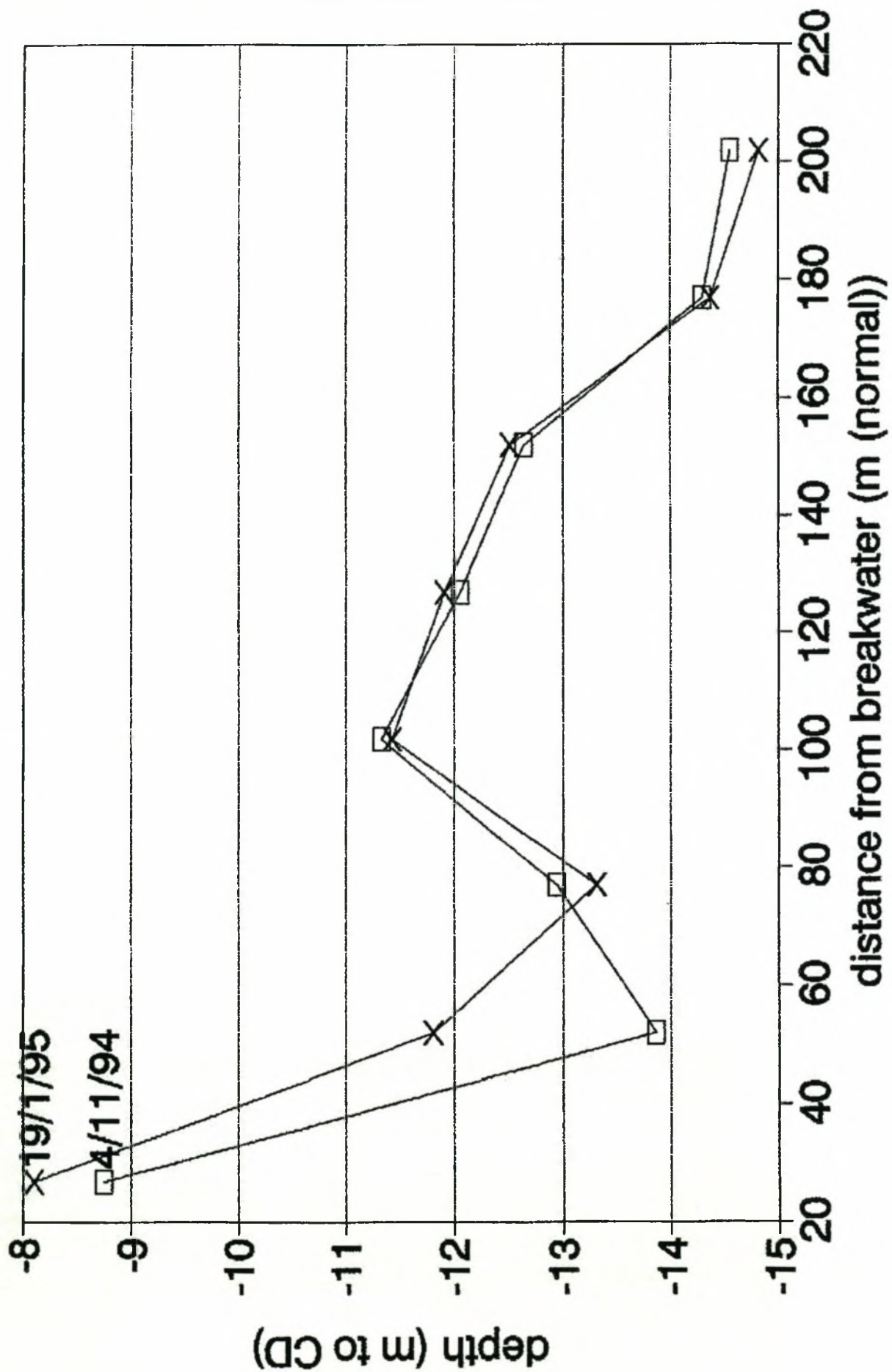
Scale 1 : 2000 (CD)

FIGURE
4.21



PROFILE COMPARISON: 04/11/1994 – 19/01/1995; PROFILE 150 m FROM HEAD OF BREAKWATER (Test Pit B)

FIGURE 4.22



PROFILE COMPARISON: 04/11/1994 – 19/01/1995; PROFILE 330 m FROM HEAD OF BREAKWATER (Test Pit A)

FIGURE 4.23

AREA OVER WHICH VOLUMES WERE CALCULATED

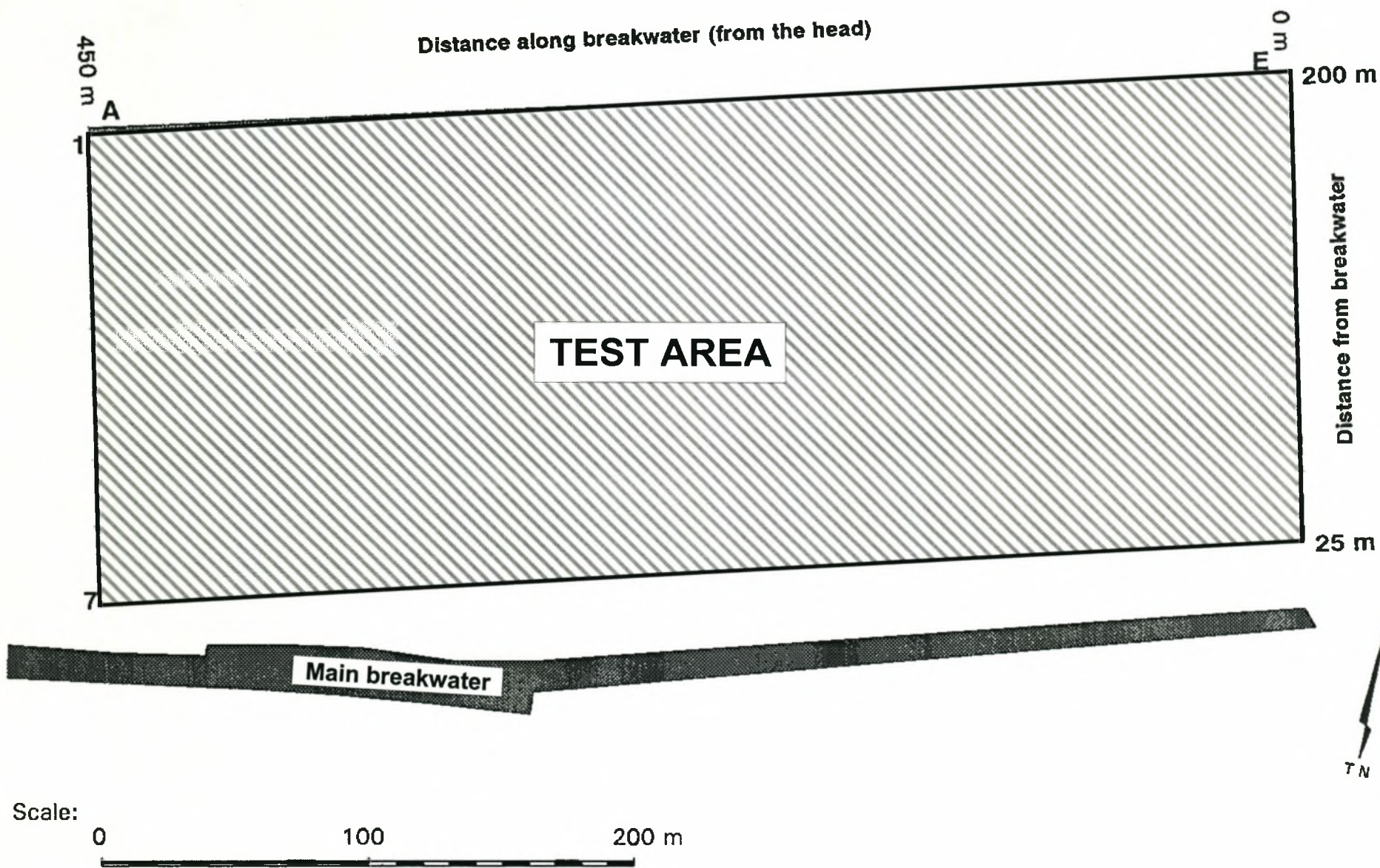
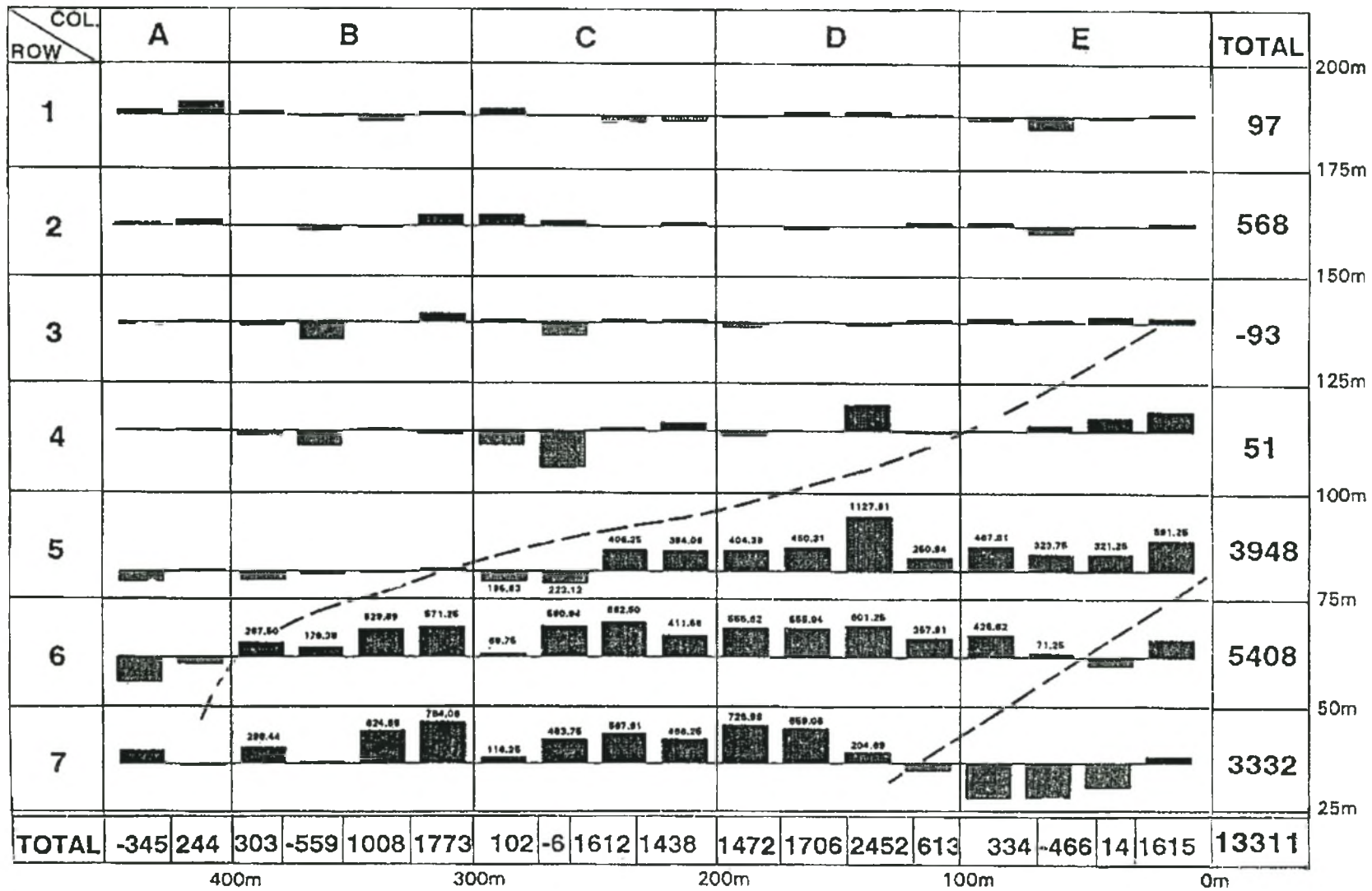


FIGURE 4.24

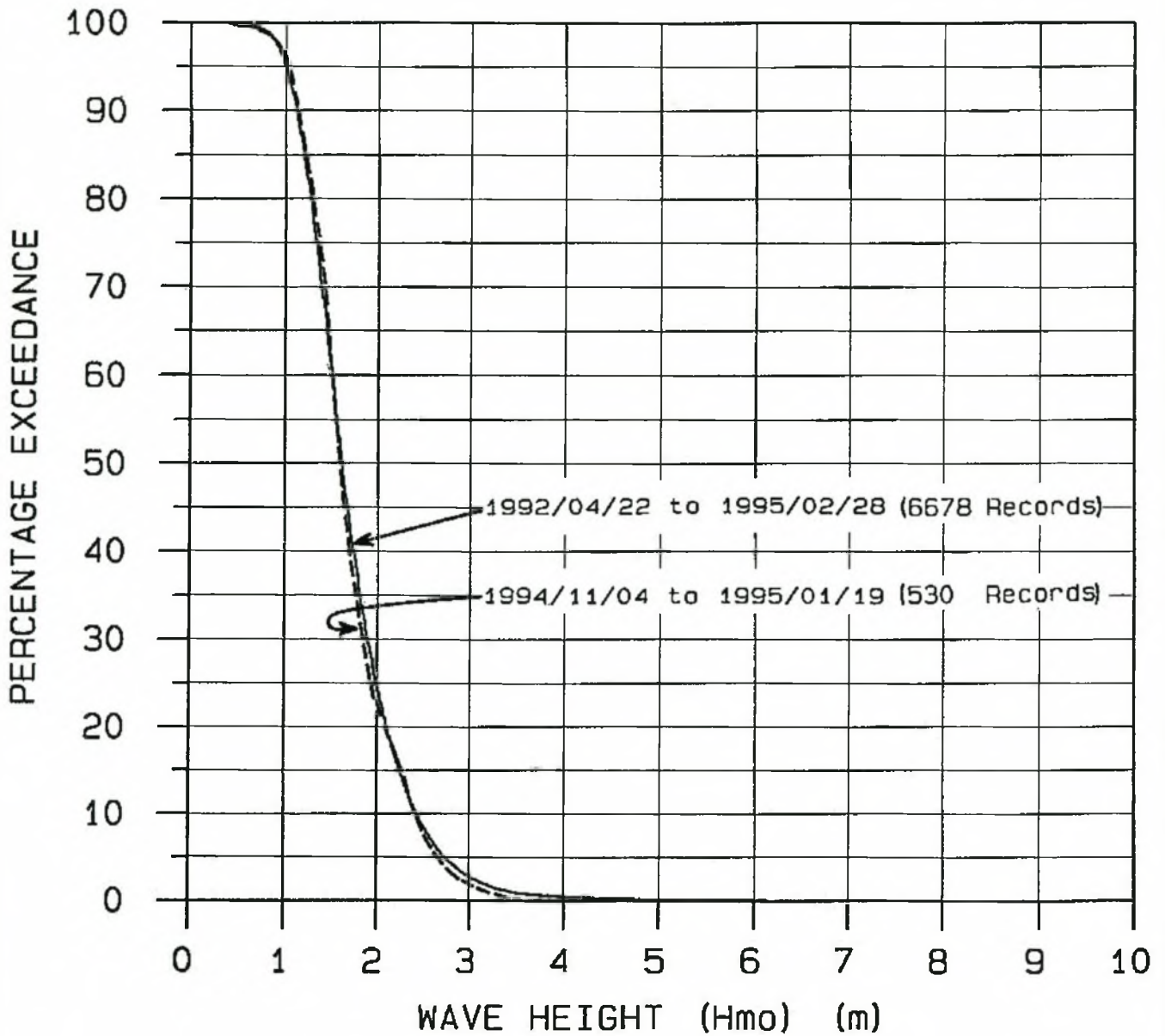
VOLUME DIFFERENCES BETWEEN SURVEYS OF
04/11/1994 AND 19/01/1995



Distance along breakwater (in m from head)

Note: The values are volume differences in m³.
Blocks above the line indicate accretion
while blocks below the line indicate erosion.

FIGURE
4.25

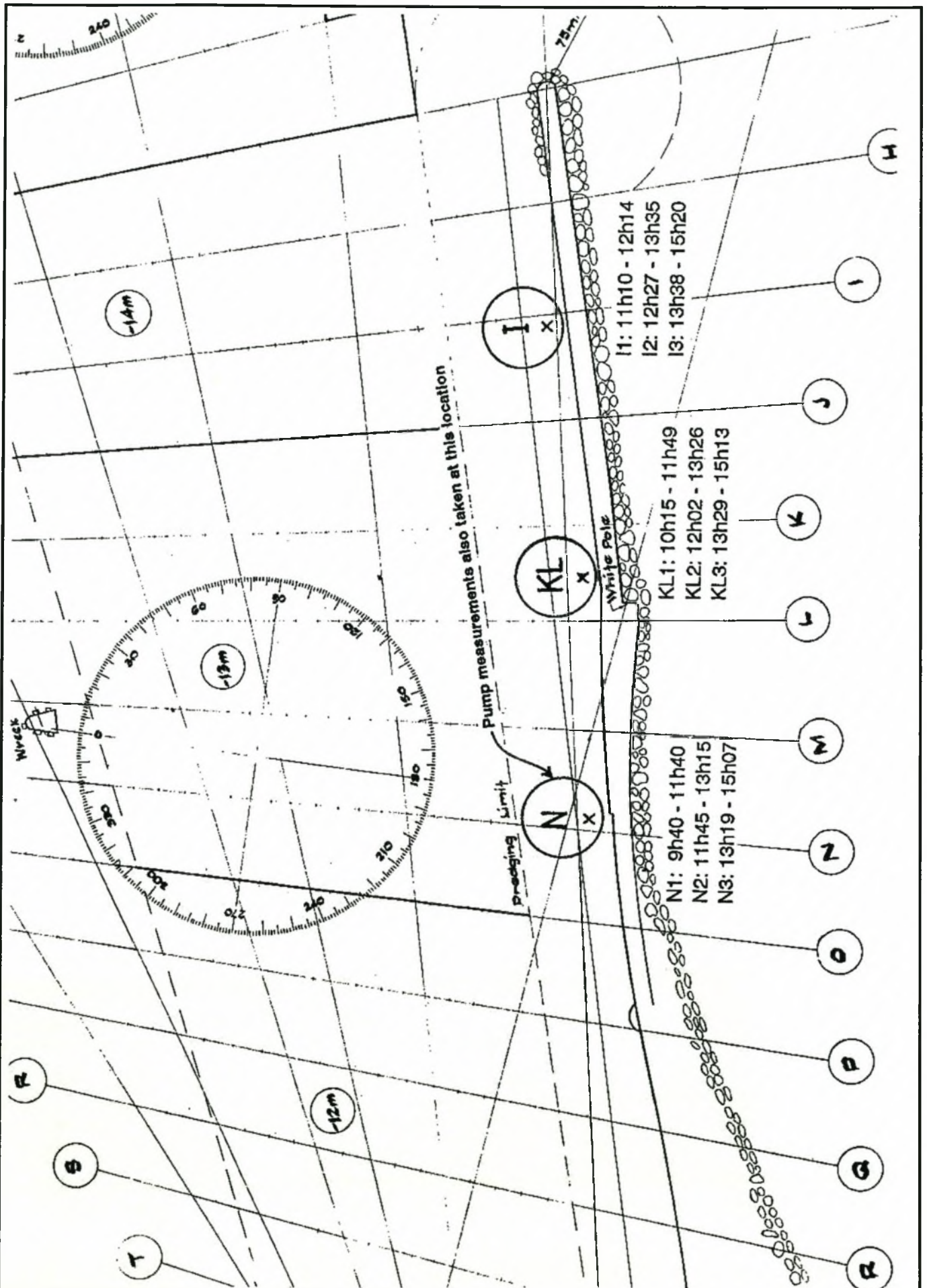


WAVE HEIGHT (Hmo) EXCEEDED					
1%	5%	10%	25%	50%	
3.48	2.75	2.42	1.99	1.63	1992/04/22 to 1995/02/28
3.28	2.66	2.41	1.95	1.61	1994/11/04 to 1995/01/19

WAVE HEIGHT (Hmo) PERCENTAGE EXCEEDANCE

FIGURE

4.26



**SEDIMENT CONCENTRATION MEASUREMENTS: 20/01/1995;
 LOCATIONS OF BAMBOO POLE AND PUMP MEASUREMENTS**

FIGURE

4.27

CONCENTRATIONS FROM BAMBOO POLE DATA:
TEST KL1, KL2 AND KL3

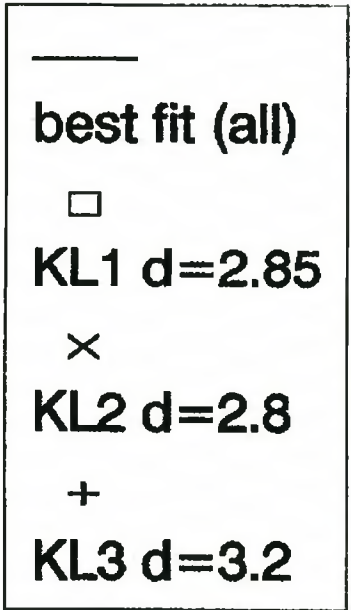
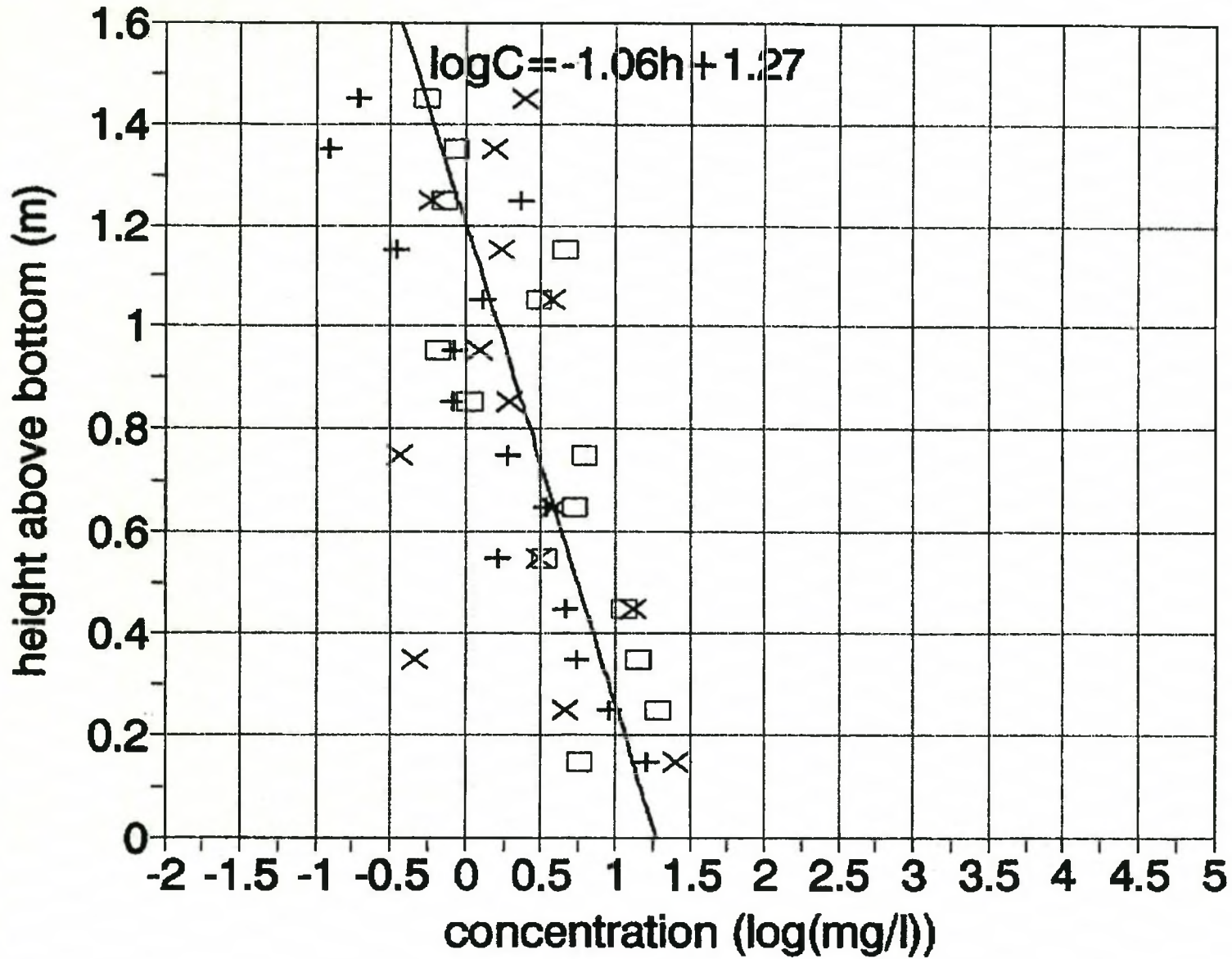
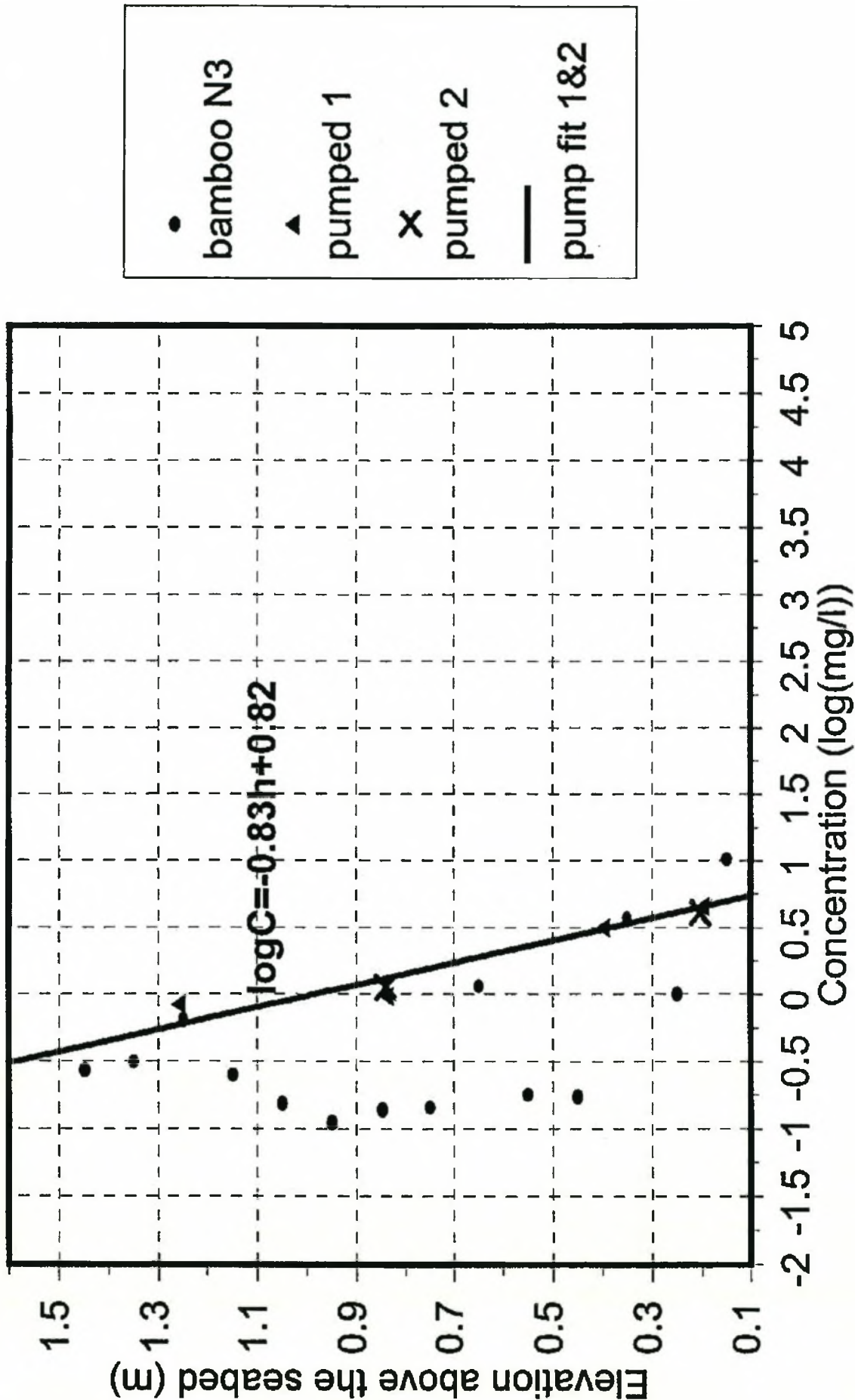
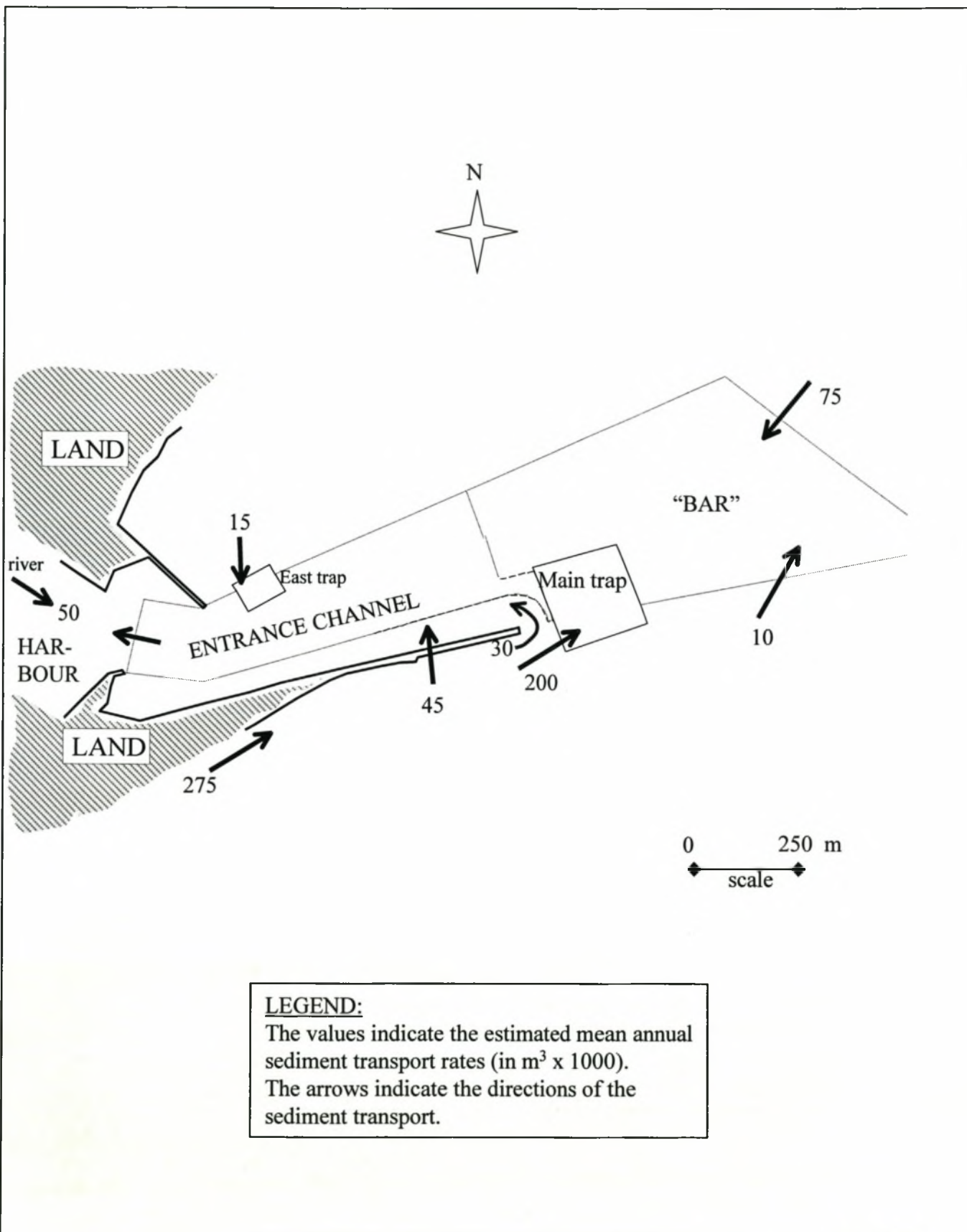


FIGURE
4.28



COMPARISON OF SEDIMENT CONCENTRATIONS:
BAMBOO POLE N3 VERSUS VACUUM PUMP

FIGURE
4.29



EAST LONDON SEDIMENT TRANSPORT REGIME

**FIGURE
4.30**

APPENDIX A

Hindcasting of deep-sea wave directions

[The wave hindcasting and wave direction determination described here, were mainly conducted by Mr M Rossouw of the CSIR. The interpretation and application of these results (Section 3.3.2) were conducted by the author.]

Sea and swell definitions

For the purpose of this study, **Sea** is defined as the wave condition resulting from wind near the area of interest. Sea wave energy is spread over a wide range of wave frequencies, primarily in the higher frequency band (above 0,1 Hz or below 10 s). In the event of high wind speeds of long duration appreciable energy also occurs at frequencies below 0,1 Hz (above 10 s).

Swell is defined as wave energy having propagated from distant areas, typically reaching the area of interest as regular, long-period waves.

Routine operational wave data processing and analysis

The six-hourly *Waverider* wave records, each of 17,5 minute duration, collected routinely at the study area were subjected to the standard FFT (*Fast Fourier Transform*) spectral analysis, resolving wave energy density with a frequency resolution of 0,00977 Hz. The spectral wave data, the *significant wave heights* and *spectral peak* and *zero-crossing wave periods* derived from the spectra were stored on a database.

Sea and swell separation

A simple method of separating **sea** and **swell** (based on their respective spectral energy-frequency distributions) was applied to the wave energy density spectra derived from the wave records.

The basis for the separation of sea and swell energy was laid down by assuming that wave energy at centre wave frequencies equal to and lower than $f=0,084$ Hz (above 11,9 s) could be entirely attributed to swell and that wave energy at centre wave frequencies equal to and higher than $f=0,123$ Hz (below 8,1 s) to sea. The wave energy at the three discrete centre frequencies in between those quoted above (namely $f=0,094$ Hz, $f=0,104$ Hz and $f=0,113$ Hz) is then allocated to swell and sea in accordance with simple relationships.

Allocation of sea and swell directions

Sea height and period data were matched with concurrent wind speed and direction data to approximate wave directions for each sea state. It was assumed that the dominant direction of any noticeable sea state could be associated with that of the wind field that caused it and that, even after the wind had subsided, the gradually decaying sea condition would maintain this direction.

Swell direction was hindcasted using synoptic weather charts. The method used took into account the movement and duration of swell generation systems over the southern ocean to identify the origin and direction of swell. Using the dispersive properties of swell, it was possible to derive expected times of arrival of swell components of known direction. These swell components could be matched with the measured spectral wave records and directions assigned accordingly.

*Sediment Transport Regime at East London***Results**

The weather and wave data (time series plots) recorded during 1 to 21 November 1996 are depicted in Figure A.1, while the synoptic weather charts for 18h00 universal time (u.t.) on 6 November 1996 to 12h00 (u.t.) on 7 November 1996 are depicted on Figure A.2 (as an example).

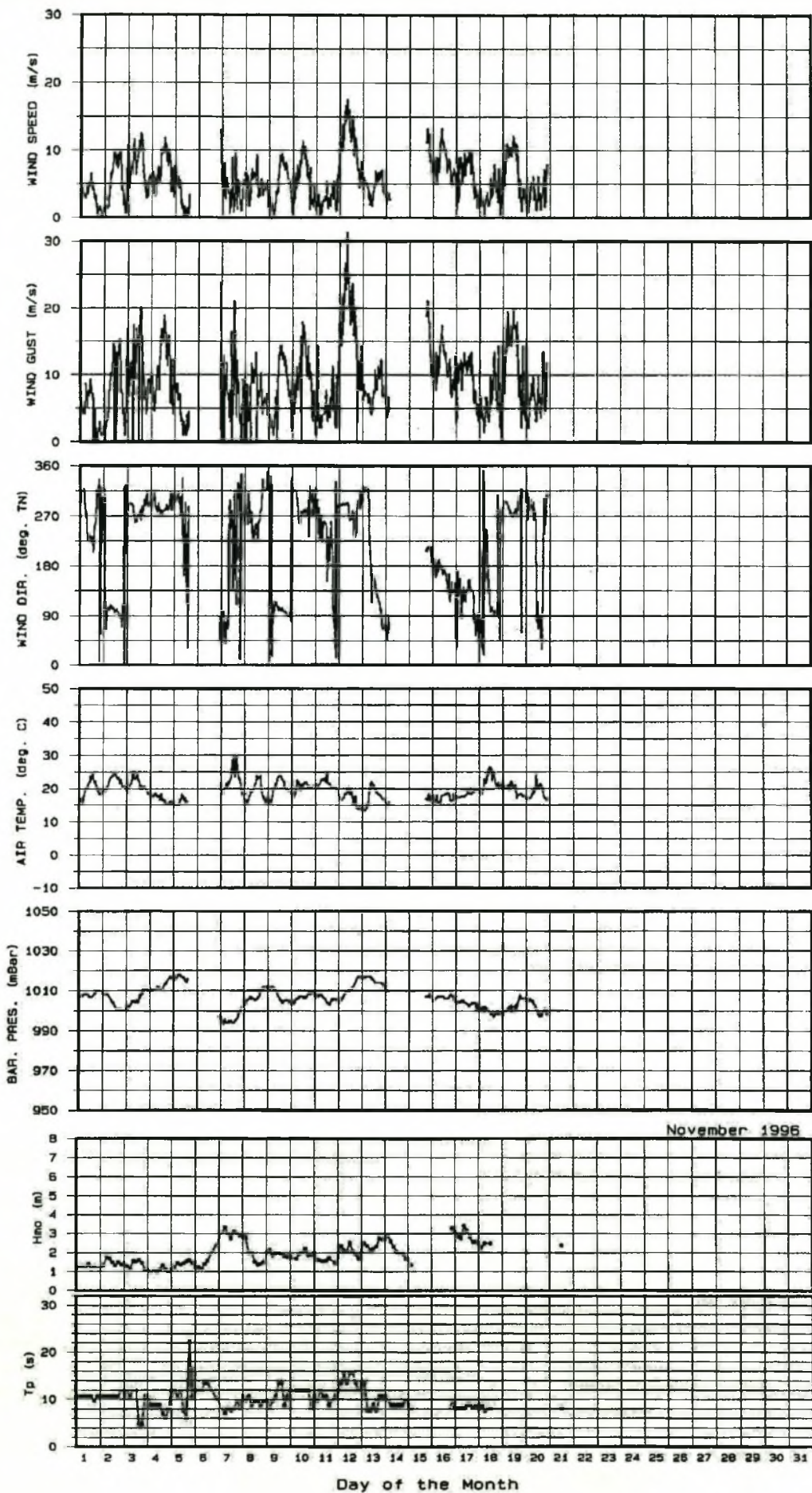
Based on this data and following the method described above, the sea and swell wave parameters including estimated deep-sea wave directions were obtained. These results are given in Table A.1.

Table A.1: Measured and predicted wave conditions at East London, 4 to 8 November 1996.

Station	Year	Month	Day	Time (GMT)	Total			Swell				Sea			
					H _{mo}	T _p	T _z	H _{mo}	T _p	T _z	Dir	H _{mo}	T _p	T _z	Dir
OL01	1996	11	4	0	1.06	10.67	3.80	0.48	10.67	12.17	SW	0.94	9.66	4.48	ENE
OL01	1996	11	4	300	0.97	8.83	4.11	0.33	10.67	12.01	SW	0.91	8.83	5.14	ENE
OL01	1996	11	4	600	1.09	8.83	4.40	0.45	10.67	12.69	SW	0.99	8.83	5.73	WSW
OL01	1996	11	4	900	0.97	8.83	4.74	0.44	10.67	10.79	SW	0.86	8.83	6.44	WSW
OL01	1996	11	4	1200	1.11	8.83	4.33	0.42	9.66	11.69	SW	1.03	8.83	5.56	SW
OL01	1996	11	4	1500	1.33	7.01	4.17	0.54	22.26	13.71	SW	1.21	7.01	4.84	SW
OL01	1996	11	4	1800	1.10	6.17	4.69	0.45	11.91	12.86	SW	1.00	6.17	5.23	SW/WSW
OL01	1996	11	4	2100	0.98	8.13	4.66	0.50	11.91	11.86	SW	0.84	8.13	5.62	SW/WSW
OL01	1996	11	5	0	1.10	11.91	4.55	0.64	11.91	11.69	SW	0.89	8.13	5.91	SW/WSW
OL01	1996	11	5	300	1.23	11.91	5.33	0.68	11.91	12.16	SW	1.03	8.13	5.60	SW/WSW
OL01	1996	11	5	600	1.44	10.67	5.08	0.75	10.67	11.60	SW	1.23	8.13	6.12	WSW
OL01	1996	11	5	900	1.36	11.91	4.50	0.69	11.91	11.94	SW	1.17	8.13	5.51	WSW
OL01	1996	11	5	1200	1.43	7.53	4.03	0.64	11.91	13.11	SW	1.28	7.53	4.92	SW
OL01	1996	11	5	1500	1.54	5.82	4.04	0.70	18.29	14.33	SSW	1.37	5.82	4.71	SW
OL01	1996	11	5	1800	1.58	22.26	4.29	0.85	22.26	13.66	SSW	1.34	4.97	4.67	SW
OL01	1996	11	5	2100	1.44	10.67	4.32	0.67	11.91	12.88	SSW	1.27	7.53	4.95	SW
OL01	1996	11	6	0	1.25	11.91	4.22	0.68	11.91	11.67	SSW	1.05	7.01	4.81	SW
OL01	1996	11	6	300	1.22	11.91	4.63	0.75	11.91	11.41	SSW	0.96	7.01	5.12	SW
OL01	1996	11	6	600	1.17	11.91	5.07	0.66	11.91	11.70	SSW	0.97	8.13	5.35	SW
OL01	1996	11	6	900	1.39	13.47	6.38	1.04	13.47	13.23	SSW	0.92	7.53	5.66	SW
OL01	1996	11	6	1200	1.56	13.47	6.89	1.08	13.47	12.36	SSW	1.11	7.01	6.25	SE
OL01	1996	11	6	1500											
OL01	1996	11	6	1800											
OL01	1996	11	6	2100											
OL01	1996	11	7	0											
OL01	1996	11	7	300											
OL01	1996	11	7	600	3.32	7.01	6.04	1.36	18.29	14.44	E	3.03	7.01	6.21	ENE
OL01	1996	11	7	900	2.96	8.13	6.45	0.97	18.29	16.11	E	2.8	8.13	6.3	ENE
OL01	1996	11	7	1200	2.73	7.53	6.14	1.05	22.26	16.31	ENE/E	2.52	7.53	6.14	ENE
OL01	1996	11	7	1500	3.12	8.13	6.07	1.39	22.26	14.39	ENE/E	2.79	8.13	6.15	ENE
OL01	1996	11	7	1800	3.01	9.66	6.36	0.97	15.52	13.5	ENE/E	2.65	8.83	6.54	ENE
OL01	1996	11	7	2100	2.88	8.13	5.58	1.2	10.67	12.68	ENE/E	2.62	8.13	6.53	ENE
OL01	1996	11	8	0	2.82	10.67	6.62	1.65	10.67	11.1	ENE/E	2.29	9.66	6.39	ENE
OL01	1996	11	8	300	2.76	9.66	6.62	1.43	9.66	11.92	ENE/E	2.36	9.66	6.78	ENE
OL01	1996	11	8	600	1.96	10.67	6.11	1.26	10.67	10.96	ENE/E	1.5	9.66	6.06	ENE
OL01	1996	11	8	900	2.01	8.83	6.41	1.05	10.67	11.04	ENE/E	1.71	8.83	6.57	ENE
OL01	1996	11	8	1200	1.53	9.66	6.66	0.93	10.67	10.94	ENE/E	1.22	9.66	6.67	ENE
OL01	1996	11	8	1500	1.38	9.66	6.78	0.69	10.67	11.24	ENE/E	1.2	9.66	7	ENE
OL01	1996	11	8	1800	1.41	8.83	6.97	0.57	10.67	11.33	ENE/E	1.29	8.83	7.24	WSW
OL01	1996	11	8	2100	1.51	9.66	7.25	0.7	10.67	10.93	SW	1.34	9.66	7.21	WSW

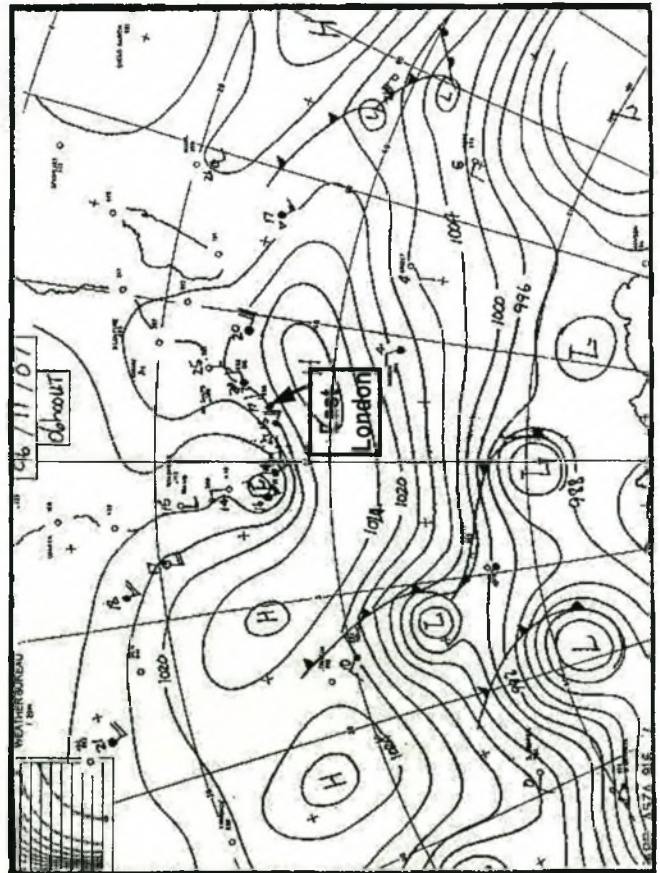
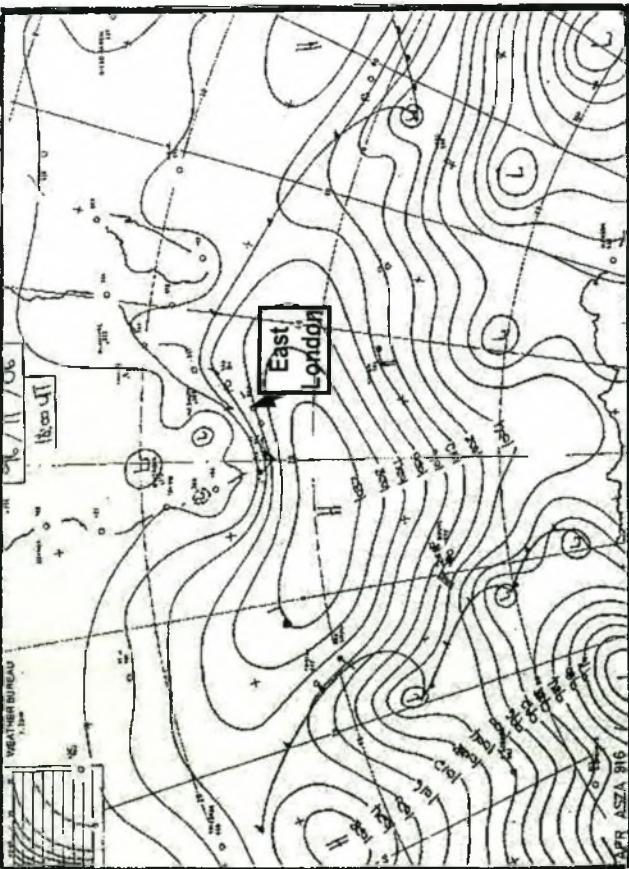
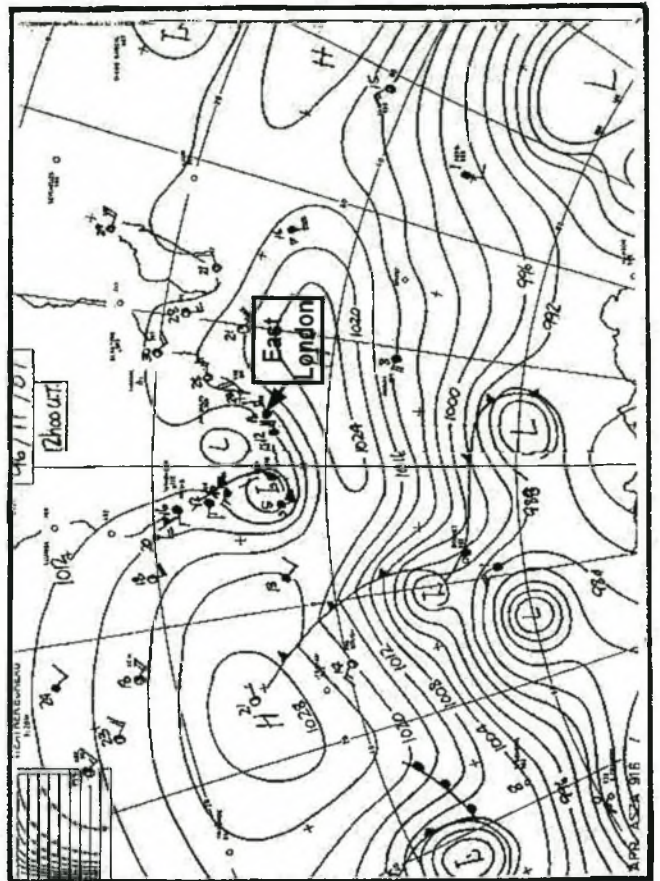
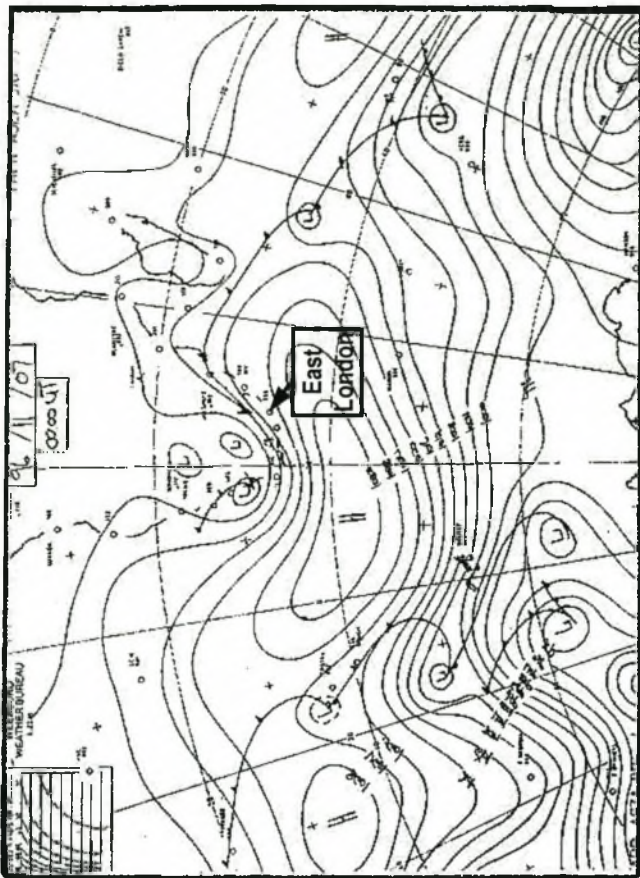
Note:

- Swell - swell component of wave (distant, long period)
- Sea - sea component of wave (local wind)
- H_{mo} - significant wave height (m)
- T_p - peak wave period (s)
- T_z - zero downcrossing wave period (s)
- Dir - wave direction (sector)



WEATHER DATA TIME HISTORIES, NOVEMBER 1996

FIGURE
A.1



SYNOPTIC WEATHER CHARTS: 6 TO 08/11/1996

**FIGURE
A.2**

APPENDIX B

Local wind effects on currents

Wind velocities and directions were recorded during all of the current measurements discussed in Section 3.3.3.3. While the currents off the main breakwater show a significant predominance of downcoast flows, the local wind climate shows a slight predominance of winds blowing in an upcoast direction. An assessment has been made of the effect of the wind on the currents.

Wind velocities recorded at the time of the current measurements ranged from 0 m/s to 14 m/s (0 to 27 knots). It was found that for wind velocities below 5 m/s the wind generally has no apparent effect on the current direction. Winds above 5 m/s start to have a small effect on the current directions but this is apparently not significant when the duration of the wind condition is short. For example, the March 1996 drogue measurements (e.g. Figure 3.31) show that during three of the four measurement periods the currents (even the surface currents) opposed the relatively strong (12 to 18 knots) winds. However, if a relatively strong wind (e.g. >10 m/s) blew consistently in the same direction for a relatively long time (> 3 days), the wind effect on the sub-surface currents eventually became evident.

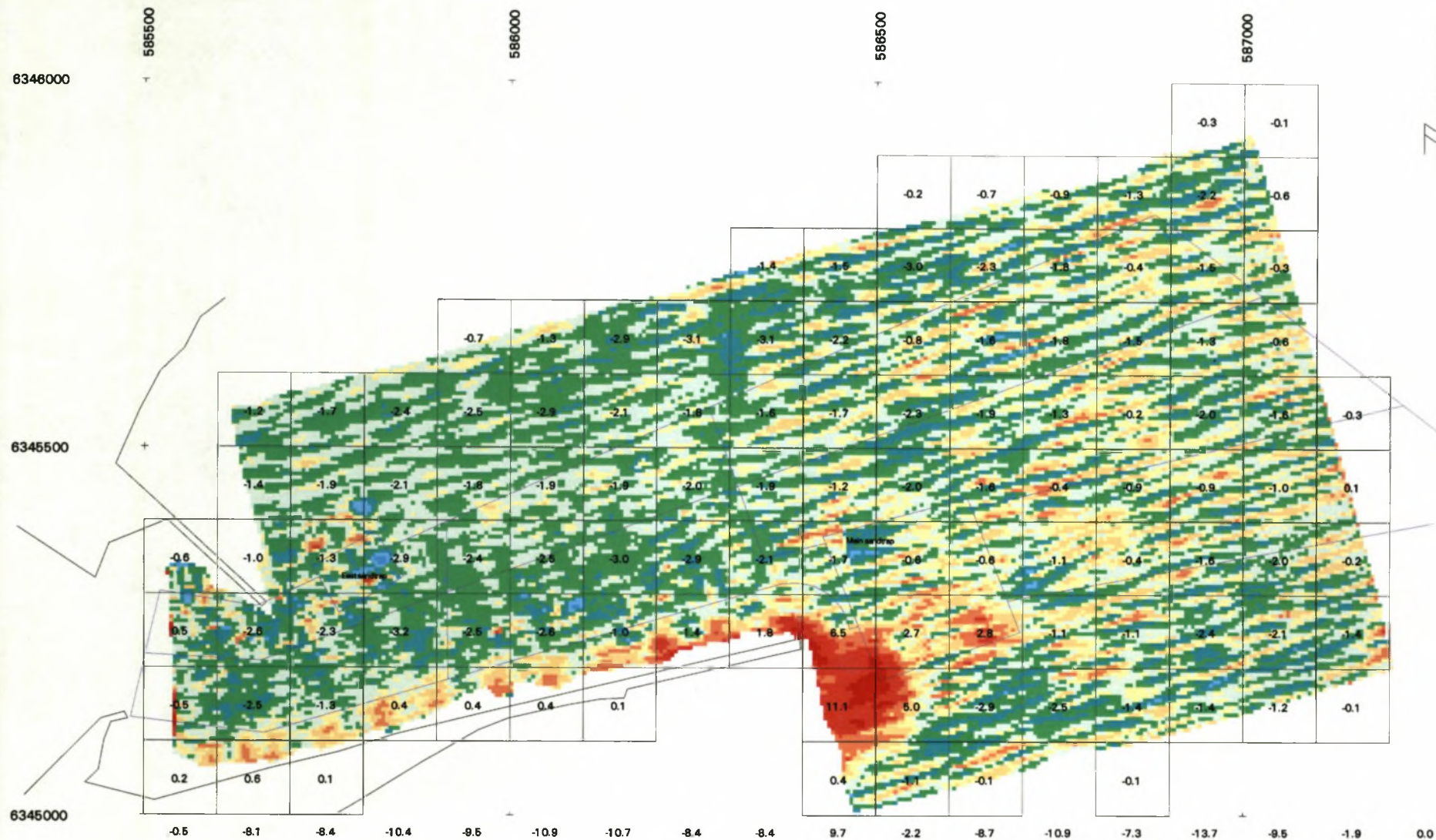
Thus, it is concluded that winds of approximately less than 10 m/s usually have an insignificant effect on sediment transports. Relatively stronger winds with long durations (at least a few days) could potentially eventually have a noticeable effect on the *sub-surface* currents and ultimately on sediment transport. For example, consistent strong south-westerly winds can cause a reversal from the normal current patterns in the nearshore zone, to a relatively weak north-easterly nearshore current (*excluding* the surf zone), when the Agulhas Current moves further offshore. At such times, there would be a potential for relatively low sediment transport in the upcoast direction in the nearshore zone, outside of the surf zone. Due to the low probability of occurrence of strong winds with long durations, local winds in general are consequently expected to have only a small impact on the overall sediment transport regime in the study area.

APPENDIX C

Additional bottom topography difference maps

These maps show changes in vertical elevation between consecutive bathymetric surveys as well as volume changes per unit area. Difference maps for the time periods July to September 1998, May to July 1998, and March to May 1996, are shown in Figures C.1, C.2 and C.3 respectively.

DIFFERENCE MAP FOR MAY TO JULY 1998

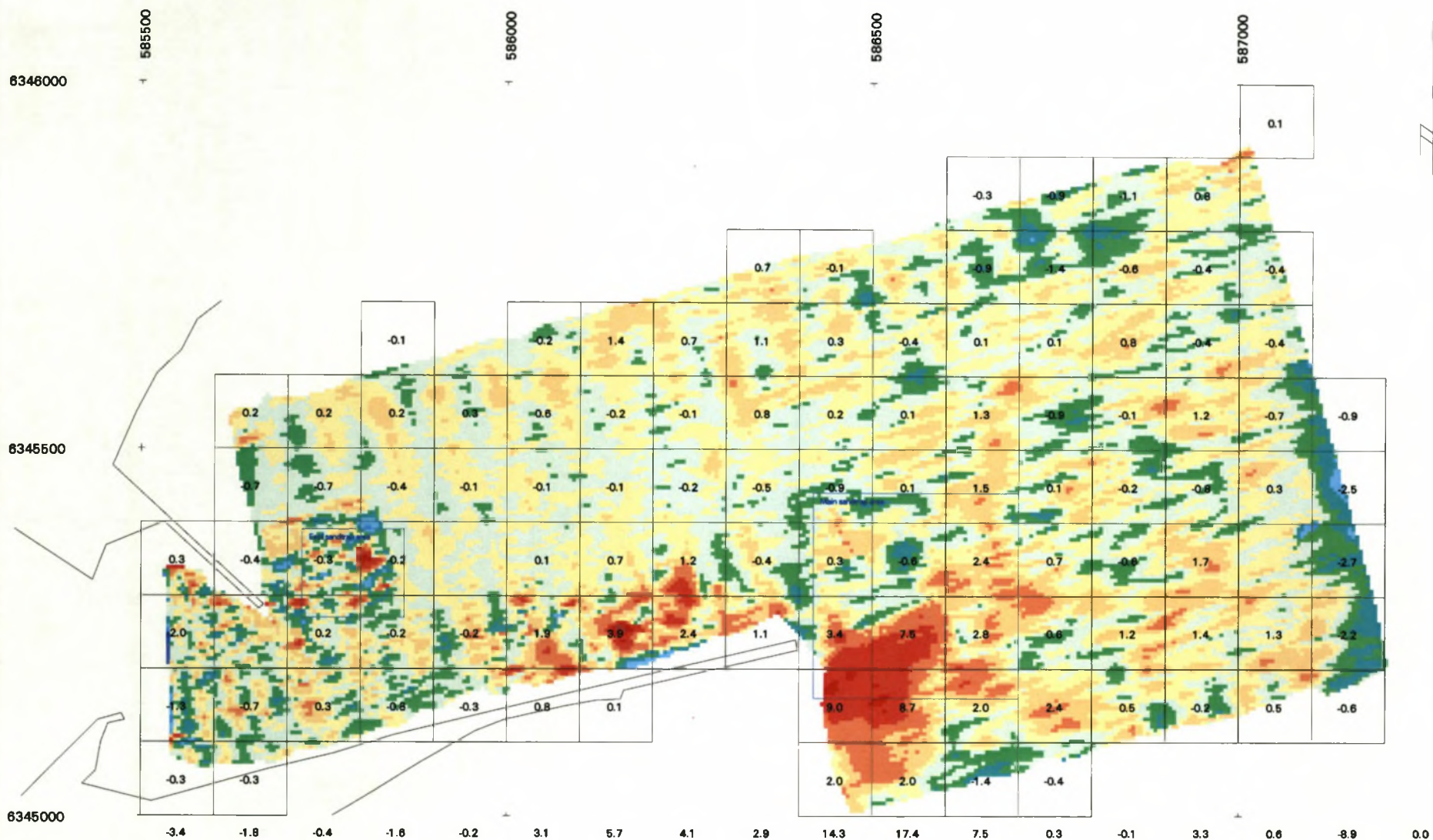


PORT OF EAST LONDON VOLUME CHART
 25 May 1998 TO combined 2 and 27 July 1998
 (UNITS : 1000m³)



FIGURE
 C.1

DIFFERENCE MAP FOR JULY TO SEPTEMBER 1998

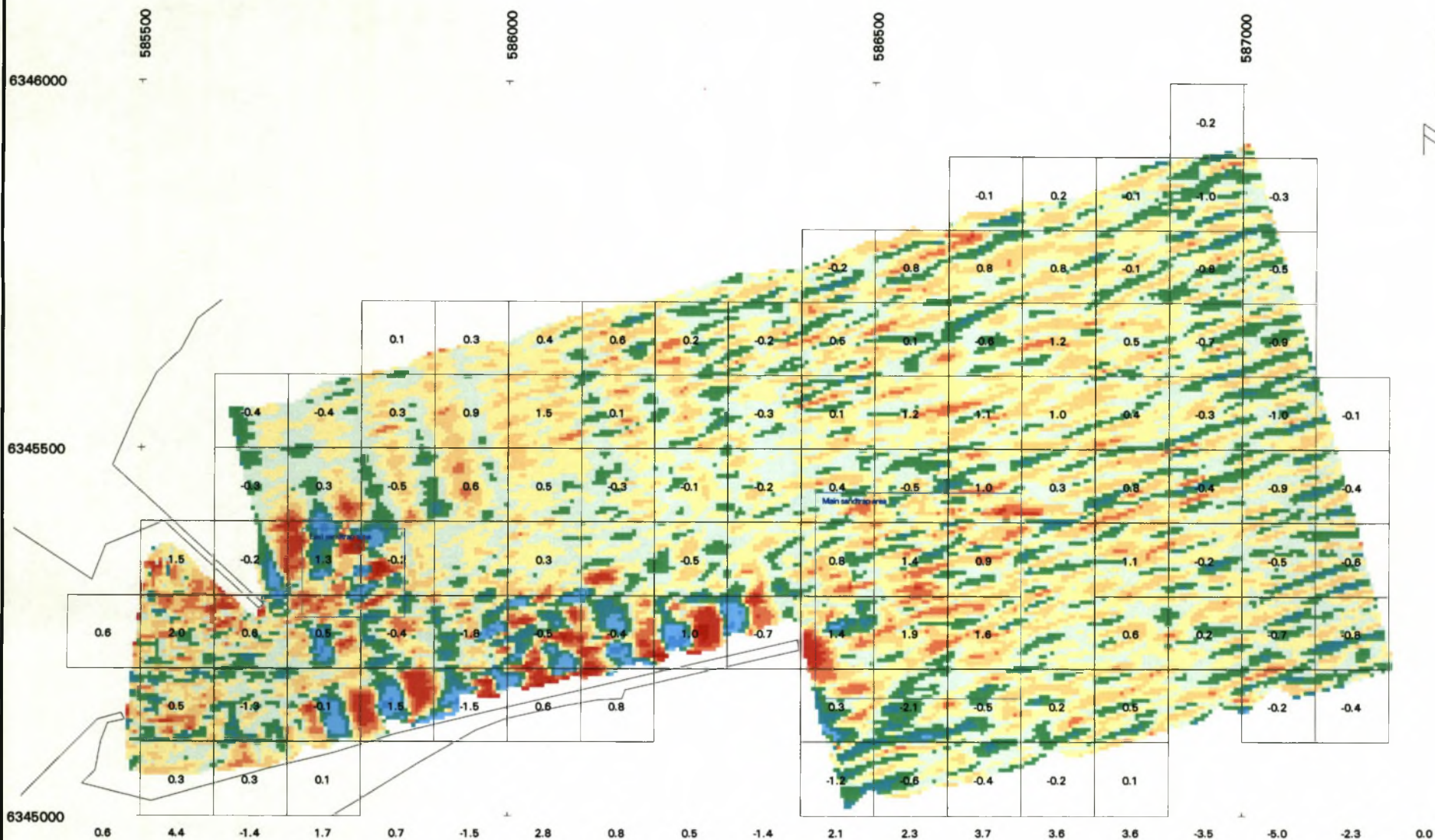


PORT OF EAST LONDON VOLUME CHART
 Combined 2 and 27 July 1998 TO 17 September 1998
 (UNITS : 1000m³)



FIGURE C.2

DIFFERENCE MAP FOR MACH TO MAY 1996



PORT OF EAST LONDON VOLUME CHART
20 March 1996 TO 15 May 1996
(UNITS : 1 000m ³)

Total volume: 11.8

0 250 metres

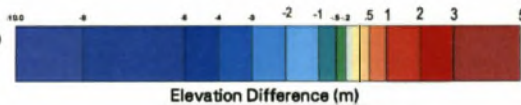


FIGURE C.3



SYNOPSIS

East London is situated on the south-eastern, Indian Ocean, coast of South Africa. The sediment transport regime at East London is quite unlike the regimes at other ports in South Africa. A major ocean current (the Agulhas) flows exceptionally close to the coastline in this area, thus significantly affecting nearshore sediment movements. The proximity of a strong ocean current *opposed* to the net longshore drift (wave driven transport) creates an anomalous **sediment transport regime** in comparison with that found at most coastlines throughout the world. Furthermore, the Port of East London (Figures 1.1 and 1.2) is the only major river harbour in South Africa, which all results in a very intricate pattern of sediment movement in the area, making it of particular interest. *The aims of this thesis are to study the littoral sediment transports at East London, achieve a holistic understanding of this complex sediment transport regime and to quantify the various transport rates as far as possible.*

The study area includes the coastal zone between the Goda and Nahoon Rivers (Figure 1.3) with the main focus on the Hood Point to Orient Beach area (Figure 1.4). The offshore marine environmental conditions are also considered as they have a strong influence on nearshore currents, waves and sediment transport patterns.

The prerequisite to understanding the sediment transport processes is a thorough investigation of the relevant coastal processes. Thus, an in-depth study is undertaken of the physical environmental data/information, nearshore processes and coastal dynamics that determine or

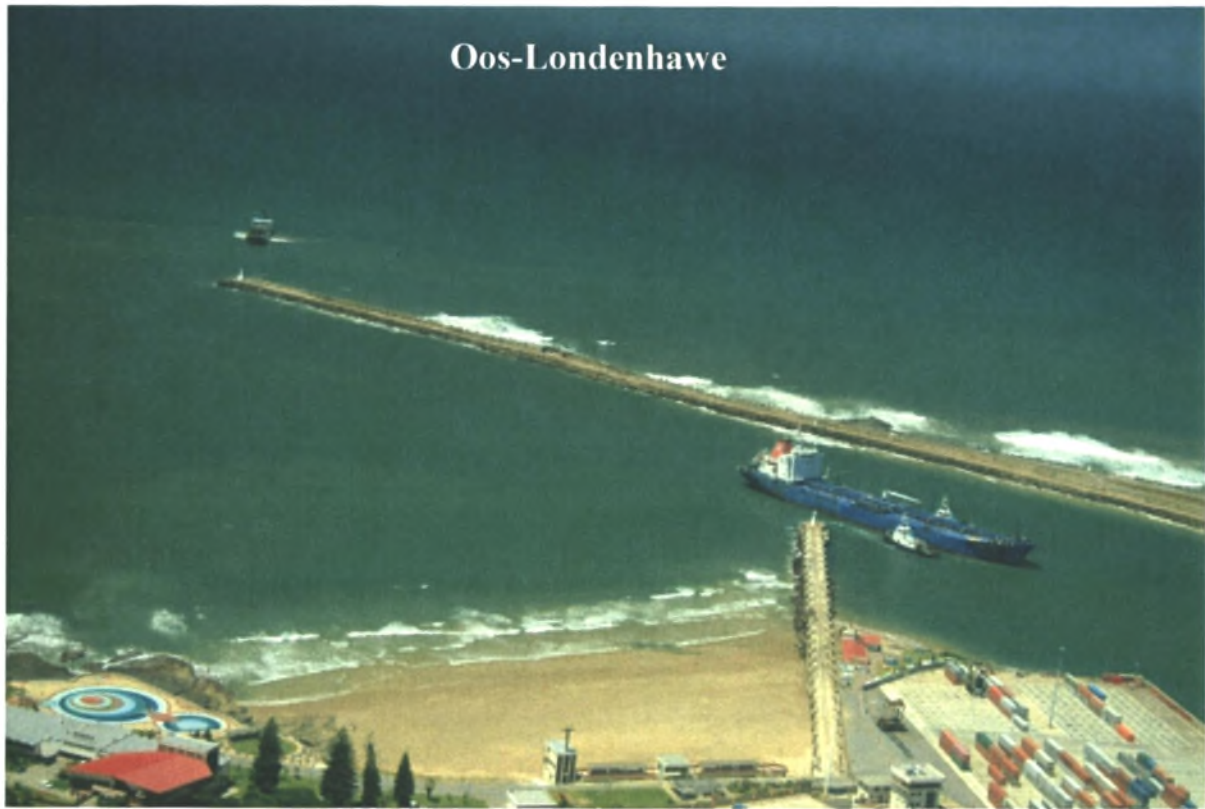
affect the sediment transport regime. These are: maintenance dredging volumes, bottom topography changes, the wave regime, the Agulhas Current, the nearshore current regime, the continental shelf sediment dynamics, sediment characteristics, seabed features, the Buffalo River, the tides, the wind regime, and coastal morphodynamics.

The specific contribution of each aspect of the environmental data/information to the qualitative understanding of the overall sediment transport regime is determined, and the various modes of sediment transport in different areas are quantified. *All of this information is then synthesised into an expose' of the sediment transport regime at East London, as briefly described in the conclusions (Section 5 and Table XI) and illustrated in Figure 4.30:*

There is a net longshore transport (wave driven) of about 250 000 m³ to 300 000 m³ per year on average from the Foreshore area towards the head of the main breakwater, with the total transport into the main sand trap and entrance channel areas from the south-west estimated at 275 000 m³/year. In the offshore zone, large amounts of sediment are transported downcoast by means of the strong Agulhas Current, which also has a significant influence on nearshore currents and sediment transport in the harbour entrance area. About 75 000 m³/year of sand is transported into the "Bar" area (the seaward part of the entrance channel) from the north-east with downcoast flowing nearshore currents, which is the predominant current direction. The riverine input into the harbour has been estimated at less than 10 000 m³/year of sand.

In this thesis, therefore, the sediment transport regime (and sediment transport balance) is derived for East London, providing for the first time a holistic understanding of the complex sediment transport regime.

It is recommended that more field data should be collected on specific aspects of this study and that the longer term effects of major weather systems should be investigated further. The numerical wave modelling should be extended and the integration of field measurements and numerical modelling to predict sediment transport and resultant bottom changes should be assessed in detail. Ultimately, the information contained in this thesis should feed into a wider regional investigation, with the aim of drawing up a sediment budget for the entire "regional macro sedimentary cell" of which the present study area forms a part.



SAMEVATTING

Oos-Londen is gelee aan die suid-oostelike, Indiese-oseaan, kus van Suid-Afrika. Die sedimentvervoer-regime by Oos-Londen is anders as dié by ander hawens in Suid-Afrika. 'n Hoof oseaan-stroom (die Agulhas) vloei besonder naby aan die kus in die gebied en het gevolglik 'n beduidende impak op sedimentvervoer-patrone in die nabystrandse gebied. Die direkte teenwoordigheid van 'n sterk diepwater stroom wat teen die netto (golfgedrewe) langsstrandse vervoer inwerk, veroorsaak 'n ongewone sedimentvervoer-regime in vergelyking met wat algemeen wêreldwyd gevind word. Daarbenewens is die Oos-Londenhawe (Figure 1.1 en 1.2) die enigste groot rivier-hawe in Suid-Afrika. Al dié ongewone toestande lei tot 'n ingewikkelde patroon van sedimentvervoer in die gebied. *Die doel van hierdie tesis is om die sedimentvervoer-regime by Oos-Londen te bestudeer, 'n holistiese begrip van die ingewikkelde sedimentvervoer-regime te verkry, en om die verskillende komponente van die sedimentvervoer regime so ver as moontlik te kwantifiseer.*

Die studiegebied sluit die kusstrook tussen die Goda- en Nagoonriviere in (Figuur 1.3). Daar word egter op die Hoodpunt tot Orientstrand-gebied gefokus (Figuur 1.4). Die diepwater, mariene omgewingstoestande word ook beskou, aangesien hul ook 'n groot impak op die nabystrandse strome, golwe en sedimentvervoer-patrone het.

'n Deeglike ondersoek van die toepaslike kusprosesse is 'n voorvereiste om 'n goeie begrip van die sedimentvervoer-prosesse op te bou. Gevolglik is 'n diepgaande ondersoek gedoen na die fisiese omgewingsdata en -inligting, nabystrandse prosesse en kusdinamika wat die sedimentvervoer-regime bepaal of beïnvloed. Dit het onderseker ingesluit na: onderhoudsbaggervolumes, bodemtopografie veranderinge, die golfklimaat, die Agulhasstroom, die

nabystrandse stroom-regime, die sedimentdinamika op die kontinentale plaat, sediment eienskappe, die windklimaat, die geaardheid van bodemvorme, die Buffelsrivier, getyaksie, en kus-morfologie.

Daar is bepaal wat elke aspek van die omgewingsdata/inligting bydra tot 'n kwalitatiewe begrip van die algehele sedimentvervoer-regime. Verder is die verskillende komponente van die sedimentvervoer in verskeie gebiede gekwantifiseer. *Al hierdie inligting is toe versoen in 'n beskrywing van die sedimentvervoer-regime by Oos-Londen, soos wat in die gevolgtrekkings (Deel 5 en Tabel XI) gegee word en in Figuur 4.30 geïllustreer word:*

Daar is 'n gemiddelde netto golfgedrewe langsstrandse vervoer van ongeveer 250 000 m³ tot 300 000 m³ per jaar vanaf die strandgebied suid van die hawe na die punt van die hoof-golfbreker. Die totale beraamde vervoer vanaf die suidweste na die hoof-sandvangput en ingangskanaal-gebied is 275 000 m³ per jaar. In die diepsee word groot hoeveelhede sediment langs die kus af vervoer deur die sterk Agulhasstroom, wat ook 'n beduidende impak het op nabystrandse strome en sedimentvervoer in die hawe-ingangsgebied. Omtrent 75 000 m³ sand word per jaar na die "Bar"-gebied vervoer vanaf die noord-ooste deur nabystrandse strome wat langs die kus af vloei. Dit is ook die oorwegende nabystrandse stroomrigting (uitgesluit die brandersone). Sandafsetting in die hawegebied afkomstig van die Buffelsrivier word op minder as 10 000 m³ per jaar geskat.

Die sedimentvervoer-regime (en sediment-balans) by Oos-Londen word dus afgelei, en vir die eerste keer saamgesnoer in 'n breë insig van die komplekse sedimentvervoer-regime.

Daar word aanbeveel dat meer velddata verkry moet word oor sekere aspekte van hierdie studie en dat die langtermyn-impakte van groot weerstelsels verder ondersoek word. Die wiskundige golf-modellering moet uitgebrei word en die gesamentlike benutting van veldmetings met wiskundige modellering om sedimentvervoere en gevolglike bodemveranderinge te voorspel, moet deeglik ondersoek word. Uiteindelik behoort die inligting vervat in hierdie tesis in te voer in breër streeks-ondersoeke, met die oog daarop om 'n sediment-begroting vir die "Ooskaapse makro-sedimentvervoer-regime" op te stel.

ACKNOWLEDGEMENTS

I would like to convey my special thanks to the following organisations and people for their active support, guidance and assistance with this study:

- The National Ports Authority of South Africa (NPA) and in particular Mr Vonk Claassens (formerly The Port Engineer of East London), for permission to make use of data and reports relevant to the study. I would also like to thank Mr Claassens and his staff for the assistance given in conducting many of the field investigations that formed part of the input into this thesis.
- The CSIR for making available various reports (including those authored by myself).
- Special thanks to Dr Koos Schoonees for valuable advice.
- Mr Eddie Bosman, my promoter, and Dr Andre van Tonder, both for valuable advice.
- Mrs Juanita van Heerden, for her accomplished typing of the original draft.

QUOTES

“O investigator (engineers and councillors), do not flatter yourself that you know the things nature performs for herself, but rejoice in knowing the purpose of those things designed by your own mind.” Leonardo da Vinci (1452-1519)

“...when you can measure what you are speaking about and express it in numbers you know something about it; but when you cannot measure it, when you cannot express it in numbers, your knowledge is of a meagre and unsatisfactory kind.” Sir William Thomson (Lord Kelvin) (1883)

“As far as the laws of mathematics refer to reality, they are not certain; and as far as they are certain, they do not refer to reality.” Albert Einstein (1879-1955)

“...if we are not careful we may easily become victims of the fallacy that conclusions arrived at in papers heavily laden with mathematical equations and numerical data, or with computer results, have, ipso facto, a higher degree of reliability than those arrived at by more “primitive” methods.” *Is Being Quantitative Sufficient*, M. King Hubbert (1974)

“The genuine goal of scientific computation in engineering should be insight, not numbers.” *Geology and Mathematics*, H. Schaeben (1988)

Course curriculum successfully completed by the candidate:

Code	Subject	Credits
WO043	Coastal Engineering (Kusboukunde I)	4
WO06	Coastal Engineering (Kusboukunde II)	4
WH05	River Hydraulics (Rivierhidroulika)	4
WD01	Dam Design (Dambou)	4
WH02	Applied Hydrology (Toegepaste Hidrologie)	4
WW01	Water and Wastewater Management (Wateromgewingsleer)	4
WW02	Water Treatment Processes (Suiweringsprosesse)	4
GK04	Management of Technology (Bestuur van Tegnologie)	4
TOTAL		32

Related peer reviewed publications by the candidate:

- Theron, A K and Schoonees, J S (1998). Defining an unusual littoral regime to optimise dredging at East London. *26 th International Conference on Coastal Engineering*, ASCE, Copenhagen, Denmark. Vol 3: 3479-3489.
- Theron, A K, Schoonees, J S, Burggraaf, A and Raw, A J (1998). Harbour sedimentation and dredging optimisation at some Southern African ports. *29 PIANC*, Netherlands, Section II, Subject 5: 47-55.
- Theron, A K and Schoonees, J S (1999). Sand Transport Through and Around the Main Breakwater at East London. *Proceedings*, Fourth International Symposium on Coastal Engineering and Science of Coastal Sediment Processes, Coastal Sediments '99, New York, ASCE. Volume 3: 2371 - 2384.
- Theron, A K and Schoonees, J S (2000). Optimization of dredging through understanding the unusual littoral regime at East London. *Civil Engineering Magazine*, SAICE. Dec 2000 Vol 8 No 10:11-12.
- Theron, A K, Schoonees, J S and Claassens, H (2002). Port of East London : design and optimisation of the sand traps. *Journal of SA Inst Civ Eng*, Vol 44(4): 8-15.

Sediment Transport Regime in the area of the East London Harbour Entrance

CONTENTS

	Page
Synopsis.....	iii
Samevatting	v
Acknowledgements.....	vii
Quotes.....	vii
Course curriculum successfully completed by the candidate.....	viii
Related peer reviewed publications by the candidate.....	viii
List of tables.....	xii
List of figures.....	xiii
List of symbols.....	xv
Definition of selected terms.....	xvi
1. INTRODUCTION.....	1
1.1 AIMS AND OBJECTIVES.....	1
1.2 THE PHYSICAL STUDY AREA.....	1
1.3 KEY QUESTIONS.....	2
1.4 LOGICAL STRUCTURE OF THESIS.....	3
2. BACKGROUND ON COASTAL SEDIMENT TRANSPORT.....	4
2.1 BACKGROUND.....	4
2.1.1 <i>Origin of marine sediments</i>	4
2.1.2 <i>Littoral sediment transport and wave effects</i>	5
2.1.2.1 General	5
2.1.2.2 Longshore sediment transport.....	6
2.1.2.3 Cross-shore sediment transport.....	7
2.1.2.4 Wind-blown sediment transport.....	9
2.1.3 <i>Sediment transport in deeper water</i>	9
2.1.4 <i>River and estuarine sediment transports</i>	10
2.2 MEASUREMENTS AND THEORETICAL METHODS TO DETERMINE SEDIMENT TRANSPORTS.....	10
2.2.1 <i>General</i>	10
2.2.2 <i>Main "measurement methods" employed to determine sediment transports</i>	11
2.2.3 <i>Main theoretical methods employed to determine sediment transports</i>	12
3. ENVIRONMENTAL DATA AND COASTAL PROCESSES AFFECTING THE SEDIMENT TRANSPORT REGIME.....	16
3.1 GENERAL AND PURPOSE.....	16
3.2 WAVE REGIME	16
3.2.1 <i>Introduction</i>	16

3.2.2	<i>General deep-sea wave climate</i>	16
3.2.3	<i>General wave exposure of the study area</i>	17
3.2.4	<i>Measured nearshore wave conditions</i>	17
3.2.5	<i>Nearshore wave directions from aerial photographs</i>	18
3.2.6	<i>East London VOS data</i>	19
3.2.7	<i>Agulhas Bank wave data</i>	19
3.2.8	<i>Simulated nearshore wave regime</i>	20
3.2.9	<i>Recent directional wave recordings</i>	23
3.2.10	<i>Surf zone widths</i>	24
3.3	CURRENT REGIME	25
3.3.1	<i>Background</i>	25
3.3.2	<i>Surf zone (wave induced) currents</i>	26
3.3.2.1	<i>Surf zone currents measured south-west of the main breakwater</i>	26
3.3.2.2	<i>1990 and 1993 field observations</i>	30
3.3.2.3	<i>Calculated longshore current velocities</i>	30
3.3.3	<i>Deeper water currents</i>	31
3.3.3.1	<i>General regional current regime</i>	31
3.3.3.2	<i>Overall current patterns in the Nahoon - Hood Point area</i>	31
3.3.3.3	<i>Currents in the vicinity of the entrance channel</i>	34
3.3.6	<i>Currents in the lee of the main breakwater</i>	36
3.3.7	<i>Numerical current modelling</i>	38
3.4	CONTINENTAL SHELF SEDIMENT DYNAMICS	41
3.5	WIND REGIME	42
3.5.1	<i>General</i>	42
3.5.2	<i>Data analyses and interpretation</i>	43
3.5.3	<i>Aeolian transport</i>	43
3.6	COASTAL MORPHODYNAMICS	44
3.6.1	<i>General</i>	44
3.6.2	<i>Long-term shoreline changes adjacent to the port</i>	44
3.6.3	<i>Sediment transports indicated from shoreline evolution</i>	45
3.7	SEABED FEATURES AND TRANSPORTS INDICATED FROM SONAR SURVEY	45
3.8	SEDIMENT CHARACTERISTICS AND GRAIN SIZE TRENDS	46
3.8.1	<i>Sediment Characteristics</i>	46
3.8.2	<i>Transport patterns from grain size trends</i>	48
4.	QUANTIFICATION OF SEDIMENT TRANSPORT REGIME	49
4.1	TRANSPORT RATES FROM SURVEYS AND DREDGING RECORDS	49
4.1.1	<i>Old and new sand trap layouts</i>	49
4.1.2	<i>Bottom Changes</i>	49
4.1.2.1	<i>Bottom changes</i>	49
4.1.2.2	<i>Sections through the sand traps</i>	50
4.1.3	<i>Dredging Records</i>	50
4.1.3.1	<i>Dredging Data</i>	50
4.1.3.2	<i>Main sand trap</i>	51
4.1.3.3	<i>Dredging areas</i>	51

4.1.4	<i>Conclusions</i>	52
4.2	LONGSHORE SEDIMENT TRANSPORT.....	53
4.2.1	<i>General</i>	53
4.2.2	<i>Theoretically determined longshore transport</i>	53
4.2.3	<i>Transport rate calculated from beach accretion</i>	55
4.2.4	<i>Distribution of longshore transport</i>	55
4.3	SEDIMENT TRANSPORT IN DEEPER WATER.....	56
4.3.1	<i>Methodology</i>	56
4.3.2	<i>Transport into the dredging areas</i>	57
4.4	MATHEMATICAL SEDIMENT TRANSPORT MODELLING.....	58
4.4.1	<i>Initial model tests</i>	58
4.4.2	<i>Morphological modelling</i>	58
4.4.2.1	<i>Background and approach</i>	58
4.4.2.2	<i>DELFT3D-MOR wave regime schematisation</i>	60
4.4.2.3	<i>Preliminary conclusions</i>	62
4.5	RIVER AND ESTUARINE SEDIMENT TRANSPORTS.....	63
4.5.1	<i>Sediment input from the Buffalo River</i>	63
4.5.2	<i>Tidally induced transports in/out of the harbour</i>	64
4.6	TRANSPORT THROUGH AND AROUND THE HEAD OF THE MAIN BREAKWATER.....	65
4.6.1	<i>Methodology</i>	65
4.6.2	<i>Transports derived from longer term measurements</i>	65
4.6.3	<i>Sediment load calculated from concentration and current measurements</i>	68
4.6.4	<i>Discussion and conclusions</i>	69
5.	CONCLUSIONS	71
5.1	COMPONENTS OF THE TRANSPORT REGIME.....	71
5.1.1	<i>Wave induced long -(and cross-) shore transports</i>	71
5.1.2	<i>Deeper water sediment transports and patterns</i>	71
5.1.3	<i>Riverine inputs and transport due to tides</i>	72
5.1.4	<i>Wind impacts</i>	72
5.1.5	<i>Transports around and through the main breakwater</i>	72
5.2	SYNTHESIS OF TRANSPORT PATTERNS AROUND THE PORT.....	73
5.3	FINAL CONCLUSIONS AND SEDIMENT TRANSPORT BALANCE.....	76
6.	RECOMMENDATIONS FOR FURTHER STUDIES	79
7.	REFERENCES	80
	APPENDIX A: HINDCASTING OF DEEP-SEA WAVE DIRECTIONS.....	86
	APPENDIX B: LOCAL WIND EFFECTS ON CURRENTS.....	89
	APPENDIX C: ADDITIONAL BOTTOM TOPOGRAPHY DIFFERENCE MAPS...90	

LIST OF TABLES

Table I:	Input wave conditions for HISWA refraction model.
Table II:	Surf zone widths calculated from Waverider data
Table III:	Wind recordings – 4 to 8 November 1996.
Table IV:	Wave and surf zone conditions at the beach adjacent to the Foreshore area.
Table V:	Comparison of observed, recorded and estimated wind and wave conditions.
Table VI:	Longshore currents calculated from dye tracking tests.
Table VII:	Average tidal levels for the Port of East London.
Table VIII:	PIANC soil classification and grain size ranges.
Table IX:	Representative “morphological” wave conditions.
Table X:	Final wave schematisation (at buoy, 22 m depth) for MOR modelling.
Table XI:	Sediment transport regime - budget and continuity

LIST OF FIGURES

- Figure i: Cross-shore definition of coastal zones
 ii: Main focus of study area
 iii: Longshore transport – schematic diagram
 iv: Example of cross-shore transport
 v: Components of transport regime “measured” or theoretically determined
 vi: Example of modelling transports
 vii: Example of modelling morphology
 viii: East London sediment transport regime
 1.1: Aerial photograph of East London Harbour on the Buffalo River
 1.2: East London location map (general)
 1.3: East London location map showing shoreline characteristics
 1.4: Detail East London location map
 2.1: Two forms of rip currents
 3.1: Some surf zone conditions between Hood Point and the main breakwater area
 3.2: Orient Beach area
 3.3: East London wave height exceedance curves
 3.4: Wave crests from aerial photographs
 3.5: East London VOS swell rose
 3.6: Comparison of VOS wave heights and directions
 3.7: Mossel Bay VOS swell rose
 3.8: Wave direction exceedance curves comparison and adapted Mossel Bay curve
 3.9: East London model bathymetry: Shelley Beach to Nahoon Point
 3.10: East London model bathymetry: area around the main breakwater
 3.11: Nearshore wave heights and directions: most common offshore wave condition
 3.12: Nearshore wave heights and directions: typical storm offshore wave condition
 3.13: Nearshore wave heights and directions: typical easterly wind wave condition
 3.14: East London wave height occurrence per direction
 3.15: East London wave period (T_p) versus direction
 3.16: Example of surf zone dye tracking measurements (1996.11.08)
 3.17: Current measurements: November 1996 - illustrations
 3.18: Comparison of current velocities: observations versus photograph method
 3.19: Current observations: June 1993
 3.20: Current patterns: 12:00 on 29 November 1993
 3.21: Sediment transport through main breakwater
 3.22: Satellite image of Agulhas Current
 3.23: East London current measurements: 1984 to 1985
 3.24: Annual current rose: Hood Point to Nahoon Point
 3.25: Current measurements and physical model simulations: 1959
 3.26: East London current patterns: 1895 and 1990
 3.27: Sub-surface drogue measurements: direction occurrence histogram
 3.28: Sub-surface drogue measurements: velocity occurrence histogram
 3.29: Endeco current vector measurements: direction occurrence histogram 5 m depth
 3.30: Endeco current vector measurements: direction occurrence histogram 20 m depth
 3.31: Drogue tracking on 19 March 1996 from 16:08 to 16:40
 3.32: Drogue tracking on 18 January 1995

- 3.33: Measured current profiles: 18 and 20/1/95; Endeco current meter
- 3.34: Current measurements on 19 and 20/1/95: drifter boys and dye tracking
- 3.35: Numerical model simulation of currents: 0,3 m/s SW current - total grid area
- 3.36: Numerical modelling of currents: 0,3 m/s SW current - near main breakwater
- 3.37: Numerical model simulation of currents: 0,5 m/s SW current
- 3.38: Numerical model simulation of currents: 0,23 m/s NE current
- 3.39: Physiographic features of the continental shelf off East London
- 3.40: Schematic block diagram of continental shelf section: physiographic features
- 3.41: East London VOS wind rose
- 3.42: Location of high-water line from aerial photographs
- 3.43: Variation of high-water line from a aerial photographs
- 3.44: Interpretation of side-scan sonar survey: 19/01/1995
- 3.45: Cross-sectional profiles perpendicular to the main breakwater (seawards)
- 3.46: Median grain sizes: September 1993
 - 4.1: Old and new (1994) sand traps
 - 4.2: East London sand traps, breakwaters and dredging areas
 - 4.3: Spot height and contour map – May 1998
 - 4.4: Spot height and contour map – September 1998
 - 4.5: Seabed difference map for May to September 1998 from hydrographic surveys
 - 4.6: Synopsis of accreted areas > 1,0 m vertical accretion
 - 4.7: Synopsis of accreted areas > 0,7 m vertical accretion
 - 4.8: Surveyed profiles along western edge of main sand trap – looking east
 - 4.9: Surveyed profiles along southern edge of main sand trap – looking north
 - 4.10: Annual volumes of sediment dredged at East London since 1890
 - 4.11: Annual volumes dredged from main sand trap
 - 4.12: Mean annual sedimentation in different areas from surveys and dredging data
 - 4.13: Sediment transport along seaward side and around the head of the main breakwater
 - 4.14: Vertical accretion and mean annual sedimentation in different dredging areas
 - 4.15: Cross-shore distribution of longshore transport (wave driven)
 - 4.16: Distribution of total annual longshore transport over wave condition occurrence
 - 4.17: Numerical model simulation of sediment transport: 0.3 m/s SW nearshore current
 - 4.18: Numerical model simulation of bottom changes due to a constant wave condition
 - 4.19: Dams on the Buffalo River
 - 4.20: Bottom topography changes: -14 m (CD) contour comparison
 - 4.21: Bathymetric survey of 4/11/94
 - 4.22: Surveyed profile comparison: 11/94 - 01/95; profile 150m from breakwater head
 - 4.23: Surveyed profile comparison: 11/94 - 01/95; profile 330m from breakwater head
 - 4.24: Area over which volumes were calculated
 - 4.25: Volume differences between surveys of 4/11/94 and 19/1/95
 - 4.26: Wave height (H_{m0}) percentage exceedance
 - 4.27: Sediment concentration measurements: bamboo pole and pump locations
 - 4.28: Concentrations from bamboo pole data: test KL1, KL2, KL3
 - 4.29: Comparison of sediment concentrations: bamboo pole N3 versus vacuum pump
 - 4.30: East London sediment transport regime
- A.1: Weather and wave data time histories, November 1996
- A.2: Synoptic weather charts: 6 to 8 November 1996
- C.1: Seabed difference map for May to July 1998 from hydrographic surveys
- C.2: Seabed difference map for July to September 1998 from hydrographic surveys
- C.3: Seabed difference map for March to May 1996 from hydrographic surveys

LIST OF SYMBOLS

a	reference level (bed concentration, related to ripple height or wave boundary layer thickness)
c	sediment concentration
D_*	particle parameter
d_{50}	median grain size (median diameter of sediment)
d_{90}	90 % diameter of bed material
d_b	depth at breakpoint
g	acceleration of gravity
h	water depth
H_s	significant wave height
H_{bs}	significant breaking wave height
H_{bmax}	maximum breaking wave height
H_{mo}	significant deepwater wave height
H_{mo}^e	representative wave height containing the average wave energy
I_1 and I_2	Einstein integrals
k_v	kinematic viscosity coefficient
k_s	bed roughness
L_o	deepwater wavelength
p	porosity
$q_{b,c}$	bedload transport rate
$q_{s,c}$	suspended sediment transport rate
$q_{t,c}$	total load transport
$\overline{v_R}$	depth-averaged value of the velocity vector
S	longshore sediment transport rate
T	bed-shear stress parameter
$\tan \alpha$	bottom slope
$\tan \alpha_x$	beach slope
T_p	spectral peak wave period
u	fluid velocity
$u^*_{*,c}$	effective time-averaged bed-shear stress
\overline{v}	mean longshore current velocity through the surf zone
v_{mid}	longshore current velocity at the middle of the surf zone
w	fall velocity
w_s	fall velocity of suspended sediment
x_b	surf zone width
z	height above the bottom
β	ratio of sediment and fluid mixing coefficient
γ	breaker index
δ_s	thickness of near-bed wave-related mixing layer
θ_b	wave incidence angle
θ_{bs}	breaking wave angle
κ	Von Karman Constant
$\kappa_{s,c}$	current-related bed roughness
$\kappa_{s,w}$	wave-related bed roughness
ρ_w	fluid density (sea water)
ρ_s	sediment density
φ	angle between wave direction and current direction

DEFINITION OF SELECTED TERMS

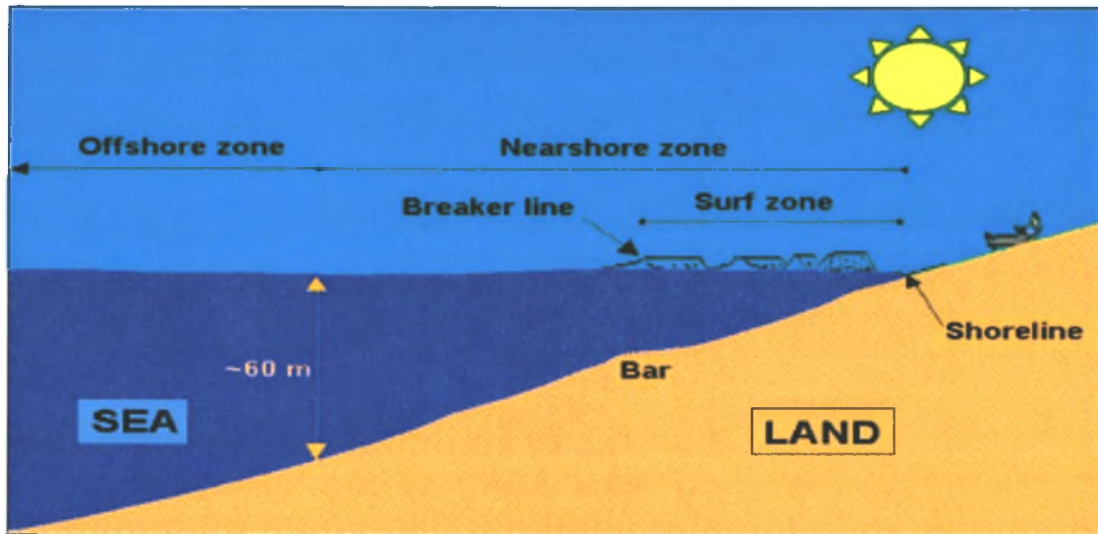


Figure (i): Cross-shore definition of coastal zones

For the purpose of clarity, specific terms used in this thesis, are defined below:

Coastal zones (refer to Figure i above): The positions along the coastline where the waves start breaking together form what is called the **breaker line**. The water depth at the breaker line usually ranges from about 0,5 m (if only small wind waves occur) to 10 m (if very large storm waves occur). The zone between the breaker line and the shoreline is called the **surf zone**. The **nearshore** zone is loosely defined as the zone extending seaward from the shoreline to well beyond the breaker line, up to the seaward edge of the central continental shelf area (in the order of about 60 m depth). The surf zone is therefore included in the nearshore zone. The **offshore** zone lies seaward of the nearshore zone (i.e. beyond the central continental shelf area).

The **wave incidence angle** is the angle between the crest of initial breakers and the local seabed contours.

Significant wave height is defined as the average of the one third highest waves in the spectrum.

The **littoral zone** is referred to as an “indefinite” zone by both the Shore Protection Manual (CERC, 1984) and the NOAA Coastal Service Center website (www.csc.noaa.gov/text/glossary). From a coastal zone management perspective, and in this thesis, the littoral active zone mainly comprises beaches, the surf zone (and slightly deeper) and river/estuary mouths. It is essentially unstable and dynamic and is located where coastal processes have a very direct influence.

A **sediment budget** includes all sources of sediment input to and sediment loss from a given section of coastline. (Department of Geography and Geology website, University of Wisconsin, <http://www.uwsp.edu/geo/faculty/ozsvath/lectures/Shorelines.htm>).

“**Upcoast**” and “**downcoast**” mean north-eastwards and south-westwards respectively for the East London coast.

Terms such as **longshore** -, **cross-shore** -, and **aeolian sediment transport**, are defined in more detail in Section 2.1.

1. INTRODUCTION

1.1 Aims and Objectives

The sediment transport regime at East London is quite unlike that found in the vicinity of other ports in South Africa. A major ocean current (the Agulhas) flows exceptionally close to the coastline in this area, thus significantly affecting nearshore sediment movements. (The 40 m isobath, which marks the start of the current-controlled central continental shelf area, is only 6 km offshore here.) Of particular interest in this case, is that this strong deeper water current predominantly flows in the opposite direction of the wave-driven longshore current in the surf zone. Furthermore, the Port of East London is the only large harbour in South Africa with a riverine character. Such diverse influences lead to a very complex pattern of sediment movement in the area. **The aims of this thesis are: to study all aspects of the physical environment which affect the sediment transport regime; to derive the baseline information necessary to understand different aspects of the sediment transport regime; to quantify the various modes of sediment transport in different areas; and finally to obtain a holistic understanding of the overall sediment transport regime at East London.**

The natural processes of sediment transport and deposition are the cause of sedimentation in ports, which necessitates routine maintenance dredging to maintain prescribed water depths (Bray, 1979, Lean, 1980 and The Dock and Harbour Authority, 1995). In order to reduce or optimise the required dredging at a specific port, it is therefore necessary to have an as complete as possible understanding of the sediment transport processes in that area. Thus, the benefit of this study, to the Port Authority of East London, could be the optimisation of various facets of the Port's maintenance dredging operations (Theron *et al.*, 1998, Theron and Schoonees, 2000).

1.2 The Physical Study Area



Figure (ii): Main focus of study area

East London is situated on the south-eastern coast of South Africa on the Indian Ocean seaboard. The Port of East London (Figure 1.1) is located on the Buffalo River. A location map of the East London area is shown in Figure 1.2. The harbour, which is one of the six largest ports in South Africa, is owned by the National Ports Authority of South Africa (NPA), who also control and operate the port. Regular dredging is needed to maintain channel depths (in total, more than half a million m³ of sand per annum on average), and maintenance dredging also represents a major annual expense (nearly R10 million at 2002 values, Theron *et al*, 2002a). (East London is also renowned as the birth-place of the dolos breakwater armour unit.)

The study area includes the coastal zone between the Goda and Nahoon Rivers (Figure 1.3) with the main focus on the vicinity of the port between Hood Point and Orient Beach (Figure 1.4). The offshore marine environmental conditions are also considered as they have a strong influence on nearshore currents, waves and sediment transport patterns. In this study, the term *East London coastline* refers to the coast between the Goda River and Nahoon River.

Along the coast from the Goda River to the Nahoon River, alternating coastal features are found: erosional wavecut rocky platforms and depositional sandy beaches (Figure 1.3). Hood Point is an exposed rocky headland, while aeolianite (dune rock) forms the erosional headlands of Nahoon Point and Cove Rock (Marker, 1988).

1.3 Key Questions

The key questions this thesis aims to address are posed below:

- Which aspects of the physical environment determine or affect the sediment transport regime?
- What can be determined from each aspect of the physical environmental data/information, nearshore processes and coastal dynamics, to derive the different transport modes contributing to the overall sediment transport regime?
- Which different modes of sediment transport occur where?
- What are the transport rates that can be deduced from surveys and dredging records?
- What is the longshore sediment transport rate towards the harbour?
- How much of the longshore transport moves through and around the head of the main breakwater, and into the main sand trap?
- Does the Agulhas Current significantly influence the nearshore currents and sediment transport at the East London harbour entrance area?
- What are the rates of the various modes of sediment transport in the different areas?
- What does the typical pattern of sediment transports in the study area look like?
- How does the overall sediment transport regime at East London function?
- What is the sediment transport balance at the Port of East London?

1.4 Logical Structure of Thesis

The thesis is structured according to the sections as listed below:

In **Section 1**, the aims and objectives of this thesis are explained. The study area is then defined and described very briefly. Next, the key questions are posed, which the thesis aims to address. The thesis structure (as described here), concludes Section 1.

Section 2 gives background to coastal sediment transports and describes the methods and theory of determining sediment transport.

Section 3 is primarily concerned with physical environmental data/information, nearshore processes and coastal dynamics, which determine or affect the sediment transport regime. Thus, this section entails providing or deriving the baseline information necessary to grasp different aspects of the sediment transport regime and which information is required to determine the various modes of sediment transport in different areas.

Section 4 relates specifically to the sediment transport regime as derived from the information given in Section 3. This basically entails providing the answer in each case to the following question: what can be determined from each aspect of Section 3, to fill in or confirm the different transport modes contributing to the overall sediment transport regime. Section 4 further relates to the various modes of sediment transport in the different areas and the quantitative determining of these rates.

Section 5 contains the main conclusions and entails the final derivation of the sediment transport regime (and sediment transport balance) at East London.

Recommendations for further studies are made in **Section 6**.

All references are listed in **Section 7**.

2. BACKGROUND ON COASTAL SEDIMENT TRANSPORT

2.1 Background

2.1.1 Origin of marine sediments

Sediment found close inshore usually originates from fluvial sources and the disintegration of rocks and shells on the seashore. The major input sources of marine sediment to the inshore area is beach, dune or cliff erosion, possible offshore sources and larger rivers in the region. Periodic flood-derived pulses of sediment are transported to the inshore area from such rivers, but the amounts can vary greatly. Vast amounts of sediment are transported along the shelf by the Agulhas Current. Meandering, large border eddies or smaller current vortices of the Agulhas could potentially transport sediment from the shelf to shallower nearshore areas.

Sediment along the coast is continuously being moved and rearranged by wind, wave and current action. Large quantities of sand are moved by wave action, particularly during storms. In South Africa, high wave energy components usually occur predominantly from the southern sector. Under the action of these prevailing wave conditions, sediments can also be moved upcoast from river mouth areas towards coastlines located further north. When wave directions become more easterly along South Africa's Indian Ocean seaboard, flood-derived pulses of sediment originating from rivers are likely to be moved south-westward along the coast towards coastlines located further south. Similarly, along South Africa's Atlantic Ocean seaboard, westerly to north-westerly wave directions could transport fluvial sediments from river mouths towards coastlines located further south. However, the waves usually approach approximately normal to the shoreline, but are much more often directed slightly upcoast than downcoast. Due to the relatively few rivers mouths along the west coast and the mostly large distances between them, the sediment dynamics along the west coast is usually not affected significantly by rivers other than the Orange and Olifants.

The nature of the drainage areas (rainfall, size, slope, vegetation, farming practices, etc.) of the large rivers, and the type of sediment source (e.g. consisting of easily eroded, fine-grained shales and mudstones, etc.), determines the character of the bulk of the sediments discharged into the sea (e.g. predominantly fine or medium grained, etc.). Rivers that drain primarily rocks that are mostly coarse grained and are more resistant to erosion, will have considerably lower sediment yields and the sediment supplied to the sea will be largely medium to coarse grained.

Periodic flood-derived pulses of sediment are also transported into the sea from smaller rivers, but the amounts are usually very small and again somewhat intermittent. Some rivers and catchments have been altered by human interference (e.g. dams), so that the sediment contribution they made in their natural state, has been significantly in- or decreased.

Thus, having arrived in the coastal zone (from various origins as described above) these sediments are now subject to many coastal processes and become marine sediments. Therefore, in the long-term, the amount and character of the marine sediments, are often ultimately determined by the larger rivers (and the nature of their catchments) within a region.

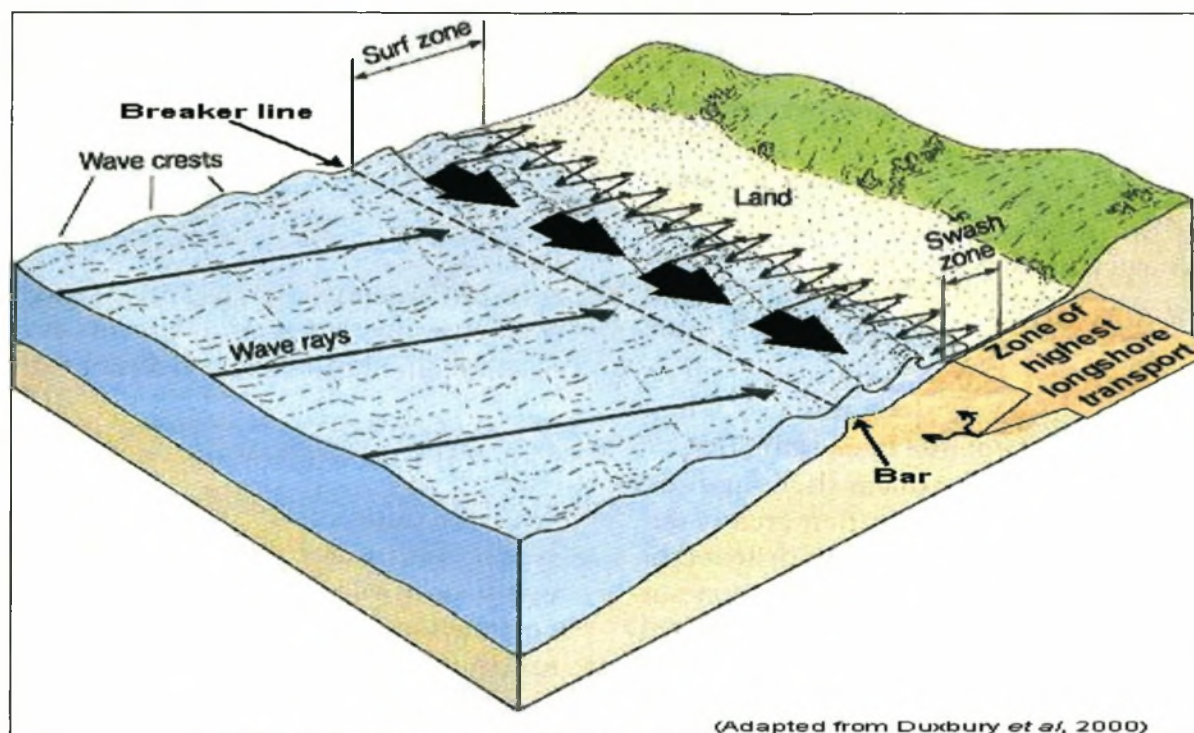
2.1.2 Littoral sediment transport and wave effects

2.1.2.1 General

Within the coastal zone, there are a number of processes that can transport varying amounts of marine sediments. Sediment transport in the nearshore region is usually categorized as longshore (parallel to the shoreline) or cross-shore (perpendicular to the shoreline) sediment transport. On a coastline with an exposed sandy area above the high-water mark, aeolian (wind-blown) sediment transport also plays a role. In general, sediment is very rarely moved by only one mode of transport in the littoral zone; longshore, cross-shore and aeolian sediment transport occur simultaneously. Even on a long straight shoreline, the current circulation pattern (including rip currents) and the associated sediment transport patterns are very complex. Furthermore, marine sediment transport is dependent on wave and tide conditions with the result that it changes continually, not only in direction and rate, but also in the location where it takes place in the nearshore zone.

The nearshore wave regime, which plays an integral role in the generation of nearshore currents and sediment transport, is controlled primarily by the characteristics of the incident waves and the bathymetry (sea-bottom topography) of the adjacent coastal zone. When deep-water waves approach the coastline, refraction, shoaling and, to a lesser extent, reflection and damping due to bottom friction occur in relatively deep water and in the nearshore zone. In shallower water diffraction also plays a role, especially in the immediate vicinity of headlands and fixed structures such as breakwaters (CERC, 1984). Combined refraction, diffraction, reflection and damping due to bottom friction therefore takes place in the nearshore zone. The effects of reflection and bottom friction are normally very small when compared to refraction and diffraction effects and are thus often assumed to be negligible. (For a description of these processes see Theron, 2003.) The wave incidence angle has a major effect on nearshore currents and sediment transport. During seasons when local winds prevail, locally generated wind waves frequently occur. Local wind waves can also have a significant impact on the sediment transport regime.

Waves approaching the coast usually break on the nearshore sandbar, reform shoreward of the bar and then break again on the shallow-water section of the beach profile (two breaker lines are then observed). The surf zone width influences the amount of energy dissipation in the surf zone. A wide surf zone with many re-breaks means that energy is dissipated over a wider area further away from the shore. The degree and type of wave breaking determine the rate of energy dissipation and are also an important parameter in other nearshore processes. Spilling waves gradually dissipate energy while plunging waves dissipate most of their energy near the breakpoint. Collapsing and surging waves dissipate energy close to the shoreline. Beaches are globally categorised according to one of six types, namely: dissipative beaches, four classes of intermediate beaches, and reflective beaches. Reflective beaches have a steep beach face with surging breakers that are reflected back towards deeper water. Dissipative beaches have flat beach slopes and the wave energy is dissipated gradually in deeper water further away from the beach (CPB, 1992).

2.1.2.2 Longshore sediment transport**Figure (iii): Longshore transport – schematic diagram**

When waves that advance towards the coast reach the nearshore zone, sediment (predominantly sand) is stirred up. Although non-breaking waves also move sediment, most of the sand is transported inside the surf zone where wave breaking is the primary agent for suspending sediment and moving sand along the bottom. Most longshore currents are generated by the longshore component of motion of waves that arrive obliquely at the shoreline (CERC, 1977 and Figure iii). Longshore currents are also generated by an alongshore variation in wave height. Longshore currents can usually not entrain sediment on their own; however, sand stirred up by the breaking waves is transported alongshore by these currents. The combined effect of breaking waves and a longshore current creates the potential for significant transport of sediment alongshore within the littoral zone (e. g. Morfett, 1990). Along an exposed coast, most of the longshore sediment transport occurs between about +2 m to MSL and depths of not more than about 8 m to 10 m below MSL. It is well known that much more sand is transported in the surf zone than outside it.

The longshore transport rate, or littoral drift, is the rate at which sediment is moved parallel to the coast in the littoral zone. The rate is usually expressed as a volume per time, that is, in m^3/s or m^3/year . Depending on the environmental conditions at the time, sediment is transported alongshore either upcoast or downcoast, but over a longer time period both directions usually can and do occur. The nett longshore transport rate is the difference between the upcoast and downcoast transport rate. Gross longshore transport rates (total of both directions) are often significantly larger than nett rates.

Actual nett (usually up-coast) longshore sediment transport of about $400\,000\ \text{m}^3$ to $1\,200\,000\ \text{m}^3$ per annum (on average) is estimated along most of the exposed, open South African coast, while the potential transport (due to wave energy) is sometimes even somewhat higher. Along rocky shorelines or sheltered areas, the nett average longshore transport rate is mostly between about $10\,000\ \text{m}^3$ and $400\,000\ \text{m}^3$ per annum. Where shorelines are located in well sheltered areas, the amount of marine

sediment transport could be significantly limited. This will mainly occur in bays and/or in the lee of points/headlands or reefs. Although the area may be sandy, little marine sediment is stirred up or transported alongshore due to the reduced wave action. In such cases the amount of sediment transport could be very low. It should also be taken into account that the longshore transport rates fluctuate considerably from year to year (Schoonees, 2000).

Local variations of the transport rate are strongly dependent on the availability of sand or the extent of rocky areas within the surf zone. Thus, extensive rocky areas within the surf zone may significantly reduce the potential transport rate. A gradient in the longshore transport rate can, in the long term, cause either shoreline erosion or accretion. These gradients can sometimes be identified by analysing long-term coastline changes (from surveys or aerial photos).

The average sediment grain size is a critical parameter affecting sediment transport rates. For example, at coastlines where finer sediments occur, the longshore transport rates are also potentially higher for the same input wave energy. Depending upon the prevailing wave conditions, wave incidence angles in the surf zone are usually another critical parameter affecting sediment transport rates. Larger wave angles generally result in greater rates of longshore transport. Prevailing wave conditions usually have high energy components occurring predominantly from the southern sector. Thus, areas which are exposed to these waves and are so orientated that surf zone wave angles are relatively larger, will potentially have higher transport rates.

2.1.2.3 Cross-shore sediment transport

Cross-shore transport may result from any currents which have a component in the cross-shore direction and which have sufficient velocity to transport sediment. A typical example of cross-shore transport is the on/offshore sediment transport resulting from (shorter term) changes in the incident wave conditions. (For a discussion of this and most other significant cross-shore transport processes, see Schoonees and Theron, 1995.) Cross-shore sediment transport is usually a swift process whereby sand is eroded near the waterline during a storm (Figure iv below). The sand is transported seawards and deposited in deeper water where it forms an underwater bar on which the storm waves break. When the sea calms down again, sand is slowly transported back to the shore, thus re-establishing approximately the original profile if no nett loss of sand has occurred. (For a more detailed description, see Birkemeier, 1985, Swart, 1974 and Van Hijum and Pilarczyk, 1982.)

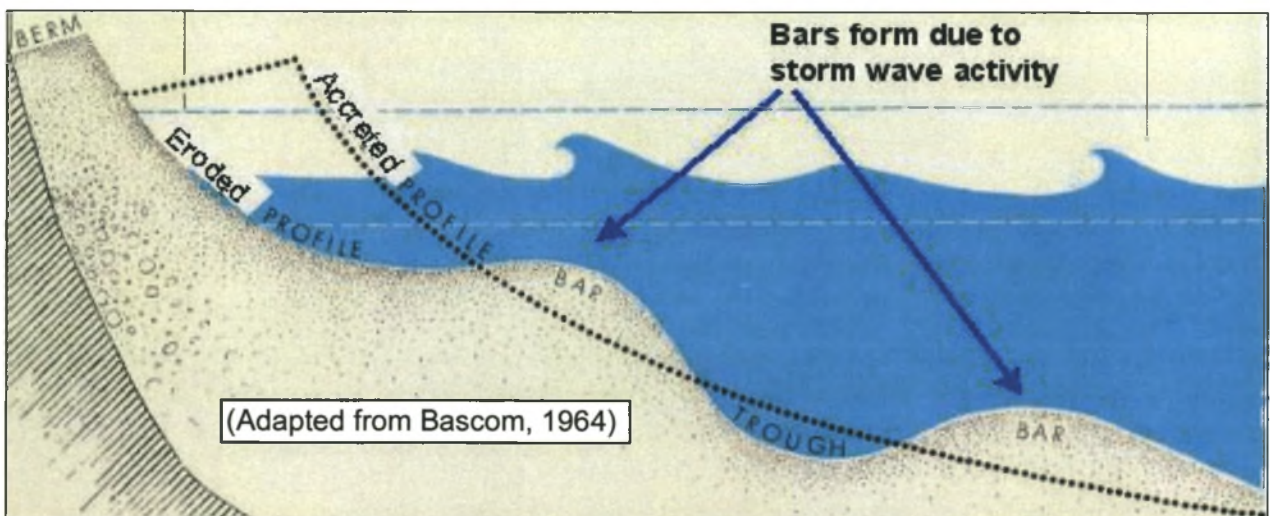


Figure (iv): Example of cross-shore transport

Although long-term nett cross-shore transport rates are often close to zero, the rate occurring at any point in time is usually quite large. Extreme cross-shore transport rates are estimated to be as high as $150\,000\text{ m}^3$ over only 2 days for very large sea storms and a shoreline length of 500 m (Theron *et al.*, 2003). Even within the somewhat sheltered Durban Bight, a nett cross-shore loss of some $100\,000\text{ m}^3$ has been recorded during a single storm event (Theron, 2000). More typical shorter-term storm nett cross-shore rates would be in the order of a few m^3/m per hour for 24 hours. (Typical southern African sea storms have durations of a few hours to a few days.) Most of the transport occurs in depths less than 10 m to MSL and typically, insignificant volumes of sand are transported cross-shore in depths greater than 10 m to 15 m to MSL along exposed shorelines. If the wave condition persists long enough an equilibrium profile develops (Swart, 1986), but because wave conditions change continuously, the profile remains in a dynamic state and rarely reaches the equilibrium condition for any of the various wave conditions.

If an area consists mainly of sediment (predominantly sand), and the wave height in the surf zone is relative large (say about 2,5 m or more) large amounts of sediment are stirred up into suspension and moved along the bottom. This will be so irrespective of the wave angle (i.e. the longshore sediment transport rate could be anything from zero to very high). Depending mainly on the bottom profile and wave characteristics, large volumes of sediment could then be mobilized. Generally, steep profiles and narrow surf zones will greatly increase the sediment load near the shoreline, while flat slopes and wide surf zones will result in more dissipation in deeper water with less wave energy penetrating to near the shoreline. (For a discussion of some of the most significant cross-shore transport processes, and an evaluation of the best known models/formulae to predict cross-shore transport rates, see Schoonees and Theron, 1995).

Another aspect relating to “cross-shore transport modes” concerns rip currents and circulation cells. Apart from the usually prevalent longshore current, water enters the surf zone by mass transport (nett water movement in the direction of the waves) caused by the waves. Rip currents, which are strong currents flowing seawards in a narrow zone, take water and some sediment out of the surf zone (Figure 2.1). Rip currents usually return water that has been “piled up” on the shore by incoming waves and wind. Another cross-shore exchange mechanism is the undertow current, which is generated in a similar fashion. This is a seaward current near the bottom on a sloping inshore zone and is caused by a return flow of water carried onshore by wave action (CERC, 1984).

A part of the longshore current feeds the rip current and some bypasses the rip current to continue alongshore to the next circulation cell. These nearshore circulation cells contribute to the longshore dispersion of sediments. On a short temporal scale (hours to months), such transient rip currents and nearshore circulation cells could potentially affect the availability of sediment, but the overall longer-term sediment transport balance is unlikely to be affected.

Although not part of the littoral zone, a form of cross-shore transport can also occur in deeper water, for example, where submarine canyons cut into the nearshore portion of the continental shelf. In such instances, nett “cross-shore” sediment losses to the offshore zone usually occur (for example, north of Cape St Lucia; Flemming, 1981). However, no such features exist within the study area.

The relevance of all of the above to this thesis is that, in the long-term, the on/offshore transport is approximately balanced and wave induced cross-shore transport is considered to have no net effect on the sediment budget. In terms of the overall sediment budget *in this particular case*, all forms of

cross-shore transport (whether within the littoral zone or beyond) are internal processes with no nett in- or output from the system boundaries, and are therefore not considered further.

2.1.2.4 Wind-blown sediment transport

Wave-induced as well as aeolian sediment transport must be considered when determining marine sediment dynamics. Aeolian, or wind-blown sediment transport, occurs when sufficiently strong winds blow over sandy areas, putting the sediment into motion. Most of this wind-blown sand is usually transported in a layer of up to a metre high above the beach or dune surface. Optimum conditions for wind-blown sand transport are the availability of dry, loose sand, strong winds, no vegetation, and a long wind fetch, that is, a long expanse of sand over which the wind can blow. Usually, the rate of aeolian sediment transport is orders of magnitude lower than the wave-driven transport rate along an exposed coast. However, the wind-blown component can nevertheless be critical to the maintenance of both shoreline stability and the natural equilibria within the littoral zone. Human impacts (e.g. removal of vegetation) within or adjacent to an area subject to significant aeolian sediment transport, can result in a nett long-term change in the sediment transport balance. (The problem of ongoing sedimentation experienced at some coastal developments is occasionally a direct result of aeolian sediment transport.)

Thus, under conditions favourable for wind-sand transport (e.g. strong winds, fine dry sediments, large open areas, etc.), significant amounts of marine sediments can be transported by means of aeolian sediment transport. Again, the amounts of sediment carried by means of wind-blown sand, is very small in comparison to the potential amount that can be transported by wave action and currents. Yet, the formation and progression of dunes can, for example, significantly affect the sediment transport balance in some instances.

2.1.3 Sediment transport in deeper water

At some distance beyond the surf zone (usually beyond 8 m to 15 m depth), the wave-induced currents/flows become insignificant and are too weak to transport sediment. However, the waves can still impart considerable stress on the bottom sediments. If a significant current is also present (for example, due to the nearshore portion of deepwater currents such as the Agulhas), the combined effect of the current and waves can result in significant sediment transport. Such transport is usually in the direction of the current flow (even if the wave direction differs greatly). The transport potential of currents is sometimes greatly enhanced by the wave stirring. Usually the role of the waves in sediment transport is the suspension of sediment, which is then advected by the net tidal, oceanic, wind-driven or wave-driven currents (e.g. Vincent *et al*, 1998 and Kleinhans, 2002).

The above description relates to sediment transport due to the combined effects of currents and waves in the nearshore zone beyond the surf zone. Sediment transport can also occur on the continental shelf and the offshore zone as a direct result of strong deepwater currents such as the Agulhas (e.g. Flemming, 1978). Although long-period storm waves can still have a significant impact on current-driven sediment transport up to considerable depths (more than 100 m), wave influence gradually decreases with depth and becomes less important beyond about 60 m water depth.

2.1.4 River and estuarine sediment transports

In addition to wave-induced and deepwater-oceanic currents, there are other nearshore currents that can affect the sediment transport, which are mainly caused by tides (and occasionally local winds). Tide-induced currents can be superimposed upon the prevailing oceanic and wave-induced circulations, especially near entrances to bays, lagoons and harbours and in regions of relatively large tidal range. Thus, the amount of marine sediment transport into a harbour can also be affected by the (nett) transport capacity of the ebb and flood tidal flows near the harbour entrance, and on the amount of sediment available outside of the harbour. Sometimes, the amount of marine sediment available near the harbour entrance can be limited. This will mostly occur where the shoreline is mainly rocky and little marine sediment is found. (Note, that a mainly rocky shoreline does not by itself imply that very little marine sediment is present. Significant amounts of sediment could still be moving along such a coast, but, for example, wave conditions are such, that a sand veneer covering the rocks is prevented from building up.)

Another potential input source of sediment to the study area is local rivers. As mentioned in the introduction, the Port of East London is located on the Buffalo River (Figure 1.3). Periodic flood-derived pulses of sediment are transported into the sea from this relatively small river, but the amounts are usually very small and somewhat intermittent. Dams on this river have significantly decreased the sediment contribution from what it used to be when the river was in its natural state. The fluvial sediment production and amount of sediment discharged into the sea, is determined by the nature of the river's catchment (area, rainfall, slope, vegetation, farming practices, etc.), the type of sediment source (type of rock and soil, erodability, grain sizes, etc.), and the nature of the flood hydrograph. Most of the *sand* supplied to the sea will come from the bedload in the river, while relatively little *sand* will be contributed by the suspended load in the river (as much thereof is too fine). In the sea, the finer particles originating from the river load will be washed out and dispersed (usually to deeper water).

2.2 Measurements and theoretical methods to determine sediment transports

2.2.1 General

Various methods have been used in the past to "measure" sediment transport rates, such as:

- Sedimentation (/erosion) from bathymetric surveys and dredging records
- Accretion against a breakwater or groyne
- Accretion plus bypassing
- Erosion downdrift of a barrier
- Growth of a spit
- Sediment concentration and current measurements
- Sediment tracers (usually radio-active or fluorescent)
- Sediment samplers
- Many kinds of mobile sediment traps

Transport rates can also be calculated with theoretical or empirical formulae and computer models. This sometimes enables a comparison of the "actual" and theoretically calculated rates and

subsequent calibration of theoretical methods.

In the following section, a brief discussion is given of the measurements and calculation methods employed in this study to determine various components of the sediment transport regime, as depicted by the arrows in Figure v below. (Note, that the letters in the blocks denote different measurements or theoretical calculations as described in the following section.)

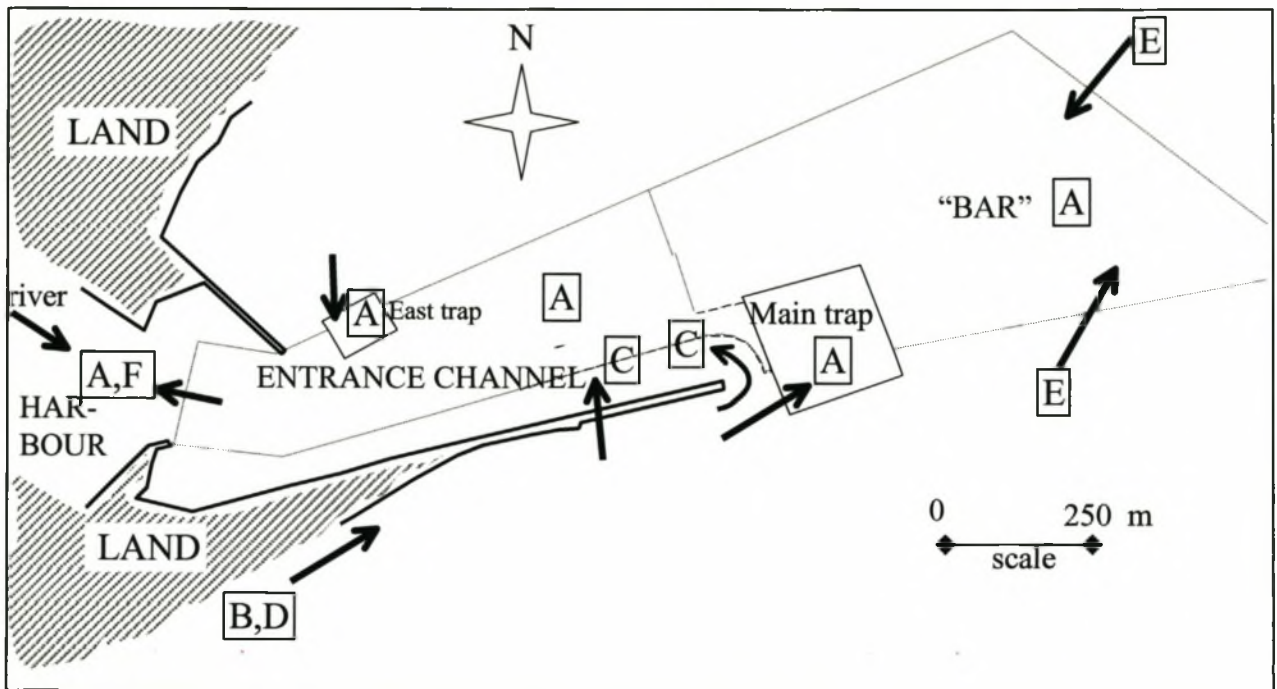


Figure (v): Components of transport regime “measured” or theoretically determined

2.2.2 Main “measurement methods” employed to determine sediment transports

Sedimentation rates from bathymetric surveys and dredging records

(This relates to the blocks denoted with an A in Figure v above.)

Seafloor contour maps can be analysed to identify changes in bottom topography, areas of sediment deposition or erosion and volume changes. Consecutive surveys should be selected between which no or very limited dredging took place, as changes due to dredging will then not distort the observed changes resulting from natural processes. Difference maps can be produced that show changes in vertical elevation between consecutive surveys as well as volume changes per unit area. Consistent deposition/infilling patterns and directions can show from which directions sediment is transported into these areas, and can also provide good information on the magnitude of these transports.

Based on the basic principle, that sediment transport in an area must ultimately be balanced, deductions about sediment transport can also be made by analysing dredging records. If there is no long-term net erosion or build-up of the sea-floor in an area, the amount of sediment moving into the area must be approximately equal to the amount of sediment dredged from this area (plus the amounts

Sediment Transport Regime at East London

possibly moving out of that area). Sediment can relatively easily move into areas that are significantly deeper than the adjacent sea-bed, but cannot easily move through or out of these areas. By implication therefore, the average sediment transport rate to each of these areas must approximate the average long-term dredging rate from each of these areas.

Longshore transport rates calculated from shoreline evolution

(This relates to the block denoted with a B in Figure v above.)

If the longshore sediment transport is interrupted by an obstruction such as a groyne or a breakwater, accretion will occur on the updrift side and erosion on the downdrift side. The latter is due to the fact that the sand that previously fed the downdrift beach is trapped and thereby prevented from reaching the downdrift beach. Harbour breakwaters sometimes function as effective (nearly total) sediment traps. By calculating the measured beach accretion over time against such a breakwater (and taking account of the aeolian transport if relevant in this area), the actual longshore transport in this area can also be determined.

Sediment load calculated from concentration and current measurements

(This relates to the blocks denoted with a C in Figure v above.)

If simultaneous measurements of sediment concentration and current velocities are available in an area, the sediment transport rate can be directly calculated. General relationships between concentration and depth, as well as between current velocities and depth can be determined from the measurements. The product of the sediment concentrations and current velocities is integrated over depth, which gives the suspended sediment load. Unfortunately, bedload measurements are usually not available, as it is extremely difficult to obtain such measurements in practise. Thus, theoretical relationships between the bedload and the suspended load are used to compute the bedload from the calculated suspended load. The total load is then simply the sum of the suspended and bedloads, and is usually converted to a sediment transport rate.

2.2.3 Main theoretical methods employed to determine sediment transports***Theoretically determined longshore transport***

(This relates to the block denoted with a D in Figure v above.)

The longshore (wave induced) sediment transport rate is a notoriously difficult physical parameter to determine accurately. Even the best theoretical methods and the most accurately measured field data have an accuracy of $\pm 50\%$ or poorer (Schoonees and Theron, 1993). Numerous means are available to theoretically determine the longshore sediment transport rate (e.g. Horikawa, 1988, Schoonees and Theron, 1994 and Swart and Fleming, 1980). If at all possible, the transport rates computed in the study area should be compared with transport rates measured nearby; for example, accretion at an adjacent harbour (as proposed by CERC, 1984). However, if no data are available with which to calibrate these theoretical methods, confidence in the results is significantly reduced.

Longshore transport rates are usually determined as follows:

A wave refraction study of the particular study area is conducted in order to calculate the nearshore wave climate. This climate is then used to compute the longshore transport for each wave condition at a specific location in the study area. As mentioned before, the waves can cause either up- or downcoast longshore transport. By adding up all the transport rates caused by the different wave conditions in the upcoast direction, the total upcoast longshore transport rate is obtained. The total downcoast transport rate is determined in a similar way. The gross longshore transport rate is then determined by adding the upcoast and downcoast rates, while the net rate is equal to the difference between the upcoast and downcoast rates.

Although the theoretical basis of sediment transport formulae vary significantly, many such formulae express the sediment transport rate as a function of some or all of the following parameters: wave height, direction and period; the density and dynamic viscosity of the water; profile characteristics such as the slope; and the sediment density and diameter (e.g. Kamphuis, 2002). The theoretical basis of the specific formulation used in this thesis to calculate the longshore transport rate, is discussed in Section 4.2.

Mathematical sediment transport modelling

One alternative theoretical method of determining the sediment transports is to utilize a hydrodynamic model. By linking a sediment transport model to the simulations of the current regime, the potential transport rates can be determined. Such relatively simple modelling does not have an interactive coupling between the calculation of currents, sediment transport rates and the resulting bed level changes. In fact, the calculated transport rates are the final model output (Figure vi, below), and the sediment mass balance (and associated bed level changes) is not determined. The sediment transport model used in this thesis, is discussed in Section 4.4.1.

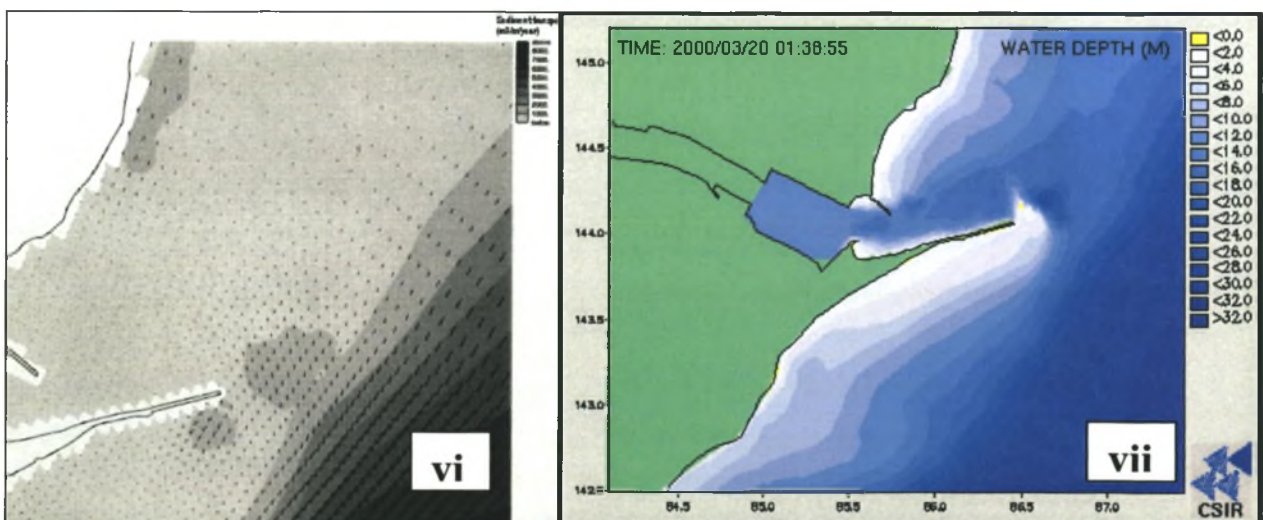


Figure (vi): Example of modelling transports

Figure (vii): Example of modelling morphology

A more sophisticated approach is to apply a full morphological model to simulate sediment transports and morphological changes. This entails the numerical modelling of the hydrodynamics, sediment dynamics and morphological changes due to the sediment fluxes induced by waves and currents (Figure vii, above). Such models provide an interactive coupling between the calculation of waves,

Sediment Transport Regime at East London

currents, sediment transport rates and the resulting bed level changes. The driving forces for the model are the offshore waves and currents. Thus, the resulting main input parameters required are: current velocity, wave height and period, water depth, roughness, grain size, and density of water and sediment. The theoretical basis of the morphological model used in this thesis, is discussed in Section 4.4.2.

Calculation of sediment transports in deeper water

(This relates to the blocks denoted with an E in Figure v above.)

In deeper water areas, sediment transport can occur as a result of the combined effects of offshore currents and wave action, or currents only. Only the basis of the theoretical method used to determine the sediment transport rates are briefly described here. The details of the formulations and the computational procedure used to calculate the transport rates, are discussed in Section 4.3.

The suspended sediment load is calculated by integrating the product of the sediment concentrations and current velocities over the depth. The formulae used in this case to determine the bedload transport is related to the bed-shear stress, the fluid density, the diameter of the bed material, a bed-shear stress parameter, and a particle parameter. The total load is then given by the sum of the suspended and bedloads. The main input parameters are: water depth, wave height, wave period, current velocity, angle between wave direction and current direction, diameter of bed material, current-related bed roughness, wave-related bed roughness, reference level (related to ripple height or wave boundary layer thickness), and the thickness of the near-bed wave-related mixing layer.

Calculation of river and estuarine sediment transports

(This relates to the block denoted with a F in Figure v above.)

Another component of the sediment transport regime is the fluvial sediment input into the coastal zone from the Buffalo River. Based on catchment area and sediment production rates (Rooseboom, 1975 and 1978), the total annual fluvial sediment production can be estimated. These calculations normally give the sediment load in tonnes/yr. By assuming a voids ratio (typically 40%) and sediment density (typically 1350 kg/m^3), the volumetric rate (m^3/yr) can be determined. The next step is to estimate the percentage of the total sediment load that consists of sand (typically 5% to 25%). If the mean annual runoff of the river is known, the sand load in the river can also be estimated directly as a percentage of the runoff (e.g. Hart, 1982). Thus, the mean annual sand load can be estimated. However, large dams on the river can act as effective sediment traps. Therefore, the proportion of the sand trapped by each of these dams also has to be estimated (e.g. Weaver, 1982). (Trapping efficiency of reservoirs can also be determined by more comprehensive techniques such as those derived by Rooseboom (1992) and Sloff (1997).) In this manner, the long-term average rate of fluvial sand input into the harbour area can be determined.

Tidal flow velocities in and out of the harbour can be estimated based on rough tidal prism calculations. Firstly, the surface area of the estuary (including the inner harbour) is determined. The spring and neap tidal ranges at East London are known. Therefore, the tidal volume entering or exiting from the inner harbour area during spring and neap tides can be calculated (assuming the estuary has a fixed surface area). Next, the cross-sectional area of the entrance to the inner harbour is calculated. Based on knowledge of the tidal cycle (phase durations, etc (e.g. Theron *et al*, 2002b)), the average and maximum flow velocities (over depth) during spring and neap tides can then be

Sediment Transport Regime at East London

calculated. (These results can be compared to current measurements conducted at the entrance to the harbour basin area (CSIR, 1998).)

Finally, based on these current velocities and typical grain size distributions in area, suitable sediment transport formulations (such as the Bijker, Engelund-Hansen-Swart and Van Rijn formulae (as described in Section 4)) can be employed to calculate the tidally driven transport rates through the entrance to the inner harbour.

Calculation of aeolian transport

Theoretically the aeolian sediment transport rate is dependent on a number of factors. These factors include:

- Wind velocity and its vertical distribution.
- Aerodynamic roughness.
- Density of air.
- Critical shear stress for suspending sediment.
Different factors affect the critical shear stress, such as the density of the sediment, the grain size distribution, as well as the moisture content and the cohesion of the sediment.
- The fetch length (that is, the length of sandy beach over which the wind blows to entrain sediment).
- Availability of sediment to be transported.

Based on wind data and sediment characteristics from sand sampled on site, aeolian transport rates can be calculated for an area (including the volumes of sand blown seasonally in specified directions by the prevailing winds). Typical South-African aeolian sediment transport rates are in the order of 20 m³/m to 80 m³/m per year. However, most predictive aeolian transport calculations are based on theoretical equations (e.g. 16 of which are described by Swart, 1986) where it is assumed that an unlimited quantity of dry, non-cohesive sand is available for transport under constant wind conditions across a flat, unvegetated surface. Since some of these criteria are sometimes not met in practice, the potential transport rates are therefore much higher than the actual rates in such instances. Still, total actual rates in the order of 20 000 m³ to 40 000 m³ per year have been recorded where significant open sandy areas occur along our coastline. The potential aeolian transport rate is also affected by the local topography and overall coastline orientation relative to the prevailing wind regime. Where the beaches are narrow, or the shoreline is predominantly rocky, the potential for wind-blow sand is of course much less.

3. ENVIRONMENTAL DATA AND COASTAL PROCESSES AFFECTING THE SEDIMENT TRANSPORT REGIME

3.1 General and Purpose

This section is primarily concerned with physical environmental data/information, nearshore processes and coastal dynamics that determine or affect the sediment transport regime. Some of the information (e.g. wave conditions and grain sizes) is utilized directly as input into sediment transport calculations (Section 4), while the other parts of the information provide circumstantial evidence about specific aspects of the sediment transport regime and contribute to a holistic understanding of the sediment transport regime (Sections 4 and 5). Thus, this section entails providing or deriving the baseline information necessary to grasp different aspects of the sediment transport regime and which information is required to determine the various modes of sediment transport in different areas. (In Section 4 the different components of the sediment transport regime are quantified.

3.2 Wave Regime

3.2.1 Introduction

Wave induced currents in the surf zone are often the dominant driving force of sediment transport in the area of harbour entrances. Waves also contribute to agitation of sediment in the shallower nearshore area seaward of the surf zone, and consequently contribute to sediment transport by nearshore currents in that zone.

The familiar waves of the sea are wind waves generated by winds blowing over the ocean. Wind waves vary in size from ripples to large ocean waves. Generally, the greater the distance the wind blows over the sea (wind fetch length), the stronger the wind, and the longer the time that the wind blows, the larger the waves that will result (CERC, 1977). When winds generated by a local storm blow toward the shore, the waves are steep, with wave lengths 10 to 20 times the wave height and wave periods usually between about 3 s and 10 s. Such waves are called seas. When waves are generated by a distant storm, they travel thousands of kilometres before reaching the shore. Under these conditions, only long low waves reach the shore. These waves normally have wave lengths from 30 to more than 500 times the wave height, with wave periods usually between about 10 s to 30 s, and are called swells.

3.2.2 General deep-sea wave climate

The east coast is dominated by south-westerly swells (Rossouw, 1984). The mean annual percent probability of swell >4 m for the East London coastline is generally about 39%, varying from 26% in March to 48% in August. During south-westerly gale wind conditions, local wind-generated surface waves (and nearshore wind-induced currents) propagate northeastward, parallel to the coastline and against the offshore Agulhas Current (Flemming, 1981). The propagation of high (north going) swells into the (south going Agulhas) current can lead to the formation of destructive "giant" waves along the continental shelf margin (Schumann, 1976; Smith, 1976; Mallory, 1977). North-easterly winds

generate surface waves (and wind induced currents) which go with the Agulhas Current (Flemming, 1981). North-westerly and south-easterly winds are much less frequent, although bedform patterns on the continental shelf indicates that heavy swells occur occasionally from the south-east (Flemming, 1980 and 1981).

3.2.3 General wave exposure of the study area

Site investigations as well as naval charts (Figure 1.4) indicate that the overall study area is exposed, particularly with respect to waves approaching from the south-westerly to north-easterly sector. It is clear that in general there is no protection (such as provided by a large headland or extensive shallow reefs) against the dominant deep-sea waves. Hood Point only has a relatively limited effect on the coastline directly adjacent to it. The coastline of the overall study area is thus exposed to deep-sea swells travelling from the south-west to north-east and even partially exposed to deep-sea swells from the west-south-west (or potentially from the north-north-east) through wave refraction. The area is also exposed to locally generated wind waves from the same south-western to north-eastern sectors (for example, Figure 3.1). In general, the study area can therefore be described as an exposed high-energy coast.

Along the Foreshore area (Figure 1.4), the breaker type is mostly spilling/plunging with one re-break. The beach type is usually about midway between a dissipative and reflective beach. The most common conditions encountered along the Foreshore area can be summarized as fully exposed to the usually rough surf conditions (for example, Figure 3.1).

With respect to the dominant deep-sea waves, Orient Beach (Figure 1.4) lies in the lee of the main breakwater. Here, the breaker type is also mostly spilling/plunging, but often with no re-breaks. The beach type is usually more dissipative than reflective. However, with respect to waves approaching from all of the easterly sectors (deep-sea swells and local wind-waves), Orient Beach is more exposed. Yet, the most common conditions encountered at Orient Beach can be summarized as partially protected to well sheltered from the usual deep-sea wave conditions (for example, Figure 3.2).

3.2.4 Measured nearshore wave conditions

Nearshore wave heights and periods at East London were initially recorded by means of a Datawell Waverider accelerometer buoy. Waves were measured about 1,2 km offshore of Hood Point (Figure 1.2) in a water depth of about 27 m from February 1984 till March 1985. A maximum estimated significant wave height (H_{mo}) of 4,7 m was recorded during this period. The wave height (H_{mo}) was above 2,5 m for 10% of the time. The average spectral peak period (T_p) was 11,2 s.

During 1992, however, the recorder was relocated to a position directly south of the harbour entrance channel in a water depth of about 22 m (Figure 1.2). Figure 3.3 shows the seasonal and all data wave height exceedance curves for the measurements since 1992. The average significant wave height (H_{mo}) is about 1,64 m while the average peak wave period (T_p) is about 11,2 s. Maximum significant wave heights of over 6 m were measured on two occasions between April 1992 and February 1996.

Wave energy is proportional to the product of the peak energy wave period (T_p) and the square of the

significant wave height (H_{mo}). Thus, a representative wave that has the average wave energy (H_{mo}^e) is calculated as follows (Schoonees and Moller, 1982):

$$H_{mo}^e = \left(\overline{H_{mo}^2} \cdot \overline{T_p} / \overline{T_p} \right)^{0.5}$$

(the lines indicate averages)

By virtue of its definition, H_{mo}^e can be used in sediment transport calculations to obtain a reasonable estimate of the wave induced longshore transport rate based on only this one representative wave condition. The energy-equivalent average wave height H_{mo}^e for East London is calculated to be about 1,9 m (based on the Waverider data recorded off the main breakwater in 22 m water depth). The value of 1,9 m (together with average open coast values for the other parameters) indicates that the potential transport rates (due to wave energy alone) are relatively high (hundreds of thousands to about a million m^3/a).

The information discussed in this section indicate that, during the early stages of this study, good nearshore wave data was available for East London in terms of wave heights and periods. However, wave directions are also critical for calculating currents and sediment transport. Alternative data sources that included directional wave data therefore had to be utilized.

3.2.5 Nearshore wave directions from aerial photographs

Fifteen different sets of vertical aerial photographs (e.g. Figure 1.1) have been analysed so as to determine nearshore wave directions. As an example, the wave crests thus identified in the Hood Point to main breakwater area, have been plotted on Figure 3.4. The following can be deduced in general.

At Hood Point (south-west of the port) as well as Eastern Beach (north-east of the port) the direction of the incident waves is such that in virtually all instances a generally north-westwardly (upcoast) flowing current (and thus longshore transport) would be generated near the shore (almost all within the surf zone). The large wave angles (relative to the coastline) together with the high wave energy at Hood Point, indicates high potential longshore transport.

Seaward of the main breakwater, the wave attack is observed to be approximately normal to the breakwater on about half of the photographs. Less than 10% of the observed waves clearly break obliquely towards the head of the breakwater. Analysis of oblique photographs confirms this pattern. (These oblique photographs were taken from the top of the grain elevator, the large crane on the breakwater and from a helicopter (e.g. Figures 3.1 and 3.2), as part of the annual breakwater monitoring over the last decade, e.g. CSIR, 2004.) This would tend to indicate that the wave attack along the seaward side of the main breakwater would mostly generate relatively weak longshore currents parallel to the breakwater, although stronger currents (and sediment transport) towards the head of the breakwater would occasionally be generated.

At Orient Beach the nearshore wave directions indicate At Orient Beach the observed wave crests are

all approximately parallel to the beach. This indicates that wave generated longshore currents in the surf zone of this beach are very weak. Together with the low wave energy in this area (Figure 3.2), this indicates low longshore transport rates in the surf zone.

Although robust, the above discussion is only based on a relatively limited number of wave directions determined from photographs. Accurate wave data including heights, periods and directions is an essential input to quantify nearshore currents and sediment transport.

3.2.6 East London VOS data

The only really long-term wave data recorded in the vicinity of East London that includes wave heights, periods and directions, is the so-called VOS data. Voluntary Observing Ships (VOS) record visual observations of wave height, wave period and wave direction at six-hourly intervals (Rossouw, 1989 and Swart and Serdyn, 1979).

The swell rose (Figure 3.5) indicates the occurrence of wave heights and directions as recorded from more than 30 000 observations made offshore of East London. The area covered by these observations encompasses the five $1^{\circ} \times 1^{\circ}$ ocean sectors closest to East London between the 32 to 34 southern latitudes and the 27 to 30 eastern longitudes (Figure 3.6). From the swell rose it is clear that the dominant offshore wave direction is southerly to west-south-westerly, with wave heights ranging from about 1 m to 7 m. A secondary (but relatively much less frequent) offshore wave direction sector appears to be easterly to north-easterly, with wave heights ranging from about 1 m to just over 4 m. Overall, wave heights of 1 m to 2 m occur by far the most frequently.

Thus, a long-term data set of wave heights, periods and directions for the wave climate offshore of East London is available. However, this data is based on visual observations, which are not sufficiently accurate for the detailed current and sediment transport calculations required in this study.

3.2.7 Agulhas Bank wave data

Up until recently, the most appropriate *long-term* data source, which includes wave directions and is of sufficient accuracy, is the Agulhas Bank data collected off Mossel Bay (CSIR, 1993a). In this data set, the wave heights and periods were measured by means of a Waverider buoy while the wave directions were hindcast from weather data. As the deep-sea swells off East London and Mossel Bay are mostly generated by the same weather systems, the wave heights are considered to be fairly similar. However, as Mossel Bay is located much further westward, the Mossel Bay swell directions are expected to be different from the East London swell directions.

Figure 3.7 shows the VOS swell rose for the area off Mossel Bay, which is fairly similar to the East London swell rose (Figure 3.5). The most common wave height (20% occurrence) for both the Mossel Bay and East London areas is about 2 m, while wave heights are in the 1 m to 3 m range for about 75% of the time. Storm waves of above 3m occur for about 17% of the time in both areas, with exceptionally large storm waves in the order of 6 m. The most common wave direction sector off Mossel Bay is 210° to 240° (20% occurrence), while a secondary peak occurs around about 90° (10% occurrence). However, off East London the most common wave direction sector is 190° to 210° (22% occurrence), while the secondary peak occurs around about 60° . Figure 3.6 shows a comparison of the

distribution of VOS wave heights and directions for the two areas. Clearly, the wave height distributions are virtually identical, while the wave directions show a marked shift (with the East London waves between about 0° to 30° more “easterly”). Thus, to utilize the Agulhas Bank wave data for East London, the Agulhas Bank wave directions have to be adapted in order to make the data applicable to East London. Figure 3.8 shows a comparison of the wave direction exceedance curves for the East London and Mossel Bay VOS data. Also shown in Figure 3.8 is the adapted exceedance curve for Mossel Bay after a shifting function has been applied to the Mossel Bay VOS wave directions. Good agreement is achieved with the East London VOS data throughout the range of wave directions.

This same shifting function was then applied to each individual record of the Agulhas Bank directional wave data set to obtain an accurate offshore wave climate for East London. Thus, a long-term data set was constructed, consisting of almost 15 000 individual wave height, period and direction conditions. (A statistical analysis of this data set showed that the average wave height was about 1.9 m, the average wave period was about 12 s, and by far the most common wave direction was south-southwest.) Based on this information, the nearshore wave regime could be derived as discussed in the following section.

3.2.8 Simulated nearshore wave regime

Modelling approach

Mathematical wave transformation models can be used to derive the nearshore wave regime (including wave directions) using the offshore wave climate as input. Two wave transformation models were available for use when this part of the study was conducted. The first is a wave refraction model, HISWA (HIndercasting of Shallow Water Waves; HISWA, 1993), which is particularly suited to describe the wave transformation process from deep water to the shore. The second is a combined wave refraction/diffraction model, REF/DIF 1, which describes the processes of both refraction and diffraction. The latter model is computationally more intensive than HISWA and is best suited to describe the transformation of waves in local areas such as in the wave shadow of a breakwater or landward of a breakwater gap. The approach adopted for the modelling described here was therefore to run the wave refraction model HISWA from deep water using the offshore wave data described in Section 3.2.7 as input. (Note, that more recently, the HISWA model has been superseded by the SWAN wave model (Holthuijsen and Booij 2003), which would at present probably be the model of choice to conduct such investigations.)

The model wave results could eventually also be compared to the Waverider measurements off the port, which would serve as a verification of the modelling process. This is, however, beyond the scope of this study. The scope of the present investigation also did not allow for a full wave climate study whereby numerous wave modelling runs are performed on a large number of wave scenarios. The initial approach was to model representative average and extreme wave scenarios so as to determine what effect the wave conditions could have on sediment transport.

In the latter stages of this study, more comprehensive wave modelling was conducted. A new wave schematisation method was developed and adapted based directly on sediment transport modelling results. This wave modelling was conducted as an integral part of the morphological modelling and cannot logically be decoupled from the morphological modelling. For this reason the later wave

modelling is described in Section 4.4.2.2 as part of the morphological modelling.

HISWA model basis

HISWA is a numerical model used to obtain realistic estimates of wave parameters in coastal areas, lakes and estuaries from given stationary wind-, bottom-, current- and offshore wave conditions (HISWA user manual, 1993). The basis of the model is a parameterized version of the action balance of the waves (or energy balance in the absence of currents). The theoretical background of the model is described in detail in Holtzhuijsen *et al.* (1989). Additional information e.g. model description, evaluation and comparison with other models has been published by Booij *et al.* (1985), Dingemans *et al.* (1986), Holtzhuijsen *et al.* (1986), Soras *et al.* (1987), Vogel *et al.* (1988) and Den Adel *et al.* (1991).

The physical phenomena accounted for in HISWA are wave shoaling, wave refraction, wind-wave growth, bottom (friction) dissipation, surf zone (breaking) dissipation and current dissipation. Traditional ray tracing models transform discretized wave components along the path the wave follows to provide a description of the wave conditions at a specified point. In HISWA the wave field is determined at all positions over a grid. The wave spectrum in HISWA is discrete only in directions and parametric in the frequencies, i.e. for each spectral wave direction a frequency-integrated energy density and mean frequency are propagated.

HISWA is capable of handling large cell sizes of the order of hundreds of metres and is therefore particularly suited to model wave transformation from deep water over large open coastal areas to provide a description of the wave climate inshore. The model does not describe wave diffraction, which is important in situations where waves travel through a gap, past a breakwater or past an island or shoal. Whilst HISWA can therefore be used to calculate the wave transformation from deep water to shore in this study, it is not suited to model the waves entering the harbour as wave diffraction becomes important.

Bathymetric input

Input bathymetric data was obtained from three separate CSIR surveys conducted off East London (1995.01.20, 1993.09.03 and 1985.02) as well from a NPA survey (1995.07.25) of the entrance channel and port area. The remaining gaps (especially the offshore areas) were filled in from SAN hydrographic charts (SAN 1027 printed 1975, SA19 printed 1971, 1843 printed 1965 and SA18 printed 1961).

By collating the information from all of these surveys, an accurate bathymetric map of the sea floor could be drawn up which includes the whole area from the -200 m contour up to the shoreline. Figure 3.9 shows the bathymetric map thus compiled for the area between Shelly Beach and Nahoon Point, while Figure 3.10 shows a closer view of the area adjacent to the Port of East London.

Wave scenarios

In Section 3.2.7 a description is given of how the deep-sea wave climate off East London was compiled. This data consists of almost 15 000 individual combined sets of wave heights, periods and directions. Deep-sea wave directions that would move away from the coast at East London were eliminated from the data base. The remaining data was analysed statistically so as to identify the

Sediment Transport Regime at East London

primary component events and individual wave conditions that are representative of specific conditions. (This was based on binning of the wave data in $12,25^{\circ}$ direction bins and 2 s period bins. The number of events, as well as average wave heights and periods were determined within each bin. The primary wave events were then selected by combining wave directions, heights and periods, with the highest occurrences that represent the primary components of the wave regime.)

Three wave scenarios were chosen for the modelling exercise. Firstly a "most typical" or "average" wave condition was considered, as this would also be representative of the "most typical" effect on sediment transports. This condition was taken to be the wave condition that occurs most frequently in deep water. Thus, the average wave height, period and direction combination was determined which is representative of the most common (highest occurrence) offshore wave condition. Similarly, the wave condition representative of a typical storm condition associated with the passage of a low pressure system was determined. This condition would also be representative of the effects of a typical low pressure frontal storm condition on sediment transports. Finally, the wave condition most representative of locally generated wind waves with an easterly direction, was determined, which would again also be representative of the effect of such conditions on sediment transports. Although a wide range of scenarios was not selected, it is considered that these three conditions are sufficiently well representative of the bimodal wave directional distribution off East London (i.e. long-period south-westerly storm swells and shorter period easterly seas) with associated wave heights, as well as the overall "most typical/common" wave condition. The actual wave conditions thus determined are shown in Table I below.

Table I: Input wave conditions for HISWA refraction model.

Case No	Wave height (H_{m0}) m	Wave period (T_p) s	Wave direction degrees north	Occurrence (approx) %	Condition represented
1	1,9	12	214	62	most common
2	4	15	214	< 1	typical SW storm
3	1,7	10	88	< 5	local NE to E wind

For this wave modelling study, no currents or wind conditions were specified.

Results

The HISWA wave refraction model was used to determine the nearshore wave conditions for each of the three offshore wave conditions given in Table I above. (The actual computer runs were conducted by Mr F Smit, then of the CSIR.) All wave heights obtained from HISWA plots are significant heights, H_s (H_s is assumed to be equal to H_{m0}).

Figure 3.11 shows the nearshore wave heights and directions thus determined for the most common offshore wave condition ($H_{m0} = 1,9$ m, $T_p = 12$ s, $\theta_b = 214^{\circ}$). Thus, significant breaking wave heights range from about 1,8 m at Hood Point to 1,6 m along the main breakwater, and 1,3 m at Eastern Beach to 1,6 m at Nahoon Point. Breaking wave angles range from as much as 45° at Hood Point to 0° about halfway along the main breakwater, and from nearly 0° at Eastern Beach to more than 45° at

Nahoon Point. Note that the HISWA model is a wave refraction model only (including wave shoaling and breaking) but does not take account of wave diffraction effects. The simulated wave conditions in the lee of the main breakwater are therefore not correct.

Similarly, Figure 3.12 shows the nearshore wave heights and directions for a typical heavy storm condition ($H_{mo} = 4$ m, $T_p = 15$ s, $\theta_b = 214^\circ$). As expected, a significant increase in wave heights is clearly seen. Significant breaking wave heights now range from about 4 m at Hood Point to 3,5 m along the main breakwater, and about 3,5 m in the Eastern Beach to Nahoon Point area. Due to the longer wave period, breaking wave angles are slightly smaller than in the previous (most common) case.

Figure 3.13 shows the nearshore wave conditions for a typical locally generated (easterly) wind wave condition ($H_{mo} = 1,7$ m, $T_p = 10$ s, $\theta_b = 88^\circ$). In this case, significant breaking wave heights range from about 1,7 m to 1,8 m in the Hood Point to main breakwater area, and about 1,5 m to 1,7 m in the Eastern Beach to Nahoon Point area. Most noteworthy is obviously the big change in wave direction as compared to the previous two scenarios. Breaking wave angles now range from nearly 0° at Hood Point to as much as 60° near the head of the main breakwater, and from nearly 0° at Eastern Beach to more than 45° at Nahoon Point. Clearly, this scenario results in downcoast longshore currents in most areas, whereas the previous two scenarios result in mostly upcoast longshore currents in most areas.

Whilst the wave modelling undertaken here, does not cover a comprehensive wave climate, it does provide an indication of what the dominant nearshore wave conditions are expected to be in the study area.

Further parameters which are important to this study and which were determined from the HISWA refraction results are the breaking wave heights and directions as well as the surf zone widths (as discussed in Sections 3.2.10 and 4.2).

3.2.9 Recent directional wave recordings

In the latter stages of this study, some directional wave data started becoming available from measurements at East London. The directional wave data is recorded at the same location as shown in Figure 1.2 (in 22 m water depth), by means of a “3D” (differential global positioning system) type wave recorder. Intermittent recordings began in November 1997 and only became more regular from about 1999. The total data set up to August 2004 consists of 30 686 records.

The directional wave data up to August 2004 is summarized in Figures 3.14 and 3.15. At this location, virtually all waves (99,9%) approach from between the east to southwest, with about 48% and 26% from the south and south-southeast respectively. The wave height is between 1 m and 1,5 m for almost 50% of the time, while the highest waves (>3,5 m) approached from the south. Wave periods were mostly between 10 s and 12 s, while only about 10% exceeded 13 s. Waves with periods exceeding 15,5 s only approached from between the south to east-southeast.

This data was used for some of the sediment transport and morphological modelling studies, as described in Section 4.4. It is considered that, in the near future, a sufficiently accurate description of the long-term nearshore wave regime at East London could be made, when 6 to 8 years of good quality directional wave data have been obtained.

3.2.10 Surf zone widths

Surf zone widths are used as input to sediment transport calculations as discussed in Section 4.2. Most longshore sediment transport occurs within the surf zone. Thus, surf zone widths also give a good indication of the main zone of longshore transport. As will become apparent in Section 4, it is the surf zone widths along the seaward half of the main breakwater, which are most relevant to this study.

Based on the wave refraction analysis (Section 3.2.8), the surf zone width along the seaward half of the main breakwater was found to be about 125 m for the most common wave condition (Case no. 1). The surf zone width was found to be about 250 m for the typical storm condition (Case no. 2) while from the easterly wind wave condition (Case no. 3, low occurrence) a width of about 140 m was obtained.

Surf zone widths can also be estimated directly from aerial photographs (Section 3.2.5 and, for example, Figure 1.1). Thus, an aerial photograph analysis based on all available (15) photos gave an average surf zone width of 110 m to 150 m along the seaward half of the main breakwater. The maximum width measured on these photographs was about 210 m.

Besides the above, surf zone widths were also calculated theoretically for the wave conditions as measured by the means of the Waverider buoy off East London (Section 3.2.4). These calculations are mainly based on the bottom slope ($\tan \alpha$) and the breaker index (γ) as derived by Nairn (1990):

$\tan \alpha$	=	d_b / x_b
with: d_b	=	depth at breakpoint
x_b	=	surf zone width
and d_b	=	H_{bs} / γ
with: H_{bs}	=	significant breaking wave height
and γ	=	$0,39 + 0,57 \cdot \tanh (33 \cdot H_{m0} / L_o)$
with: H_{m0}	=	significant deepwater wave height
L_o	=	deepwater wave length
and L_o	=	$1,561 \cdot T_p^2$ (approximately)
with T_p	=	peak wave period

Sediment Transport Regime at East London

The mean bottom slope for the area adjacent to the main breakwater was determined from the survey data (as discussed in Section 3.2.8). The results are summarised in Table II below.

Table II: Surf zone widths calculated from Waverider data.

Wave condition exceedance (%)	Surf zone width (m)
maximum measured	510
1	300
5	230
10	195
25	160
50 (median)	125

The above independent method of determining the surf zone widths thus provides very similar results to those determined from the wave refraction analysis (Section 3.2.8) and the aerial photographs (Section 3.2.5). This significantly increases the confidence of these findings. Based on the results, it would appear that the median width of the longshore transport zone along the seaward half of the main breakwater, would be about 125 m (a narrower surf zone would in this case mean low wave heights and resulting low wave energy). The maximum width would mostly be around 250 m (surf zone widths would exceed this width less than 5% of the time). The weighted mean surf zone width based on the calculated widths is about 150 m. In view of the relatively higher transports associated with higher waves, it is therefore concluded that the effective longshore transport zone width along the seaward half of the main breakwater is between 150 m and 250 m.

3.3 Current Regime

3.3.1 Background

The current regime at East London is of particular importance to this study because of the ability of the currents to transport sand. In particular, the velocity, location and persistence of the currents were investigated. Different types of currents within the East London coastal zone are distinguished here:

- Wave driven currents in the surf (breaker) zone.
- Ocean currents such as the Agulhas Current - usually in the offshore zone, but can also act in the nearshore, such as found at East London.
- Tidal currents in the nearshore, but more prominent in river and harbour mouths.
- Wind driven currents in the nearshore zone (including the surf zone).

All of the above currents can potentially transport sediment and cause sand to be deposited in various areas.

3.3.2 Surf zone (wave induced) currents

The wave induced surf zone currents are the main mechanism responsible for the sediment transport in the surf zone and are normally responsible for the bulk of sediment accretion in a harbour entrance.

3.3.2.1 Surf zone currents measured south-west of the main breakwater

Method

During November 1996 surf zone currents were measured along the "beach" to the south-west of the main breakwater (adjacent to the Foreshore area, Figure 1.4). In this relatively high wave energy environment, the best practical way of measuring surf zone currents was by means of dye tracking tests.

The procedure was basically as follows:

Reference markers and beacons were first constructed along the beach, above the high tide run-up line (e.g. Figure 3.16). Dye was released into the surf zone and the position of the dye patch was tracked by observation from the shoreline and photography from the top of the adjacent grain silo complex. By determining the temporal and spatial location of the centroid of the dye patch, a reasonable estimate of the surf zone currents were made. From these measurements, the full cross-shore distribution of the longshore current can be determined theoretically. Five days of field work provided a reasonable amount of data (sufficient, for example, to calibrate a mathematical model).

The second (and also important) part of the information required on the surf zone currents was to determine the wave conditions causing the measured currents. This entailed the following:

As wave directions were not measured at East London at the time, deep-sea wave directions (at the time of the current measurements) were determined by means of wave hindcasting techniques. By means of the wave refraction model (described in Section 3.2.8) the nearshore and breaker wave conditions (wave height, period and direction) can then be deduced from the deep-water wave conditions. The simultaneously recorded Waverider data (wave height and period) can ultimately be utilized to verify the deduced nearshore wave conditions to ensure the best possible accuracy in the wave refraction modelling.

The surf zone current measurements were conducted during the week of 4 to 8 November 1996 approximately over the neap tidal cycle (in conjunction with other drogue measurements). The wave hindcasting analysis was conducted shortly thereafter, when the relevant data were available from the Weather Bureau.

*Sediment Transport Regime at East London***Wind and wave conditions**

Wind velocities and directions were recorded during all of the current measurements. The wind recordings are given in Table III below.

Table III: Wind recordings – 4 to 8 November 1996.

Date	Velocity range (knots)	Direction (sectors)
4.11.96	8 to 29	south-west
5.11.96	6 to 20	south-west
6.11.96	0 to 3	west-south-west
7.11.96	10 to 20	north-east
8.11.96	1 to 6	east to west

The *breaking* wave and surf zone conditions observed along the beach directly adjacent to the Foreshore area are given in Table IV below.

Table IV: Wave and surf zone conditions at the beach adjacent to the Foreshore area.

Date	Time	H_{bs} (m)	H_{bmax} (m)	θ_b (deg)	T_p (s)	x_b (m)	Wave induced current direction
4.11.96	10h00	1-1,2	1,5	5-15	9	~5	towards b.w.
4.11.96	11h00	1-1,2	1,8	5-15	9	~5	towards b.w.
5.11.96	10h00	1,0	1,5	10-15	8	5-7	towards b.w.
6.11.96	09h00	1,0		~5	10-13	~7	
7.11.96	09h00	1,5	2,0	15-30	8-10	30-150	towards H.P.
8.11.96	09h00	1,3	1,6	15-30	10-13	30-150	towards H.P.
8.11.96	12h30	1,7	2,0	20-25	10	15-30	towards H.P.

Note: b.w. - main breakwater (thus, towards b.w. indicates that the induced longshore current flowed towards the breakwater)

H.P. - Hood Point (towards H.P. indicates that the induced longshore current flowed towards Hood Point)

(See the list of symbols (page xv) for definitions of the other parameters.)

Figure 3.17 shows the wave angle at 13:00 on 8 November 1996 (as an example).

Based on the recorded weather and wave data and following the wave hindcasting method described in Appendix A, the sea and swell wave parameters including estimated deep-sea wave directions were obtained. These results are also given in Table A1 in Appendix A. In general, it was found that the wind and wave conditions observed on site concur reasonably well with the recorded and estimated conditions. A comparison is shown in Table V below.

*Sediment Transport Regime at East London***Table V: Comparison of observed, recorded and estimated wind and wave conditions.**

Wind direction (sectors) comparison			
Date	Site observations	Port control recorder	Weather chart hindcast
04.11.96	SW	WNW	SW to WSW
05.11.96	SW	-	SW
06.11.96	WSW	-	SW
07.11.96	NE	NE-S-NW	ENE
08.11.96	E to W	W	ENE to WSW
Relative wave height comparison			
Date	Site observations (m)	Waverider recording (H_{m0})	
04.11.96	1,0 - 1,5	1,1 - 1,3	
05.11.96	1,0 - 1,5	1,4 - 1,6	
06.11.96	1,0	1,2 - 1,6	
07.11.96	1,5 - 2,0	2,7 - 3,1	
08.11.96	1,3 - 2,0	1,4 - 2,0	

(It is interesting to note that the wind conditions determined from the weather charts corresponded better with the observed on site conditions than did the wind data recorded at Port Control. This is probably due to the fact that Port Control is situated on the slope of a hillside, which could result in significant topographical effects of the local wind flows.)

Current measurements

Figure 3.16 depicts the movement of a dye patch on 8 November 96, as an example. From the dye tracking tests, the longshore currents were calculated as given in Table VI below.

*Sediment Transport Regime at East London***Table VI: Longshore currents calculated from dye tracking tests.**

Date	Time	Current velocity (m/s)		Current direction (towards breakwater or Hood Point)	Calculated from
		Range	Average		
4.11.96	10h05-11h17	0,05-0,18	0,09	to b.w.	observations
5.11.96	08h55-09h10	0,13-0,23	0,18	to b.w. head (at spur)	observations
5.11.96	09h50-10h30	0,13-0,27	0,16	to b.w.	observations
6.11.96	09h00-11h25	0,0-0,14	0,07	to b.w.	observations
7.11.96	08h43-09h57	0,42-0,83 0,31-0,60	0,52 0,47	to H.p to H.p	observations photographs
7.11.96	13h35-14h17	0,44-0,71 0,39-0,73	0,58 0,59	to H.p to H.p	observations photographs
8.11.96	08h55-09h41	0,42-0,63 0,35-0,76	0,54 0,55	to H.p to H.p	observations photographs
8.11.96	12h25-13h26	0,14-0,42 0,16-0,44	0,28 0,29	to H.p to H.p	observations photographs

Both observations from the shoreline and oblique photographs were used so as to obtain at least some measure of the relative accuracy of the values. The correlation between the current velocities obtained from the observations and the photos (Figure 3.18) is considered to be good (especially if the average values are compared). Thus, it was found that the average surf zone current velocities ranged from 0,28 m/s to 0,59 m/s towards Hood point, and from 0,07 m/s to 0,18 m/s towards the main breakwater, at the time of the measurements. The relatively stronger downcoast longshore current during 7 and 8 November 1996 resulted from the larger wave heights and wave incidence angles (Table IV) that occurred then.

General Conclusions

The following is concluded in general from the surf zone currents that were measured along the beach to the south-west of the main breakwater. Waves with a deep-sea wave direction of south-west to west-south-westerly (the most common scenario) and relatively low wave heights ($H_{bs} = 1$ to 1,2 m) resulted in surf zone currents flowing towards the harbour with fairly low average velocities, and (probably low) longshore transport towards the harbour. Waves with a deep-sea wave direction of east-north-easterly (an uncommon scenario) and about average wave heights ($H_{bs} = 1,3$ to 1,7 m) resulted in surf zone currents flowing towards Hood Point with about medium average velocities, and (probably significant) longshore transport from the root of the main breakwater towards Hood Point. The correlation between deep-sea wave directions and surf zone current directions, as well as between wave height and current velocities is also clear. (The surf zone wave angle obviously also has a major effect on the current velocity with larger angles potentially resulting in orders of magnitude greater longshore transport.)

3.3.2.2 1990 and 1993 field observations

During a site visit in June 1993, various field observations were conducted in conjunction with NPA. Rhodamine dye was released at 3 locations along the seaward side of the main breakwater (Figure 3.19). The wave direction at the time was more easterly than “normal”. Under these circumstances relatively little dye moved through the breakwater. The general movement of the dye is shown in Figure 3.19.

Surf zone observations of sediment plumes were also conducted during a site visit in November 1993. The wave attack was virtually normal to the main breakwater, which coincides with the general wave regime. The current patterns as derived from these observations, are depicted in Figure 3.20. It was obvious that relatively large amounts of sediment were moving through the main breakwater (e.g. Figure 3.21), while there was also a current flowing parallel to the breakwater towards the head.

Dye tests were conducted by NPA during November 1990 (Withers, 1991). Rhodamine dye was released at five different locations on two consecutive days. The observed current patterns in the surf zone at Orient Beach (and near the head of the secondary breakwater) are also indicated on Figure 3.20. Thus, a weak surf zone alongshore current was observed flowing from north to south (towards the secondary breakwater) along Orient Beach.

3.3.2.3 Calculated longshore current velocities

In order to compute the longshore current velocities in the surf zone, the wave characteristics at the breaker line have to be available at the sites of interest. In this case it is the surf zone currents seaward of the main breakwater that were calculated. The mean significant breaker height (mean H_{bs}) and the mean wave incidence angle for this beach were obtained by analysing the refraction results described in Section 3.2.8 and by using a breaker index ($= H_{bs}/d_b$; d_b = breaker depth) of 0,7. The results were averaged along the seaward 300 m of the main breakwater.

The longshore current velocities in the middle of the surf zone (v_{mid}) were calculated with the method of Komar (1979), which is well verified:

$$v_{mid} = 1,17 \cdot (g \cdot H_{bs})^{0,5} \cdot \sin \theta_b \cdot \cos \theta_b \text{ [m/s]}$$

with θ_b = breaking wave angle [degrees]
 g = acceleration of gravity [m/s^2]
 H_{bs} = breaking wave height [m]

The mean longshore current velocity (\bar{v}) through the surf zone (which is required for sediment transport calculations) was assumed to be one half of the velocity at the mid-surf position ($\bar{v} = 0,5 \cdot v_{mid}$). Because the maximum current velocity usually occurs close to the centre of the surf zone and because the longshore current velocity can be roughly approximated by a (smoothed) triangular distribution (Longuet-Higgins, 1970), this is a reasonable assumption.

In accordance with the occurrences of the input wave conditions, it was assumed that the calculated current velocities are similarly representative of the occurrences of the actual long-term current conditions, which is reasonable. Thus, it was determined that the mean velocity of the longshore current in the surf zone along the seaward 300 m of the main breakwater, ranges from about 0 m/s to more than 1 m/s. This indicates that the potential longshore transport can also range from 0 to very high rates depending on the incident wave conditions. For typical wave incidence angles, the mean

velocity would normally be low, between 3 and 5 cm/s towards the head of the breakwater (normally also indicating low longshore transport). Under strong easterly wave conditions a mean longshore current velocity of more than 1 m/s could be generated in the opposite direction (towards the Foreshore area), generating transports in the same direction (towards the Foreshore area). However, the occurrence of such strong easterly wave events is relatively low (probably less than 5% based on the wave data).

3.3.3 Deeper water currents

3.3.3.1 General regional current regime

The Agulhas Current is a major western boundary current flowing in a south-westwards direction along the east coast of South Africa (Figure 3.22). It is the most important factor controlling sediment transport in the deeper waters (beyond about 40 m depth) on the continental shelf. It is fed by the Mozambique Current, the East Madagascar Current, and the Agulhas Return Current (Flemming, 1981). Lutjeharms, *et al.* (1989) show that the northern Agulhas Current (including the East London area) follows the continental shelf edge quite closely with no perceptible regular meandering or large border eddies (Figure 3.22). Due to the extremely narrow continental shelf, the Agulhas Current is one of the few fast-flowing ocean currents found close to the coastline for appreciable distances (over 1 000 km). Surface current velocities of > 2,5 m/s have been reported for the core of the current, just beyond the shelf break (Pearce *et al.*, 1978). Harris (1978) concludes that small cyclonic (clockwise) current vortices occur between Nahoon Point and the harbour as well as between the harbour and Hood Point. Such phenomena often occur when currents flow past headlands (Boyer and Tao, 1987 and Pattiaratchi *et al.*, 1986).

3.3.3.2 Overall current patterns in the Nahoon - Hood Point area

1984 to 1985 measurements

A detailed data collection programme of the East London marine environment was undertaken from February 1984 to June 1985 (CSIR, 1989). The data collection aimed at providing a sound concept of the relevant physical marine processes. The data collection programme included the operation of fixed recording meters for currents (two locations), waves and wind, as well as direct recordings from a light vessel. The latter were done during six field trips to East London involving a total of 96 days at sea. The current recordings obtained in this programme were mainly carried out in the nearshore zone, but excluded the surf zone. Fixed measurement stations were used with electronic position fixing to accurately collect data from (Figure 3.23):

- 470 releases of drogues to determine surface and sub-surface current patterns
- 555 profiles of currents
- 690 profiles of salinity and temperature

The results and conclusions from the above measurements can be summarised briefly as follows:

The presence of the swiftly flowing Agulhas Current from north-east to south-west, parallel to the shore, was the dominant influence on the local water movements. The current mostly flows relatively

close to the coastline of East London. For about two thirds of the observations the current flowed swiftly in a south-westerly (downcoast) direction, sweeping all waters with it. The opposing south-westerly winds were seen to “turn” the shallower waters occasionally in a north-easterly direction. When the Agulhas Current was further offshore, the south-westerly winds could dominate and cause a reversal to a slower north-easterly (upcoast) current, assisted occasionally by a return current from an eddy trapped inshore of the Agulhas Current. Onshore and offshore currents were generally weak and short-lived being transient between the shore-parallel current directions. The strongest surface current recorded was 70 cm/s in a south-westerly direction. The observed current patterns are also shown in Figure 3.23.

Figure 3.24 shows the statistical occurrences based on the Aanderaa current data collected off Hood Point and Nahoon Point in 30 m water depth. (The total recording period of about 311 days was made up of two periods: 12 April to 26 September 1984 and 4 November 1984 to 24 February 1985.) The median current speed is 0,2 m/s, and values of 0,3 m/s, 0,4 m/s, and 0,5 m/s are exceeded for approximately 20%, 5% and 1% of the time respectively. As described above, the downcoast currents are clearly dominant, while the upcoast (northerly) components in total represent less than 20% of the observed currents.

1959 measurements and physical modelling

During 1959, a small hydraulic model of the coastline at East London was constructed to determine the effect of the strong offshore Agulhas current on the nearshore circulation of water (Whillier, 1962). The movement of water to simulate the Agulhas current in the model, was obtained by pumping. The model was to a horizontal scale of 1 in 6 250, with 16- fold vertical exaggeration, and covered an 8 km length of coast. The overall model size was about 3 m by 1,2 m. The depth contours were modelled down to about 30 m, and thereafter the bottom was flat. It was verified that the small scale of the model, the large vertical exaggeration, and the water velocity in the model, were not critical factors, due to the nature of the problem that was being investigated. No attempt was made to study wave action and the resulting littoral current in the model.

Also during 1959, several *in situ* measurements of deeper water current patterns were conducted by means of surface and sub-surface floats (~3 m deep) as well as dye tests (Whillier, 1962). Wind conditions during these tests ranged from calm to storm winds, with directions from northeast to southwest. The current measurements and model simulation are both shown on Figure 3.25. Despite the various wind conditions encountered during the measurements and their possible effects on observed flow patterns, the measurements do generally fit the pattern found in the model quite well. Most evident is the overall strong downcoast flow, with a clockwise eddy just southwest of the main breakwater, and larger eddies / counter currents in the area between Nahoon Point and the main breakwater. The model results are considered only a rough indication of the Agulhas Current’s influence on the nearshore current regime (excluding surf zone currents).

Current patterns from aerial photographs

All available vertical aerial photographs (nine sets) were analysed so as to investigate current patterns. In general, current patterns could not be clearly identified on the available photographs. Nevertheless, a clockwise eddy south of the main breakwater can be seen on some of the photographs. A general south-westerly flow, parallel to the coastline but further seaward (from the head of the main breakwater) can also be deduced from some of the photographs.

Current observations by ships pilots

Since December 1995, the harbour pilots at East London observe and record current velocities and directions as well as general wind conditions as they bring each ship into the port. These recordings apply to the zone seaward of the head of the East London main breakwater. The observations may appear to be very subjective, but are actually based on their ship navigation operations and their long practical experience of local conditions, which in fact give a reasonably good indication of current conditions. Statistics based on their observations, show downcoast currents for about 62% of the time and upcoast for 38%. This agrees well with the occurrence of current patterns presented in Figure 3.23.

The current velocities estimated by the harbour pilots are considered to be relatively inaccurate, but perhaps more importantly, they also indicate that the mean downcoast velocity is approximately twice the upcoast velocity.

1895 field observations

During February and December 1895 extensive measurements were conducted by means of surface floats (NPA East London Drawing Office, 1993). Although conditions in 1895 are not totally representative of the present situation (due mainly to the absence of the breakwaters), this data does provide valuable corroborating information about current patterns in the study area. The general current patterns that can be deduced from this data are shown on Figure 3.26. The main difference between this data and the other information discussed above, is perhaps that in 1895 the clockwise eddies formed south of the main breakwater were much smaller and not “fixed” in place but moved in a downcoast direction. The present stronger and less transient nature of the eddy is a direct result of the relatively larger protrusion of the main breakwater from the “original” 1895 shoreline.

Discussion - Nearshore portion of the Agulhas current

The information derived from all the different data sources are very consistent and in good agreement for the entire Nahoon - Hood Point area. The Agulhas Current, flowing from the north-east to the south-west, parallel to the shore (i.e. downcoast), is the dominant influence on the local deeper water flows and has the potential to transport very large amounts of sediment in the deeper nearshore zone (40 m to 60 m depth) reducing shorewards. In the nearshore zone, seaward of the surf zone off the main breakwater, the current flows swiftly in the south-westerly direction for about 70% of the time, thereby also transporting sediments in a downcoast direction. When the Agulhas Current is further offshore, with consistent south-westerly winds, this can cause a reversal to a slower north-easterly current in the nearshore, which has the potential for transporting sediment in the upcoast direction (this occurs for less than 30% of the time). As the mean downcoast current velocity is about twice the upcoast velocity and the downcoast occurrence is also much higher, the potential for downcoast sediment transport in the nearshore zone (excluding the surf zone) is an order of magnitude higher than upcoast transport. Onshore and offshore directed currents in the nearshore zone (excluding the surf zone) are generally weak, of short duration and occur very rarely, and are therefore not significant in terms of the sediment transport regime. Small cyclonic (clockwise) current vortices occur just to the south of the main breakwater when the deeper water current flows in a downcoast direction. The surf zone currents in the Hood Point to main breakwater area, together with the deeper water currents, probably induce this clockwise eddy adjacent to the Foreshore area. Further field measurements would be required to accurately quantify the effects of such eddies on sediment

transport in the vicinity of these eddies (such as described by Sasaki and Sakuramoto, 1984).

For the dominant scenario at East London (i.e. relatively swift downcoast currents in the deeper water), the following can be deduced in general. The velocity of the downcoast current increases steadily from the offshore (in deeper water, where the influence of the Agulhas Current is strongest) towards the coastline (in shallower water, where the edge of the current has weaker influence). However, the main breakwater causes a significant concentration or increase in current velocity in the area seaward of the head of the breakwater (as often found in similar instances, e.g. Ferentinos and Collins, 1980). Current directions are mainly parallel to the coast and in the area adjacent to the main breakwater the direction is about north-south. Obviously, increasing current velocity indicates greater potential for sediment transport, while the sediment transport direction generally follows the current direction.

3.3.3.3 Currents in the vicinity of the entrance channel

The information presented in the previous section (Section 3.3.3.2) provides a very good overview of the currents in the greater East London area. In order to obtain more quantitative information on the currents closer to the harbour, the extensive data set of the 1984/85 CSIR measurements was reanalysed. *In this case only measurements within 2 km from the main breakwater and in water depths less than 35 m were considered.* The current data in this area consists of measurements by means of drogue tracking and an Endeco electronic vector-averaging current profiler. (Possible wind effects on the currents are discussed in Appendix B.)

1984 to 1985 drogue tracking measurements

Data from both surface and sub-surface drogues (5 m deep) are available for the area of interest. *In this case only the sub-surface data was used* as these give a more accurate representation of the actual sub-surface (sediment transporting) currents. The bottom depths where these measurements were made ranged from -8 m to -35 m CD with an average bottom depth of -19 m CD. These measurements were recorded at 140 m to about 2 000 m (with an average distance of about 1 200 m) from the head of the main breakwater.

The data was analysed statistically and the direction occurrence histogram is shown in Figure 3.27. The data was also subdivided into two groups depending on whether the measurements were made upcoast (designated NE for north-east on the figure) or downcoast (designated SW for south-west on the figure) of the main breakwater. This was done to determine if there is any relative change in current characteristics between the areas upcoast and downcoast of the breakwater. Clearly, the current direction distributions for the two areas are very similar. Thus, it can be concluded that there is no significant difference between the two areas in terms of current direction characteristics. Only the results for the total data set (designated TOTAL on the figure) are therefore discussed further.

The current directions have a distinct bimodal (up- and down-coast) directional distribution centred around about 225° (from true north) and 30° . In total the currents flowed downcoast for about 70% of the time, while upcoast flow occurred less than 30% of the time. This is very similar to the results based on all the current measurements between Hood Point and Nahoon Point, where it was found that downcoast flows occurred for about two thirds of the time.

The velocity occurrence histogram is shown in Figure 3.28. The sub-surface current velocities ranged

Sediment Transport Regime at East London

from about 6 cm/s to 93 cm/s with an overall average velocity of about 34 cm/s. More significant in terms of the sediment carrying capacity is that the mean downcoast velocity was 40,5 cm/s while the mean upcoast velocity was 20,4 cm/s. (Sediment carrying capacities are discussed further in Section 4.3.)

1984 to 1985 Endeco current measurements

In the vicinity of the harbour entrance (in this instance within 2 km from the main breakwater and in water depths less than 35 m), current vectors were measured at 5 m depth and 20 m depth. The measurements at 5 m depth were located at between 460 m to 1 940 m from the head of the main breakwater (average distance of 1 120 m) with bottom depths ranging from -8 m CD to -35 m CD (average bottom depth of -17 m CD). The direction occurrence histogram of the 5 m deep measurements is shown in Figure 3.29. The results are very similar to the sub-surface drogue measurements with the current generally flowing downcoast for 69% of the time and upcoast for less than 31% of the time.

The current measurements at 20 m depth were located at between 880 m to about 2 000 m from the main breakwater head (average distance of 1 490 m) with bottom depths ranging from about -19 m CD to -35 m CD (average bottom depth of -30 m CD). The direction occurrence histogram of the 20 m deep measurements is shown in Figure 3.30. Once again the results are very consistent, with generally downcoast currents for 72% of the time and less than 28% generally upcoast currents.

1996 drogue tracking measurements near the harbour

During March 1996 limited drogue tracking measurements were conducted in order to obtain current data relatively close to the head of the main breakwater. Currents were measured on the surface and at 5 m, 10 m and 15 m below the surface, all within 300 m seaward of the main breakwater head. An example of the results is depicted in Figure 3.31. (It was noted during some of the measurements that the deep (15 m) drogue was dragging on the bottom. Thus, the depth of this drogue was reduced to 14 m for the final deployment.) Sub-surface current velocities ranged from 7 cm/s to 58 cm/s. The current flowed downcoast during three recording periods and upcoast during the fourth. The average sub-surface downcoast velocity was about 45 cm/s while the average upcoast velocity was about 13 cm/s. Although these measurements are too limited to be of statistical significance, they do agree very well with the general current regime information as described before in this section. These measurements are also useful in showing typical values of the current characteristics relatively close to the main breakwater. The high downcoast velocities and much lower upcoast velocities are particularly significant (as discussed further in Section 4).

General conclusion

As expected, the current regime in the vicinity of the outer entrance channel (within 2 km seaward from the main breakwater head and in water depths less than 35 m) displays the same overall characteristics as the current regime within the larger encompassing Nahoon Point to Hood Point area (as discussed in detail in Section 3.3.3.2). The information is very consistent, with generally downcoast currents occurring for about 70% of the time while upcoast flows occur less than 30% of the time. On/off-shore flows occur very rarely.

3.3.6 Currents in the lee of the main breakwater

Tides

Forces caused by the gravitational attraction between mainly the moon and sun acting on the rotating earth, result in the periodic level changes in large bodies of water, which is called the tide or astronomical tide. Significant currents generated by tides can occur at inlets to lagoons and bays or at entrances to harbours. At such constricted places, tidal currents generally flow in when the tide is rising (floodtide) and flow out as the tide falls (ebb tide) (CERC, 1977).

Tide gauge measurements are available from the South African Navy Hydrographer. These are used to predict astronomical tides and to determine the magnitude of additional meteorological effects adding to (or deducting from) the height of astronomical tides. The characteristics of the tides at East London are listed in Table VII below. (Note, that levels are relative to Chart Datum (CD), which at East London is 0,716 m below the national land levelling datum called mean sea level, or MSL).

Table VII: Average tidal levels for the Port of East London.

Tide	Level (m above Chart Datum)
Highest Astronomical Tide	2,08
Mean High Water Spring Tide	1,82
Mean High Water Neap Tide	1,25
Mean Level	1,02
Mean Low Water Neap Tide	0,78
Mean Low Water Spring Tide	0,23
Lowest Astronomical Tide	0,00

Source: South African Navy Tide Tables (2004)

Current measurements

During January 1995 currents were measured on the entrance channel side of the main breakwater by means of an Endeco electronic vector-averaging current profiler, drogue tracking, drifter buoys and dye tracking (Theron and Schoonees, 1999).

Figure 3.32 shows an example of the drogue tracking measurements on the entrance channel side of the main breakwater. (Note, that drogue tracking measurements seaward of the main breakwater are also shown on the figure. However, these are not relevant to the present discussion.) The effect on the surface drogues of the windy conditions that prevailed during the measurements on 18 January 1995, are clearly visible (Figure 3.32). In this case only the 5 m and 10 m deep drogues give an estimate of the actual sub-surface (sediment transporting) currents. The measurements on the entrance channel side of the main breakwater were conducted from just before low-tide to just before high-tide. The flow directions are mainly parallel to the breakwater and these currents are considered to be largely due to tidal action. The current velocities are mostly very low, with an overall average of only about 0,07 m/s.

Figure 3.33 shows representative current profiles measured at three different positions on the entrance channel side of the main breakwater. These three positions (on lines N, KL and I in Figure 3.19) were chosen to be relatively representative of nearly the whole area on the leeward side of the breakwater.

The measurements were done by means of an Endeco electronic current meter over periods of a few hours. (The values were averaged over $\frac{1}{2}$ hour periods to coincide with concentration measurements, which are discussed in Section 4.6.3.) The measurements show that at each position there is little variation in the current strength over depth. Thus it can be assumed (for these conditions) that current measurements made at any depth are approximately representative of the current strength over the whole water column at that position. Surface currents could, however, be very different from sub-surface currents if strong winds occur (as shown in Figure 3.32). Currents very close to the bottom are also expected to be somewhat weaker than higher up in the water column.

Currents were also measured by means of drifter buoys and dye tracking on 19 and 20 January 1995. The area covered by these measurements ranged from the head of the main breakwater to line P (Figure 3.19) and within 75 m from the leeward side of the breakwater. The currents at the surface to 2 m below the water surface were measured with drifter buoys. The wind speeds measured on site were less than 8 km/h throughout 19 and 20 January (during these current measurements). Thus, the wind effects on these current measurements were negligible. The measured current strengths ranged from 0 m/s to 0,26 m/s, with an average velocity of 0,07 m/s. Figure 3.34 shows a compilation of all the individual measurements in terms of current velocity and direction on the leeward side of the main breakwater from the drifter buoys and dye tracking in January 1995.

Heavy rains had fallen in the catchment of the Buffalo River just prior to the January 1995 current measurements. A fairly large flood (the magnitude was not recorded) was observed in the river at the time of the current measurements. The currents recorded on the leeward side of the main breakwater do, however, not reflect any noticeable net effect from the river discharge into the harbour. Thus, the assumption that river flows generally do not influence the currents on the leeward side of the main breakwater, appears to be valid.

Theoretical tidal currents due to the tidal prism at different tidal stages (for example, neaps and springs) can be calculated at the harbour entrance to obtain rough estimates of the current velocities. Further calculations of tidally induced currents and sediment transport in the harbour mouth area are addressed in Section 4.5.

Conclusions

Investigation of the measured currents and current patterns lead to a number of general conclusions.

The effects of tidal flows on the current patterns (and sediment movement) along the leeward side of the main breakwater increase as the distance normal to the breakwater increases. Close to the leeward side of the breakwater (within 20 m distance), tidal effects are relatively small. In the entrance channel further away from the leeward side of the breakwater (beyond 50 m distance) tidal flows dominate the current patterns. Thus, in the deeper water leeward of the breakwater, there are relatively stronger currents (up to about 0,25 m/s, Figure 3.34) parallel to the breakwater (between tides) that would potentially also move sediments parallel to the main breakwater.

Close to the main breakwater (<10 m) pulsating currents in and out of the breakwater (on the leeward side) were often observed. This is due to wave action on the outside of the breakwater. In fact, wave induced flow through the breakwater could be seen along almost all of the breakwater, from about line N to the head (the locations of the lines are indicated on Figure 3.19). A mixture of air, water and sand being blown out of the leeward side of the breakwater, was especially noticeable (for example,

Figure 3.21) between about lines M to N and at line I. Wave action along the leeward side of the breakwater (the effect thereof on sediment movement) gradually decreases from the head towards about line L where it is still fairly noticeable. Thereafter (i.e. in the direction of the inner harbour or west) the wave action is much reduced. A current flowing parallel and close to the leeward side of the main breakwater towards the harbour was observed near the head. This is most probably due to the wave action around the head and along the leeward side of the breakwater. This current would tend to draw sediment from adjacent to the head towards the leeward side of the breakwater.

River flows generally do not influence the currents and sediment transport along the leeward side of the main breakwater.

3.3.7 Numerical current modelling

Motivation and background

In order to obtain an indication of current patterns and velocities close to the main breakwater, a numerical model study was undertaken. A two dimensional numerical model of the Delft Hydraulics Laboratory was utilized to simulate the complex flow patterns in the vicinity of the port. Existing information and data on current measurements, as described in Section 3.3.3.2, were used as input conditions for the model boundaries. (Wave induced currents in the surf zone were excluded from the simulations described in this Section. *Wave-driven currents were however, included in the morphological modelling studies as described in Section 4.4.*)

Description of the model

The Delft hydrodynamic model (WL|Delft Hydraulics, 1996) solves the unsteady shallow water equations in two dimensions (depth-averaged, as applied in this case) or in three dimensions (not applied in this case). The system of equations comprises the horizontal momentum equations, the continuity equation and the transport equations. These equations are described in detail in WL|Delft Hydraulics (1996). The equations are solved on an orthogonal curvilinear grid. The time integration method is the Alternating Direct Implicit type where the water levels and velocities are solved implicitly along grid lines. The accuracy of wave propagation is related to the Courant number, which should generally be less than 10. An appropriate time step is determined by comparison of the relevant results for decreasing time steps. The open boundaries may be prescribed as tidal levels, currents or flow rates.

The Delft model includes formulations and equations that take into account:

- tidal forcing
- wind shear stress on the water surface
- the effect of the earth's rotation (Coriolis force)
- bed shear stress on the bottom
- turbulence induced mass and momentum fluxes
- water with variable density due to temperature or salinity (equation of state)
- free surface gradients (barotropic effects)
- horizontal density gradients in pressure (baroclinic effects)
- transport of conservative constituents

In this preliminary study the Delft model was run in the depth-average (2 dimensional) mode and many of the above-mentioned capabilities of the model were not utilized, as discussed below. (The actual model runs were conducted by Mr S Luger of the CSIR. The interpretation and application of these results were conducted by the author.)

Set-up of the model

The numerical grid extended approximately 8 km in a direction parallel to the coast and approximately 5 km offshore (Figure 3.9). (Note that a False Easting of -3 600 000 m was used in order to reduce the number of significant digits in the model.) The grid sizes ranged from 40 m near the breakwater to 200 m near the model boundary. The model bathymetry was obtained from the GIS (Geographical Information System) data base set up for the refraction study (Section 3.2.8).

As discussed below, the dominant currents flow parallel to the coastline. The model was thus driven by prescribing the velocities on the upstream open boundary. On the downstream open boundary a stationary water level was prescribed. This water level included a slope in the offshore direction that accounted for the Coriolis effect. A closed boundary was specified for the offshore boundary orientated parallel to the coast (Figure 3.35).

The currents specified at the open boundary were based on the current measurements (Section 3.3.3.2) made for a proposed outfall at East London (CSIR, 1988). Aanderaa current meters were deployed approximately 1,4 km offshore at Hood and Nahoon Points for the period April 1984 to February 1985. The measured current directions showed a strong preference for the longshore directions of SW and, to a lesser extent, NE. The average velocity for the south-westerly current was 0,25 m/s and for the north-easterly current 0,18 m/s at the location of the current meters. The strongest currents were generally south-westerly and a current speed of 0,40 m/s was exceeded 10% of the time for this direction. The current meters were in a water depth of approximately 30 m and the meters were located 3 m above the seabed. Assuming a logarithmic current profile, the depth-averaged current magnitude will be 25% higher than the measurements. The following depth-averaged currents were thus tested in the model:

- 0,31 m/s SW Average current velocity in the south-westerly direction
- 0,50 m/s SW Velocity exceeded for 10% of the time in the south-westerly direction
- 0,23 m/s NE Average current velocity in the north-easterly direction

Current profiles were also measured at three positions offshore of Hood Point and four positions offshore of Nahoon Point (CSIR, 1988). This data enable the variation in current strength with distance from the coast to be estimated. A linear regression of this data gives the following relationship:

$$\text{Average velocity at a specific offshore location (m/s)} = 0,166 + 0,0000727 \times \text{distance offshore of that location (m)}.$$

A similar linear increase in the velocity with distance from the shore was applied along the model boundary. The velocity magnitudes were scaled to ensure that the magnitude at the position of the Aanderaa current meter (1 400 m offshore) corresponded to either 0,31, 0,50 or 0,23 m/s (as discussed above).

The model was run until a steady state condition was reached (approximately two days in real time). The sensitivity of the model results (current speeds and directions) were checked for the following parameters: time step, bottom friction and eddy viscosity. A time step of 30 s was found to give accurate results, i.e. further reduction in the time step did not improve the model accuracy. The currents were found to be relatively insensitive to the bottom friction coefficient and a Chezy coefficient of $75 \text{ m}^2/\text{s}$ was used. For eddy viscosities of 0,1 and $1 \text{ m}^2/\text{s}$, the currents were deflected offshore by the breakwater and only reattached to the coastline approximately 5 km downstream. This did not correspond with the actual current measurements and the eddy viscosity was thus increased until the results were similar to the measurements, which was the case for an eddy viscosity of $20 \text{ m}^2/\text{s}$.

Limitations of the modelling approach

The model was driven by the currents prescribed on the upstream open boundary, which were based on the prototype current measurements (as described in the model set-up above). The effect of local wind forcing was not modelled - this effect was assumed to be included in the current measurements. Tidal effects were also not included. The current measurements did not indicate significant tidal currents, but the tide could have a small effect in the entrance channel area.

Wave-driven currents were not included in the preliminary model study. These will be the dominant forcing mechanism for currents in the surf zone. The initial model results were thus not applicable in the surf zone. The wave-driven currents also extend along the south side of the main breakwater. Wave-driven currents were, however, included in the morphological modelling studies as described in Section 4.4.

Since the model was run in depth-averaged mode, flow variations in the vertical direction are not resolved. These variations may be generated by wind forcing, bed stress, Coriolis force, topography or stratification.

Calibration and validation of the model

Calibration is the process whereby the model parameters are modified until a good agreement between the model output and the measured conditions is obtained. Ideally, simultaneous measurements of water level, current velocity, wind and water temperature are therefore required. Measured data suitable for calibrating the model was in this case limited to the data described in Section 3.3.3.2. No specific measurements were undertaken for this study. Model simulations of the existing scenario gives results that correspond well to the available measurements (as discussed in the following section), thus also indicating that the simulations are realistic. The two-dimensional model therefore gives an adequate representation of the general current regime in the Nahoon to Hood Point area. However, these calibrations do not necessarily indicate that the hydrodynamic model is able to reproduce the detailed current regime in the vicinity of the main breakwater with sufficient accuracy for modelling the transport of sediment. The model may now be used to simulate the current regimes for an extended range of environmental conditions, but further calibration of the model may be required before sediment transport modelling can confidently be undertaken.

Results of model simulations and conclusions

Figure 3.35 shows the contour and vector plots of the steady state currents as simulated for the average (0,31 m/s) downcoast (SW) current regime. The results for the total model grid area are shown. The existing breakwater layout was simulated. This simulation represents the situation that mostly exists at present at East London. In general, the following features are observed: as expected, there is a steady increase in current velocity in the offshore direction (as induced on the model boundary, based on measurements). The main breakwater causes a significant concentration or increase in current velocity in the area seaward of the head of the breakwater (as often found in similar instances, e.g. Ferentinos and Collins, 1980). Current velocities inshore and downcoast of the main breakwater are very low. Current directions are mainly parallel to the coast except in the area adjacent to the main breakwater, where the direction changes to about north-south.

Figure 3.36 shows exactly the same simulation (most common situation) except that the view is zoomed in to show a more detailed picture of the area in the vicinity of the main breakwater. Current velocities off the head of the main breakwater are generally between 0,2 m/s to 0,4 m/s. This corresponds well with the measurements described in Section 3.3.3.3. This simulation does not show a distinct eddy downstream of the main breakwater (as in Figure 3.25). However, these model simulations do not include surf zone currents which would probably induce / trigger eddy formation. (The surf zone currents in the Hood Point to main breakwater area would tend to add a northerly to easterly flow to the circulation, thus providing a strong impetus for a clockwise eddy adjacent to the Foreshore area.)

Figure 3.37 shows the results for a strong (0,5 m/s) downcoast (SW) current regime. This velocity is only exceeded for about 10% of the time in the southwesterly direction. The current pattern is generally very similar to the previous case except for the increased velocities. Velocities off the breakwater range from about 0,4 m/s to 0,7 m/s. In this case, an eddy is formed downstream of the breakwater. (An animation of the current patterns shows this eddy much more clearly than the small arrows in Figure 3.37.)

Figure 3.38 shows the results for the average (0,23 m/s) upcoast (NW) current regime. The most significant difference (except from the current direction) from the previous two cases is obviously the much lower velocities. Off the head of the breakwater the velocities range from about 0,1 m/s to 0,3 m/s. Once again this corresponds well with the measurements described in Section 3.3.3.3. No perceptible eddy is formed downstream (in this case north) of the main breakwater. The absence of such an eddy is mainly due to the low current velocity, as well as the current direction in relation to the breakwater. In this case the upcoast current flows obliquely parallel to the seaward side of the breakwater (Figure 3.38). The downcoast current, on the other hand, passes the head of the breakwater almost perpendicularly (Figures 3.36 and 3.37), which results in a stronger impetus for eddy formation. (Also, in contrast to the clockwise eddy formed just south of the main breakwater during the downcoast current scenario, the surf zone currents in the Nahoon Point to main breakwater area would in reality not providing any impetus for an anti-clockwise eddy north of the breakwater during upcoast currents.)

3.4 Continental Shelf Sediment Dynamics

In terms of obtaining a holistic understanding of the macro sedimentary dynamics and shelf sediment transport regime along the eastern Cape coast, very valuable work has been published; mostly by

Flemming (e.g. Flemming, 1978, 1980, 1981, 1982 and Martin and Flemming, 1986). The findings from these references relevant to this study are briefly described here.

The continental margin of the east coast is characterised by an extremely narrow shelf. At East London the shelf is about 25 km wide and the shelf break is located at about the 100 m isobath (Figure 3.39). The south-westwardly flowing Agulhas Current reaches a peak surface velocity of over 2,5 m/s just beyond the shelf break east of East London. The information clearly indicates that a vast amount of sediment is transported along the shelf by the Agulhas Current. The total downcoast sediment transport on the shelf along the East London coastline, mainly in a zone between 40 m and 60 m depth (i.e. the central shelf dune field area, Area B in Figure 3.40) is estimated to be as high as $24 \times 10^6 \text{ m}^3/\text{year}$ (Flemming, 1981).

In general it is possible to distinguish three, more or less shore-parallel, physiographic seabed regimes, each reflecting specific wave and current characteristics (Figure 3.40). The narrow nearshore zone is subjected to a high-energy swell regime, and is covered by a thin wedge of sandy sediment. This wedge appears to have achieved dynamic equilibrium with the prevailing energy regime, and additional (fluvial) sediment is rapidly dispersed and fed into a sand-stream, situated slightly further offshore on the broad central shelf, where the Agulhas Current dominates sediment transport. Thus, the nearshore sediment wedge progrades seaward until it meets sufficient current strength for sand to be entrained. This sand is entrained and carried on the central shelf by the so-called *conveyer-belt process*, driven by the Agulhas Current. This current-controlled part of the shelf can be further subdivided into two parallel zones: a broad central-shelf sand stream and a narrow outer-shelf gravel pavement. The current-scoured gravel pavement stretches along the outer margin of the shelf and probably extends onto the upper continental shelf slope. The lateral sequence of physiographic zones is illustrated in an idealized block diagram (Figure 3.40). This lateral sequence clearly indicates a progressive increase in current velocity in the offshore direction - a phenomenon that is consistent with available current data. It is also clear that any excess sediment transported onto the current-dominated zone of the shelf or deposited on the nearshore sediment wedge near the margin of the current-dominated zone would (eventually) be transported away by the south-westwardly flowing Agulhas Current.

3.5 Wind Regime

3.5.1 General

When wind blows over the ocean, it exerts a stress that results in the generation of both waves and ocean currents (Pond and Pickard, 1986). The most direct effect of wind is on the surface layer of the ocean, where surface currents drift in the direction of the wind. These surface currents have typical velocity values equal to 2-3% of the wind speed (CERC, 1977). Due to the Coriolis force the surface current would be 10 degrees to the left of the wind direction (looking in the direction towards which the current flows) in the Southern Hemisphere. The influence of the wind also extends deeper as the deeper layers of the ocean come under the influence of the shear stress applied by the upper layers (Pond and Pickard, 1986). Wind-induced surface currents toward the shore cause significant bottom return flows, which may transport sediment seaward. Similarly, strong offshore winds can result in an offshore surface current, and a resultant onshore bottom current which can aid in transporting sediment landward (CERC, 1977).

The wind regime along the east coast of Southern African is influenced by the semi-permanent South

Indian Anticyclone (high-pressure cell), the continental high and the South Atlantic Anticyclone. The seasonal movement of the high-pressure systems results in surface winds during summer to have a predominant northerly component. Coastal lows usually initiate on the west coast and propagate southward. Thereafter, they move eastward and north-eastward around the coast. All coastal lows produce offshore winds ahead of the system and onshore winds behind. This weather phenomenon is common in late winter and early spring (Preston-Whyte and Tyson, 1988).

3.5.2 Data analyses and interpretation

The East London airport is situated about 4 km from the coast (Figure 1.3) at an elevation of 120 m above sea level. Long-term wind data (1951 - 1970) at the airport shows that East London receives about equally strong south-westerly and north-easterly winds. The dominant winter wind blows from the west to the north-west sector. Summer winds tend to blow parallel to the coast from between the west to south-west, and east to north-east sectors. The south-westerly wind is considered to be the dominant wind throughout the year, while strong north-easterlies may occur in all seasons. Both of these wind directions are approximately *parallel* to the coastline. The same general pattern (i.e. strongest and most common wind directions are parallel to the coastline) is derived from the VOS wind data as depicted in Figure 3.41. (The VOS wind data consisted of more than 45 000 observations covering the 35-year period from 1960 to 1995. The area covered by these observations encompasses the five $1^{\circ} \times 1^{\circ}$ ocean sectors closest to East London between the 32 to 34 southern latitudes and the 27 to 30 eastern longitudes, Figure 3.6.)

Local winds were recorded on the main breakwater of the East London harbour by an automatic weather station from March 1984 to June 1985. This short-term wind data compares reasonably well with the long-term wind data discussed above. The average wind speed recorded was 4,5 m/s. The data gathered during this period revealed that the wind direction generally has a preference for *alongshore* directions of west to south and, to a lesser degree, north to north-east. The south-westerly winds are generally also slightly stronger than the north-easterlies. These alongshore winds could potentially generate waves, currents and ultimately sediment transport in the same direction as the wind, or alternatively, reduce currents and thus sediment transport moving in directions opposite to the wind direction.

3.5.3 Aeolian transport

Waves and currents are normally the dominant forcing mechanisms effecting sediment transport in the littoral zone. The wind (or aeolian sediment transport) usually has a much smaller effect. The coastline of the study area is mostly rocky with only a few small and narrow sandy beaches. The backshore area is either developed or fully covered by vegetation and there are no dune fields or extensive open sandy areas. The local wind regime also shows a predominance of approximately shore parallel wind directions. The significance of all of these factors is that there is very little on/offshore aeolian transport (and thus losses from or feeding into the littoral sediment budget) from the already limited sandy beach areas. It can thus be firmly concluded that aeolian transport is not significant in terms of the overall sediment transport regime in the study area. Hence, only the water-borne transports (e.g. due to waves and currents) are considered further.

3.6 Coastal Morphodynamics

3.6.1 General

Harbour breakwaters sometimes function as effective (nearly total) sediment traps. By calculating the (measured) sand accretion against such a breakwater and taking account of the aeolian transport in this area, the actual longshore transport in this area can also be determined.

Shoreline changes can be quantified by analysing vertical aerial photographs or beach survey data. Beach survey data is much more accurate than aerial photographic data. However, aerial photographs often span a much longer time period than existing beach surveys and provide a longer term perspective. Aerial photographs are, therefore, especially useful in quantifying long-term trends, while beach surveys usually provide accurate information on shorter term variability.

The limitations of assessing shoreline changes using aerial photograph analysis are the level of accuracy when establishing the location of the high-water mark and the availability of good aerial photographs. By using the high-water runup mark and not the water line, difficulties relating to the tidal level at the time of the photography are eliminated. (An elevation of approximately +3 m CD often indicates the line of wave run-up during normal high tides (Theron 1991).) Thus, the location of the high-water mark can be established with a horizontal accuracy of about 10 m. Aerial photographs covering the study area and used in this analysis were available for the years 1938, 1954, 1966, 1970, 1972, 1978, 1981, 1987 and 1989. In order to compare the aerial photographs quantitatively they had to be converted to the same scale. Historical shorelines were referenced relative to ortho-corrected aerial photography (taking the necessary care in identifying coastal features, etc.). All photographs were projected onto a master (taken from the 1972 1:10 000 orthophoto), using a Bausch and Lomb Zoom Transfer Scope, to correct for photographic distortion where possible.

3.6.2 Long-term shoreline changes adjacent to the port

The port development, especially the construction of the main breakwater, resulted in a major change in the nature of the sediment transport regime. Thus, shoreline changes prior to the final extension of the main breakwater between 1935 and 1938 (Figure 1.4) are not relevant to the present ambient sediment transport regime (which includes the effects of the original port development).

The location of the high-water runup mark as determined from the photographs is depicted in Figure 3.42. Shoreline changes were measured at three representative cross-sections along the study area. The locations of these cross-sections are shown in Figure 3.42. Shoreline changes were quantified by measuring the horizontal distance from a fixed reference point to the approximate high-water runup mark at the time that the photograph was taken. Using the 1938 photograph as basis, the shoreline changes relative to this date were determined, as shown in Figure 3.43.

The following can be deduced from the aerial photographs analysis:

- Between 1938 and 1954 the Orient Beach shoreline prograded by about 50 m, after which it eroded by about 40 m up to 1966. Since 1966 this shoreline again accreted somewhat with relatively smaller variations. Over the long-term, this shoreline appears to be approximately stable.

- The shoreline at the base of the main breakwater prograded by a large amount (about 150 m) between 1954 and 1966. Thereafter, this shoreline stabilized over the long-term with smaller variations occurring.
- The shoreline in the West Bank area (at Section 3 in Figure 3.42) prograded somewhat (about 40 m) between 1938 and 1966. Thereafter, this shoreline has remained relatively stable over the long-term.

It is obvious that especially the construction of the main breakwater, which was completed by 1938, had a very significant effect on the adjacent beaches, with the beaches to the south of the main breakwater accreting substantially. It also appears that all of the beaches have remained relatively stable since 1966. The foregoing discussions do not prove absolutely that the beaches of the study area are at present necessarily in a state of long-term equilibrium. Without further detailed investigation (such as for instance described by Gravens, 1990 and Kraus *et al.*, 1984) it cannot be conclusively determined if the beaches in the study area have fully adjusted to the existing port developments and that the shoreline has completely attained a new long-term equilibrium. However, it is considered that any potential further adjustments of the coastline as a result of the existing port developments will most likely be very small. If any progressive beach changes do still occur in future, careful consideration will have to be given to the possible ongoing effects of the existing port developments, future port development, other man induced effects or even (changes in) long-term natural processes, in determining the cause of such beach changes.

3.6.3 Sediment transports indicated from shoreline evolution

The original construction of the breakwaters, the main sandtrap and other dredging have affected the natural sediment transport along the beaches of the study area. The beach on the southern side of the main breakwater has accreted by about 150 m (since 1954), while the beach just to the north of the harbour accreted by a relatively small amount. The large accretion south of the main breakwater clearly indicates that this structure has acted as a sediment trap and has disrupted the natural upcoast longshore sediment transport. Since the nineteen-seventies, the shorelines on both sides of the harbour appear to have obtained dynamic equilibrium over the long-term, which indicates that total sediment transport to and from these beaches is also approximately balanced over the long term. The possibility of calculating the longshore sediment transport from the shoreline accretion on the southern side of the main breakwater, is discussed in Section 4.2.3.

3.7 Seabed features and transports indicated from sonar survey

In 1995, a detailed sonar survey was conducted of the leeward side of the main breakwater (Theron and Schoonees, 1999). The purpose was to identify seabed features, ultimately providing information on sediment transport (and breakwater stability).

Figure 3.44 shows an interpretation of seabed features from the side-scan sonar survey conducted in January 1995. Two distinct features relevant to this study were identified. These are the depression and mound features to the west of the navigation light and to the east of survey line I (Lines G to N are lines along which NPA conduct regular surveys). These approximately fan-shaped mounds adjacent to depressions against the main breakwater are clear indications of large "blow holes" through the breakwater at these locations.

The feature to the west of the navigation light is particularly large (about 25 m by 40 m). However,

the position of the present shoreline on the outside of the main breakwater opposite this feature, would indicate that sediment would have to travel almost 50 m through the breakwater to form this mound. This is highly unlikely and the feature is most probably a relic from the past when the shoreline was much closer to the breakwater (i.e. shorter sediment pathway). More recently (last decade), NPA has repaired extensive erosion to this part of the breakwater. The "blow hole" at this location was probably formed when the breakwater was fairly narrow at that point. Previously, relatively large volumes of sediment must have moved through this hole, but this pathway and "blow hole" is most probably no longer active.

It cannot be said how active the blow hole to the east of line I is, but this sediment pathway is probably still at least partially open, even though the bathymetric survey of January 1995 shows a build up of sand on the outside of the breakwater (Figure 3.45, the location of Profiles G, K and N are also indicated on Figure 3.44). The entrance to this large pathway could become blocked when sediment builds up on the outside of the main breakwater or could become active again when erosion occurs.

The absence of other identified blow holes does not mean that no other such holes exist. The seabed features are simply not large enough or distinct enough to be identified from the side-scan sonar records (or they are obscured by loose concrete armour blocks) originating from the breakwater. A large number of smaller holes spaced relatively close to each other all along the breakwater would not produce distinct identifiable features (on the sonar records). Relatively larger areas of sand build up with smoother contours would also not produce the sharper "shadow" areas that are identifiable on the side-scan sonar recordings. A sand bank that was visually observed approximately between lines M and N (Figure 3.44) could be such a feature as it was not identifiable on the sonar recordings.

The identification of at least a few distinct blow holes indicates that the sediment movement through the breakwater is in the form of separate "point sources" (e.g. Figure 3.21). The nature of most of these seabed features (due to relatively small blow holes) is such that they cannot be clearly identified with presently available technology. Most of the holes could probably be mapped by means of a comprehensive and detailed diver survey. However, there would be little point in carrying out such an expensive exercise if the dynamic (ever changing) nature of the seabed is kept in mind. Actions taken by NPA to make the main breakwater more impermeable (e.g. by means of grouting) would obviously reduce sediment movement through the breakwater.

Depending largely on local wave conditions and sand levels along the seaward side of the main breakwater at the time, the flows through the main breakwater (mostly from south to north) can range from insignificant to substantial. High waves, low sand levels (and possibly more southerly waves) all lead to higher flows and thus sediment transport through the main breakwater (mostly from south to north). At present a few larger and many smaller pathways and blow holes contribute to transport through the main breakwater (e.g. Figure 3.21).

3.8 Sediment Characteristics and grain size trends

3.8.1 Sediment Characteristics

Knowledge of the nature of the beach and bottom material is necessary in determining the characteristics of the sediment such as the grain size and fall velocity. These parameters play a critical

Sediment Transport Regime at East London

role in the magnitude of sediment transports. Thus, the purpose of this section is to present the basic characteristics of the beach and bottom material relevant to this study; that is, the grain size ranges of the sediments. The soil classification according to PIANC (1984) has been used. The PIANC soil classification and grain size ranges are given in Table VIII below.

Table VIII: PIANC soil classification and grain size ranges.

Main soil type	Range of particle sizes (mm)
Fine gravel	2 - 6
Coarse sand	0,6 - 2
Medium sand	0,2 - 0,6
Fine sand	0,06 - 0,20
Silt	0,002 - 0,06
Clay	< 0,002

The silt/clay fraction (which is also called mud, or the fine fraction) is the material smaller than 0,063 mm (or 63 microns).

In September 1993, sand samples were collected from 15 locations around the port (Theron and Schoonees, 1998). The grain size distributions as well as the median grain sizes (d_{50}) of these samples were subsequently determined by means of the fall velocity method in a settling tube. Theron (1992) found that the fall velocity (w) is related to d_{50} as follows:

$$w = ((0,11892 \times d_{50} + 9398721)^{0,5} - 4173) / 59460 \quad [\text{m/s}]$$

The median grain size at each location is indicated on Figure 3.46.

During a site investigation in June 1993, three sand samples were also collected from the leeward side of the main breakwater. The median grain sizes (d_{50}) of these samples are also indicated on Figure 3.46. The close correlation between the grain sizes on the seaward and leeward sides of the main breakwater is obvious. In conjunction with the identification of blow holes through the main breakwater (Section 3.7), this indicates that the source of the sediments directly in the lee of the main breakwater is most probably the sediment on the seaward side and that some sediment moves directly through the breakwater from the seaward to the leeward side (e.g. Figure 3.21).

During 1992 sand samples were also collected to the south of the main breakwater (Cummings, 1992). The average d_{50} of all these samples was 0,21 mm (210 micron), which correlates well with the d_{50} grain sizes of the September 1993 samples.

In November 1990 sand samples were also collected at Orient Beach (Figure 3.46), just north of the secondary breakwater (Withers, 1991). The average d_{50} grain size of these samples was again approximately 0,21 mm.

It can thus be stated in general that the sediments in the area around the harbour are relatively uniform (in terms of median grain size) and can all be classified as fine to medium sands. For a median grain size of 0,21 mm the fall velocity is calculated to be only 0,028 m/s. The relative fineness of the sediment together with the energetic wave conditions and relatively strong currents, leads to potentially high sediment transport rates.

3.8.2 Transport patterns from grain size trends

Sediment distribution generally reflects energy levels at the seabed, which are primarily related to prevailing wave regimes. A selective “sifting/washing out” process results in residual deposits of coarse sediments in high-energy areas, whereas finer sediments accumulate in low energy areas. This is generally reflected in the sampling carried out at East London where the coarser fractions were found in higher energy zones (south-west of the main breakwater). The finer fractions are most prominent in deposition areas such as the sheltered part of the harbour entrance channel.

The direction in which grain sizes decrease normally also give a fair indication of the direction of net sediment transport (HAECON, 1992; Gao and Collins, 1994). Kleinhans (2002), found that the grading of seabed sediment has a direct correlation with the sediment transport directions, mostly because of grain size-selective suspended sediment transport (coarser sediment is transported in bedload mode, while finer sediment is transported in suspended load).

From the grain size differences in relation to the relative locations (Figure 3.46), the following trends (indicated by the dashed arrows in the figure) can be deduced in general. The grain sizes gradually decrease from the vicinity of the Foreshore area (Figure 3.46) towards the deeper water near the main sand trap. The grain sizes also decrease from the leeward side of the main breakwater towards the centre of the entrance channel. Finally, grain sizes also decrease from Orient Beach towards the vicinity of the head of the secondary breakwater.

These trends indicate the following (refer to the arrows on Figure 3.46):

- Sediment is generally transported from the area adjacent to the Foreshore (i.e. near the beach south of the harbour) towards the deeper water near the main sand trap.
- Transport occurs from the leeward side of the main breakwater towards the centre of the entrance channel.
- Sediment is transported from Orient Beach towards the vicinity of the head of the secondary breakwater.

4. QUANTIFICATION OF SEDIMENT TRANSPORT REGIME

4.1 *Transport rates from Surveys and Dredging Records*

4.1.1 Old and new sand trap layouts

In previous investigations by the author (Theron, 1994a, Theron and Schoonees, 1998, Theron *et al*, 1998) a new layout and location of the main sand trap near the head of the main breakwater was recommended, as well as a new sand trap near the head of the secondary breakwater. The NPA implemented these recommendations in about mid-1994 and the so-called new sand traps have therefore been in use for some time. The old and new (i.e. present) sand traps are depicted in Figure 4.1. On recommendation from the author (Theron, 1994a), dredging data has been collected for nine separate sub-areas (Figure 4.2) since 1995. The dredging data is discussed further in Section 4.1.3.

4.1.2 Bottom Changes

4.1.2.1 *Bottom changes*

Seafloor contour maps were studied so as to identify changes in bottom topography, areas of sediment deposition or erosion and volume changes. More than 20 contour maps of the port area dating from 28 July 1976 to 18 November 1999 were obtained from NPA. Data from hydrographic surveys of the surrounding areas conducted in February 1985 and in October 1993 (Theron *et al*, 2002a) were also utilized in this study.

It was possible to select consecutive surveys (here called survey couples) between which no or very limited dredging took place, for example, the survey maps of May 1998 and September 1998 (Figures 4.3 and 4.4). This is important in analysing bottom changes, as changes due to dredging cannot then distort the observed changes resulting from natural processes. The surveys also need to be of good quality and contain no anomalies.

From the selected survey data, difference maps were produced. These maps show changes in vertical elevation between consecutive surveys as well as volume changes per unit area. For example, the difference map for the survey couple of May 1998 to September 1998, is shown in Figure 4.5. The largest accretion by far occurred at the south-western corner of the main sand trap, while notable accretion also occurred on the leeward side of the main breakwater and in the East sand trap. (Difference maps for three other survey couples (time periods) are shown in Appendix C, Figures C.1, C.2 and C.3. The patterns of most significant accretion are very similar.)

To clearly identify the most significant depositional patterns found in the difference maps, a summary chart has been drawn up which shows all the areas where more than one metre of vertical accretion occurred in each of four selected survey couples. This is depicted in Figure 4.6. The pattern now becomes quite clear: significant deposition occurs at the south-western corner of the main sand trap, between this sand trap and the head of the main breakwater, along the leeward side of the main breakwater, within the East sand trap, between this sand trap and the head of the secondary breakwater and finally on the leeward side of the secondary breakwater.

To identify slightly smaller depositional patterns, a similar summary chart now showing all areas where more than 0,7 m of vertical accretion occurred, is depicted in Figure 4.7. The same pattern as described above clearly emerges. However, in addition, widely-spread areas of limited accretion to the north and east of the main sand trap are now also indicated. (This can also be observed directly by careful scrutiny of the difference maps (Figure 4.5, and C.1, C.2 and C.3 in Appendix C).)

4.1.2.2 Sections through the sand traps

To analyse and explain the bottom changes that have taken place, a number of sections were taken through the two existing sand traps. The bottom changes can be observed by studying the two profiles that make up a specific survey couple, that is, by comparing sections through the sand traps that reflect changes due to natural processes only. For example, Figures 4.8 and 4.9 show two different sections through the main sand trap (the locations of these sections are indicated on Figure 4.7). In Figure 4.8, for example, the large accretion at the south-western corner of the main sand trap between May 1998 to September 1998, is clear.

Two main conclusions are reached regarding the *main sand trap*:

- The main sand trap primarily accretes from the south-western corner.
- Very little sediment enters the trap from any other direction.

4.1.3 Dredging Records

4.1.3.1 Dredging Data

Dredging records in terms of volumes of sand dredged over time in specific areas, were obtained from NPA, Whillier (1962) and Cummings (1992). These records were compiled, analysed and tabled to determine the amount of dredging conducted in the various dredging areas, which are depicted in Figures 4.1 and 4.2.

The volumes of sand dredged annually from the entire port, are shown in Figure 4.10. (No annual data could be obtained for the period from 1961 to 1981.) During 1950 to 1960 about 490 000 m³ of sand was dredged annually on average, while about 720 000 m³ was annually dredged on average from 1983 to 1993. It cannot be ascertained whether the values for the 1950'ties in fact include all the amounts dredged at the port, in other words both regular maintenance dredging, as well as capital dredging for port developments. Furthermore, up to about 1966 the main breakwater was still trapping a proportion of the sand transport from south of the harbour. Only when the fillet accreted against the southern side of the breakwater had built up to equilibrium capacity would most sand transport from the south have ended up in the main sand trap and entrance channel. This accounts for some of the differences between the 1950-60 average and the 1983-93 average value. The dredged material is dumped in the offshore area (beyond the 30m depth contour ~ 3 km offshore) to the south-east of the port, from where it cannot easily be transported back to the port. (It is too deep for significant direct wave driven transport, and the deeper water currents would tend to transport the sediment downcoast away from the harbour.)

Maintenance dredging at the Port of East London is conducted mostly in three zones (Figure 4.2), named:

1. the "main sand trap" (Area 8),
2. the "Bar" area (Areas 6,7 and 9) and
3. the "entrance channel" (Areas 1, 2, 3, 4 and 5).

Maintenance dredging is also conducted in the inner harbour (the harbour basins and quays). The total volume of sediment dredged annually from the main sand trap was found to be about 320 000 m³ on average (up until 1994). In the Bar and entrance channel areas, an amount in the order of 200 000 m³ has annually been dredged in total, while about 50 000 m³ in total has been dredged annually from the inner harbour on average.

Apparently there is no long-term net erosion or build-up of the sea-floor in any of these dredging areas. Thus, the amount of sediment moving into each of the areas must be approximately equal to the amount of sediment dredged from each area plus the amounts moving out of that area. This observes the basic principle that sediment transport in an area must ultimately be balanced (e.g. CERC, 1984 and many others). The sand traps, and to a slightly lesser degree the other above mentioned areas, are significantly deeper than the adjacent sea-bed, with the result that sediment can relatively easily move into these areas but cannot easily move through or out of these areas. (This phenomenon is described in more detail in Bijker, 1980, Fredsoe, 1978, Mayor-Mora *et al*, 1976, O'Connor, 1985, Van Rijn, 1986 and Vincente and Uva, 1984.) By implication therefore, the average sediment transport rate to each of these areas must approximate the average long-term dredging rate. The only area where a small divergence from this "rule" possibly occurs, is the Bar area, as will become clear in the following sections.

4.1.3.2 Main sand trap

Figure 4.11 shows the annual volumes dredged from the main sand trap since 1976. The mean annual volume since 1994 (when the existing traps were completed) is about 245 000m³, while the longer-term average for 1976 to 1984 is about 320 000m³. In view of the significant reduction over the last few years, the existing sand trap layout is most probably more effective than the previous layout. (This is due in part to a measure of over-trapping that occurred with the previous layout; for a discussion of this and other factors see Theron *et al*, 2002a).

4.1.3.3 Dredging areas

From the data collected for the nine separate sub-areas (Figure 4.2), the average annual volumes of sediment dredged from the different areas for the period 1995 to 1999, could be determined. To determine this as accurately as possible, the volume changes as derived from surveys were also taken into account. (The surveys for their part are estimated to have a vertical accuracy of about 0,3 m and possibly a little better in the sheltered area leeward of the main breakwater.) For example, if the bathymetric surveys indicated that the sea-floor in the area was higher at the end of the period over which the sedimentation rates were calculated, compared to the beginning of the period, then the volume difference between the surveys was added to the dredged volumes. This is because the nett build up (in this example) means that less sediment was dredged than what was deposited in this area.

A comparison of the mean annual sedimentation rates for the nine dredging areas is shown in Figure 4.12, which also shows where these sediment volumes are deposited. Clearly, by far the largest amount of sedimentation occurs in the main sand trap, which accounts for more than half of the total. The other areas where significant sedimentation occurs are Areas 3, 5, 6, 7 and 9. This shows that except for the main sand trap, sedimentation mainly occurs along the central entrance channel to the port and in the deeper areas east of the harbour. The sedimentation rate per unit area calculated for each of the dredging areas shows that by far the highest unit rate occurs in the main sand trap ($4,5 \text{ m}^3/\text{m}^2/\text{a}$), followed by the East sand trap ($1,2 \text{ m}^3/\text{m}^2/\text{a}$) and then Area 5 ($1,0 \text{ m}^3/\text{m}^2/\text{a}$). Areas 3, 6, 7 and 9 have smaller, relatively similar sedimentation rates ($0,3$, $0,4$, $0,3$ and $0,3 \text{ m}^3/\text{m}^2/\text{a}$ respectively), with a small decreasing trend from Area 6 towards Area 9. Area 2 has a low rate ($0,1 \text{ m}^3/\text{m}^2/\text{a}$) followed by Area 4 with a zero rate.

4.1.4 Conclusions

The findings derived from the dredge data can be compared to the conclusions reached in Section 4.1.2 from the bottom changes. Not surprisingly, both the survey and dredge data indicate major sedimentation in the main sand trap and significant sedimentation in the East sand trap. The sedimentation between the main sand trap and the breakwater head, and along the leeward side of the main breakwater, as derived from the survey data, correlate with the relatively high sedimentation found in dredging Areas 3 and 5, as derived from the dredge data. After the main sand trap the most significant sedimentation is in dredging Area 5, which results from sediment transport through (Figure 3.21) and around the head of the main breakwater (Figure 4.13). The survey data showed significant sedimentation between the East sand trap and the head of the secondary breakwater, as well as on the leeward side of the secondary breakwater. The dredge data also showed significant sedimentation in the East trap and Area 2, but the volumes are relatively small. The survey data indicates widely spread areas of more limited accretion to the north and east of the main sand trap. This correlates to the moderate sedimentation in Areas 6, 7 and 9 deduced from the dredge data. Both the survey and dredge data indicate virtually no sedimentation in Area 4. These comparisons indicate that the conclusions derived from the surveys and dredged volumes correlate extremely well.

As discussed before (Section 4.1.3.1), the sand traps, entrance channel area and to a lesser extent the Bar area, by nature act as sediment traps with little transport through or out of these areas. Considering this, and most importantly, the consistent patterns of deposition/infilling and the direction from which this deposition occurred, unambiguous deductions about the overall movement of sediment could be made. Thus, these deposition/infilling patterns and directions clearly show from which directions sediment is transported into these areas, and also provides good information on the magnitude of these transports, as depicted in Figure 4.14 and described below:

The main sand trap accretes virtually only from the south-western corner, but also and to a very small degree from the north-eastern corner. The small build-up in the north-eastern corner (e.g. Figures 4.8 and 4.9) indicates a very small amount of sand movement *through* the Bar area into this corner. In the Bar area (Figure 4.14), the sand build-up mainly occurs from the north-eastern corner, while there is also a much smaller build-up from the south-east. In the entrance channel area, there is a build-up of sand along the seaward half of the main breakwater (on the lee-side). A small amount of deposition also occurs in the entrance channel from approximately the north.

4.2 Longshore sediment transport

4.2.1 General

Longshore transport obviously occurs in both directions along the coast (depending on the direction from where waves approach the beach). The general coastline orientation of the East London coastline between Cove Rock and Nahoon Point (Figure 1.3) is approximately north-east (or south-west). Thus, it follows that in general, waves with a direction of between 150°N and 330°N would theoretically generate a north-easterly (upcoast) longshore current. According to the deepwater wave direction occurrences (Figure 3.6), a north-easterly longshore current would be generated for about two-thirds of the time, while a south-westerly (downcoast) longshore current would occur for about a third of the time. This would clearly result in a net north-easterly longshore transport in the long-term.

Although this does not take into account further variances due to the differences in wave heights and periods from the various wave direction sectors, these variances will not have a major effect on the average net transport direction.

4.2.2 Theoretically determined longshore transport

In a comprehensive study of existing longshore sediment transport formulae and models (more than 50 in total), Schoonees and Theron (1996) recalibrated and improved the then best formulation. This was the Kamphuis formulation, which was originally derived by means of dimensional analysis, based on extensive model tests and calibration against these and field data (Kamphuis, 1991). The improved formulation is referred to as the modified Kamphuis formulation:

$$S = 41\,025 X_{\text{Kamphuis}} \text{ (m}^3\text{/year)}$$

with

$$X_{\text{Kamphuis}} = \frac{1}{(1-p)\rho_s} \cdot (\rho / T_p) L_o^{1,25} H_{bs}^2 (\tan \alpha_\kappa)^{0,75} \cdot (1/50)^{0,25} (\sin 2\theta_b)^{0,6}$$

where	S	=	longshore sediment transport rate	(m ³ /year)
	p	=	porosity	(e.g. 0,4)
	ρ _w	=	density of sea water	(kg/m ³)
	ρ _s	=	density of sediment	(kg/m ³)
	T _p	=	peak wave period	(s)
	L _o	=	deepwater wavelength	(m)
	H _{bs}	=	significant breaking wave height	(m)
	tanα _κ	=	beach slope	(e.g. 0,03)
	d ₅₀	=	median grain size	(m)
	θ _b	=	wave incidence angle	(degrees)

The modified Kamphuis formulation was used to calculate theoretically the longshore transport rates adjacent to the root of the main breakwater (on the seaward side). This was done because it is considered that almost all of the sediment dredged from the main sand trap and from the leeward side of the main breakwater, is due to longshore transport along the outside of the breakwater (combined with a rip current near the head). (The sources of the dredged sediments are discussed further in Section 5). Input data in terms of bottom slopes, wave climate and sediment characteristics were

determined from the data as described in Section 3.

Initially, averaged breaking wave conditions (wave height, period and direction) were determined from the wave modelling results discussed in Section 3.2.8, as well as the wave data derived in Sections 3.2.4 and 3.2.7, combined with wave refraction and shoaling calculations. Thus, applying the modified Kamphuis formulation, it was estimated that the potential mean longshore sediment transport rate is about 600 000 m³/year along the outside of the main breakwater (towards the head). This is based on a representative (average) breaking wave condition ($H_{bs} = 2,3$ m; $T_p = 11,2$ s; $\theta_b \simeq 1$ deg.). Being representative of the most common (predominant) offshore wave scenario, this rate is also considered to approximate the most common longshore transport rate in this area. Also, taking account of the fact that the effects of storms are compensated by the low wave conditions which occur at other times, the transport rate based on the most common wave scenario is considered to give an acceptable first approximation of the long-term mean rate.

Storms can obviously have a dramatic short-term effect on sediment transport, which could also have a significant effect on the annual transport rate. The most accurate estimate of the long-term mean annual transport rate would be based on a fully representative offshore wave climate including all wave scenarios that are likely to occur as well as the persistence of each of these scenarios. Although this was somewhat beyond the scope of this study, it was in fact done later, once a significant amount of good quality *directional* wave data had been recorded by means of a directional wave buoy (Section 3.2.9). The procedure that was followed is basically as follows:

Out of the few years of available directional wave data, a year was selected in which the data coverage and quality was good. The selected year (2000) had about 3 000 wave records. Each of the wave conditions, as measured in 22 m water depth, were refracted and shoaled in, based on the wave transformation model of Battjes and Janssen (1978) and assuming parallel contours. Thus, the breaking wave conditions (wave height, period and direction) were determined for each of the conditions measured in 22 m water depth. The modified Kamphuis formula was then used (as described previously) to determine the sediment transport for each breaking wave condition. By adding all of the transports together (plus and minus), the total net annual sediment transport could be determined. Using this method, it was determined that the potential mean longshore sediment transport rate is about 500 000 m³ per year just north-east of the Foreshore area (Figure 1.4).

It is important to note, however, that the above theoretically determined rates are potential rates. The actual sediment transport also depends on (amongst other factors) the availability (or supply) of sediment to be transported and is often significantly less than the potential rate. The coastline to the south of the harbour consists of intermediate sand and rocky areas (Figure 1.3). In terms of the availability in this whole area, of sediment to be transported (in relation to the occurrence of rocky areas) the estimated net transport rate of about 500 000 m³/a is considered to be somewhat excessive. (Gonsalves and Bartels, 1990 discuss how sediment transport is limited along a rocky coast.) Thus, it is foreseen that the available sediment will not be sufficient to sustain a long-term net longshore transport rate of 500 000 m³/a (towards the main breakwater). Based roughly on the area of the nearshore zone covered by rock, it is estimated that the actual sediment transport rate is between 50% (250 000 m³/a) and 60% (300 000 m³/a) of the potential rate, with a best estimate of around 275 000 m³/a.

4.2.3 Transport rate calculated from beach accretion

A comparison of the “actual” and theoretically calculated longshore transport rates can sometimes be made, by calculating the rate of sand accretion against a breakwater that traps the littoral drift.

The East London main breakwater has acted as a partial sediment trap resulting in beach accretion since 1954 of more than 150 m adjacent to the base of the breakwater (Section 3.6 and Figure 3.42). Thus, by calculating the volume of sediment trapped during the nineteen-fifties, the net long-term mean rate of accretion adjacent to the root of the main breakwater (due to transport from the area south of the harbour) is calculated to be about 58 000 m³ per year. As expected, this does not correspond with the theoretically determined transport rate of 275 000 m³ per year (Section 4.2.2). This is mainly because the main breakwater is not correctly aligned (approximately parallel to the main wave directions) to initially form a total sediment trap. In fact, the alignment is almost perpendicular to the main wave directions, which would allow a large amount of sand to move from the base of the breakwater out of the fillet area towards the breakwater head (also due to rip currents along the breakwater). Therefore, the volumes of sand dredged (and possibly bypassing the harbour) during the period over which the beach accretion is calculated, should also be taken into account to determine the total longshore sand transport rate. However, as the dredging records for 1954 to 1966 are incomplete and possibly include capital dredging volumes (for port developments), the transport rate cannot in this case be determined in this manner from the shoreline evolution.

If at all possible, the theoretically determined longshore transport rates should be compared with measured transport rates, such as the accretion adjacent to the breakwater. As discussed above, good calibration data did not exist for the present study area. However, the theoretically determined rate could be calibrated to some extent, based mainly on the survey and dredging information, once the overall sediment transport regime had been determined.

4.2.4 Distribution of longshore transport

To determine where the bulk of the longshore sediment transport occurs, the *longshore transport distribution normal to the beach* was determined. This required the use of a detail predictor, which determines the specific sediment transport rate at each cross-shore distance (or depth). In this case, the Engelund-Hansen-Swart model (Swart, 1976; Swart and Flemming, 1980) was used to determine the transports. Schoonees and Theron (1996) found this to be one of the best detail predictors. Figure 4.15 shows the weighted mean transport distribution over cross-shore distance (calculated from the individual transports due to the wave data time series as determined in Section 3.2.7). Figure 4.15 indicates that the transport rate peaks at about 100 m from the breakwater, while very little transport occurs beyond 300 m from the breakwater. Also shown on Figure 4.15 is the percentage of the total longshore transport accumulated over the cross-shore distance from the breakwater. Thus, it can be seen that about 39% of the transport occurs within 100 m of the breakwater while about 89% occurs within 200 m and 97% within 300 m of the breakwater.

The above findings are also in accordance with the location of a relatively flat area adjacent to the main breakwater (as clearly shown by the bathymetry). This flat area stretches to about 150 m to 200 m from the breakwater or up to about the -5 m MSL contour (e.g. Figure 3.10). Seaward of the -5 m MSL contour, the bottom slope increases towards deeper water. Almost all littoral transport occurs within the surf zone on this flat area. Only during very rare storm events when the waves break seaward of the -5 m MSL contour, would significant littoral transport occur seaward of the -5 m MSL

contour.

To investigate the relative contribution of different wave conditions, the *distribution of the total annual longshore transport in relation to the occurrence of specific wave conditions* was also determined. The wave height occurrence statistics is indicated in Figure 3.3. Thus, for example, it is calculated that the accumulative effect of all wave conditions below the 50% exceedance value ($H_{mo} = 1,64$ m in 22 m water depth) would cause a total of only about 35% of the average annual longshore transport. In comparison, the largest waves that occur for only 1% of the time, ($H_{mo} > 3,44$ m in 22 m water depth) cause about 3,5% of the annual transport despite their low occurrence. Figure 4.16 shows the cumulative distribution of the annual longshore transport in relation to the cumulative occurrence of wave conditions. (Note that the wave conditions represent increasing "storminess" along the x-axis.) The increasing upward curve of the line indicates the relatively larger contribution to the annual transport due to the more stormy conditions. (This analysis shows the major effects of different wave heights alone. To obtain the complete picture of the relative contribution to the total annual transport by different wave conditions, the combined occurrence of specific wave height, period and direction conditions needs to be taken into account. Such a detailed analysis of the occurrence distribution of the different transport rates is however beyond the scope of this thesis.)

4.3 Sediment transport in deeper water

4.3.1 Methodology

In the deeper water areas, sediment transport is affected by both the offshore currents (the Agulhas) and wave action (and, to a lesser extent, wind driven currents). Thus, the method by Van Rijn (1989) was utilized to determine the potential transport due to the combined effects of currents and waves.

Van Rijn derived the following formulae to determine the different components of the sediment transport (per unit width normal to the current direction):

$$\text{suspended load transport (numerical integration): } q_{s,c} = \int_a^h u c dz \quad (\text{m}^2/\text{s})$$

$$\text{bedload transport: } q_{b,c} = 0,25 u_{*,c} d_{50} \frac{T^{1,5}}{D_*^{0,3}} \quad (\text{m}^2/\text{s})$$

$$\text{total load transport: } q_{t,c} = q_{b,c} + q_{s,c} \quad (\text{m}^2/\text{s})$$

with	$u_{*,c}$	=	current-related grain bed-shear velocity	(m/s)
	h	=	water depth	(m)
	a	=	reference level (related to ripple height or wave boundary layer thickness)	(m)
	u	=	fluid velocity	(m/s)
	c	=	sediment concentration	(-)
	z	=	height above the bottom	(m)
	d_{50}	=	median diameter of bed material	(m)
	T	=	bed-shear stress parameter	(dimensionless)
	D_*	=	particle parameter	(dimensionless)

The computation procedure for the method of Van Rijn is basically as follows:

- (1) Specify the input data:
 - water depth (m)
 - significant wave height (m)
 - peak wave period (s)
 - depth-averaged value of the velocity vector (m/s)
 - angle between wave direction and current direction (E)
 - median diameter of bed material (m)
 - 90% diameter of bed material (m)
 - fall velocity of suspended sediment (m/s)
 - current-related bed roughness (m)
 - wave-related bed roughness (m)
 - reference level (bed concentration) (m)
 - thickness of near-bed wave-related mixing layer (m)
 - acceleration of gravity (m/s^2)
 - fluid density (kg/m^3)
 - sediment density (kg/m^3)
 - kinematic viscosity coefficient (m^2/s)
 - Constant Von Karman (0,4)
 - ratio of sediment and fluid mixing coefficient (.1)
- (2) Compute sediment characteristics. (The suite of formulae to calculate the variables in Steps (2) to (12) are given in Van Rijn, 1989.)
- (3) Compute wave length.
- (4) Compute wave parameters.
- (5) Compute apparent bed roughness.
- (6) Compute friction factors.
- (7) Compute effective time-averaged bed-shear stresses.
- (8) Compute bed-shear stress parameter.
- (9) Compute velocity distribution over the depth.
- (10) Compute sediment mixing coefficient distribution over the depth.
- (11) Compute concentration distribution over the depth by numerical integration.
- (12) Compute transport rates (by means of the formulae given before).

From the information in Sections 3.2 and 3.3 average values were determined for the depth, wave and current input parameters for the zones over which the transports take place. Appropriate values for the sediment input parameters were determined from the information described in Section 3.8. Typical values were also determined for the roughness, viscosity and density input parameters for the area. Finally, it was also assumed that the downcoast currents would occur for two thirds of the time, while the upcoast currents would occur for one third of the time (according to what was found in Section 3.3.3).

4.3.2 Transport into the dredging areas

In the deeper water dredging areas, that is the “Bar” (Areas 6, 7 and 9) and main sand trap

(Area 8) in Figure 4.2, sediment transport is affected by both the offshore currents and wave action. Thus, the above method of Van Rijn was used to determine the volume of sediment which would annually be transported into the Bar area with the south-westwardly flowing Agulhas Current. It was computed that, on average, about 75 000 m³ of sediment would be transported into the Bar area from the north-east. Of this 75 000 m³ of sediment, a small percentage could potentially again be transported further into the deeper main sand trap (also from the north-east). Taking into account the occurrence of current reversals (i.e. north-eastwardly flowing nearshore currents) as well as the velocity of these currents (Section 3.3.3), it was similarly computed that on average about 10 000 m³ of sediment would annually be transported into the Bar area from the south. These results confirm that the downcoast currents transport significant amounts of sediment into the study area, while the weaker upcoast currents have a much smaller sediment transport capacity.

A limited sensitivity analysis of the above methodology and calculations, indicated that the results (transported volumes) could vary by about a factor of 2. The main variations are due to uncertainties in the input parameters in terms of the currents (velocity and direction), bed roughness and transport zone widths. As such, the general accuracy of the Van Rijn formulations was not assessed. The results given above are however considered to be the best theoretical estimates.

4.4 Mathematical sediment transport modelling

4.4.1 Initial model tests

An additional or alternative means of determining the sediment transports is to utilize the Delft hydrodynamic model (Section 3.3.7). By linking a sediment transport model to the simulations of the current regimes, the potential transport rates can be determined. These initial tests simulated transports due to the offshore currents (combined with wave stirring effects), but *excluded* wave driven longshore currents (as opposed to the further modelling described in Section 4.4.2). In this case, the Engelund-Hansen-Swart model (Swart, 1976; Swart and Flemming, 1980) was used to determine the transports. Schoonees and Theron (1996) found this to be one of the best detail predictors to determine sediment transport due to currents and waves. Figure 4.17 shows the potential transport rates thus simulated for the average situation/conditions (i.e. current is 0,3 m/s at 1,4 km offshore; H_{mo} = 2 m; T_p = 12 s). It should be noted that this exercise was preliminary for the purpose of testing the type of detailed modelling simulation is being utilized in present ongoing studies. In this simulation for instance, the wave heights are not correctly incorporated into the calculations over a part of the modelling terrain. (Nicholson *et al.*, 1997 give a comparison of a few other models which should be suitable to model sediment transport in this case.)

4.4.2 Morphological modelling

4.4.2.1 Background and approach

Following the preliminary model tests described above, the morphological model DELFT3D-MOR (WL|Delft Hydraulics, 2001) was applied to model the sedimentation and morphological changes at the entrance of the East London harbour. This entailed the numerical modelling of the hydrodynamics, sediment dynamics and morphological changes due to the sediment fluxes induced by waves and currents. (These simulations therefore *included* wave driven currents, whereas the initial tests described above in Section 4.4.1 did not.) The main reason for selecting this model is that

ultimately it is required to predict morphological changes that cannot be predicted with one-dimensional models. As outlined by Bos *et al* (1996) the Delft3D-MOR model provides an interactive coupling between the calculation of waves, currents, sediment transport rates and the resulting bed level changes. This implies that if the morphological changes are above a selected limit, the flow field will automatically be recalculated to allow for the influence of the bottom changes on the flow.

The study area is exposed to the incident wave regime, strong currents occur and has a well-mixed system without stratification. This type of environment is more suitable to a two-dimensional depth-averaged modelling approach as was conducted here. The driving forces for the model are the offshore waves and currents (which also include wind and tidal effects). Bottom friction was calculated using the approach of Colebrook-White.

The sediment transport formula of Bijker (1971) was used, since this is the only formula that has been programmed in the DELFT model to determine the bottom and suspended transport separately. This means that sediment deposition, re-suspension and sediment availability can be accounted for. Bijker's method can be classified as a shear stress (modified steady flow) approach. He introduced the average bed shear stress due to combined wave and current action instead of the bed shear stress due to current alone.

Based on the concept of Einstein (1950), Bijker proposed:

$$q_{s,c} = 1.83 q_{b,c} [I_2 + I_1 \ln(33 h/k_s)]$$

in which:

- $q_{s,c}$ = suspended sediment transport rate (m^2/s)
- $q_{b,c}$ = bedload transport rate (m^2/s)
- I_1 and I_2 are the Einstein integrals (Einstein, 1950)
- k_s = bed roughness (m)
- h = water depth (m)

The bedload transport rate ($q_{b,c}$, m^2/s) is expressed as a function of :

- Overall bed shear velocity
- Mobility parameter
- Bed form factor
- Overall Chezy coefficient
- Grain related Chezy coefficient
- Bijker coefficient

Thus, the resulting main input parameters required are: current velocity, wave height and period, water depth, ripple height (roughness), grain size, density of water and sediment, and the Bijker coefficient. The method of Einstein assumes a logarithmic velocity distribution over the depth.

Sensitivity analyses were conducted on different input processes and parameters and the most suitable set-up was selected for the modelling (similar to that described in Section 3.3.7). The first step in the modelling is to ensure that the model simulates the wave and current induced hydrodynamics of the system correctly.

4.4.2.2 DELFT3D-MOR wave regime schematisation

To start off with, the input wave climate that is required by the model was chosen to be the same as the wave climate determined for the wave refraction modelling described in Section 3.2.8. Therefore, just three wave scenarios representative of specific conditions were chosen for the modelling exercise. (These were the “most typical” or “average” wave condition, a typical south-westerly storm condition and a typical easterly wind wave.) However, it was soon evident that although quantitative deductions could be made regarding the sediment transport and morphological changes caused by each different wave condition, the combined result did not reflect reality at all. Thus, it was found that the simplified wave climate determined in this manner is insufficient for the calculation of morphological changes resulting from a wider range of wave conditions (as is the case for most of South Africa). It was concluded that a wave climate more representative of the actual wave climate should be constructed.

The principles for an alternative method were put forward, namely:

- The total annual upcoast (taken as positive by convention) and downcoast (taken as negative by convention) longshore transports should both be correct. Therefore both the nett and gross annual longshore transports will be correct (resulting, for example in this case in more realistic volumes of sediment caught in the sand traps).
- The zones/areas in which the transport occurs should be approximately correct. Thus, for example, the wave heights should not be increased unrealistically, which would result in wider surf zones, with more transport further away from the shoreline than in reality.
- The average breaking wave angle should be correct, because, for instance, the true equilibrium shoreline alignment is highly correlated with the average breaking wave angle.
- The duration of discrete wave conditions should be correct. An important reason for setting this principle is that sediment transports can reach a so-called “point of no return”. This relates to the fact that if a certain wave condition persists for too (unrealistically) long, too much sediment can be transported into an area from where it cannot return, even if the wave condition is eventually reversed (or changed). In reality, the changing wave conditions would have stopped such transport sooner, or reduced the amount.

Thus, a limited (i.t.o. number of conditions) new wave climate was constructed, while attempting to adhere to the above principles. This wave climate was intended to simulate the minimum number of key components of the wave driven sediment transport regime, resulting in an acceptable approximation of the annual morphological response. The wave conditions are summarised in Table IX below.

Table IX: Representative “morphological” wave conditions.

Duration (days)	Significant offshore wave height (m)	Peak period (seconds)	Offshore direction
17,5	3	9,6	East
7,5	3	9,6	East-south-east
50	3	10,7	South
93,5	3	10,7	South-south-west
112	3	10,7	South-west

Although the modelling results showed improvements compared to the first set of runs, the simulations were still not acceptable. This emphasized the difficulty and necessity of determining a proper wave climate for sediment transport and morphological modelling. The main objective of this part of the study was to identify a better method to determine a truly representative wave climate (i.t.o. wave driven sediment transport).

From the initial work, it became obvious that the sequence and duration of wave events was critical in obtaining realistic simulations. Thus, a way was sought of simulating as realistically as possible a complete annual wave time series, but keeping in mind the major limitation that it is not practical/possible to simulate more than about 200 wave conditions in DELFT3D-MOR. The fact that larger wave heights or larger wave incidence angles result in relatively much greater sediment transports was used to select those events from the annual record which resulted in the major part of all sediment transport.

A separate model was programmed and used to transform every wave condition from the wave recording buoy (which data was used as input for the model) to the shoreline. This wave transformation model was based on the bore model of Battjes and Janssen (1978) (tested with success by Nairn, 1990 amongst others) with linear, cnoidal and vocoidal shoaling. The breaking wave heights as determined with the vocoidal shoaling are considered to be the most accurate (Swart and Crowley, 1988, CSIR, 1993b) and were thus used in this study. Each individual wave condition was thus transformed from the recording position, through the surf zone up to the point of maximum wave run-up. Data from hydrographic surveys of the area conducted in February 1985 and in October 1993 (Theron *et al*, 2002a) were utilized to determine the input bottom profile.

The same transport model as used in DELFT3D-MOR (i.e. the Bijker model, Section 4.4.2.1) was then used to determine the transport due to each wave condition (this also required some additional programming). The transports were ranked (up- and downcoast) enabling the selection of those conditions resulting in the top 30% of transports. The time series of these “top 30%” conditions was analysed to determine the duration of each discrete event (e.g. 24h of SW storm conditions followed by 12h of local easterly wind waves.) Wave heights and periods were then averaged over these durations to further reduce the number of wave conditions. Thus, a specific sequence of less than 20 wave conditions with distinct durations was derived from the original time-series record of about 3 000 wave conditions.

Sediment Transport Regime at East London

The wave conditions are summarised in Table X below. A complete annual record is simulated by extrapolating or repeating this sequence (in this case 5 repetitions are required). This method was tested and it was found that the schematised wave regime (18 conditions) gave results very similar to that obtained from the total (~ 3 000 conditions) wave record (i.t.o. sediment transports).

Table X: Final wave schematisation (at buoy, 22 m depth) for MOR modelling.

Condition No.	Duration h	H_{mo} m	T_p s	Direction °N	Direction Coast °	Blqs. Unit m ³
1	3,0	2,4	13,5	122	-36,0	-1080
2	40,9	2,5	11,6	183	24,6	14180
3	3,0	2,2	5,8	135	-23,1	-470
4	21,4	2,1	12,9	182	24,2	3140
5	3,0	2,2	5,5	101	-57,3	-430
6	22,0	2,3	10,4	184	26,0	5730
7	3,0	2,0	6,6	132	-26,0	-350
8	2,0	2,1	6,8	209	50,6	1020
9	13,1	2,4	11,9	174	16,4	9400
10	8,5	1,8	9,5	124	-34,2	-3730
11	1,0	2,0	7,5	199	40,5	450
12	19,8	2,4	10,6	177	18,7	15620
13	6,0	2,2	9,6	140	-17,8	-3320
14	8,7	2,2	10,2	187	28,6	6530
15	1,0	2,4	6,2	106	-51,9	-450
16	5,9	2,3	11,9	178	19,6	4000
17	16,1	2,1	8,8	119	-38,7	-10830
18	23,5	2,4	13,2	177	19,2	17900

Based on the above results, a few test conditions were selected on which wave transformation simulations were modelled, and the fully dynamic hydraulic, transport and morphological simulations were conducted. (The actual model runs were conducted by Dr H Diedericks of the US. The interpretation and application of these results were conducted by the author.) As an example, the morphological changes resulting from a constant wave condition (i.e. current is 0,3 m/s at 1,4 km offshore; $H_{mo} = 2$ m; $T_p = 11,9$ s; wave dir. = 214 °N (all deep-sea) are illustrated in Figure 4.18. The top figure shows the initial bathymetry at the start of the simulation, while the middle and bottom figures show the resulting bed-level changes after 78 and 171 days respectively. The most significant results are clearly the sand transport into the main sand trap, around the head of the main breakwater and into the entrance channel. The modelling also indicated that such continuous transport would lead to the formation of a sandbank/bar across the port entrance, such as has been documented in the past along the western edge of what is aptly named the “Bar” area. However, wave conditions would not remain virtually the same for such a long period. In reality, the sediment transport balance in the area is determined by the constantly varying wave conditions in conjunction with the varying current regime.

4.4.2.3 Preliminary conclusions

The suitability of the Delft3D-MOR morphological model to simulate the field conditions and to utilize the field data to predict hydro- and sediment dynamics in the East London coastal zone was assessed, and the results were promising. It is concluded that the numerical model is a good tool for

studying hydro- and sediment dynamics at East London (but also anywhere along the South African coast), as the model achieves good agreement with measured local water velocities and at this initial stage appears to simulate sediment dynamics sufficiently well. The model showed that the sediment transport balance in the study area relies on a subtle balance between the varying wave conditions (and current regime). It is therefore not correct to simply conclude that a representative wave and current condition will simulate long-term sedimentation realistically. Although the model performed acceptably, there are still additional processes to include such as more accurate wave refraction modelling, as discussed in the following paragraph. Although the model results are preliminary (simulating only a few wave and current conditions), it illustrates the sedimentation trend that can be expected in the study area for typical wave conditions with a downcoast nearshore (in the deeper waters seaward of the surf zone) current condition.

The method as described above relied on linear wave refraction of the measured waves in deep water to the nearshore area. The DELFT3D model uses the more sophisticated DELFT3D-WAVE (SWAN) model. SWAN (Simulating Waves Nearshore) is a third-generation wave model that computes random, short-crested wind-generated waves in coastal regions, including lakes and estuarine waters (Holthuijsen and Booij, 2003). To correct the possible error in the initial linear wave refraction, the more accurate wave transformation as simulated in the DELFT model could be applied. This is, however, beyond the scope of this thesis. Once all the wave transformation simulations have been modelled with DELFT3D-WAVE (SWAN), the fully dynamic hydraulic, transport and morphological simulations can be conducted. The results can then be compared to the available knowledge regarding the sediment transport regime.

4.5 River and estuarine sediment transports

4.5.1 Sediment input from the Buffalo River

As mentioned in the introduction, the Port of East London is located on the Buffalo River (Figure 1.2). A further aspect of the sediment transport regime in the study area is thus the fluvial sediment input into the coastal zone from the Buffalo River.

The Buffalo river has a relatively small catchment area of about 1 250 km² (DWA, 1986). Sediment production (including sand and silt) for the total catchment is estimated to be about 660 000 ton per annum (based on the work of Rooseboom, 1975 and 1978). The mean annual runoff of the river at the Bridle Drift Dam (Figure 4.19) is estimated to be some 41 x 10⁶ m³. The sand load in the river is estimated to be 0,2% of the runoff (Weaver in Hart, 1982). Thus, the mean annual sand load is estimated to be about 80 000 m³.

However, there are three relatively large dams (Laing, Rooikrantz and Bridle Drift, Figure 4.19) on the river that act as effective sediment traps. It is estimated that each of these dams trap a very large proportion of the sand flowing into them; in the case of Bridle Drift virtually 100% (Weaver in Hart, 1982). Of the dams, Bridle Drift is located the furthest downstream and there are no additional significant inflows into the river between this dam and the sea. Consequently, very little sand of fluvial origin is eventually deposited in the harbour area. This is also confirmed by observations (of dredging works) made by Mr V Claassens (formerly the Port Engineer of East London). Although larger volumes of mainly muddy (with some silty) sediment is deposited in the harbour area during large river floods, it can be conservatively stated that in the long-term, on average less than 10 000 m³/a of fluvial sand is input into the harbour area. The dredging records (Section 4.1.3)

indicate that on average about 50 000 m³/a in total has been dredged from the inner harbour. It is estimated that between 40 000 m³ to 45 000 m³ of this material consists of mainly muddy (with some silty) sediment, while about 5 000 m³ to 10 000 m³ consists of sand of mostly fluvial origin.

Reservoir sedimentation and therefore trapping efficiency of reservoirs could also be determined by more comprehensive investigations/state-of-the-art techniques such as those derived by Rooseboom (1992) and Sloff (1997). Sloff investigated the sedimentation processes and for example developed and tested a two-dimensional depth-averaged (2-DH) two-layer mathematical model to simulate turbidity currents in reservoirs. However, the conclusions regarding fluvial inputs into the coastal zone are robust and it is therefore unwarranted to investigate this single aspect of the overall study in such fine detail (also keeping in mind that the fluvial sand input is between 1% and 3% of the total marine sediment input for the study area).

4.5.2 Tidally induced transports in/out of the harbour

Based on a rough tidal prism calculation, tidal flow velocities in and out of the harbour are estimated as follows:

The average depth of the entrance to the harbour (basin area) is about 13 m, while the entrance width is about 188 m. Thus, the cross-sectional area of the entrance is about 2 450 m². It is estimated that the surface area of the Buffalo River Estuary and the harbour is about 975 000 m². The spring tidal range at East London is about 1,63 m, while the neap tidal range is about 0,5 m (Section 3.3.6). Therefore, the tidal volume entering or exiting from the harbour area is about 1 590 000 m³ during spring tides and 490 000 m³ during neap tides (assuming the estuary has a fixed surface area). Assuming a sinusoidal tidal cycle (i.e. ebb and flood tides are symmetrical), but a significantly more peaked flow velocity cycle (as found in nature at many South African estuaries, Theron *et al*, 2002b), the average flow velocity (over depth and time) during spring tides is calculated to be 5 cm/s, while the maximum velocity (over depth) is 14 cm/s. Similarly, average flow velocities are calculated to be 1 cm/s with a maximum of 4 cm/s during neap tides.

These results can be compared to current measurements conducted by IMT over a two-month period at the entrance to the harbour basin area, at 2 m above the bottom (CSIR, 1998). Current speeds were found to be relatively low, ranging from about 1 to 19 cm/s with an average speed of only 5 cm/s. Further measurements conducted over a spring tidal cycle gave current velocities ranging from 1,4 to 13,3 cm/s with an average of only 4,4 cm/s. Thus, it can be said that the calculated current velocities and measurements match very well.

Based on these current velocities and typical grain size distributions in area (Section 3.8.1), the Bijker (Section 4.4.2.1), Engelund-Hansen-Swart (Section 4.2.4) and Van Rijn formulae (Section 4.3.1) all give zero transport rates. This indicates that these current velocities are too low to initiate significant sand transport. Thus, it can be said that sand transport into or out of the harbour due to tidal flows alone is insignificant.

4.6 Transport through and around the head of the main breakwater

The purpose of this part of the study is to determine the volume of sand deposited on the leeward side of the main breakwater and from where this sand originates. This entails determining the transport rate through the breakwater and the transport rate to the leeward side of the breakwater from around its head.

4.6.1 Methodology

Two temporary sandtraps or test pits (A and B) were planned for the purpose of studying sediment infill patterns over time and general sand movement. This led to an area on the leeward side of the main breakwater being dredged deeper than the surrounding seabed (Figures 4.20 and 4.21). Bathymetric surveys of the whole area leeward of the breakwater were undertaken before and after this dredging. Another four surveys of this area were completed after the dredging so that changes in bottom topography could be investigated. (All these surveys were undertaken by NPA.) In this way the volumes of sand deposited and eroded could be determined as well as the areas in which these changes took place. A study of the sedimentation and erosion patterns also lead to some conclusions regarding the origin of this sediment and the processes involved.

Limited current and sand concentration measurements were also done on the leeward side of the main breakwater. These measurements and observations gave some insight into the actual transport and sedimentation mechanisms. From the measured currents and concentrations, the sediment load was also calculated.

The results of a side-scan sonar survey of the area are also considered, as this is relevant to this study.

4.6.2 Transports derived from longer term measurements

Changes in bottom topography

A total of eight bathymetric surveys (all done by NPA in a consistent manner) were utilized for this study. The dates of these surveys covering the area on the leeward side of the main breakwater are shown on Figure 4.20. (The volumes of sand dredged from this area between June 1994 and November 1994 were also obtained from NPA.) No dredging activities took place in this area after the survey of 4 November 1994. Thus, volume differences were only calculated from this survey onwards. The earlier surveys are, however, also useful in studying the changes in bottom topography.

Figure 4.20 shows a direct comparison of the eight surveys. In this case only the -14 m CD (Chart Datum) contour from each of the surveys is shown. It is clear from the figure that relatively little change took place in this area over the period under consideration (21 September 1993 to 19 January 1995) except in the area in and between the two test pit areas. The greatest changes here are due to the dredging activities. The longest undisturbed period (without dredging) is that between the surveys of 4 November 1994 and 19 January 1995. The areas of significant accretion and erosion between these two dates are also shown in Figure 4.20. It can be seen that most accretion took place approximately parallel to the breakwater in the two test pit areas.

Cross-sectional profiles

Specific changes in the bottom topography can be more clearly shown by comparing cross-sectional profiles. Figure 4.22 is an example of such a comparison and shows a cross-section through the middle of test pit B (150 m from the head of the breakwater and perpendicular to the breakwater – approximately midway between lines I and J, Figure 4.21). Likewise, Figure 4.23 shows a cross-section through test pit A (330 m from the head of the breakwater). The significant accretion, which occurred over approximately the first 100 m from the breakwater between these dates, is clearly shown. The smaller differences further away from the breakwater (>100 m) are within or close to the accuracy of the survey methods.

Sediment volume differences

Volume changes were calculated between the surveys of 4 November 1994 and 19 January 1995 over an area of 450 m by 200 m parallel to the breakwater (Figure 4.24). The volume differences in each 25 m by 25 m block over this whole area are shown in Figure 4.25. It should be noted that volumes of 60 m³ or less represent vertical differences of less than 0,1 m which is within the accuracy of the survey methods. Volume changes of this order of magnitude are thus not significant and should be disregarded (over the total area the small survey errors should cancel out approximately). The total volume change over the whole area indicates that accretion of some 13 000 m³ occurred over the 45 days between the surveys. This represents sedimentation of about 100 000 m³/year on the leeward side of the main breakwater. The assumption that the 45 days between the surveys is approximately representative of the long-term average situation is based on the recorded wave conditions. Figure 4.26 shows that the wave heights recorded between 4 November 1994 and 19 January 1995 match the long-term record almost exactly.

Derived sediment movement patterns

Virtually all of the significant accretion occurred between the two dashed lines on Figure 4.25. Investigation of the sedimentation and erosion patterns provides some insight into the source of the sedimentation.

Sediment transported *around the head of the breakwater* (Figure 4.13) would be deposited on the leeward side in a fan-like pattern (in the relatively deeper and calmer waters). Peak tidal currents parallel to the breakwater would tend to spread this sediment to a certain degree along the breakwater. (In general, however, the tidal currents are too weak to have a significant effect.) Wave action on the leeward side of the breakwater would also tend to move some of the sediment towards the harbour. There is a relatively steep gradient in the bottom topography from the breakwater towards the entrance channel. This would add a downslope component to the movement of sediment and cause sediment also to move away from the breakwater into deeper water. It is highly unlikely that sediment would move back up the slope into shallower water. The turbulence (and possibly stronger currents) close to the head of the breakwater would prevent deposition in this area (Garde *et al.*, 1961 and Przedwojski, 1995).

Sediment moving through the breakwater (Figure 3.21) would likewise be spread parallel to the breakwater by tidal currents and also have a downslope component of movement away from the breakwater. As the distance increases from the head of the breakwater there is a marked decrease in wave action and turbulence on the leeward side of the breakwater. Thus sediment moving through the

breakwater is much less prone to wave action than sediment moving around the head, especially as the distance from the head increases. Being less turbulent than near the head, sediment would also be deposited closer to the breakwater as one moves from the head in a landward direction.

Calculated source of sedimentation

All of the above is consistent with the general pattern of sedimentation shown in Figure 4.25. This leads to an approximate division of the sources of the sedimentation. From the pattern of sedimentation it is calculated that at most about 46% of the sediment deposited could be from around the head of the breakwater, while the minimum could be 25%. Thus it can be estimated that on average between 25 000 m³ and 46 000 m³ of sand moves around the head per year, while between 54 000 m³ and 75 000 m³ moves through the breakwater per year (total 100 000 m³/year). These estimates are given not taking into account subsequent actions by NPA to "plug" the breakwater, which would reduce transport through the breakwater. Subsequent to 1995, NPA has "plugged" a small portion of the main breakwater by pumping a total volume of 89 m³ of concrete into the breakwater at about 500 m landward from the head. The Port Engineer estimates that the porosity of the breakwater has been reduced by about 80 % in that area. The plugged area, however, only constitutes about 15 % of the total length of the breakwater over most of which it is known that sediment moves through. Thus, the effect of the plugging on the sediment transport patterns has been relatively small. It is therefore estimated that since the plugging, the amount of sediment transported around the head of the breakwater could be slightly increased to between about 30% to 55%, or 30 000 m³ to 55 000 m³ per year. Thus, on average between 45 000 m³ and 70 000 m³ would move through the breakwater per year.

Possible effects of "test pits"

Originally, the plan had been to create two approximately rectangular test pits as shown on Figures 4.20 and 4.21 (indicated by A and B). The rectangular areas indicate the floor of the test pits, which were supposed to be about 2 m below the average surrounding bottom elevation. The idea behind these test pits was to create two temporary sand traps. By studying the patterns of sediment infill into these traps over time, the general sand movement (and volumes) in the area could be determined. Test pit A would tend to trap most sediment moving through the breakwater between about lines K to M (Figure 4.20). Test pit B would tend to trap sediment moving around the head as well as movement through the breakwater between about lines I to J (Figure 4.20).

Due to cost and time constraints, two distinct test pit areas were not dredged in practise. The actual situation after completion of dredging activities is shown on Figure 4.21 (bathymetric survey of 4 November 1994). It can be seen that a generally deeper area (below -14 m CD) was attained between about lines I to L with the deepest part of this "hollow" about 100 m from the breakwater. This was the result of utilizing an existing deeper area within test pit A and additional dredging towards test pit B.

The uneven shape of the actual deeper area, makes clear determination of sand infill patterns more difficult. Thus, it was decided to study the changes in bottom topography over the whole area (including this deeper area) as shown in Figures 4.24 and 4.25. In this way, it was also possible to obtain a clear picture of the sediment movement in the area as a whole.

Neither the originally proposed test pits, nor the actually achieved deeper area could cause more sand

to move through the breakwater or around the head, than if these bottom features were not present. The test pits and deeper area are all too far away from the breakwater to have a noticeable effect on the physical processes forcing sediment to move through the breakwater or around the head.

It is possible that the deeper than "normal" area cause by the dredging may have resulted in a small additional "abnormal" sediment movement towards this deeper area because of the increased downward slope. This does however, not have any bearing on the main results of and conclusions reached in this study. This is because the area considered for the volume computation (Figure 4.24) covers an area beyond the deeper area and as such, redistribution of the sediment within the volume area cancels out. In addition, the profiles on Figures 4.22 and 4.23 show that significant accretion occurred on the sloped area of the seabed relatively close to the breakwater and not on the flatter area further away. This substantiates the above discussion and shows clearly that the volumetric calculations were not influenced by the deeper dredged area.

4.6.3 Sediment load calculated from concentration and current measurements

Concentration measurements

Sediment concentrations were measured at three locations (called N, KL and I) on the leeward side of the main breakwater (Figure 4.27) on 20 January 1995. These three positions were chosen to be adjacent to areas where significant sand movement through the breakwater was expected and also to be representative of nearly the whole area on the leeward side of the breakwater. Segmented "bamboo pole" samplers were used to trap suspended sediment. (More detail on these samplers is given in Nicholson and Swart, 1985 and Schoonees, 1991.) Three deployments were done at each location. Sediment was trapped at 14 different levels in the water column over a period of at least half an hour, so as to obtain good time-averaged sediment entrainment values (mg/h). (The individual measurement periods at each location are shown on Figure 4.27).

Gonsalves and Bartels (1990) found good correlation between "bamboo pole" data and directly pumped samples. From their relationship, sediment concentrations (mg/l) were calculated from the entrainment values (mg/h). Figure 4.28 shows the concentrations thus obtained at location KL (as an example). Good agreement is shown between the individual measurements and a general relationship between concentration and depth could be established for this location. Similar relationships were also determined for the other two locations (I and N).

A vacuum pump suction sampler was also used to obtain simultaneous measurements at location N (Figure 4.27). Samples were extracted at various levels in the water column over a period of at least half an hour. Figure 4.29 shows a comparison of the "bamboo pole" and vacuum pump measurements. There is excellent agreement between the two pumped measurements and reasonable agreement between the pumped measurements and the "bamboo pole" data. (Note that the bottom samples of the two pump measurements were directly on the sand bottom and thus not comparable to the other suspended sediment samples). The conclusion is thus that all of the "bamboo pole" measurements should be of acceptably good quality.

Current measurements

In conjunction with the concentration measurements, currents were measured on the leeward side of the main breakwater by means of an Endeco electronic vector-averaging current profiler, drogue tracking, drifter buoys and dye tracking. These measurements are described in Section 3.3.6.

Calculated sediment load

From the measured sediment concentrations and currents the volume of sediment being transported to the leeward side of the main breakwater, could be calculated. From the concentration measurements general relationships between concentration and depth were determined for representative areas along the leeward side of the main breakwater. Average depths were determined for each area taking into account the bottom topography and the predicted tidal levels for East London. Vector averaged currents were also determined for each area from the measured current velocities and directions. By integrating the concentrations over depth, and multiplying by the averaged currents, depths and widths of the areas, the suspended sediment load could be calculated. The bedload in each area was determined by using the method of Einstein (1950) to calculate the relationship between the bedload ($q_{b,c}$) and the suspended load ($q_{s,c}$). (In this case it was determined that $q_{b,c} = 1,13 q_{s,c}$.) Thereafter the total load ($q_{t,c} = q_{b,c} + q_{s,c}$ (kg/s)) was converted to a sedimentation rate ($m^3/year$).

The wave heights measured by the Waverider off the Port of East London on 20 January 1995 were about 17% below the long-term average. The wave periods were approximately equal to the long-term average. Unfortunately, wave directions were not measured at East London at that time. However, the observed wave directions (approximately south to south-easterly seaward of the main breakwater) were considered fairly typical and not uncommon. Thus, the sedimentation rate was adapted only to account for the below average wave heights. The above approach gave a total sedimentation rate of about 16 000 $m^3/year$ for sand moving through the breakwater. However, this was previously determined to be at least 45 000 $m^3/year$ from the survey results (Section 4.6.2). The reasons for this "discrepancy" are discussed in the following section.

4.6.4 Discussion and conclusions

From further investigations of the measurements and observations it has become evident why the above approach (Section 4.6.3) would give different answers from the long-term measurements (Section 4.6.2).

The bottom topography during the concentration and current measurements was most probably not representative of the usual long-term conditions. Previously a relatively large "blow hole" was clearly visible between lines K and L (Figure 3.44). The survey of 3 September 1993 (Theron and Schoonees, 1999) also clearly shows a "hole" opposite this position on the outside of the breakwater. No blow hole could be seen at all at this position on 19 and 20 January 1995. A more recent survey (CSIR, 1995) also shows no indication of such a hole. In fact, the more recent survey shows that most of the area on the outside of the breakwater had accreted when compared to the previous survey. Especially the gully close to the outside of the breakwater appears to have sanded up (Figure 3.45). This would tend to close off many of the holes through the breakwater and further limit the sand transport through the wall. It is thus concluded that far less sand was moving through the breakwater during 19 and 20 January 1995 than was previously the case.

Observations during the concentration and current measurements indicated that sediment movement through the breakwater (e.g. Figure 3.21) is in the form of strongly pulsating point sources (in other words, specific "blow holes"). At a relatively small distance from the breakwater, these point loads are then spread laterally by water movement parallel to the breakwater. The concentration measurements were done at approximately 15 m from the breakwater where the sediment load had already become somewhat diffused. It cannot be determined how representative the three measurement locations are of the whole area - in fact, the amount of sand coming through each hole is expected to vary in time depending on the wave conditions and the sea bed levels seawards of the breakwater. The current measurements made near the location of the concentration measurements are also not representative of the strongly pulsating water flows directly at the "holes". The steep slope from the breakwater towards the channel would cause a relatively large downslope bedload (which is extremely difficult to measure accurately) towards the entrance channel area. Thus, it can be said that the current and concentration values used in the calculation of the sediment load are not totally representative of the conditions causing sedimentation on the leeward side of the breakwater. It would however, be impossible to locate almost every "hole" and to measure the concentrations and currents at each hole continuously over a longer time period (e.g. one year).

A final point of uncertainty is the effect of storms. The fact that the sediment transport during storms is much larger than during normal conditions, is a given. In the long-term a relatively larger proportion of the sedimentation is due to storms (Section 4.2.4). The measurements for this part of the study were conducted during below average conditions, but the results were adjusted to account for the *average* condition. Although the long-term average wave height includes storm events, the adjustment is probably still insufficient. Study and data constraints limit the present effort to primarily longer term average predictions. A comprehensive environmental database and a more detailed and complex initiative, beyond the scope of the present study, would be required to assess the effects of sporadic or short-term events.

The current and concentration measurements and observations were most useful in obtaining a proper understanding of the mechanics and processes involved. They also reinforce the interpretation of the bathymetric surveys (Section 4.6.2). It is, however, concluded that the results obtained from the current and concentration measurements are not fully representative of the actual average long-term situation. Therefore, the results and conclusions reached in Section 4.6.2 are more applicable and are considered to be the most accurate. The best estimates are, thus, that the amount of sediment transported around the head of the breakwater is about 30 000 m³ per year, while, on average, about 45 000 m³ moves through the breakwater per year.

5. CONCLUSIONS

5.1 Components of the transport regime

5.1.1 Wave induced long -(and cross-) shore transports

The port has disrupted the natural upcoast longshore transport, but the shorelines adjacent to the harbour appear to have obtained dynamic equilibrium over the long-term with approximately balanced sediment transports.

Waves with a deep water direction of between 150 degrees and 330 degrees north theoretically generate upcoast longshore transport (mainly in the surf zone). Such transport would be generated for about two-thirds of the time while a downcoast longshore current would occur for about one-third of the time. This results in a net upcoast longshore transport in the long-term. Waves with a deep-sea direction of south-west to west-south-westerly, the most common scenario, cause longshore transport from the Foreshore area (Figure 1.4) towards the harbour and the head of the main breakwater. East-north-easterly waves, which are uncommon, cause longshore transport from the port towards the Foreshore area and Hood Point. At Hood Point as well as near Eastern Beach (Figure 1.3), upcoast longshore transport virtually always occurs with high potential transport at Hood point. At Orient Beach the longshore transport rates are low.

For typical wave incidence angles, relatively low longshore currents are generated along the main breakwater. Stormy sea conditions contribute relatively larger amounts to the gross annual transport rates than do average conditions. Along the outside of the main breakwater the sea bed has a relatively flat area that stretches to about 150 to 200 m from the breakwater. Almost all longshore transport occurs within the surf zone on this flat area. Only during rare storm events would significant transport occur beyond the -5m MSL contour. The potential mean longshore sediment transport rate is estimated to be about 500 000 m³/year along the outside of the main breakwater (towards the head). In terms of the availability in this area of sediment to be transported, this estimated net wave induced transport rate is excessive. The actual rate is estimated at between 250 000 to 300 000 m³/year (Section 4.2).

In this case, the net effect of cross-shore transport in the inshore zone is not significant in terms of the overall sediment transport regime.

5.1.2 Deeper water sediment transports and patterns

In the central shelf area the Agulhas Current transports very large amounts of sediment downcoast. The Agulhas Currents is also the dominant influence on the local deeper water flows and has the potential to transport significant amounts of sediment in the nearshore zone in the area of the East London harbour entrance. In general, there is an increase in current velocity in the offshore direction, while the main breakwater also causes an increase in current velocity seawards of the head. Current directions are mainly parallel to the coast. For about 70 per cent of the time the current flows swiftly in the south-westerly direction. When the Agulhas Current is further offshore, the south-westerly winds can dominate and cause a reversal to a slower north-easterly nearshore current. The potential for downcoast transport is orders of magnitude higher than upcoast transport. Off the head of the main breakwater, the carrying capacity of the weaker upcoast currents is only about 15 per cent of the downcoast currents.

It is estimated that, on average, about 75 000 m³/year of sediment would be transported into the Bar area (areas 6,7 and 9; Figure 4.2) from the north-east. A very small amount of sediment is transported from the Bar area further along and into the north-eastern corner of the main sand trap. On average about 10 000 m³ of sediment would annually be transported into the Bar area from the south.

On/offshore transport is not significant (in the deeper water zone). A clockwise current vortex occurs south of the main breakwater when the deeper water current flows in a downcoast direction. Further field measurements will be required to quantify the effects of such eddies. During upcoast currents, no eddy is formed south of the main breakwater.

5.1.3 Riverine inputs and transport due to tides

Annually, less than 10 000 m³ of fluvial sand is input into the harbour area on average (due to trapping of most of the sand by dams on the river, Section 4.5.1). Apart from localized sedimentation (consisting mainly of mud with some silt) confined to the inner harbour, river flows generally do not influence sediment transport in the study area.

As a result of the relatively large cross-sectional area of the entrance to the harbour in relation to the relatively small estuarine tidal volume, current velocities in/out of the harbour due to tides are too low to initiate significant sand transport (Section 4.5.2). Thus, it can be said that sand transport into or out of the harbour due to tidal flows alone are not significant. Although river and tidal flows can result in fine material (such as mud and fine slit) being transported, most of the fine material is considered to remain in suspension (to be widely dispersed into the ocean).

5.1.4 Wind impacts

Apart from the ability to occasionally reverse the direction of nearshore flows (as discussed above in Section 5.1.2), local winds in general do not have a significant impact on the overall sediment transport regime. Wind-blown sediment transport is also not significant (Section 3.5.3).

5.1.5 Transports around and through the main breakwater

The current on the lee side of the head of the main breakwater would tend to draw sediment from adjacent to the head, towards the lee side of the breakwater. Sediment transported *around the head of the main breakwater* (Figure 4.13) would be deposited on the leeward side in a fan-like pattern (in the relatively deeper and calmer waters in the lee of the breakwater). Flows parallel to the breakwater (mainly due to tidal currents and wave action along the leeward side) would tend to spread this sediment to a certain degree along the breakwater. Wave action along the lee side of the breakwater would also tend to move some of the sediment towards the harbour. There is a relatively steep gradient in the bottom topography from the breakwater towards the entrance channel. This would add a downslope component to the movement of sediment and cause sediment also to move away from the breakwater into the deeper water of the channel. The turbulence (and possibly stronger currents) close to the head of the breakwater would prevent deposition in this area.

Sediment movement through the main breakwater (from the south, Figure 3.21) is in the form of separate point sources through distinct blow holes (due to wave induced pulsating currents). High waves, low sand levels and more southerly waves all lead to higher transport from south to north through the main breakwater. Sediment moving through the breakwater would likewise be spread parallel to the breakwater by tidal currents and also have a downslope component of movement away from the breakwater. Along the leeward side of the main breakwater in the deeper water (between tides), sediments move parallel to the breakwater. Wave action and sediment movement gradually decrease from the head towards the harbour. Being less turbulent than near the head, sediment would also be deposited closer to the breakwater as one moves from the head in a landward direction.

It is estimated that on average about 30 000 m³ of sand moves around the head per year, while about 45 000 m³ moves through the breakwater per year (a total of 75 000 m³/year). (This estimate takes into account actions by NPA to “plug” the breakwater during recent years, which slightly reduced transport through the breakwater.)

5.2 Synthesis of transport patterns around the port

The mean volume of sediment dredged annually from the entire port (since 1994, when the existing traps were completed) is about 480 000 m³. Since 1994, about 245 000 m³ has been dredged from the main sand trap on average. In the Bar and entrance channel areas, an amount in the order of 200 000 m³ has annually been dredged in total, while about 50 000 m³ in total has been dredged annually from the inner harbour on average. (However, this last volume (50 000 m³) is known to have a high *mud* and *silt* content (similar to the examples of Fredsoe, 1978, Mayor-Mora *et al*, 1976 and O’Connor, 1985).)

Sediment is transported from the area adjacent to the Foreshore (Figure 1.4) towards the deeper water adjacent to the head of the main breakwater. Transport also occurs from the vicinity of the main breakwater towards the centre of the entrance channel, as well as from Orient Beach towards the vicinity of the head of the secondary breakwater. The main sand trap accretes from the south-western corner. In the Bar area, the sand build up mainly occurs from the north-eastern corner, while there is also a much smaller build up from the south-west. In the entrance channel area, there is a small build up of sand along the seaward half of the main breakwater (on the leeside). A small amount of build up also occurs in the entrance channel from approximately the north. These patterns show from which directions sediment is transported into these areas.

The main components of the sediment transport patterns around the port can be inferred from a synthesis of all of the foregoing information. (To facilitate the following discussions, reference should be made to Figure 4.2.)

Main sand trap

Virtually all sediment deposited in the main sand trap is due to sediment transport from the southwest. Some sediment also passes through the gap between the breakwater head and the main sand trap (Figure 4.13), to be deposited in the lee of the main breakwater. Sediment also moves through the main breakwater to be deposited in the lee thereof (Figure 3.21).

Dredging Areas 4 and 5

Dredging Areas 4 and 5 (Figure 4.2) are generally at about the same depth, with no significant slope between these areas. There is also no evidence of any other process, which could transport significant volumes of sediment from Area 4 to Area 5, or from the deeper areas to the east and northeast towards Area 5. It is also known that virtually no sedimentation occurs in Area 4 while there is relatively high sedimentation in Area 5. This means that sediment is not transported into Area 5 from the north (Area 4) or the northeast. It can thus be concluded without doubt that the sedimentation in Area 5 is almost exclusively due to the sediment transported through and around the main breakwater. It is concluded (Section 4.6) that of the total volume of sediment deposited in the lee of the main breakwater (dredging Areas 3 and 5), the majority (~60%) is due to sediment moving through the breakwater, while a smaller proportion (~40%) results from sediment transport around the head of the main breakwater. The NPA has "plugged" a small portion of the main breakwater by pumping concrete into the breakwater and thereby reducing the porosity of the breakwater in that area. However, the effect of the plugging on the sediment transport patterns has been relatively small. It is estimated that since the plugging, the proportion of sediment transported around the head of the breakwater has increased slightly. (This also conforms to the continuity principle, in that the energy or driving forces remain the same and the same amount of sediment is transported to the area, which roughly means that if less sediment can move through the breakwater, more sediment will be transported around the head.)

East sand trap and dredging Area 2

Virtually all sediment deposited in the East sand trap is due to sediment transport from the north to west. Some sediment also passes through the gap between the secondary breakwater head and the East sand trap, to be deposited in dredging Area 2 or in the lee of the secondary breakwater. There is no significant slope between dredging Areas 2 and 3 and there is no apparent mechanism, which could transport sediment from Area 3 to Area 2. The only other potential source of sedimentation in Area 2 is from the river through the harbour to the west. However, it has been shown (Section 4.5.1) that potential sedimentation due to river floods is very low in this part of the port. Furthermore, it has also been found that the sediment dredged from the East sand trap and Area 2 is predominantly sandy and usually has a low mud or silt content (while riverine sediments would have high mud or silt content). Thus, it is concluded that most sedimentation in the East sand trap and Area 2 is due to sediment transport from the north and northwest (parallel to the secondary breakwater).

Area 3

The sedimentation in Area 3 has three potential sources: from the river through the port on the west, from Area 2 on the north and from the east through sediment transported along the leeward side of the main breakwater. As stated before, sedimentation due to river floods is very low in this part of the port. Also (as in Area 2), the sediment dredged from Area 3 is predominantly sandy usually with low mud or silt content (while riverine sediments would have high mud or silt content). There is no significant slope between dredging Areas 2 and 3. However, an anti-clockwise current eddy is often generated to the north of the port, which could possibly transfer finer sediments from Area 2 to Area 3, as the western boundary of this eddy generally flows parallel to the secondary breakwater in this direction. However, because these eddy currents have low velocities, such transfer is very small. The main source of sedimentation in Area 3 is therefore considered to be transport from the east along the main breakwater.

Area 4

From the above discussions and the apparent lack of any significant driving force, it follows that sediment transport rates in the vicinity of Area 4 are very low. This is corroborated by the fact that the mean annual sedimentation (1995 to 1999) in Area 4 was found to be zero (Figure 4.12).

Areas 6, 7 and 9

The bathymetric difference maps (e.g. Figure 4.5) show that sedimentation in Areas 6, 7 and 9 generally occurs east of a line drawn along the eastern border of the main sand trap (Figure 4.6). Water depths in the areas to the east of this line are relatively greater and in these deeper areas the effects of waves on sediment transport are reduced, while the effect of the Agulhas current become more significant. It has been shown (Section 3.3.3.3) that in Areas 6, 7 and 9 the Agulhas current predominantly (80 %) flows in a downcoast direction and that the downcoast currents are generally twice as strong as the upcoast currents. The sea floor generally has a small upward gradient from the southeast (Area 9) towards the northwest (Area 6). The significance of this is the bottom transport (which is totally dominant in this area) is not easily driven up the slope. It has also been determined (Section 4.1.4) that sedimentation generally decreases from Areas 6 towards Area 9. All of this clearly indicates that the sedimentation in Areas 6, 7 and 9 is primarily the result of downcoast sediment transport due to the effects of the Agulhas current.

5.3 Final conclusions and sediment transport balance

The final interpretation of the foregoing synthesis led to the development of a relatively complicated pattern of sediment transports in the study area, as described below and illustrated in Figure viii. The sediment transport budget is summarized in Table XI below.

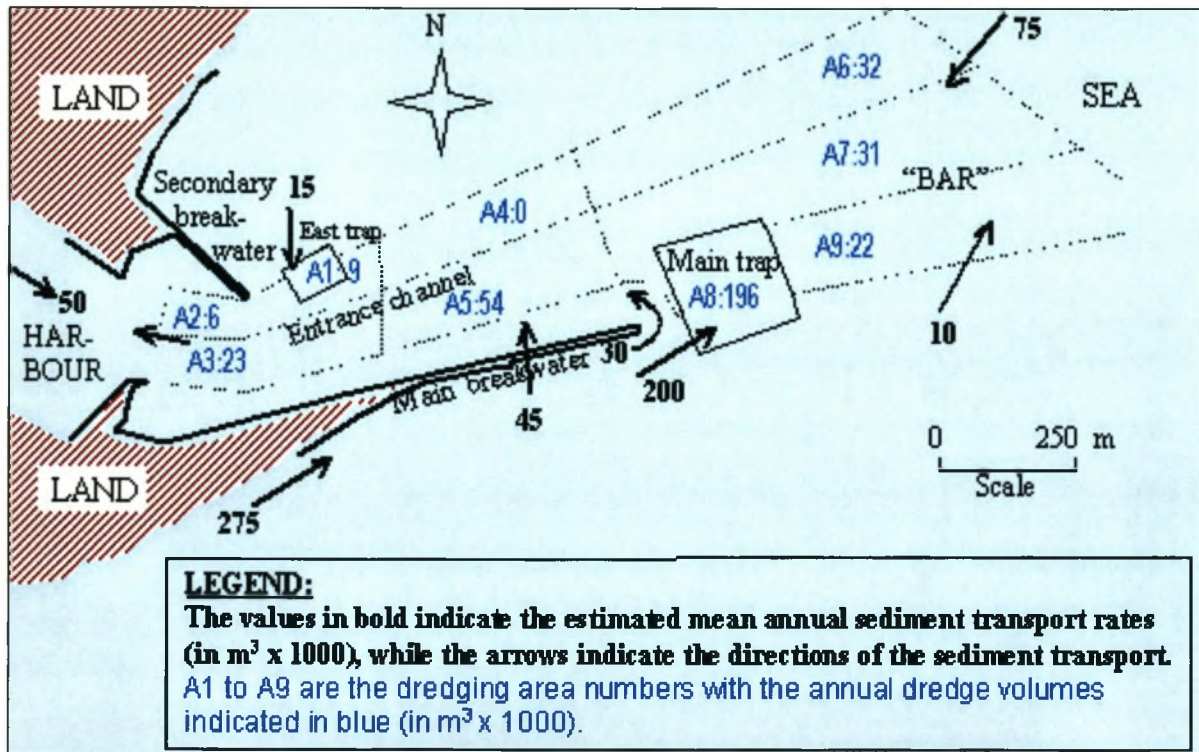


Figure (viii): East London sediment transport regime

Table XI: Sediment transport regime: budget and continuity

Sediment transports (1 000 m ³ /a) into study (control) area (Figure viii)			Observed sediment accretion volumes (1 000 m ³) inside study (control) area from bathy & dredge records (Figure viii)			
Component of transport	Volume	Sub totals	Area	Area #	Volume	Sub totals
Longshore transport from south: (goes into main trap, through main breakwater, and around main breakwater head)	275		Main trap	8	196	
		275	Entrance channel: SW part	3	23	
			Entrance channel: SE part	5	54	273
Transport due to deeper water currents: into Bar area from northeast	75		Bar: northern part	6	32	
into Bar area from southwest	10	85	Bar: central part	7	31	
			Bar: southern part	9	22	85
Transport from north and north-west into East trap and entrance channel		15	East trap	1	9	
			Entrance channel: NE part	2	6	
			Entrance channel: NW part	4	0	15
TOTAL		375	TOTAL			373
From river (mud, silt) plus fine suspended marine sediments into inner harbour	50		Inner harbour (mainly mud, some silt, little sand)		50	

There is a net wave induced longshore transport (mainly in the surf zone) of about 250 000 to 300 000 m³/year (estimated mean of 275 000 m³/year) on average from the Foreshore area towards the head of the main breakwater. Near Hood Point and Eastern Beach there is a high potential wave induced net longshore transport in the upcoast direction. The longshore transport at Orient Beach is low.

About 30 000 m³/year of sand is transported around the head of the main breakwater into the entrance channel (e.g. Figure 4.13) while about 45 000 m³/year moves through the main breakwater into the entrance channel (e.g. Figure 3.21). A smaller amount is also transported into the entrance channel and East sand trap from approximately the north to north-west, which is estimated to be about 15 000 m³/year to maintain the long-term sediment transport balance. A relatively large amount of sediment is transported into the main sand trap from the south-west. As virtually no sand is transported into the sand trap from the north-east, the transport from the south-west into the trap is estimated to be about 200 000 m³/year. The total transport into the main sand trap and entrance channel areas from the south-west (200 000 + 30 000 + 45 000 = 275 000 m³/year) is mainly fed by the wave driven longshore transport (mainly in the surf zone) from south-west of the port (estimated at 250 000 to 300 000 m³/year, Section 4.2.2).

In the deeper nearshore zone, mainly between 40 m to 60 m depth, very large amounts of sediment are transported downcoast by means of the Agulhas Current. This strong downcoast flowing current also has a significant influence on nearshore currents and sediment transport at the East London harbour entrance area. About 75 000 m³/year of sand is transported into the Bar area from the north-east with downcoast flowing nearshore currents, which is the predominant current direction. Almost none of this amount moves through the Bar area into the main sand trap (from the north-east). About 10 000 m³/year is also transported into the Bar area from the south-west with upcoast flowing nearshore currents, which is the less frequent current direction. These transport values give an approximate net annual accumulation of sediment in the Bar area of 75 000 m³ from the northeast plus 10 000 m³ from the southwest = 85 000 m³/year.

At Orient Beach the longshore transport rates are low. Some transport occurs from Orient Beach towards the vicinity of the head of the secondary breakwater. Most sedimentation in the East sand trap (9 000 m³/year) and Area 2 (6 000 m³/year) is due to sediment transport from the north and northwest (parallel to the secondary breakwater); thus about 15 000 m³/year in total. Some sediment passes through the gap between the secondary breakwater head and the East sand trap, to be deposited in dredging Area 2 or in the lee of the secondary breakwater.

Annually about 50 000 m³ of sediment (mostly mud with some silt and little sand) has been dredged from the inner harbour (the basins and quays). The sand content of this material is low, which implies that the actual *sand* transport from the entrance channel area into the inner harbour, is also low. The riverine input into the study area has been estimated at less than 10 000 m³/year of *sand*. It is estimated that the bulk of the 50 000 m³/year is mud and silt from the river, with some fine sediments of marine origin carried into the inner harbour in suspension.

Total sediment transports (from all sources) into the nine dredging areas (Figure viii and Table XI) therefore add up to 275 000 m³/year (longshore transport from the south-west) + 85 000 m³/year (deeper water currents into the Bar area) + 15 000 m³/year (from the north and northwest into the East sand trap and Area 2) = 375 000 m³/year. The mean annual sedimentation (since 1994), in the nine

Sediment Transport Regime at East London

dredging areas (from bathymetry and dredge records, Figure viii and Table XI), totals to about 373 000 m³. The difference (~2 000 m³) between the two totals is very small (~0,5%) and a good sediment transport balance is achieved.

Finally, it can be stated that the various effects of a multitude of environmental processes and systems such as waves, the Agulhas Current, the Buffalo River, local winds, etc. have been synthesized into a holistic understanding of the complex East London sediment transport regime, as depicted in Figure viii (and Figure 4.30).

6. RECOMMENDATIONS FOR FURTHER STUDIES

Many investigations (e. g. Theron, *et al.*, 1998, Theron, *et al.*, 2000) have shown that a good quantitative understanding of the sediment transport processes is required before any meaningful recommendations can be made regarding sedimentation and optimisation of dredging operations at any port. The prerequisite to understanding the sediment transport processes is a thorough investigation of the relevant coastal processes (e.g. wave regime, current patterns, etc.) and the sediment transport balance.

More detailed, high quality survey and dredge volume data will aid the accurate determination of sediment transport rates. In order to obtain more quantitative information on the currents closer to the harbour, further field data should preferably be collected. The information on surf zone currents also needs to be expanded on. Eddies often occur adjacent to the main breakwater. A literature review and field measurements are required to quantify the effects of such eddies on local sediment transports and to determine if the eddies have any effect on the overall sediment transport regime.

The longer term effects of major weather systems (especially strong winds with long durations) on local flow patterns and ultimately on sediment transports should be investigated further, as this will contribute to a more complete understanding of the current and transport regimes.

In terms of wave modelling, the scope of the present investigation did not allow for the completion of full wave climate time series wave modelling runs. The adopted approach was to model representative average and extreme wave scenarios, or alternatively to schematise the wave regime with less than 20 wave conditions. Thus, the wave modelling undertaken in this study does not cover a totally comprehensive wave climate and should be extended in more comprehensive future investigations. A two dimensional numerical model (the Delft hydrodynamic flow model) was utilized to simulate the complex flow patterns. In more comprehensive modelling studies, the tides should be included and the model should be run in full 3 dimensional mode to confirm that the omission of these effects do not have significant impacts on the results. By utilizing the Delft sediment transport model, preliminary results were presented, mainly to demonstrate the type of detailed modelling simulation that could be utilized in future studies. Finally, the integration of the field measurements and the modelling to predict sediment transport and resultant bottom changes should be assessed. This would be especially useful in quantifying the effects on the transport regime of different proposed modifications to the existing scenario (e.g. breakwater extensions).

Ultimately, the information contained in this thesis should feed into a wider regional investigation. The aim would be to draw up a sediment budget for the entire "regional macro sedimentary cell" of which the present study area (the coastal zone between the Goda and Nahoon Rivers) forms a part. (In engineering/geology type studies the "standard" is to define a cell's boundaries based on the dispersal of sediment from its source and/or based on topographic limits to its travel. A macro cell is usually defined as that entire coastal area or zone that receives most of its sediment from a given major source.) The consequences of (local) human interventions can only be fully appreciated, if the interaction with "the bigger picture" is properly understood.

7. REFERENCES

- Bascom, W N (1964). Waves and beaches. *Beaches*, Doubleday, New York, Chapter IX: 184 - 212.
- Battjes, J A and Janssen, J P F M (1978). Energy loss and set-up due to breaking of random waves. *16 Inter Conf on Coastal Eng*, Hamburg, Germany. ASCE, Vol 1: 569-587.
- Bijker, E W (1971). Longshore Transport Computations. *Journal of the Waterways, Harbours and Coastal Engineering Division*, Vol 97, No WW4.
- Bijker, E W (1980). Sedimentation in channels and trenches. *17 Inter Conf on Coastal Eng*, Sydney, Australia. ASCE, Vol 2: 1708-1718.
- Birkemeier, W A (1985). Field data on seaward limit of profile change. *Journal of Waterway, Port, Coastal and Ocean Engineering*, Vol. 111, No. 3.
- Booij, N, Holthuijsen, L H and Herbers, T H C (1985). A numerical model for wave boundary conditions in port design. *International Conference on Numerical and Hydraulic Modelling of ports and harbours*, Birmingham, BHRA, IAHR, Birmingham University, England, pp. 263-268.
- Bos, K.J., Roelvink, J.A., and Dingemans, M.W. (1996). Modelling the impact of detached breakwaters on the coast. *Proceedings 25th Intn. Conf On Coastal Eng.*, Orlando, Florida. ASCE, Chapter 157.
- Boyer, D L and Tao, L (1987). On the motion of linearly stratified rotating fluids past capes. *Journal of Fluid Mechanics*, 180, 429-449.
- Bray, R N (1979). *Dredging: A Handbook for Engineers*. Issued by Edward Arnold (Pub.) Ltd., London. P. 93.
- CERC (1977). Shore Protection Manual. Volume 1. U.S. Army Coastal Engineering Research Center, Fort Belvoir, Virginia.
- CERC (1984). Shore protection manual. Department of the Army, U S Army Corps of Engineers, CERC, Vicksburg, Mississippi. Vols. 1,2.
- CPB (1992). Coastal erosion, flooding and sea level rise standards and protection policy. *Coastline, South Australian Coast Protection Board*, No 26, 6 p.
- CSIR (1986). Breaker wave characteristics and longshore sediment transport along a bay, by J S Schoonees. *CSIR Research Report 570*, NRIO, Stellenbosch, 61, pp.
- CSIR (1987). East London Outfall Studies. Report No 4. Geophysical site investigations Hood Point-Nahoon Point. *CSIR Report C/SEA 8727*, Stellenbosch.
- CSIR (1988). East London Outfall Studies. Report No 3. Physical data interpretation and summaries. *CSIR Report C/SEA 8804*, Stellenbosch.
- CSIR (1989). Feasibility of a marine outfall pipeline for East London - executive summary report. *CSIR Report EMA-C 89105*, Stellenbosch.
- CSIR (1992). CLEO observers manual for estuaries and beaches. Ematek, Stellenbosch. 60 pp.
- CSIR (1993a). Agulhas Bank metocean data summary 1993 update of environmental design parameters: waves. *CSIR Report EMAS-C 93046*, Stellenbosch.
- CSIR (1993b). Modelling of Wave Height and Water Level Transformations Through the Surf Zone. *CSIR Research Report EMA-S-R 715*, Stellenbosch.
- CSIR (1995). East London breakwater survey, echo-soundings, side-scan sonography and seabed probing. *CSIR Draft Report EMAS-C 95025*, Stellenbosch.
- CSIR (2004). Port of East London Photographic Survey of the Main Breakwater, February 2004. *CSIR Report ENV-S-C 2004-029*, Environmentek, Stellenbosch.
- Cummings, G (1992). Report on the dredging requirements for the Port of East London, NPA. Submitted to The Harbour Engineer, East London. December 1992. 50 pp.

- Den Adel, J D, Franken, A, Niemeyer, H D, Booij, N, Stive, M J F and Vogel, J A (1991). Wave model application on a Wadden Sea area, *Proc 22nd International Conference on Coastal Engineering*, Delft, ASCE, New York.
- Dingemans, M W, Stive, M J F, Bosma, J De Vriend, H J and Vogel, J A (1986). Directional nearshore wave propagation and induced currents, *Proc. 20th International Conference on Coastal Engineering*, Taiwan, ASCE, New York, pp. 1092-1106.
- Duxbury, Alyn, Duxbury, Alison and Sverdrup, K A. (2000). *Introduction to the World's Oceans*. 6th ed. New York: McGraw-Hill.
- DWA (1986). Bestuur van die waterhulpbronne van die Republiek van Suid-Afrika. Dep. Of Water Affairs, Pretoria.
- Einstein, H A (1950). The bed-load function for sediment transportation in open channel flows. *Technical Bulletin* No. 1205, U S Dep. Of Agriculture, Soil Conservation Service, Washington, D.C.
- Ferentinos, G and Collins, M B (1980). Effects of shoreline irregularities on a rectilinear tidal current and their significance in sedimentation processes. *Journal of Sedimentary Petrology*, 50(4), 1081-1094.
- Flemming, B W (1978). Underwater sand dunes along the Southern African continental margin - observations and implications. *Marine Geology*, v. 26, p. 177-198.
- Flemming, B W (1980). Sand transport and bedform patterns on the continental shelf between Durban and Port Elizabeth (southeast African continental margin). *Sedimentary Geology*, v. 26, p. 179-205.
- Flemming, B W (1981). Factors controlling shelf sediment dispersal along the southeast African continental margin. *Marine Geology*, V. 42. 259-277.
- Flemming, B W (1982). Dynamics of large transverse bedforms on the southeast African continental shelf. *11th International Sedimentological Congress*. Hamilton, Ontario, Canada, p. 73.
- Fredsøe, J (1978). Sedimentation of river navigation channels. *J. Hydraulics Div.*, ASCE, Vol 104 (HY2): 223-236.
- Gao, S and Collins, M B (1994). Analysis of grain size trends, for defining sediment transport pathways in marine environments. *Journal of Coastal Research*, Vol 10, No 1: 70-78.
- Garde, R J, Subramanya, K and Nambudripad, K D (1961). Study of scour around spur-dikes. *Journal of the Hydraulics Division*, ASCE, Proc paper 2978: 167-175.
- Gonsalves, J W and Bartels, A (1990). Sediment movement over a rocky coast: An evaluation. *CSIR Research Report* 686, Stellenbosch.
- Gravens, M B (1990). A new ocean-entrance system at Bolsa Chica Bay, California: Preconstruction assessment of potential shoreline impacts. *Miscellaneous Paper* CERC-90-2, WES, CERC, Vicksburg.
- HAECON (1992). Granulometrische sediment-trend analyse techniek. HAECON n.v. Harbour and Engineering Consultants, BME/VMT/DDT/T/SAF0961/00015. 10pp.
- Hallermeier, R J (1981). A profile zonation for seasonal sand beaches from wave climate. *Coastal Engineering* 4: 253 - 277.
- Harris, T F W (1978). Review of coastal currents in Southern African waters. *S. Afr. Natl. Sci. Programme, Rep.*, 30 : 103pp.
- HISWA user manual (1993). Prediction of stationary short-crested waves in shallow water with ambient currents. By N Booij and L H Holthuijsen. *Delft University of Technology*, Delft, The Netherlands.
- Holthuijsen, L H and Booij, N (1986). A grid model for shallow water waves, *Proc. 20th International Conference on Coastal Engineering*, Taiwan, ASCE, New York, pp. 261-270.

- Holthuijsen, L H, Booij, N and Herbers, T H C (1989). A prediction model for stationary, short-crested waves in shallow water with ambient currents, *Coastal Engineering*, 13, pp 23-54.
- Holthuijsen, L H and Booij, N (2003). SWAN User Manual: SWAN Cycle III version 40.20. Delft, Netherlands, Faculty of Civil Engineering and Geosciences, Environmental Fluid Mechanics Section, Delft University of Technology : 128.
- Horikawa, K (1988). Nearshore Dynamics and Coastal Processes: Theory, Measurement and Predictive Models. University of Tokyo Press, Japan.
- Kamphuis, J W (1991). Alongshore sediment transport rate. *J. Waterway, Port, Coastal and Ocean Eng.*, ASCE, (117), 624-640.
- Kamphuis, J W (2002). Alongshore Transport of Sand. *28 th International Conference on Coastal Engineering*, ASCE, Cardiff, Wales.
- Kleinhans, M G (2002). Sediment dynamics on the shoreface and upper continental shelf, a review. EC MAST Project No. MAS3-CT97-0086, *Utrecht University*, Physical Geography.
- Komar, P D (1979). Beach-slope dependence of longshore currents. *J Waterway, Port, Coastal and Ocean Div*, ASCE, Vol 105(WW4): 460-464.
- Kraus, N C, Hanson, H and Harikai, S (1984). Shoreline change at Oarai Beach: Past, present and future. *19 International Conference on Coastal Engineering*, ASCE, Vol. 2: 2107-2123, Houston.
- Larsen, M, Hanson, H and Kraus, N C (1987). Analytical solutions of the one-line model for shoreline change. WES, CERC, *Technical Report CERC-87-15*, Vicksburg, USA.
- Lean, G H (1980). Estimation of maintenance dredging for navigation channels. *Hydraulics Research Station Report*, Wallingford.
- Longuet-Higgins, M S (1970). Longshore currents generated by obliquely incident sea waves. *Journal of Geophysical Research*, 75, no33: 6778-6801.
- Lutjeharms, J R E, Catzel, R and Valentine, H R (1989). Eddies and other boundary phenomena of the Agulhas Current. *Continental Shelf Research*, 9, 597-616.
- Mallory, J K (1977). Abnormal waves on the south-east coast of South Africa. *Inst. Oceanogr. Univ. Cape Town, Occas. Rep. 77/1*; 18 pp.
- Marker, M E (1988). Geology and Geomorphology. In: Lubke, R A; Gess F W & Bruton M N (eds) (1988). *A Field Guide to the Eastern Cape Coast*. Published by: The Grahamstown Centre of the Wildlife Society of southern Africa, Grahamstown, South Africa.
- Martin, A K and Flemming, B W (1986). The Holocene shelf sediment wedge off the south and east coast of South Africa. In Knight, R J and McLean J R (Eds) *Shelf Sands and Sandstones. Canadian Society of Petroleum Geologists, Memoir II*, p 27-44.
- Mayor-Mora, R, Mortensen, P and Fredsøe, J (1976). Sedimentation studies on the Niger River Delta. *15 Intern. Conf. On Coastal Eng.*, ASCE, Honolulu, Hawaii, Vol. 2: 2151-2169.
- Morfett, J C (1990). A "virtual power" function for estimating the longshore transport of sediment by waves. *Coastal Engineering* 14: 439-456.
- Nairn, R B (1990). Prediction of cross-shore sediment transport and beach profile evolution. *PhD thesis*, Dept of Civil Engineering, Imperial College, London.
- Nicholson, J and Swart, D H (1985). Measurements of suspended sediment concentrations in the field. *CSIR Report T/SEA 8513*, NRIO, Stellenbosch. 12pp.
- Nicholson, J, Broker, I, Roelvink, J A, Price, D, Tanguy, J M and Moreno, L (1997). Intercomparison of coastal area morphodynamic models. *Coastal Engineering* 31 (1997) 97-123.
- O' Connor, B A (1985). Siltation in navigation channels, dock entrances and marinas. 3 day Short Course: Dredging for waterways and harbours, Dept Civil Eng, University of Liverpool, Liverpool.

Sediment Transport Regime at East London

- Pattiaratchi, C, James, A and Collins, M B (1986). Island /wakes and headland eddies: A comparison between remotely-sensed data and laboratory experiments. *Journal of Geophysical Research*, 92, 783-794.
- Pearce A F, Schumann E H and Lundie, G S H (1978). Features of the shelf circulation off the Natal coast. *S. Afr. J Sci.* 74, 328,331.
- PIANC (1984). Classification of soils and rocks to be dredged. Permanent International Association of Navigation Congresses, Supplement to Bulletin No. 47(1984), PIANC, Brussels. 14pp.
- Pond, S and Pickard, G L (1986). *Introductory dynamical oceanography*. Oxford: Pergamon Press.
- NPA East London Drawing Office (1993). Unpublished maps depicting current measurements. NPA Drawing Office, East London.
- Preston-Whyte, R A and Tyson, P D (1988). *The atmosphere and Weather of Southern Africa*. Cape Town; Oxford University Press.
- Przedwojski (1995). Bed topography and local scour in rivers with banks protected by groynes. *Journal of Hydraulic Research*, Vol 33, no 2: 257-273.
- Rooseboom, A (1975). Sedimentproduksiekaart vir Suid-Afrika. Dep. Of Water Affairs, Techn. Report 61, unpubl.
- Rooseboom, A (1978). Sedimentafvoer in Suider-Afrikaanse Riviere, Water S.A. 4,1,15-17.
- Rooseboom, A (1992). Sediment transport in rivers and reservoirs - a Southern African Report to the Water Research Commission by Sigma Beta Cons. Eng., WRC Report No 297/1/92.
- Rossouw, J (1989). Design waves for the South African coastline. Dissertation approved for the degree doctor of philosophy at the University of Stellenbosch. 140pp.
- SANHO-2 (2004). South African *tide tables*. SANHO-2, Hydrographer, South African Navy, Tokai.
- Sasaki, T O and Sakuramoto, H (1984). Effect of rip current barrier on harbor shoaling. *ASCE, Proc 19 Int Coastal Eng Conf*, Houston, Texas, Vol II: 2091-2106.
- Schoonees, J S (1991). Field measurements of suspended sediment concentrations in the surf zone at Walker Bay. *Euromech 262 - Sand Transport in rivers, Estuaries and the Sea*, Soulsby & Bettess (eds). Balkema, Rotterdam. P 131-138.
- Schoonees, J S (2000). Annual variation in the net longshore sediment transport rate. *Coastal Eng.*, Vol. 40(2): 141-160.
- Schoonees, J S and Möller, J P (1982). Design and calibration of False Bay sediment model. 18th International Conference on Coastal Engineering, ASCE, Volume 2: 1161-1180, Cape Town.
- Schoonees, J S and Theron, A K (1993). Review of the field-data base for longshore sediment transport. *Coastal Eng.*, Vol. 19: 1-25.
- Schoonees, J S and Theron, A K (1994). Accuracy and applicability of the SPM longshore transport formula. *24 Intern. Conf. On Coastal Eng.*, ASCE, Kobe. Vol. 3: 2595-2609.
- Schoonees, J S and Theron, A K (1995). Evaluation of 10 cross-shore sediment transport/morphological models. *Coastal Eng.*, Vol. 25: 1-41.
- Schoonees, J S and Theron, A K (1996). Improvement of the most accurate longshore transport formula. *25 Intn. Conf. On Coastal Eng.*, Orlando, Florida. ASCE, Volume 3, Chapter 282, page 3652-3665.
- Schumann, E J (1976). High waves in the Agulhas Current. *Mar. Weather Log*, 20, 1-5.
- Sloff, C J (1997). Sedimentation in reservoirs. Communications on Hydraulic and Geotechnical Engineering, Report No. 97-1. TUDelft, Faculty of Civil Engineering, Delft University of Technology. 269pp.
- Smith, R (1976). Giant waves, *J. Fluid Mech.*, 77, 417-431.
- Soras, P E, Scholberg, P and Thendrup, A (1987). Wave data in shallow waters provided by the HISWA numerical model, *Proc Advances in Underwater Technology, Ocean Science and Offshore Engineering*, Vol. 12, Modelling the Offshore Environment, Society for

Sediment Transport Regime at East London

- Underwater Technology, London, publ. Graham and Trotman, pp. 89-95.
- Swart, D H (1974). *Offshore sediment transport and equilibrium beach profiles*, D.Sc Thesis, Delft University of Technology.
- Swart, D H (1976). Coastal sediment transport computation of longshore transport. *Report R968*, Volume 1, Delft Hydraulic Laboratory, Delft, The Netherlands. 112 pp.
- Swart, D H (1986). Prediction of wind-driven sediment transport rates. *Proc. Of 20th International Conf. on Coastal Eng.*, ASCE, Taipei, Taiwan. Vol. II: 1 595-1 611.
- Swart, D H and Serdyn, J de V (1979). Unpublished. Statistical analysis of visually observed wave data from voluntary observing ships for South African west coast. NRIO, CSIR, Stellenbosch.
- Swart, D H and Fleming, C A (1980). Longshore water and sediment movement. *17 th International Conference on Coastal Engineering*, ASCE, Sydney, Australia, Volume 2: 1275-1295.
- Swart, D H and Crowley, J B (1988). Generalized wave theory for a sloping bottom. *Proc. 21st International Conference on Coastal Engineering*, Malaga, ASCE, New York.
- The Dock and Harbour Authority (1995). Maintenance and environmental dredging. *Journal of the Dock and Harbour Authority*, Vol. 75, No 859, London, UK. 31 pp.
- Theron, A K (1991). Setback line for Sunrise Beach, Muizenberg. *CSIR Report EMA-C 91161*, Stellenbosch. pp 28.
- Theron, A K (1992). Unpublished computer program ("SEDVM") to determine beach slopes and shoreline erosion/accretion.
- Theron, A K (1994a). Oos-Londenhawe: Sedimentasie, sandvangput en storing. *CSIR Report EMAS-C 94020*, Stellenbosch.
- Theron, A K (1994b). Oos-Londenhawe: Beplanning en invloed van golfbreker-uitsteeksel. *CSIR Report EMAS-C 94046*, Stellenbosch.
- Theron, A K (1995). Port of East London: Sedimentation on the inside of the southern breakwater. *CSIR Report EMAS-C 95034*, Stellenbosch.
- Theron, A K (1996). Reduction of dredging costs by limiting sediment transport towards the Port of East London: Feasibility Study. *CSIR Report EMAS-C 96018*, Stellenbosch.
- Theron, A K (1998). Current Measurements at the Port of East London Since, July 1996. *CSIR Report ENV/S-C 98023*, Environmentek, Stellenbosch.
- Theron, A K (2000). Durban Beach Monitoring Progress Report: July 1998 to June 1999, Volume I. *CSIR report ENV-S-C 2000 – 022A*. Environmentek, Stellenbosch.
- Theron, A K (2003). Setback line for the coastal zone: Msimbazi- to Mahlongwana River Mouth, and Mgeni- to Ohlanga River Mouth. *CSIR Report EMAS-C 2003-088*. Environmentek, Stellenbosch.
- Theron, A K and Schoonees, J S (1998). Defining an unusual littoral regime to optimise dredging at East London. *26 th International Conference on Coastal Engineering*, ASCE, Copenhagen, Denmark Vol 3: 3479-3489.
- Theron, A K, Schoonees, J S, Burggraaf, A and Raw, A J (1998). Harbour sedimentation and dredging optimisation at some Southern African ports. *29 PIANC*, Netherlands, Section II, Subject 5: 47-55.
- Theron, A K and Schoonees, J S (1999). Sand Transport Through and Around the Main Breakwater at East London. *Proceedings*, Fourth International Symposium on Coastal Engineering and Science of Coastal Sediment Processes, Coastal Sediments '99, New York, ASCE. Volume 3: 2371 - 2384.

- Theron, A K and Schoonees, J S (2000). Optimization of dredging through understanding the unusual littoral regime at East London. *Civil Engineering Magazine*, SAICE. Dec 2000 Vol 8 No 10:11-12.
- Theron, A K, Schoonees, J S and Claassens, H (2002a). Port of East London : design and optimisation of the sand traps. *Journal of SA Inst Civ Eng*, Vol 44(4): 8-15.
- Theron, A K, Diedericks, G P J, Huizinga, P, Basson, G R and Kemp, A (2002b). Measurement and modelling of sediment dynamics in estuaries. In : ENVIRO FLOWS. 2002. Proceedings of the International Conference on Environmental Flows for River Systems, incorporating the 4th International Ecohydraulics Symposium. *Proceedings*. Cape Town, South Africa. March 2002.
- Theron, A K, Schoonees, J S, Huizinga, P and Phelp, D T (2003). Beach Diamond Mining Design at the Rocky Namaqualand Coast. *Proceedings*, 4th Coastal Structures Conference, ASCE, Portland, Oregon, 2003.
- Van der Meer, J W and Veldman, J J (1992). Singular points at berm breakwaters: scale effects, rear, round head and longshore transport. *Coastal Engineering* 17: 153-171.
- Van Hijum, E and Pilarczyk, K W (1982). Equilibrium profile and longshore transport of coarse material under regular and irregular wave attack. Publication No 274. Delft Hydraulics Laboratory, Delft, The Netherlands.
- Van Rijn, L C (1986). Sedimentation of dredged channels by currents and waves. *Journal of Waterway, Port, Coastal and Ocean Engineering*, ASCE, Vol 112 (No 5): 541-559.
- Van Rijn, L C (1989). Sediment transport by currents and wave - Handbook. *Delft Hydraulics, Report H461*, Vol. 2 p. 10.15-10.21.
- Vincente, C M and Uva, L P (1984). Sedimentation in dredged channels and basins. Prediction of shoaling rates. 19 *Intern Conf on Coastal Eng*, Houston, Texas. ASCE, Vol 2: 1863-1878.
- Vincent, C E, Stolk, A and Porter, C F C (1998). Sand suspension and transport on the Middelkerke Bank (southern North Sea) by storms and tidal currents. *Marine Geology* 150, 113-129.
- Vogel, J A, Radder, A C and De Reus, J H (1988). Verification of numerical wave propagation models in tidal inlets, *Proc, 21st International Conference on Coastal Engineering*, Malaga, ASCE, New York, pp. 433-447.
- Weaver, A B (1982). In Hart R C (1982): Water Quality in the Buffalo river catchment. A Synthesis. University of Rhodes, Grahamstown. pp. 63-82.
- Whillier, A (1962). Ocean currents at East London. *Die Siviele Ingenieur in suid-Afrika*, January 1962. pp 1-8.
- Withers, A W (1991). A preliminary investigation into the dynamics of the physical processes and sediment movement along the Orient Beach shoreline with respect to beach front planning, East London. *Dennis Moss Partnership Inc*. Ref L2017.
- Whitford, D J and Thornton, E B (1993). Comparison of wind and wave forcing of longshore currents. *Continental Shelf Research*, Vol. 13, No 11, pp. 1205-1218, Great Britain.
- WL|Delft Hydraulics (1996). Delft3D-FLOW version 0.1, User Manual release 2.48, WL|Delft Hydraulics, the Netherlands.
- WL|Delft Hydraulics (2001). Delft 3D MOR *User Manual* version 3.00, WL|Delft Hydraulics, the Netherlands.